EFFECT OF MACROMOLECULAR BINDING AND SELF-ASSOCIATION ON THE PHOTOPHYSICAL AND PHOTOCHEMICAL PROPERTIES OF TRIARYLMETHANE DYES

BY

LAVINIA M. LEWIS

A dissertation submitted in partial fulfillment of

the requirements for the degree of

Doctor of Philosophy

(Pharmaceutical Sciences)

at the

UNIVERSITY OF WISCONSIN-MADISON

2001

EFFECT OF MACROMOLECULAR BINDING AND SELF-ASSOCIATION ON THE PHOTOPHYSICAL AND PHOTOCHEMICAL PROPERTIES OF TRIARYLMETHANE DYES

Lavinia M. Lewis

Under the supervision of Dr. Guilherme L. Indig

At the University of Wisconsin-Madison

In response to transmembrane potentials, which are negative on the inner side of energized mitochondria, extensively conjugated cationic molecules (dyes) with appropriate lipophilic/hydrophilic character naturally accumulate inside these subcellular compartments. Because enhanced mitochondrial membrane potential is a prevalent cancer cell phenotype, the selective destruction of tumor cells *via* mitochondrial targeting is currently under investigation in this laboratory as a novel therapeutic strategy for photochemotherapy of neoplastic diseases. Cationic triarylmethane dyes (TAM^+) represent a class of photosensitizers whose phototoxic effects develop at least in part at the mitochondrial level. The aim of this project was to determine how the molecular structure of TAM^+ dyes affects their noncovalent binding to model host biopolymers (hexokinase, DNA, and low density lipoprotein), and explore the effects of these noncovalent interactions on photosensitization efficacy (or drug potency).

Depending upon the degree of biopolymer loading, TAM^+ dyes were found to bind to hexokinase (HK) and DNA both as monomers and as aggregates. Laser irradiation of TAM^+-HK and TAM^+-DNA complexes has indicated that photosensitization efficacy decreases upon increasing the degree of dye aggregation. While dye aggregates were extensively destroyed (photobleached) upon laser irradiation, little damage was inflicted by them on the

host macromolecules. On the other hand, dye monomers were less susceptible to photobleaching and more effective in promoting the destruction of HK and DNA. TAM^+ dyes were also found to bind to low density lipoprotein (LDL) in aqueous media. The dominant mechanism of TAM^+ binding to LDL has been characterized as the partitioning of these dyes into the lipid core of the host lipoprotein. No evidence has been found for the formation of TAM^+ aggregates in the presence of LDL. Accordingly, in LDL-TAM^+ complexes the degree of photoinduced macromolecular damage was found to increase with increasing drug concentration.

Biopolymer-assisted dye aggregation can thus be expected to control, at least in part, the photosensitization efficiency of TAM^+ dyes in complex biological environments. Our findings indicate that considerations on how molecular structure affects dye aggregation are of relevance for the rational design of new photosensitizers specifically tailored for the selective destruction of tumor cells via mitochondrial targeting.

APPROVED

DATE: 05/07/01

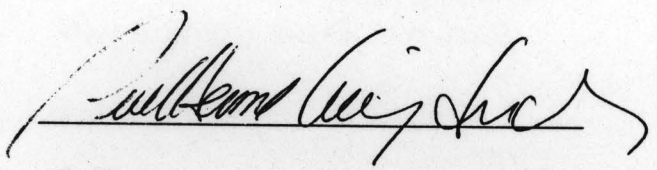

Guilherme L. Indig, Ph.D.; Major Advisor

Dedicated to my parents Frank E. Lewis and Josephine M. Lewis, my sister Dr. Preeti Lewis and to Mother of Perpetual Succor

There is nothing that my Lord and I,

together cannot accomplish today.

ACKNOWLEDGEMENTS

I would like to acknowledge Dr. Guilherme L. Indig, my major advisor for his support and guidance through out my Ph.D. and for teaching me the importance of good experimental design and analytical thinking. I must state that the five years that we worked together have been scientifically very rewarding. I would also like to thank my committee members namely Dr. George D. Zografi, Dr. Glen S. Kwon, Dr. Timothy D. Heath and Dr. Samuel H. Gellman for their time and input .

There are many people who contribute towards a candidate's Ph.D. other than the major advisor and the committee members. Along those lines I would like to acknowledge Dr. Mauricio S. Baptista, a Post Doctorate Fellow, in our laboratory for help during the initial year of my Ph.D., Dr. Kenneth A. Connors for teaching me the principles of mathematical models, Dr. William S. Mellon for allowing me to use his laboratory facilities, Dr. Monika V De Arruda for teaching me the basic aspects of gel electrophoresis, Moises Rivera and Surawut Watana for help with the finer aspects of gel electrophoresis and Subramanya Sastry for help with expediting computational procedures.

Life in the laboratory is often influenced by the people in the lab. I have been fortunate to be with extremely good lab mates, especially Jeremy A. Bartlett with whom I spent a great part of my Ph.D. and to whom I owe a lot both on a scientific and personal level. Also on a personal level, there were many friends with whom I could feel free to shed a tear or share a laugh, and they include Vidya Sridhar, Bonnie J. Fingerhut, Sue Stein, Judy

Thompson and Pornanong Aramwit. I would also like to thank Dr. Joseph R. Robinson for the time and help that he lent during my job hunting endeavors.

Five and a half years is a long and hard journey in a foreign country, away from home. I would not have been able to complete this journey that I embarked on five years ago, without the love, support and prayers of my family. Though physically absent they have been with me in their thoughts, words and deeds. Last but not the least, I would like to thank God for taking care of every minute detail of my life, including my Ph.D.

TABLE OF CONTENTS

List of Figures

List of Tables

Chapter 1 . Introduction

Photodynamic Therapy:

Photodynamic therapy (PDT) is a new treatment modality that involves the combined use of light and photosensitizers, for the photochemical destruction of targeted tissue (Dougherty T. J., 1987). It involves the systemic injection and accumulation of a photosensitizer within neoplastic tissue followed by tumor destruction upon irradiation with light of an appropriate wavelength. Neoplastic cell death and tumor eradication is promoted through the photochemical generation of highly reactive (cytotoxic) species *in situ* (Dougherty T. J., 1987). PDT was first approved in 1993 by the Canadian FDA (US FDA approval was in 1995) for the prophylactic treatment of bladder cancer (Dougherty T. J. et al, 1998), but it has rapidly progressed from the field of oncology to other fields like ophthalmology, cardiology and dermatology (Rouhi M., 1998). In ophthalmology, it is used for the treatment of age related macular degeneration, a leading cause of blindness in the world. In the field of cardiology, its use in the removal of arterial plaques by a procedure called as photoangioplasty is under active investigation (Rouhi M., 1998). In dermatology, the potential of PDT is being explored for the treatment of superficial skin lesions, acne and for cosmetic purposes. Currently its applications in urology (enlarged prostate and prostate cancer), gynecology (dysfunctional uterine bleeding), rheumatoid arthritis (for the selective destruction of pathological synovium), periodontal diseases and localized wound infections are also being examined (Rouhi M., 1998).

Following its first FDA approval in Canada in 1993, approvals for PDT were obtained in The Netherlands and France for treatment of advanced esophageal and lung

cancers, in Germany for treatment of early stage lung cancer, in Japan for early stage lung, esophageal, gastric and cervical cancers and in the United States for advanced esophageal cancer and early stage lung cancer (Dougherty T. J. et al, 1998). Taking into consideration the current regulatory status of PDT, the work done in this project focuses on its use in the treatment of malignant tumors. The success of PDT thus rests on the preferential accumulation of photosensitizers by neoplastic tissue over the adjacent healthy tissue in which the tumor arose. One possible way of achieving this selectivity is by targeting the mitochondria of tumor cells, since tumor cell mitochondria have enhanced mitochondrial membrane potentials compared to normal cell mitochondria (Chen L. B., 1988). This enhanced mitochondrial membrane potential is associated with increased uptake and retention of a variety of cationic photosensitizers by tumor cells as compared to normal cells.

Mitochondrial Targeting and Cationic Photosensitizers :

Based on a comprehensive investigation involving more than 200 cell lines/types of melanoma, adenocarcinoma, transitional cell carcinoma, squamous cell carcinoma, and normal epithelial cells, Chen has demonstrated that enhanced mitochondrial membrane potential is a prevalent cancer cell phenotype (Chen L. B., 1988). Only approximately 2% of all cells tested so far disobey this dominant precept. Typically, the mitochondrial membrane potential of carcinoma cells is over 60 mV higher than in normal epithelial cells. Evidence pointing to a higher plasma membrane potential in a variety of carcinoma cells, as compared to normal epithelial cells has also been previously described (Chen L. B., 1988; Davis S. et al, 1985). Because enhanced mitochondrial membrane potential is a prevalent cancer cell phenotype the selective destruction of tumor cells *via* mitochondrial targeting is being

explored as a novel therapeutic strategy for both chemo- and photochemotherapy of neoplastic diseases.

Photofrin II™ (PII), the clinically approved photosensitizer and other anionic porphyrin oligomers target primarily tumor vasculature, while a variety of cationic photosensitizers target primarily the malignant cells (Henderson B. W. et al, 1985). Accumulation around the tumor vasculature in the case of anionic photosensitizers has been attributed to the large size of the porphyrin oligomers, to their association with serum proteins and to the tumor architecture which includes a leaky vasculature, a large interstitial space, and a compromised lymphatic drainage system (Dougherty T. J. et al, 1998). Since anionic photosensitizers target primarily the tumor vasculature and not the tumor cells, their toxicity toward tumors stems from destruction of the tumor vasculature and subsequent tumor starvation. Despite their extensive clinical application, PII and other porphyrins have a number of undesirable properties. Penetration of light into tissue is best at the edge of visible and into the near infra red regions of the spectrum. However, PII has only a small absorption peak in the relevant region of the spectrum (ε = 1170 $M^{-1}cm^{-1}$ at 630 nm) (Dougherty T. J., 1992; Stewart F., 1998). Porphyrins target the tumor vasculature and require the presence of molecular oxygen to mediate the photochemical destruction of targets, and are therefore not effective in poorly perfused regions of tumor mass. Besides, destroying the tumor vasculature results in the generation of hypoxic tumor zones which are often the origin of tumor recurrences, because oxygen is no longer available in these zones for the photodynamic action to take place (Foster T. H. et al, 1991). Porphyrins also show long persistence in normal tissues, including skin, thus keeping the patient photosensitive for more than a month after treatment.

On the other hand, in response to transmembrane potentials, which are negative on the inner side of energized mitochondria, extensively conjugated cationic molecules with appropriate lipophilic/hydrophilic character naturally accumulate inside these subcellular compartments. Indeed mitochondrial toxicity is one of the mechanisms for cell death typically associated with cationic photosensitizers (Davis S. et al, 1985). With appropriately tailored cationic molecules, the dye concentration within the mitochondria can be 10^3 to 10^4 fold higher than that observed outside the cell, thus offering a greater degree of direct cellular phototoxicity than anionic photosensitizers (Davis S. et al, 1985). When mitochondrial accumulation is controlled solely by membrane potentials, the difference in concentration inside and outside the cell can be rationalized in terms of the Nernst equation (Chen L. B., 1988, Davis S. et al, 1985, Wong J. R. et al, 1988). At equilibrium, the cytoplasmic and mitochondrial concentrations can be theoretically predicted by the Nernst equation as follows:

$$[\text{Cytoplasm}] = [\text{Extracellular}] * 10^{(\Delta\Psi_{\text{cytoplasm}})/(2.303RT/nF)} \qquad \text{Equation 1}$$

$$[\text{Mitochondrion}] = [\text{Cytoplasm}] * 10^{(\Delta\Psi_{\text{mitochondrion}})/(2.303RT/nF)} \qquad \text{Equation 2}$$

where $\Delta\Psi_{\text{cytoplasm}}$ and $\Delta\Psi_{\text{mitochondrion}}$ are the potentials across the cell and mitochondrial membrane respectively. At 25°C, the exponential term within parenthesis, 2.303RT/nF, takes on the value of 59 mV. Thus, for illustrative purposes, if $\Delta\Psi_{\text{mitochondrion}}$ is –180 mV, and $\Delta\Psi_{\text{cytoplasm}}$ is –60 mV, the equilibrium concentration of a cationic photosensitizer in the cytoplasm would be approximately 10 times that outside the cell, while in the mitochondrial compartment the concentration would be approximately 10,000 times that in the cytoplasm.

Rhodamine 123 (Rh123) is the cationic dye most extensively investigated with respect to selective mitochondrial accumulation. Rh123 stains mitochondria with remarkable

efficiency and selectivity, with no simultaneous staining of the plasma membrane, nuclear envelope, lysosomes, endoplasmic reticulum, Golgi complex and any other cellular component (Bernal S. D. et al, 1983; Chen L. B., 1988). For this particular dye, the potential driven component of mitochondrial accumulation is clearly the dominant contribution to cell accumulation. Upon depolarization of the mitochondrial membrane of living cells, Rh123 is no longer retained in the mitochondria. Rh123 is retained for a prolonged period of time (2 to 5 days) by the mitochondria of a large variety of carcinomas, whereas normal epithelial cells release it within a few hours (Bernal S. D., et al 1983; Wong J. R., et al 1995). Cancer therapy experiments carried out on mice have demonstrated that Rh123 has anticarcinoma activity *in vivo*. Rh123 has also been identified as a reasonably efficient purging agent for the selective removal of tumor cells from contaminated bone marrow grafts (Wong J. R. et al, 1995).

Triarylmethane (TAM^+) Dyes as Photosensitizers:

The cationic photosensitizers used in this project belong to a family of dyes called triarylmethanes (Figure 1.1), namely Crystal Violet (CV^+), Ethyl Violet (EV^+), Victoria Blue R (VBR^+) and Victoria Pure Blue BO ($VPBBO^+$). The rationale for choosing TAM^+ dyes as our model photosensitizer is as follows. One of our motivations in exploring mitochondrial targeting as a novel modality of photodynamic treatment of neoplastic diseases was based on a putative limitation of Photofrin II and other vascularly-targeted photosensitizers presently in clinical use in PDT. Although Photofrin II does not target *exclusively* tumor vasculature, there is little doubt that its *primary* mechanism of tumor destruction is based on vasculature impairment, and, interestingly, this major determinant of tumor destruction simultaneously

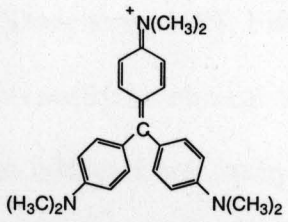

Crystal Violet (CV^+)

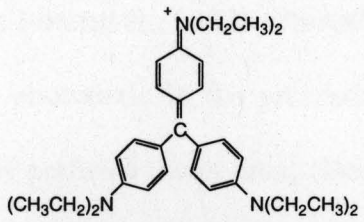

Ethyl Violet (EV^+)

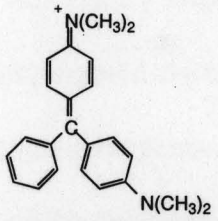

Malachite Green (MG^+)

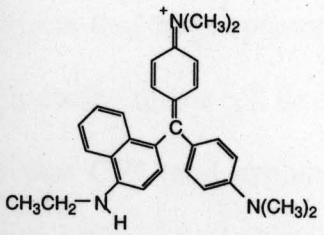

Victoria Blue R (VBR^+)

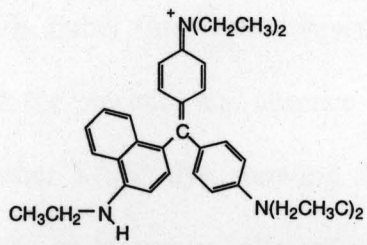

Victoria Pure Blue BO ($VPBBO^+$)

Figure 1.1 Triarylmethane dyes

represents a potential limiting factor for the success of this drug in certain therapeutic applications (Dougherty, 1998; Fisher et al, 1995; Bonnett R., 2000). Photofrin II and other PDT drugs presently in clinical use are highly phototoxic in the presence of molecular oxygen but do not work well in hypoxic or poorly perfused tumor areas (Dougherty, 1998). Therefore, as a result of the vascular damage incurred during irradiation, along with the natural consumption of oxygen by the cytotoxic photochemical reaction, tumor zones that at the onset of the treatment were sufficiently oxygenated may become hypoxic before sufficient damage is inflicted on the targeted tissue. The presence of hypoxic or poorly perfused areas in solid tumors (due to endogenous conditions or secondary to vascular damage) is thought to represent one of the determinants of tumor recurrence in PDT (Foster T. H. et al, 1991). Therefore, there is substantial interest in the development of new photosensitizers that target primarily tumor cells rather than tumor vasculature and are capable of inducing tumor cell destruction both in the presence and absence of oxygen. We now know that CV^+ (and hypothetically any other TAM^+ dye showing the appropriate lipophilic/hydrophilic character) is efficiently taken up by tumor cells and shows selective toxicity against these cells as compared to normal cells. We also know that the mechanisms of phototoxicity of CV^+ and other TAM^+ dyes do not require the involvement of molecular oxygen to operate (Baptista M. S. and Indig, G. L., 1998; Bartlett, J. A. and Indig, G. L., 1999; Indig, G. L. 1997; Baptista M. S. and Indig G. L., 1997, Lewis, L. M. and Indig, G. L., 2001). Therefore, mitochondria-specific TAM^+ dyes have the potential to increase the efficacy of PDT of solid tumors when used either in isolation or in combination with vasculature-targeted photosensitizers.

In addition to the importance of molecular oxygen in determining dye phototoxicity, other parameters to consider in conceptually constructing our idealized new photosensitizers include chemical stability, low systemic toxicity, and a low energetic requirement for electronic excitation. Again, TAM^+ dyes show very satisfactory characteristics with regard to all of these requirements. The properties listed below represent the minimum set of characteristics that must be present in an ideal photosensitizer. TAM^+ dyes meet these specifications. Based on these considerations, an ideal photosensitizer should present:

- *Strong absorption towards the red edge of the visible and into the near infra-red region of the electromagnetic spectrum, regions in which the penetration of light into tissue is better.* Most TAM^+ dyes show high extinction coefficients (> 70,000 M^{-1} cm^{-1}) above 600 nm (Lewis L. M. and Indig, G. L., 2000; Davis C., 1967).
- *Good chemical stability.* TAM^+ dyes are stable in solution. For example, in pure water or in ethanol the half-life of concentrated TAM^+ solutions kept in the dark can reach several years (Davis C., 1967).
- *Low systemic toxicity.* Over the years TAM^+ dyes have developed an excellent track record for biological safety. They have been employed, for example, as anthelmintics, antiseptics in burn patients and umbilical cords of newborns, antifungals to treat both topical and vaginal infections caused by Candida (Davis C., 1967; Duxbury D. F., 1993; RTECS 1997; Gennaro A. R. et al, 1990). Furthermore, our lead compound, CV^+, has been used for over 50 years for cleansing blood to remove the protozoan parasite Trypanosoma cruzi to prevent transfusion-associated transmission of Chaga's disease (Moras-Souza et al, 1996; Ramirez L. E. et al, 1995;

Docampo R. et al, 1988). Transfused patients receive a high dose of CV^+ intravenously. After transfusion, the skin of Caucasian patients becomes bluish-purple, and yet no significant side effects have ever been associated with this procedure (Moras-Souza et al, 1996)

- *Good cell penetration properties and preferential retention by neoplastic tissue.* Our lead compound, CV^+, apparently satisfactorily fulfills this requirement.
- *High phototoxicity in both normally oxygenated and hypoxic tumor areas.* Using laser flash photolysis and classical photochemical methods, we have described the mechanisms by which CV^+ and other TAM^+ dyes can damage biopolymers, including DNA and hexokinase (Baptista M. S. and Indig, G. L., 1998; Bartlett, J. A. and Indig, G. L., 1999; Indig, G. L. 1997; Baptista M. S. and Indig G. L., 1997, Lewis, L. M. and Indig, G. L., 2001). These last two biopolymers are considered putative targets for the phototoxic action of these dyes at the mitochondrial level. Mitochondrial DNA is particularly prone to oxidative damage due to its lack of protective histones, proofreading, and the mitochondria's incomplete repair mechanisms (Kowalowtoski M. J., 1999). Hexokinase is known to be over expressed in highly glycolytic tissues such as tumors, and this enzyme has been previously considered as a possible target for anti-tumor therapy (Penso J. and Beitner R., 1998). The mechanisms of TAM^+-induced biopolymer damage were found to be independent of molecular oxygen. Accordingly, the phototoxic action of CV^+ against L1210 cells was in a great extent (although not entirely) conserved upon extensive (but gentle) purging of cell

suspensions with argon to remove dissolved molecular oxygen before irradiation (Indig, G. L., 2000).

- *Must be converted during PDT to a photoproduct transparent to the excitation light to avoid the optical shielding effect that prevents the irradiation light from reaching deeper locations in photosensitizer-loaded tumors.* CV^+-mediated damage to biopolymers is initiated by a photoinduced electron transfer from the biopolymer to the photosensitizer (Baptista M. S. and Indig, G. L., 1998; Bartlett, J. A. and Indig, G. L., 1999; Indig, G. L. 1997; Baptista M. S. and Indig G. L., 1997, Lewis, L. M. and Indig, G. L., 2001), an event that simultaneously leads to dye decomposition and bleaching. The final products of CV^+ photodecomposition only absorb light in the ultra-violet region of the electromagnetic spectrum. Accordingly, upon irradiation of L1210 cells loaded with CV^+, dye bleaching was found to parallel cell kill.

Mitochondrial Accumulation of TAM^+ Dyes:

To obtain preliminary information on subcellular distribution and mitochondrial accumulation of CV^+ and EV^+ in rat basophilic leukemia cells, two photon laser scanning microscopy has been employed by Indig et al (Indig G. L. et al, 2000). RBL cells were chosen as the intial model system because they display well-defined discrete spherical mitochondria that makes morphological alterations easy to detect. The experimental strategy involved the use of a mitochondrial marker (Rh123) and the cellular NADPH autofluorescence to probe the cellular distribution of TAM^+ dyes and characterize the early alterations in mitochondrial morphology and bioenergetics associated with the dark

(cytotoxic) effects of these photosensitizers. Simultaneous two photon images of NADP(H), Rh123, and TAM^+ fluorescence were obtained by exciting RBL cells at 750 nm using a Ti:Sapphire laser (75 fs) as the excitation source. The RBL cells were incubated in the dark for periods ranging from 1 minute to 1 hour with growth media containing 1 μM TAM^+ dye and subsequently incubated for 30 minutes in the dark with fresh growth media containing 0.05μM Rh123. After a final cycle washing and incubation for 15 minutes in fresh growth media, the cells were subjected to two photon imaging. No morphological alterations or induction of fluorescence attributed to cellular damage was observed during the brief imaging period. The cell fluorescence was analyzed in three different detection channels for the simultaneous characterization of the spatial distribution of each fluorophore of interest.

When RBL cells were incubated for 10 minutes with CV^+, the fluorescence associated with CV^+, Rh123 and NADP(H) showed similar perinuclear, punctuate distribution in the cell, which is consistent with mitochondrial localization. The mitochondria were still energized at this point as indicated by their ability to retain Rh123. After 30 minutes of CV^+ incubation Rh123 was no longer retained by the cell and cellular NAD(P)H fluorescence was less intense and less punctuate, indicating that the mitochondrial inner membrane potential has been reduced and NADH has been oxidized to NAD^+. This approach of monitoring NAD(P)H fluorescence in living cells for the assessment of mitochondrial bioenergetics was originally introduced by Chance (Chance B. et al, 1970).

With the replacement of CV^+ by EV^+ similar mitochondrial effects were observed. The comparison of the fluorescence patterns of EV^+, Rh123 and NADPH after 10 minutes of RBL incubation with EV^+ has indicated that this dye also accumulates in cell mitochondria.

However, significant EV^+ background fluorescence was observed throughout the cytoplasm, suggesting that a substantial fraction of the EV^+ molecules taken up by the RBL cells may also localize in subcellular compartments other than mitochondria.

Cellular Uptake and Phototoxicity of TAM^+ Dyes:

TAM^+ dyes have been previously considered as photosensitizers for PDT (Fiedorowicz M., 1997; Viola A., 1996) and are thought to develop their cytotoxic effect primarily at the mitochondrial level (Ramirez L. E. et al, 1995). To explore whether a series of structurally related TAM^+ dyes can promote the selective destruction of tumor cells with minimum toxicity towards normal cells, a model preclinical study was conducted in which the phototoxicity of TAM^+ dyes towards leukemia L1210 cells and normal hematopoietic cells (murine granulocyte-macrophage progenitors, CFU-GM) was compared under conditions in which the respective thermal (dark) toxicity was small or negligible for both cells (Indig et al, 2000). Figure 1.2 shows the efficiency with which a series of TAM^+ dyes photoinactivate L1210 cells and CFU-GM cells as a function of irradiation time. It is evident that among the four commercially available TAM^+ dyes investigated so far, CV^+ is the only dye that was substantially more efficient in photoinactivating L1210 cells than CFU-GM cells. After relatively short periods (*circa* 20 minutes) the surviving fractions of L1210 cells represented only 0.3 to 0.4% of their initial values, whereas in the case of CFU-GM cells the respective surviving fractions were still in the range of 60 to 70% of their initial values. The phototoxic effects of the other three TAM^+ dyes do not show appropriate selectivity toward

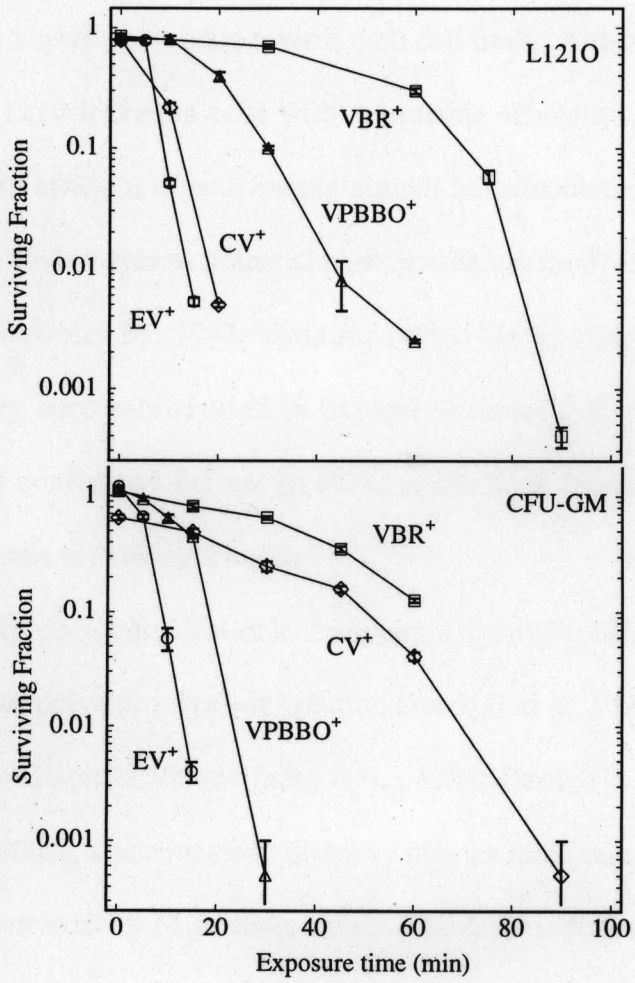

Figure 1.2 Photoinactivation of L1210 leukemia cells (upper panel) and murine CFU-GM (lower panel) sensitized by TAM^+ dyes. Data points represent mean colony counts ± standard errors of four replicate culture dishes. Cells were incubated for 10 minutes with 1μM TAM^+. Fluence rate = 27 W/m^2. (Reproduced from Indig et al, 2000)

leukemia cells. VBR^+ displayed low efficacy in destroying both L1210 and CFU-GM cells, and EV^+ is highly phototoxic toward both cell lines. Although $VPBBO^+$ mediates the inactivation of L1210 leukemia cells with reasonable efficiency, this dye was found to be even slightly more efficient at inactivating normal hematopoietic cells. Interestingly, most attention given to TAM^+ dyes as potential photosensitizers for PDT has to date been focussed on $VPBBO^+$ (Fiedorowicz M., 1997; Viola A., 1996). On the other hand CV^+, the TAM^+ dye that has been very successfully used in tropical medicine for several decades, but to our knowledge never considered for use in PDT, is the most promising TAM^+ dye for PDT among those we have investigated to date.

Extensively conjugated cationic compounds typically bind to natural and synthetic anionic biopolymer polyelectrolytes in solution (Jones II et al, 1991; Jones II et al, 1994; Pal M. K. et al, 1994; Baptista M. and Indig G. L., 1998; Bartlett J. A. and Indig G. L., 1999; Indig G. L. et al, 2000), a phenomenon that may play an important role in the mechanisms of mitochondrial phototoxicity of cationic dyes. The total mitochondrial membrane protein content, including both inner and outer membranes, varies between 60 and 65%, while the inner membrane protein content is believed to be as high as 75% (Nicholls D. G., 1982). Because of the high protein content of the inner membrane, these proteins can be expected to be one of the primary targets for the toxic action of cationic mitochondrial photosensitizers. Indeed, these proteins are thought to be one of the primary targets of mitochondria-generated reactive oxygen species during oxidative stress (Kowaltowski A. J. et al, 1999). Among the possible mitochondrial targets are hexokinase (HK), a mitochondrial enzyme and mitochondrial DNA (mt-DNA), the latter especially being prone to oxidative damage

(Kowaltowski A. J. et al, 1999), because of a lack of protective histones and an incomplete repair mechanism.

Hexokinase (HK):

Cancer cells are characterized by a high rate of glycolysis, which is their primary energy source. All glycolytic enzymes bind to the cytoskeleton, except HK, which binds reversibly to mitochondria (Gots R. E. et al, 1972). HK has been shown to bind to porin at the contact sites between the outer and inner mitochondrial membranes (Kottke et al, 1988). The mitochondrially-bound HK utilizes mitochondrially generated ATP to phophorylate glucose to glucose-6-phosphate (Gotts R. E. et al, 1972; Gotts R.E. et al, 1974; Viitanen P. V. et al, 1984). This phosphorylation represents the first step of the glycolytic process. Glucose-6-phosphate then enters the glycolytic pathway that results in the generation of cellular ATP. In addition to this, glucose-6-phosphate also enters the pentose phosphate pathway, leading to the synthesis of excess amounts of nucleic acids and lipids, which are essential for cancer cell proliferation and maintenance.

The levels of mitochondria bound HK in highly glycolytic tumor cells greatly exceeds that of normal tissues, and the bound enzyme was shown to have a preferred access to mitochondrially generated ATP (Arora K. K. and Pedersen P. L., 1988, Smith T. A. 2000). It was also found that NIH/3T3 cells transfected with tumor HK cDNA, showed increased HK, increased glycolytic rate and enhanced growth rate (Fanciulli et al, 1994). These findings show that the exceptionally high mitochondria bound HK in cancer cells plays a key role in regulating cell energy metabolism and cell growth rate.

HK catalyses the transfer of the phosphoryl group to the sixth hydroxyl group of glucose according to the following biochemical reaction that requires the initial formation of a ternary enzyme-glucose-ATP-Mg^{2+} complex (Wilson J. E., 1995).

$$\text{D-glucose} + \text{ATP} \xrightarrow{\text{HK/Mg}^{2+}} \text{D-glucose-6-phosphate} + \text{ADP}$$

The binding sites for both substrates namely ATP and glucose are located in the C-terminal half of the molecule, and therefore this portion of the molecule is associated with catalytic function (Wilson J. E., 1995). Glucose-6-phosphate serves as a potent allosteric inhibitor of the enzyme (Crane R. K. and Sols A., 1954; Wilson J. E. and Chung V., 1989). The regulatory site to which glucose-6-phosphate binds, is located in the N-terminal half of the enzyme (Wilson J. E., 1995).

Yeast HK is structurally well characterized, and there is extensive similarity in amino acid sequences between yeast HK and other members of the HK family (Wilson J. E., 1995). Both the N- and C-terminal halves of the mammalian enzyme are presumed to resemble the yeast HK. Yeast HK is a homodimer and each subunit consists of two readily distinguishable domains, generally referred to as the 'large lobe' and the 'small lobe'. The binding site for glucose lies at the bottom of the cleft between the lobes and binding of glucose induces closure of the cleft by a hinge bending movement (Steitz, T. A. et al, 1977). The change in the conformation upon binding of glucose enhances the binding of the metal-ATP substrate and apparently protects the activated ATP from attack by water. There is one nucleotide binding site per monomer of the enzyme molecule.

HK has been explored as a potential target in the chemo and photochemotherapy of neoplastic diseases. Dose dependent detachment of HK from mitochondria of B-16 melanoma cells has been investigated as a possible strategy for cancer therapy using clotrimazole and bifenazole (Penso J. and Beitner R., 1998). The decrease in mitochondria bound HK preceded the decrease in cell viability, with concomitant detachment of other cytoskeleton bound glycolytic enzymes. Glioma metabolism requires the presence of mitochondria bound HK which generates glucose dependent energy (Miccoli L. et al, 1998). A decrease in cellular pH leads to release of HK, which in turn decreases glucose phosphorylation, ATP content and cell proliferation. Thus agents that can decrease intracellular pH can be used in therapy against gliomas. In human glioma cells treated with hypericin, a naturally occurring photosensitizer, HK was inhibited in a light and dose dependent manner (Miccoli L. et al, 1998). HK was released from mitochondria as measured by ELISA using a specific anti-HK antibody. The action of hypericin thus involved the alteration of mitochondria bound HK, initiating a cascade of events that ultimately alter the metabolism and survival of glioma cells.

Photodynamic treatment of yeast (Kluyveromyces Marxianus) with toluidine blue resulted in an inhibition of alcohol dehydrogenase, cytochrome c oxidase, glyceraldehyde-3-phophate dehydrogenase and hexokinase (Paardekooper M. et al, 1995). However, when the same yeast cells were treated with light and chloroaluminium phthalocyanine, no significant inhibition of HK activity, but significant inhibition of activity of other enzymes was observed, indicating that not all photosensitizers inhibit HK. In this work we demonstrate that TAM dyes belong to the family of photosensitizers capable of inducing photoinactivation of HK.

Mitochondrial DNA (mtDNA):

Defective mitochondrial function is one of the distinct phenotypes of many cancer cells (Pedersen P. L., 1978; Pedersen P. L., 1997; Rempel A. et al, 1996). Most cancer cells have few mitochondria (≤ 50% of normal) and less mitochondrial content (Pedersen P. L., 1978). In addition to having an altered membrane potential, cancer cell mitochondria are small, have few cristae and altered membrane composition (Rempel A. et al, 1996). Mitochondria occupy about 50% of the cytoplasmic volume of animal cells and hold approximately 1000 proteins that are encoded by nuclear DNA. Mitochondria contain their own DNA that encodes 13 proteins consisting of 4 enzyme complexes of the respiratory chain viz. Complex I, III, IV and ATP synthase. This information is retained within a 16.5 kb DNA sequence, there are about 10 copies of the genome in each mitochondrion, and up to 10,000 mitochondria in each cell (Schatz G., 1995; Singh K. K., 1998).

Changes in mitochondrial genome have been reported in cancer cells (Hochhauser D., 2000). Damage to mtDNA occurs more commonly than nuclear DNA, presumably through the production of reactive oxygen species during oxidative phosphorylation. Repair of mtDNA is less efficient than nuclear DNA, because mtDNA lacks histones and has an incomplete repair mechanism (Kowaltowski, A. J., 1999). MtDNA has a higher copy number than has nuclear DNA, and therefore its mutations are easier to detect. According to a study conducted by Fliss and co-workers (Fliss, M. S. et al, 2000) the sensitivity with which cancer is diagnosed can be improved with the identification of mtDNA mutations. By sequencing 80% of the mtDNA genome from primary tumors, they found somatic mtDNA mutations in samples of body fluids in 64% cases of bladder cancers, 46% of head and neck

cancers, and 43% of lung cancers. The sensitivity of identifying mtDNA mutations is about 200 times higher than nuclear DNA mutations like mutant p53 (Hochhauser D., 2000).

Singh et al have examined the role of mtDNA in cancer therapy, by comparing the response of two tumor cell lines to different cancer therapeutic agents (Singh K. K., 1999). The cell lines they compared were HSL2 (Rho+) having mtDNA, and its derivative cell line that lacks mtDNA (Rho0). The cancer therapeutic agents included adriamycin a DNA intercalating drug, an alkylating agent (MNNG), PDT (photosensitizer – Mesoporphyrin IX) and gamma radiation. Cell death induced by adriamycin and PDT in Rho+ cells was much more pronounced than that observed in Rho0 cells that lack mtDNA. Rho0 cells were in fact resistant to both PDT and adriamycin. However, both cell lines were equally sensitive to ionising radiation and the alkylating agent. Adriamycin and PDT produce cytotoxic reactive oxygen species that make an already susceptible mtDNA, even more susceptible to oxidative damage. The importance of mtDNA and the functions it encodes thus play an important role in cancer cell sensitivity and response to a therapeutic agent.

It has also been observed that anionic photosensitizers like the haematoporphyrins, which localize in the mitochondrial membranes, do not target the mitochondrial DNA because they probably cannot access the interior of the mitochondria. Although anionic photosensitizers target primarily the tumor vasculature, localization in the membranes of subcellular organelles can occur if tumor cell colonies are incubated for long enough periods with haematoporphyrins. There was no difference in the survival curves between the parent cell line 143B, and its mitochondrial DNA negative derivative, p° 206, after exposure to x-rays or visible light in the presence of Photofrin II (Barrett J. T., 1993). The finding that the

parent cell and its mt DNA–negative derivative do not differ in their sensitivity to PDT strongly suggests that mitochondrial DNA is not a target susceptible to Photofrin II.

Morgan and co-workers (Morgan J. et al, 2000) compared phototoxicity in two cell lines with photosensitizers that localize in different cellular compartments. The two cell lines were a human ovarian carcinoma cell line 2008 and its mitochondrial DNA-deficient derivative, ET3. Photosensitizers included Victoria Pure Blue BO (that localizes in the mitochondria) and probably in other lipophilic subcellular compartments, Photofrin II (that localizes in cell membranes), and Nile Blue A (that localizes in the lysosomes). For photosensitizers like Photofrin II and Nile Blue A that do not localize in the mitochondria, no significant difference was observed between 2008 and ET3 toxicity. Because Victoria Pure Blue B O ($VPBBO^+$) localizes in cell mitochondria, ET3 cells that lack a mitochondrial DNA were less susceptible than 2008 to both dark- and light-mediated phototoxicity of $VPBBO^+$. These results indicate that damage to mitochondrial DNA may be a major element of toxicity mediated by $VPBBO^+$. In this work we demonstrate that TAM^+ dyes induce the photochemical destruction of DNA, although among the dyes studied, $VPBBO^+$ is less effective in promoting such destruction.

TAM^+s and their Interaction with Serum Proteins:

Early observations on the strong interaction of albumin with porphyrins encountered in the porphyria disease lead to the assumption that albumin was the most important carrier of photosensitizers in the blood (Maziere' J. C., 1991). However, Reyftmann P. et al (1984) and Jori et al (1984) independently demonstrated that a variety of hydrophobic

photosensitizers show a strong association with human blood lipoproteins. Lipoproteins are macromolecular complexes described as emulsion or microemulsion particles, that transport lipids through vascular and extravascular compartments (Spady D. K., 1991). They have a common structural organization, which consists of a hydrophobic core of triglycerides and esterified cholesterol, surrounded by a monolayer of phospholipid, unesterified cholesterol and apoproteins. The major lipids transported via lipoproteins are triglycerides and cholesterol.

Plasma lipoproteins can be separated into various classes according to their density, size, surface charge and other surface properties. Chylomicrons are the largest of the lipoproteins found under conditions of abundant dietary triglyceride intake (Spady D. K., 1991). They are synthesized in the intestine and are rich in triglycerides, have the highest lipid to protein ratio and therefore the lowest density. Very low density lipoprotein (VLDL) is the next largest of the lipoproteins also rich in triglycerides and synthesized by the liver (Spady D. K., 1991). Intermediate density lipoprotein (IDL) is the product of VLDL metabolism and is mainly comprised of cholesteryl ester along with some triglycerides (Spady D. K., 1991). LDL, in turn is the product of IDL metabolism and has an internal core predominantly made of cholesteryl esters (Havel R. J., 1984). High density lipoprotein (HDL), is the smallest of the lipoproteins, has the highest protein to lipid ratio and its lipid core contains both cholesteryl esters and triglycerides (Tall A. R. et al, 1978). Because cancer cells over-express LDL receptors compared to normal cells due to their increased requirement for cholesterol and phospholipids (Gal D. et al, 1981), studies in this project will focus on low density lipoprotein.

Low Density Lipoprotein

LDL is a 3.6 million Da macromolecule that has been described as a microemulsion particle (Rosenberger V. and Margalit R., 1993). It is isolated in the density region between 1.063 and 1.019 g/ml; and is composed of 19% protein, 1% carbohydrate, 43% cholesteryl ester, 11% unesterified cholesterol, 4% triglycerides and 22% phospholipids (Schumaker V. N. et al , 1994). Apo B is the only protein associated with LDL (Spady, D. K., 1991; Schumaker V. N. et al, 1994). It is a hydrophobic glycoprotein with a major portion of β structure and very little α helical character. It surrounds the LDL particle in the form of a surface belt and because of its hydrophobic nature does not easily dissociate from LDL.

Synthesis and Catabolism of LDL:

VLDLs are synthesized in the liver to transport endogenous lipids (Spady, D. K., 1991). Once exocytosed into the plasma they are acted upon by the enzyme lipoprotein lipase, resulting in hydrolysis of the triglycerides and formation of remnants (Havel, R. J., 1984). VLDL remnants can either be further endocytosed by liver hepatocytes or they can follow an alternative pathway that converts them to LDL via the IDL pathway. In humans most of the VLDL is converted to LDL, the transformation representing continued activity of lipases and takes place in the vascular space (Havel, R. J., 1984). Thus the rate of LDL production is determined both by the rate of VLDL production and by the rate of conversion of VLDL to LDL. LDL is removed from the plasma by various organs of the body by receptor dependent and receptor independent pathways. In humans two thirds of the LDL is removed by receptor-mediated pathways and the plasma half life of LDL is 3 to 4 days (Spady, D. K., 1991).

LDL receptors are membrane proteins that have a domain rich in cysteine and negatively charged amino acids which play an important role in the recognition and interaction of LDL receptors with positively charged amino acids of Apo B (Allison B. A. et al, 1994). Upon binding of a circulating LDL to the receptor, the receptor-ligand complex is internalized into vesicles and eventually transformed into an endosome. Inside the endosome, the receptors dissociate from the lipoprotein and are recycled back to the cell surface while LDL is delivered to lysosomes where it is finally degraded. The entire cycle takes 10 to 20 minutes and continues irrespective of the presence or absence of ligand (Spady, D. K., 1991).

LDL as a potential drug carrier

A fascinating concept in the field of drug delivery is the idea of targeting macromolecular drug conjugates to a specific cell population. The endogenous nature of LDL makes it a suitable carrier because it is well tolerated in the body, does not cause immunological reactions, is biodegradable, and is not rapidly cleared by the reticuloendothelial system. Its receptor-mediated uptake lends further credence to its potential use as a 'targeting shuttle'. Much attention has been focused on the possible exploitation of LDL as a carrier for targeting antitumoral drugs to neoplastic cells, which have higher LDL receptor activity due to their high mitotic index than corresponding normal cells.

Anionic photosensitizers especially porphyrin derivatives have been coupled to LDL; and indeed such complexes have shown increased PDT activity (Allison B. A. et al, 1994). One such example is benzoporphyrin complexed with LDL, which has shown great promise

in the treatment of experimental choroid melanoma (Scmidt-Erfurth V. et al, 1994). In the case of anionic photosensitizers tumor necrosis is brought about by destruction of the vasculature surrounding the tumor tissue (Foster T. H. et al, 1991). This cuts off the supply of oxygen (which is essential for PDT) to the irradiated tissue, resulting in hypoxic areas, often the origin of tumor recurrences. Zhou *et al* (Zhou C. et al, 1988) have observed that, anionic photosensitizers carried by LDL bring about photodynamic effects by direct damage to neoplastic cells and are mostly deposited in mitochondria, lysosome and plasma membrane. These observations have been based on electron microscopic studies performed on tumor tissues taken from mice at different times after phototreatment (Zhou C. et al, 1988). This suggests that complexation of a photosensitizer to LDL increases photosensitizer uptake within neoplastic tissue and can therefore take PDT beyond the level of the tumor vasculature. LDL also plays an important role in carrying the photosensitizer to arterial plaques in photoangioplasty and to newly forming blood vessels that are the cause of blindness in wet-type macular degeneration (Rouhi M., 1998).

The probability that an injected photosensitizer becomes associated with serum lipoproteins is governed by factors such as the chemical structure of the photosensitizer, the delivery system and serum composition, which can vary depending on diet and metabolic function. As a general trend, the fraction of injected compounds that associate with LDL, tends to decrease with increasing polarity, for example the association of chlorin e6 with lipoproteins decreased twofold upon condensation with aspartic acid (Jori G. and Reddi E., 1993). In the case of sulfonated derivatives of tetraphenyl porphyrins, a partial hydrophobic-hydrophilic nature was found to be optimal for association with lipoproteins (Chris de Schmidt P. et al, 1993). Thus the monosulfonated and disulfonated derivatives were found to

associate with lipoproteins while the tetrasulfonated porphyrin showed very little association. The delivery system used for systemic administration of the photosensitizer also affects its association with lipoproteins. Over 80% of injected Hematoporphyrin was delivered to lipoproteins when administered in liposomes, while only a 30% association with lipoproteins was observed when administered in phosphate buffer saline (Jori G., 1990). In all such instances where photosensitizers have been delivered in liposomes, oil emulsions or as a LDL complex, a preferential interaction with serum lipoproteins was observed (Jori G. and Reddi E., 1993). Another property of the photosensitizer that can have an impact on its therapeutic ability is its tendency to self- associate (Rotenberg M. and Margalit, R., 1985). Thus three kinds of equilibria could co-exist in systemic circulation and at the target site (i) self-association, (ii) protein binding as a monomer and (iii) protein binding as aggregates. All three could be major factors in determining the fraction of dose available to the target and in modulating both photoreactivity and phototoxicity. The role of these equilibria on the photosensitization efficiency is specifically addressed in this study.

Dye Aggregation:

TAM^+ dyes are known to self-associate in aqueous solutions (Leuck H. et al, 1992, Stork W. H. et al, 1972, Duxbury D. F., 1993). Dye aggregation has been characterized for TAM^+s in highly concentrated solutions (*circa* 80 μM for EV^+) and in solutions with high ionic strength (Bartlett J. A. and Indig, G. L.; unpublished data; Lueck H. B. et al, 1992, Stork W. H. et al, 1972). Self-association of TAM^+s at high dye to protein ratios has also been detected in the presence of bovine serum albumin (BSA) (Bartlett J. A. and Indig G. L., 1999). It has been observed that the tendency of TAM^+s to aggregate in water increases with

increase in the size and hydrophobic character of the N-substitutents on the aromatic rings. The nature of the driving force that controls aggregation is not well understood. Since the aggregation of TAM^+ dyes is observed in water but not in methanol, ethanol and acetonitrile and other organic solvents, the hydrophobic effect has been hypothesized to play an important role in the aggregation phenomenon (Lueck H. B. et al, 1992). The formation of dye aggregates is most commonly studied by absorption spectroscopy, using the concentration and temperature dependence of the absorption spectrum (Leuck H. B. et al, 1992; Jones II et al, 1994) The formation of TAM^+ dye dimers in aqueous solutions is indicated by the appearance of a hypsochromically (blue) shifted absorption band. The formation of larger dye aggregates leads to larger hypsochromic shifts.

According to the exciton model in molecular spectroscopy (Kasha M. et al, 1965), dye aggregation causes the excited singlet levels of the aggregate to split relative to those of the monomer. The wavelength of absorption of the composite molecule (aggregate) depends on the relative geometry of the monomeric components of the dimer. In the case of H-type (face-to-face) dimers, the transition dipoles are parallel to each other (Figure 1.3). The out-of phase dipole arrangement is represented by the exciton state S_1 that lies lower than S_2, the exciton state of the repulsive in-phase dipole interaction. The transition moment is given by the vector sum of the individual transition dipole moments in the component. Thus transition from the ground state to exciton state S_1 is forbidden (transition moment = 0), while transitions from the ground state to the exciton state S_2 are allowed, giving rise to a blue shift in the singlet-singlet electron transition in the dimer.

In the monomer transition from the ground state to the lowest singlet state is allowed, fluorescence occurs under favorable conditions, while phosphorescence is limited by

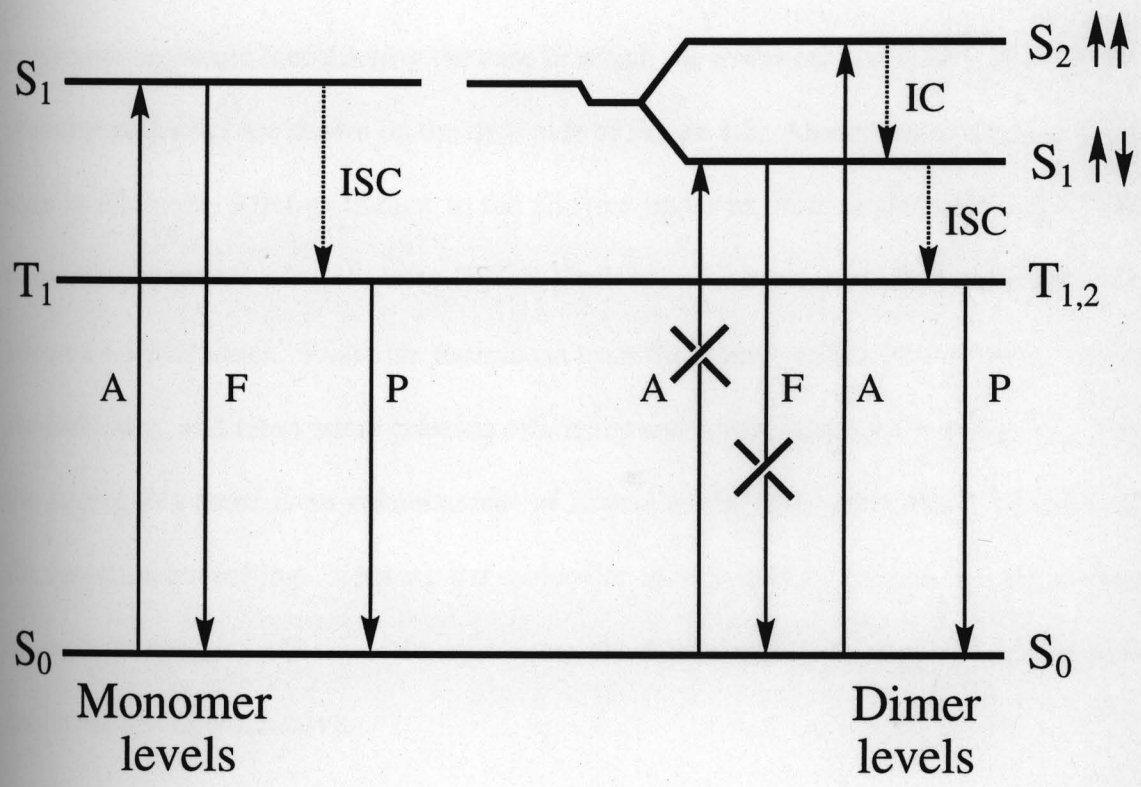

Figure 1.3 Paths of excitation between singlet and triplet states without and with exciton splitting (parallel transition dipole dimer case): A = Absorbance, D = Dimer, F = Fluorescence, IC = Internal Conversion, ISC = Intersystem crossing, M = Monomer, P = Phosphorescence.

intersystem crossing efficiency to the corresponding triplet state (Figure 1.3). In the composite molecule (considering the case in which the lower exciton state is forbidden), the probable pathways are shown on the right side of Figure 1.3. Absorption to the upper exciton state is allowed. After excitation to the allowed upper exciton singlet state, rapid internal conversion between singlet states ($S_2 \rightarrow S_1$) occurs, which prevents fluorescence from the allowed excited states. Radiative transitions from the lower exciton state to the ground state are forbidden, and intersystem crossing efficiency and triplet formation is enhanced. Thus in the aggregates there is an enhancement of lowest triplet state excitation accompanied by fluorescence quenching. Because the molecular exciton theory predicts an ehancement in intersystem crossing efficiency in aggregates, the formation of aggregates should lead to an enhanced dye photoreactivity.

Photochemistry of photosensitizers bound to macromolecules

Photodynamic action is brought about by the combined involvement of light, oxygen and photosensitizer. Foote (Foote C. S., 1968) considered two types of photoreactions that can play an important role in PDT. The first type involves a primary interaction of the electronically excited sensitizer with a molecule of substrate S; while in the second type the electronically excited sensitizer reacts with a molecule of oxygen. The excited triplet state of the photosensitizer (^{3}Sens*) lives much longer than its corresponding singlet. This long lifetime of the triplet favors sensitizer-substrate and sensitizer-oxygen interactions. In this context, the more important biological photooxidation processes occur via electron or hydrogen atom transfer events between the excited sensitizer and the substrate (Type I

reaction) or via energy transfer from the triplet sensitizer to molecular oxygen (Type II reaction).

$^3Sens^* + S \rightarrow$ Radical Pair $+ O_2 \rightarrow$ Reactive oxygen species Type I

$^3Sens^* + O_2 \rightarrow {}^1O_2^*$ Type II

The Type I reaction generates the radical pair which subsequently reacts with dissolved molecular oxygen to produce a variety of cytotoxic reactive oxygen species such as peroxyl, hydroxyl and superoxide radicals. The Type II reaction results in the formation of the highly reactive singlet oxygen species which can then react with biological substrates. The relative importance of Type I and Type II reactions depends on the respective reaction rates and the concentrations of substrate and oxygen. In cases where noncovalent binding of photosensitizers to proteins, nucleic acids and other biological substrates is predominant, the variables controlling the competition between Type I and Type II are no longer those that are true for free species in solution (Indig, G. L., 1996; Indig, G. L., 1997; Baptista M. S. and Indig G. L., 1997; Baptista M. S. and Indig G. L., 1998). Since the ground state photosensitizer is physically attached to a substrate, the Type I mechanism may become much more competitive, especially when the excited photosensitizer is protected from diffusional oxygen quenching by virtue of it binding to a macromolecular domain that offers such protection. Thus reaction paths not observed for species free in solution may be observed in restricted reaction spaces and may be governed by the nature of the microenvironment.

Detailed studies on the mechanisms of photoreaction of TAM^+s are currently under active investigation in our laboratory. Previous work in this laboratory has explored the

photochemical behavior of TAM^+s, both when free in solution and when noncovalently bound to BSA (Indig G. L., 1997; Baptista M. S. and Indig G. L., 1997; Baptista M. S. and Indig G. L., 1998; Bartlett J. A. and Indig, 1999; Bartlett J. A. and Indig, 1999). It has been found that when TAM^+s are noncovalently bound to BSA, their photoreactivity undergoes a remarkable enhancement, and that the photooxidation mechanism, Type I is favored in the macromolecular environment. The nature of the spectral changes observed upon photolysis of TAM^+s bound as monomers to BSA was highly conserved among the dye series, suggesting that the mechanism of photobleaching may also be conserved among the dye series. One such reaction mechanism is depicted in Figure 1.4. Both benzophenone type photoproducts (oxidized) and leuco forms (reduced) of the TAM^+ dyes were identified in photolysed samples of BSA-TAM^+ complexes. The reduction of CV^+ to its leuco derivative is a two electron process, (formally $H + e^-$ or $2e^- + H^+$), initiated in BSA-TAM^+ complexes by a photoinduced electron or hydrogen atom transfer from the protein to the dye moiety. The semi-reduced carbon-centered dye radical can either react with dissolved molecular oxygen to produce the benzophenone type photoproduct or accommodate a second electron to form the leuco derivative of CV^+.

Comparative studies on the photobleaching efficiencies of TAM^+ monomers and dimers, free in solution and noncovalently bound to BSA have also been carried out. Substantial enhancements in the photobleaching efficiency were obtained upon formation of dye aggregates on the biopolymer template, indicating that dye aggregation is another phenomenon that may play a significant role in the mechanism of photosensitization in complex biological environments. As predicted by the molecular exciton theory, the formation of H type dimers leads to an enhancement in the intersystem crossing efficiency

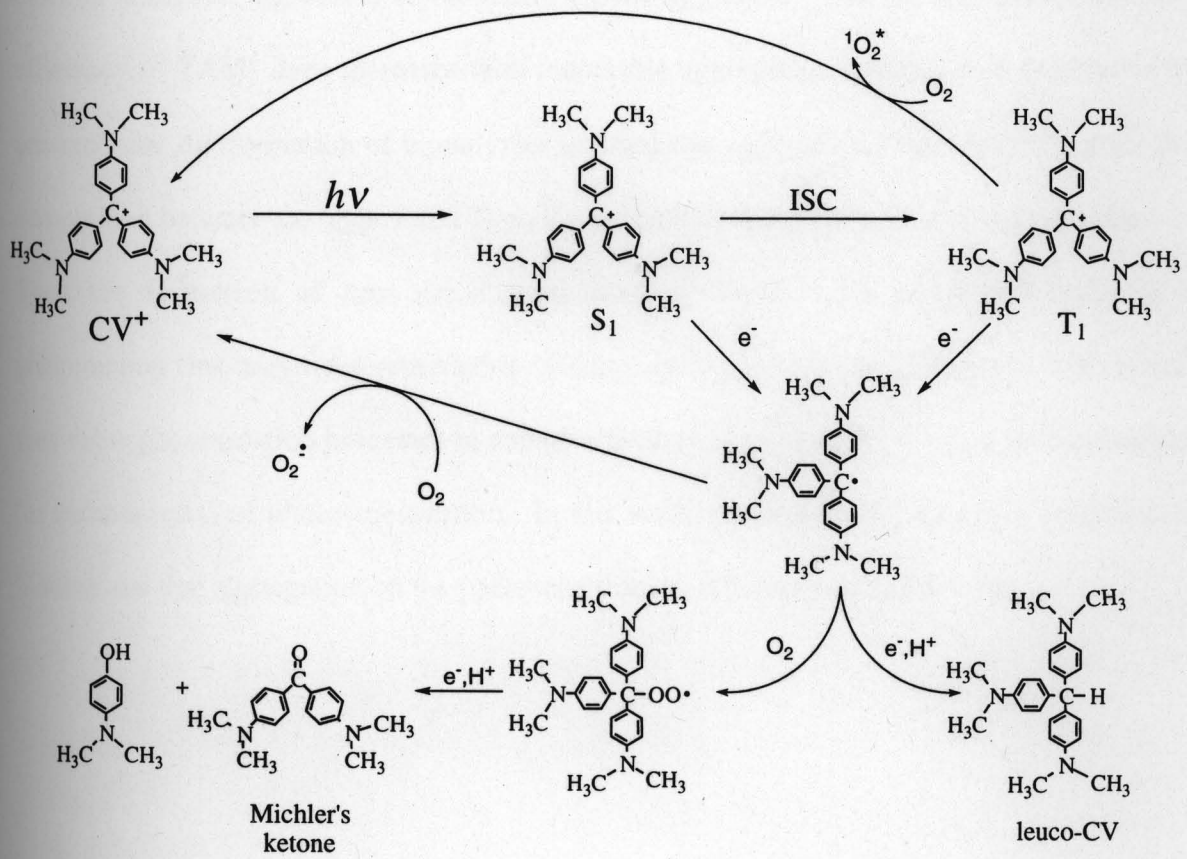

Figure 1.4 Routes of deactivation and photobleaching of CV^+. (Reproduced from Indig et al, 2000)

within the aggregates as compared to the monomers, and this enhancement typically leads to enhanced photoreactivity. Besides, photoinduced electron transfer events are intrinsically favored within dye aggregates as a result of physical contact between electron donor and electron acceptor, regardless of the nature of the aggregate. Because the photobleaching efficiency of TAM^+ dyes increases with increasing aggregation number, it is reasonable to presume that the formation of biopolymer-assisted dye aggregates would typically shift the competition between the Type I and Type II mechanisms more toward the Type I process. Thus the formation of host guest complexes of TAM^+ dyes with bioploymers is a phenomenon that may have remarkable consequences not only on the efficacy with which they drive photoxidation processes in complex biological systems but also on the mechanism (or mechanisms) of photosensitization. In this work we explore the effects of biopolymer binding and dye aggregation on the photosensitization efficiency of TAM^+ dyes.

Chapter 2. Statement of Problem, Research Plan and Working Hypotheses

Statement of Problem:

The PDT strategy is aimed at promoting neoplastic cell death and tumor eradication through the photochemical generation of highly reactive cytotoxic species *in situ*. The currently approved clinical photosensitizers (Photofrin II and Verteporfin) are anionic by nature, accumulate primarily around the tumor vasculature and operate via the Type II pathway that results in the generation of singlet oxygen (Stewart F., 1998; Rouhi M., 1998). Because they primarily target the destruction of the vasculature rather than direct tumor cell kill, they are not effective in poorly vascularized internal regions of tumor mass. Besides by damaging blood vessels, tissue that at the outset of irradiation was sufficiently oxygenated to support the formation of singlet oxygen may become hypoxic, and such poorly perfused tumor zones are often the origin of tumor recurrences. Thus some of the present day limitations of photodynamic therapy are a lack of direct tumor cell kill and an inability of currently approved photosensitizers to operate in poorly perfused or hypoxic areas of tumor tissue.

Since elevated mitochondrial potential is a prevalent cancer cell phenotype, a number of cationic dyes preferentially accumulate and are retained for longer time periods in tumor cell mitochondria compared to normal cells (Chen L. B., 1988). This preferential uptake and retention of cationic species by tumor cells makes mitochondrial targeting an attractive therapeutic strategy in the photochemotherapy of neoplastic diseases. This has motivated the investigation of the use of Triarylmethanes (TAM^+s), a class of cationic photosensitizers, as photochemotherapeutic agents for mitochondrial targeting in PDT in our laboratory.

Besides, having a good track record with regard to biological safety, it has been shown using two photon laser scanning microscopy that TAM^+s naturally accumulate into the mitochondria of rat basophilic leukemia cells. Thus cationic photosensitizers, like the triarylmethanes can offer a greater degree of direct cell kill and eliminate some of the limitations that are associated with anionic agents currently in clinical use. However for TAM^+ s to act efficiently at the level of the mitochondria, two important aspects need to be taken into consideration viz. transport of the photosensitizer and photochemical destruction of mitochondrial targets.

Working Hypotheses:

Since TAM^+ dyes are known to bind very efficiently to natural and synthetic macromolecules and supramolecular structures through noncovalent interactions (Jones II et al, 1991; Jones II et al, 1994; Pal M. K. et al, 1994; Baptista M. and Indig G. L., 1998; Bartlett J. A. and Indig G. L., 1999; Indig G. L. et al, 2000), they may not be free in solution to any significant extent when present in complex environments, such as isolated cells and biological tissues. Moreover, because TAM^+s are extensively conjugated they tend to self-associate under conditions of high dye concentration and high ionic strength. Such events can influence both the transport and the photoreactivity of the triarylmethane. When present in the blood stream, TAM^+s could bind to various serum proteins like albumin and lipoproteins, and within the mitochondria, they could interact with various mitochondrial components. Thus it is highly probable that the photodynamic action may be predominantly initiated within such dye-macromolecule complexes.

Our working hypothesis is that LDL, one of the serum proteins, the receptors for which are over expressed in cancer cells compared to normal cells, may play an important role in the transport of the injected TAM^+s to their site of action. Since the TAM^+s exert their phototoxic action at the mitochondrial level, it is also reasonable to hypothesize that this phototoxic action may be mediated by the photochemical destruction of mitochondrial targets, which in turn may be influenced by both, macromolecular binding and self-association of dye molecules. An ideal photosensitizer should be capable of destroying tumor cells both in the presence and absence of oxygen. It has been shown previously in this laboratory that TAM^+ dyes do not require the involvement of molecular oxygen to operate (Indig G. L., 1997; Baptista M. S. and Indig G. L., 1997; Baptista M. and Indig G. L., 1998; Bartlett J. A. and Indig G. L., 1999). It is therefore possible to hypothesize that the photoinduced destruction of mitochondrial targets may also proceed *via* oxygen independent pathways.

Research Plan:

The specific aims of this project were to characterize the formation of noncovalent complexes of TAM^+s and model biological hosts and to determine the extent to which noncovalent binding affects the photophysical and photochemical properties of these photosensitizers. The plan was to outline the interdependence between dye structure and photoreactivity of the TAM^+s, under conditions that resemble those encountered *in vivo*, i.e. with the TAM^+ dyes non covalently bound to a series of model biological hosts. Accordingly, hexokinase, DNA and LDL, were chosen as model biological hosts. Hexokinase, a mitochondrial enzyme that is over expressed in cancer cells was chosen

because it has been used in the past as a target in both chemo and photochemotherapy of neoplastic diseases (Penso J. and Beitner R., 1998; Miccoli L. et al, 1998). Mitochondrial DNA is particularly prone to oxidative damage, both because of a lack of protective histones and an incomplete repair mechanism and therefore represents a target that can be destroyed with relative ease compared to nuclear DNA (Hochhauser D., 2000). LDL was chosen not only because it is a serum protein that can carry the photosensitizer to its site of action, but also to provide a microenvironment that represents those typically encountered at protein lipid interfaces of cell membranes.

To study binding it is imperative to determine how spectral distribution, extinction coefficients and fluorescence quantum yield are influenced by noncovalent binding. For this it was necessary to carry out studies on different systems that could corroborate the binding data obtained with the biological hosts. In order to do this we carried out systematic studies with various solvents to study the effects of these solvents on the spectroscopic characteristics of TAM^{+}s. For similar reasons we also studied the binding of TAM^{+}s to various non-biological macromolecules and supramolecular structures like cyclodextrins and anionic and nonionic detergents and their corresponding micelles. The micellar structures with a nonpolar core and charged polar heads specifically served as a simple mimic for LDL, which also has a charged surface surrounding a nonpolar core.

The stoichiometry of noncovalent complexes involving small ligands and biopolymer polyelectrolytes has been traditionally characterized with the use of Langmuir isotherms. A linear representation of these isotherms derived by Scatchard (Scatchard G., 1949) is one of the equations most frequently used in the investigation of protein binding. A linear Scatchard plot indicates the presence of one or more indistinguishable binding sites in a

macromolecule for a specific substrate, while deviations from linearity indicate the presence of different types of binding sites for that ligand. The question of whether the Scatchard analysis can permit the distinction between the aggregation of ligand molecules in a single binding site from the existence of different types of binding sites for that ligand was addressed in this study. We have built mathematical models that in combination with our experimental data have pointed out limitations of the Scatchard analysis with regard to the distinction of these two different scenarios.

To determine how binding affects the photoreactivity of the TAM^+s, noncovalent complexes of dye and model biological hosts obtained under different binding conditions, were subjected to laser photolysis. Photoinduced macromolecular damage was assessed using a variety of techniques. In the case of HK, changes in enzymatic activity were used to measure the extent of photoinduced macromolecular damage, while in the case of DNA, it was photoinduced DNA cleavage. Because the protein–lipid type architecture of LDL resembles the proten-lipid type environment encountered in cell membranes, LDL was considered as a model for a biological membrane that could also serve as putative PDT target. The extent of lipid peroxidation provided a measure of photoinduced damage in LDL. Appropriate experiments were also designed to explore whether the TAM^+s can bring about photoinduced damage in HK and DNA in the absence of molecular oxygen. In these experiments the photoinduced macromolecular damage in air-equilibrated and nitrogen purged samples was compared. In addition, the contribution of the Type II pathway (that results in the generation of singlet oxygen) towards photoinduced damage was also investigated.

Chapter 3. Experimental

MATERIALS:

Chemicals and Reagents:

The TAM^+s used in the experiments were chloride salts of Ethyl violet (EV^+), Victoria Blue R (VBR^+) and Victoria pure blue BO ($VPBBO^+$) from Aldrich and Crystal violet (CV^+) from Sigma. These salts were recrystallized from methanol and dried under vacuum. The purity of crystallized TAM^+s was assessed by Thin layer Chromatography (silica gel, methanol-acetic acid 95:5, v:v). Water used in all experiments was distilled, deionized and filtered prior to use (Millipore Milli-Q system; resistivity 18MΩ cm).

Solvents used in the studies of solvent effects on the spectroscopic properties of TAM^+ dyes, namely, acetone, acetonitrile, methanol, and 1-propanol from Fisher, ethanol from AAPER Alcohol and Chemical Co., 2-propanol from Aldrich, 1-butanol from Mallinckrodt, and t-butanol from Baker were of high purity grade and used as supplied. Biopolymers like HK (from yeast), DNA (from calf Thymus) and LDL (human) were purchased from Sigma and used as supplied. Similarly, β cyclodextrin (Sigma), Triton X 100 and Sodium dodecyl sulfate (Sigma), γ cyclodextrin (Aldrich) and deuterium oxide (Aldrich) were used as supplied. Sodium Phosphate (monobasic and dibasic salts) and Trizma-HCl salt was purchased from Sigma and used in the preparation of various buffers used in the experiments.

Reagents used in the HK activity assay namely, β-NADP (β-Nicotinamide Adenine Dinucleotide Phosphate), D- Glucose, Magnesium Chloride, ATP (Adenine Nucleotide Phosphate) and Glucose-6-Phosphate Dehydrogenase (G6PDH) were purchased from Sigma

and used as recommended. Pre-cast SDS-Polyacrylamide Gels from Novex (12% Tris-Glycine gel, 1.0mm x 12 wells) were used in all protein gel electrophoresis experiments. Tris Glycine Buffer (Bio-Rad), Glacial Acetic Acid (EM), Isopropyl Alcohol (Aldrich), Coomasie Blue R (Aldrich), Protein Markers (Benchmark Protein Ladder; Life Technologies) were the other reagents used in SDS gel electrophoresis. Seakem Le Agarose (FMC Bioproducts) was used to prepare gels in the DNA gel electrophoresis experiments. Trizma Base (Sigma), Acetic Acid (EM), Disodium EDTA Dihydrate (Sigma), Glycerol (EM), Bromophenol Blue (Aldrich, 16423E), DNA Marker (Lambda DNA / EcoRI + Hind III, Promega), Ethidium Bromide (Sigma), Sodium Sulfite (Fisher Scientific), were the other reagents used in agarose gel electrophoresis. Thiobarbituric acid (TBA) and trichloroacetic acid (TCA) from Sigma were used as reagents in the lipid peroxidation experiments. Nitrogen gas used in the nitrogen purging experiments was purchased from Praxair Gas Technology.

INSTRUMENTS AND METHODS:

BINDING STUDIES:

Binding studies using UV-VIS Spectroscopy:

Spectrophotometric titrations were performed at 25°C using a Shimadzu UV-2101PC spectrophotometer equipped with a temperature-controlled cuvette holder to characterize the binding of TAM^+s to various macromolecules. The concentration of macromolecule was varied, while the dye concentration was kept constant and the change in absorption spectrum was monitored as a function of titrant (macromolecule) concentration. In the case of LDL, DNA, and cyclodextrins, titrations were carried out in 10 mM sodium phosphate buffer, pH 7.3. In the case of HK, titrations were carried out in 50 mM Tris buffer, pH 7.6 at 25°C and also in water (pH adjusted to 7.6). With Triton X 100 and sodium dodecyl sulfate, titrations were carried out in water to eliminate influence of salt on the CMC and/or micelle size and aggregation number. Because of the tendency of TAM^+s to adhere to quartz cuvette walls, titrations were carried out in polystyrene cuvettes and the spectrum was taken from 400 to 800 nm. The recorded absorption spectra were analysed using the Igor Pro Graphing Program (Wavemetrics Inc.).

Binding studies using Fluorescence Spectroscopy:

Binding of TAM^+s to various macromolecules was also characterized using fluorescence spectroscopy under conditions of pH and temperature that were identical to those used in the UV-VIS spectrophotometric binding experiments. Fluorescence measurements were carried out on a Timemaster Strobemaster fluorometer equipped with a

temperature-controlled cuvette holder from Photon Technology International. Samples were excited at 540 nm and the emission spectrum collected from 560 to 800 nm. An emission and excitation bandwidth of 3 nm was maintained during the fluorescence measurements. The recorded fluorescent spectra were also analyzed using the Igor Pro Graphing Program, with the integral of the area under the fluorescence spectrum being used as a measure of fluorescence intensity.

In the case of LDL, binding was also characterized by monitoring the intrinsic fluorescence of apo B. The fluorescence spectra of tryptophan and tyrosine residues in apoB when free and complexed with crystal violet was recorded, after excitation at 280 nm, and integrated between 330 to 400 nm. Inner filter effects were negligible in these experiments because the dyes do not absorb at 280 nm or between 330 and 400 nm.

Binding studies using ultrafiltration:

Ultrafiltration studies were carried out on a IEC MicroMB Centrifuge at 14,000 rpm for a period of 8 minutes using a molecular cut off filter of 30,000 Daltons (Millipore). The molecular cut off filter excludes the LDL bound dye and the resultant dye concentration in the filtrate equals the free dye concentration in the presence of the macromolecule. Adsorption of dye to the ultrafiltration membrane was accounted for by running parallel controls.

Viscosity measurements:

In order to distinguish between intercalative and non intercalative binding of TAM^{+}s to DNA, viscosity of DNA samples with and without ligand was measured as a

function of their flow times through a Ubbelohde viscometer at 25°C. Similar such viscosity measurements were done on samples containing DNA and ethidium bromide, a dye that is known to intercalate between DNA base pairs. Small aliquots of CV^+ or Ethidium bromide (3000 μM) were added to 9 ml of 300 μM (100 μg/ml) DNA and the flow time readings were measured using a stopwatch (Fisher Scientific). Flow times were used to calculate η, the viscosity of DNA in the presence of ligand by using the equation $\eta = (t-to)/to$, where to is the flow time for the buffer without DNA. The helix lengthening ratio was calculated using the equation $L/Lo = (\eta/\eta o)^{1/3}$, where ηo is the viscosity of DNA in the absence of ligand, and is represented by $\eta o = (t-to)/to$ (Seifert J. L. et al, 1999).

STUDIES ON PHOTOREACTIVITY OF NONCOVALENT COMPLEXES OF TAM^+ AND BIOPOLYMERS:

Photolysis Experiments:

In the photolysis experiments samples were placed in a standard 10 mm (optical path) quartz cell at a distance of approximately 10 cm from the light source, and irradiated using the 532 nm line of a Nd:Yag laser model 7010 from Continuum operating at a repetition rate of 10 Hz. The defocused laser beam (circular profile with diameter of about 5 mm) was directed toward the centre of the quartz cell. The cell holder allowed continuous magnetic stirring of the samples during photolysis. The photolysed samples were maintained at room temperature using a laboratory-built forced-air cooling system. The absolute photolysis energy was kept constant over the course of any specific experiment, and measured with a calibrated solid-state joulemeter model PM30VI from Molectron.

Measurement of photoinduced inactivation of HK:

Relative values of HK activity were determined using the spectrophotometric method described by Easterby, J. S. and O' Brien, M. J. (Easterby, J. S. and O' Brien, M. J., 1973). It is based on the following biochemical reactions catalyzed by HK and G6PDH.

$$\text{D-glucose} + \text{ATP} \xrightarrow{\text{HK}} \text{D-glucose-6-phosphate} + \text{ADP}$$

$$\text{D-glucose-6-phosphate} + \beta\text{-NADP} \xrightarrow{\text{G6PDH}} \text{6-phosphogluconate} + \beta\text{-NADPH}$$

HK catalyses the phosphorylation of D-glucose to D-glucose-6-phosphate, which in turn is converted to 6-phosphogluconate by G6PDH in the presence of β-NADP. The reaction was followed by monitoring spectrophotometrically, the formation of β-NADPH at 340 nm as a function of time. The pH of the final reaction mixture consisting of 7.62 mM D-Glucose, 19.04 mM $MgCl_2$, 9.5mM ATP, 0.095 mM β-NADP, 50mM Tris Buffer and 5.0 units of G6PDH was adjusted to 7.6 and the temperature was maintained 30°C. The reaction was triggered with 0.013 μM HK.

Photoinduced damage of HK was additionally characterized using fluorescence spectroscopy and SDS polyacrylamide gel electrophoresis. Photolysed samples were excited at 280 nm to detect changes in the fluorescence attributed to the tryptophan and tyrosine residues of HK, and at 360 nm to detect changes that could result in the intrinsic fluorescence spectrum (380 to 600 nm) of HK, because of possible oxidation of amino acid residues. Photolysed samples were also subjected to extensive ultrafiltration and the resuspended

enzyme fractions were excited at the above-mentioned two wavelenghts (viz. 280 and 360 nm) to eliminate fluorescence from low molecular weight photoproducts. An emission and excitation bandwidth of 3 nm was maintained during the fluorescence measurements. Photoinactivation and photoinduced damage of HK was also monitored in buffered D_2O. Because the use of glass electrodes for the measurement of acidity of D_2O solutions leads to pH meter readings that are 0.4 pH units lower than those obtained in comparable H_2O solutions, the acidity of the D_2O solutions employed in this study were determined using the equation pD = pH (meter reading) + 0.4 (Glasoe P.K. et al, 1960). Comparative studies of photoinduced inactivation of HK were also carried out between air-equilibrated and nitrogen-purged samples.

SDS polyacrylamide gel electrophoresis was used to detect protein fragmentation. Novex Pre-Cast gels (12% Tris-Glycine Buffer, 1.0mm x 12 well) were mounted on a vertical gel electrophoresis unit (Aladin Enterprises Inc.). The electrophoresis was run for 90 minutes at 120 V. The Tris Glycine Buffer (0.1%SDS, 25 mM Tris, 192 mM Glycine, pH = 8.3) served as the running buffer. The samples to be loaded had a 2.6:1 composition of loading buffer (12.5% of 0.5 M Tris HCl, 10% Glycerol, 20% of 10% SDS, 5% of β-mercaptoethanol, 5% of 0.05% bromophenol blue) and HK respectively. A sample volume of 10µl equivalent to 500 ng of HK was placed in each well, and the protein ladder marker volume was 5 µl. Gels were stained with a solution made up of 15% Acetic acid, 25% Isopropyl alcohol and 0.15% Coomasie Blue R, and after extensive destaining with water were viewed over a transilluminator (Desktop Lightbox - Logan). Photographs of gels were

taken using the Polaroid Camera (DS 34) loaded with Polaroid Film 667 (Fisher Scientific) and equipped with an orange filter (Filter #15, ISS-Enprotech).

Measurement of photoinduced damage in DNA:

Photoinduced DNA damage was assessed by agarose gel electrophoresis using the Easy-Cast™ Electrophoresis System (Model #B1, ISS-Enoprotech). Agarose gels containing 1% agarose and 0.0001% ethidium bromide with either 10 or 15 wells were prepared. The fluorescence of the DNA intercalating dye, ethidium bromide was observed using a UV Transilluminator (ISS-Enprotech). The running buffer (24.2% trizma base, 5.71% glacial Acetic acid, 0.05 M disodium EDTA dihydrate, pH 8.0) was diluted 50 times before use. The samples to be loaded had a 1:4 composition of loading buffer (50% Glycerol, 10 mM Trisma Base, 50 mM Disodium EDTA dihydrate, a pinch of bromophenol blue, pH 8.0) and DNA respectively. A sample volume of 25 µl (equivalent to 400 ngs of DNA) was placed in each well, and the DNA marker volume was 5 µl. The electrophoresis was run at 120 V for 60 minutes, and photographs of the gels after the run were taken using the Polaroid Camera (DS 34) equipped with an orange filter (Filter #15, ISS-Enprotech). The camera was loaded with Polaroid Film 665 (Fisher Scientific) that provides both a print and a high resolution negative. The negative was developed in 18% aqueous sodium sulfite solution, washed with water and dried in air. The density of the photographed DNA bands was quantified using a digital densitometer (Model 300A) from Molecular Dynamics.

Photoinduced damage of DNA was also monitored in buffered D_2O and comparative studies on photoinduced damage of DNA were also carried out between air-equilibrated and nitrogen-purged samples.

Lipid Peroxidation:

Lipid peroxidation of LDL, both in the presence and absence of photosensitizer was assayed using the thiobarbituric acid (TBA) method (Wilbur K. M. et al, 1949). 400 µl of 50% TCA (Trichloroacteic acid) and 800 µl of 2% TBA was added to 2800 µl (0.07 µM LDL) of the irradiated sample, and the resultant mixture was left in a hot water bath at 75°C for 30 minutes. After cooling, the precipitate was removed by centrifugation at 14,000 rpm and amount of malondialdehyde (MDA) formed was quantified by measuring the absorbance of the supernatant at 532 nm. An extinction coefficient of 156,000 M^{-1} was used for MDA (Hunter, F. E. et al 1963) .

Photolysed LDL samples were excited at 360 nm to detect any formation of products that result from the conjugation of aldehydic lipid peroxidation products with protein amino acid groups, and also excited at 280 nm to detect changes in the intrinsic apoB fluorescence.

OTHER STUDIES:

Solvent Effects on Spectroscopic Properties of TAM^+s:

The spectrophotometric studies were performed with a Shimadzu UV-2101PC spectrophotometer using cuvettes with either a 10 mm or 100 mm optical path length. The

effects on Kamlet-Taft's solvent solvatochromic parameters π^*, α and β (Kamlet, M. J., 1983) on the electronic spectra of TAM^+ dyes were analyzed in terms of the magnitude of the solvent-dependent splitting between two overlapped TAM^+ visible absorption bands observed in different media. The magnitude of splitting between overlapped electronic transitions was evaluated through the measurement of the difference in frequency ($\Delta\nu$) between the maximum and shoulder of the respective absorption band (or between two maxima of spectra showing better resolution). Accurate frequency values were taken from the first derivative of the electronic spectra, although the parameter ($\Delta\nu$) represents a phenomenological (approximated) spectroscopic parameter rather than a precise difference in energy between two distinct vertical electronic transitions. Unless otherwise stated the measurements were carried out at 25°C.

Mathematical models:

Various mathematical models that describe binding of ligands to macromolecules were built, beginning from a simple one site model and increasing the complexities from there on stepwise. In order to expedite the computational and graphing procedures, several software routines (macros) were written for Igor Pro. A macro allows assignment of numerical values to different model parameters or variables, and solves the function that these variables define. Each of the models involved different functions, and therefore needed different macros for their execution. Detailed information on these macros is provided in Appendices I to III.

Miscellaneous Measurements and Equipment:

The concentration of TAM^+s was determined using measured extinction coefficients provided in Table 4.1. The amount of LDL in lyophilised LDL samples supplied by Sigma is described in terms of protein weight. LDL concentrations were therefore determined using the molecular weight of LDL (3.5 million Daltons) and taking into consideration that protein comprises 20% of the total LDL mass (Rosenberger V. and Margalit R., 1993). HK concentrations were determined using a molecular weight of 99,000 (Wilson, 1995). DNA concentrations were determined spectrophotometrically by taking into consideration that an optical density of 1 at 260 nm corresponds to a concentration of 50 μg/ml DNA (Sambrook, J., 1989). Alternatively, when required an extinction coefficient of 6600 M^{-1} cm^{-1} per nucleotide, at 260 nm was used (Minchin R. F., 1987). Concentrations of cyclodextrins were determined by molecular weight (Beta Cyclodextrin-1,135g; Gamma Cyclodextrin-1,297g), and concentration of Triton X 100 using an approximated molecular weight of 625g and a specific gravity of 1.07g/ml (Supplier data). The pH of various buffers was measured using the Orion Benchtop pH meter (Orion, Model 520A). Temperatures of solutions were measured using a digital thermometer (Fisher Scientific, capable of measuring temperatures from –50°C to 750°C).

Other equipment used on a routine basis included a Sartorius Balance (Model # U611293), a sonicator (Fisher Scientific) operating at 22 Watts, a benchtop centrifuge (International Equipment Company), a Maxi Mix II mixer (Bransted/Thermolyne) for vortex mixing, water baths (Fisher Scientific), microwave (Sharp Carousel) and a stopwatch (Fisher Scientific).

Chapter 4. Solvent Effects on the Spectroscopic Properties of Triarylmethanes

RESULTS AND DISCUSSION:

A systematic study on the effects of solvents on the spectroscopic properties of TAM^+ dyes was carried out in order to characterize change in spectral signatures as a result of change in solvent character. Since the project involved characterizing the binding of TAM^+s to various biological macromolecules using spectrophotometric techniques, a study on the effects of solvents on the spectroscopic properties of TAM^+s was imperative. The data obtained in this study would not only help the interpretation of the binding data obtained with the various biological macromolecules, but would also shed some light on the relationship between the molecular structure of TAM^+s and the characteristics of their electronic spectra. Moreover the study would help distinguish spectral signatures obtained due to a change in dye environment from those observed as a result of self-association (aggregation).

The spectral profile of TAM^+ dyes in different media is presented in Figure 4.1. The overall observation was that for the symmetric dyes, CV^+ and EV^+, the solvent effect on the structure of the maximum absorption band was modest, while more pronounced effects were observed in the case of $VPBBO^+$ and VBR^+. To facilitate visual inspection, the spectra shown in Figure 4.1 represent solutions containing a different dye concentration for each specific solvent (1 μM to 5 μM range). Values of extinction coefficient at λ_{max} are given in Table 4.1. For $VPBBO^+$ and VBR^+, the splitting of a single well defined absorption

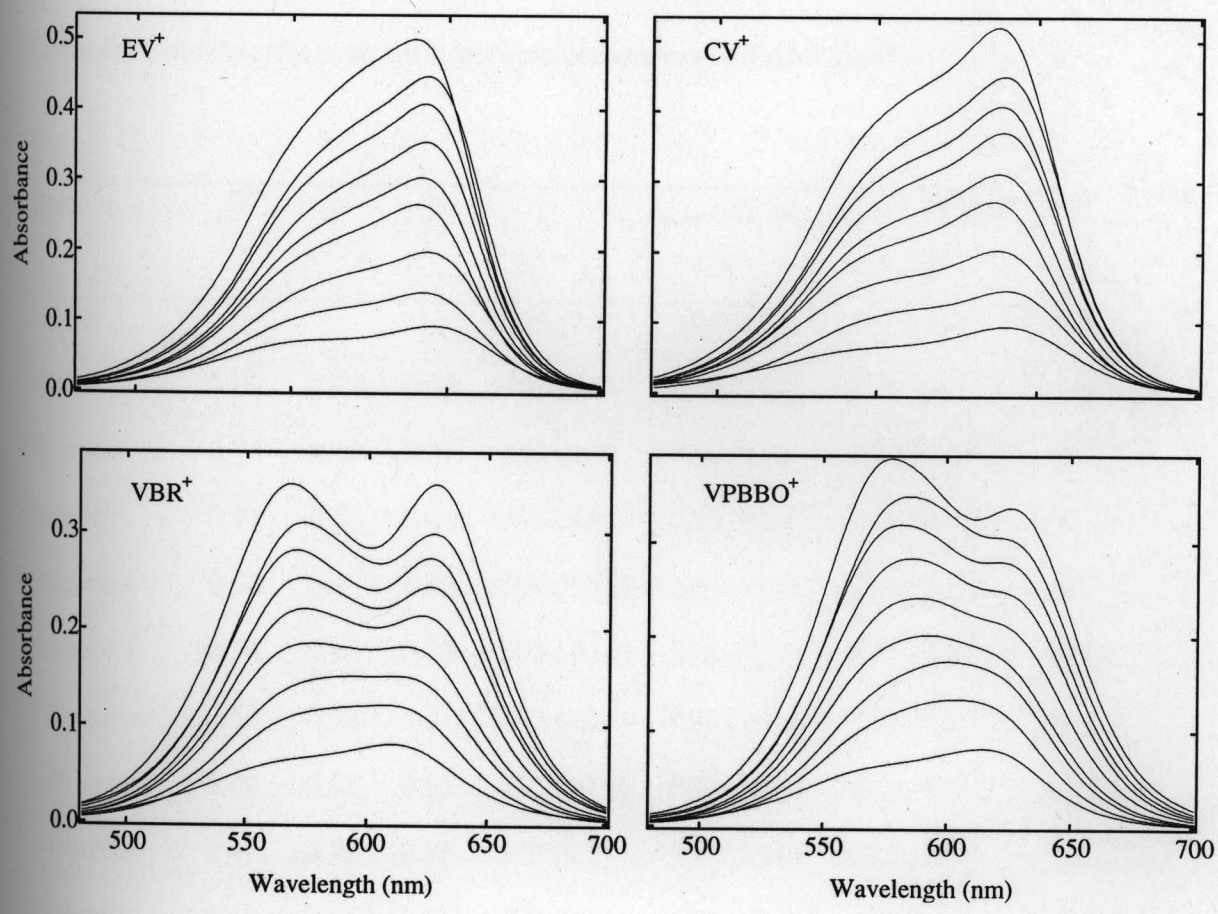

Figure 4.1 Absorption spectra of EV^+, CV^+, VBR^+, and $VPBBO^+$ in different solvents. From the bottom of each panel the solvents and dye concentrations (in micromolar units) were water (1.0), acetonitrile (1.5), acetone (2.0), methanol (2.5), ethanol (3.0), 1-propanol (3.5), 2-propanol (4.0), 1-butanol (4.5), and t-butanol (5.0).

Table 4.1 Solvent effects on spectroscopic parameters of TAM^+dyes‡.

Solvent	Π^*	α	β	λ_{max}, nm (ε_{max} x 10^{-4}, $M^{-1}cm^{-1}$)			
				EV^+	CV^+	VBR^+	$VPBBO^+$
Buffer	-	-	-	595 (9.1)	590 (9.0)	612 (7.4)	615 (8.8)
Water	1.09	1.17	0.18	595 (9.2)	590 (9.5)	611 (8.1)	614 (8.3)
Acetonitrile	0.75	0.19	0.31	592 (9.4)	588 (9.8)	607 (8.1)	604 (9.0)
Acetone	0.71	0.08	0.48	593 (9.9)	590 (10.2)	611 (7.6)	601 (8.7)
Methanol	0.60	0.93	0.62	590 (10.6)	586 (10.9)	578 (7.4)	592 (8.8)
Ethanol	0.54	0.83	0.77	591 (10.1)	589 (10.4)	574 (7.4)	589 (8.1)
1-Propanol	0.52	0.78	-	592 (10.1)	589 (10.6)	573 (7.2)	586 (8.1)
2-Propanol	0.48	0.76	0.95	592 (10.2)	588 (10.2)	570 (7.0)	582 (8.0)
1-Butanol	0.47	0.79	0.88	593 (9.9)	589 (10.0)	573 (7.1)	585 (7.9)
t-Butanol	0.41	0.68	1.01	590 (9.8)	588 (10.4)	568 (6.9)	578 (7.5)

‡Solvatochromic parameters (Π^*, α and β values) from (Kamlet M. J., 1993).

maximum into two well defined maxima was observed upon going from aqueous to organic media, as can be clearly seen through the comparison of the electronic spectra of these dyes in water and in t-butanol (Figure 4.1). The extinction coefficients of the dyes do not change substantially as the medium changes from water to t-butanol (Table 4.1). The wavelength of maximum absorption of the dyes in solvents with low polarity shifts to the blue compared to that observed in water. Note however that for VBR^+ and $VPBBO^+$, the λ_{max} shifts to the red by 1 nm in phosphate buffer (10 mM) compared to water (Table 4.1). A possible explanation for this small red shift in phosphate buffer would involve the formation of small quantities of ion pairs in solution, namely the phosphate ion with the cationic TAM^+ dyes. This is probably because the negative phosphate ion in the buffer and the dye molecule exist as an ion pair. This is in keeping with the observation that the λ_{max} shifts to the red region of the spectrum for TAM^+s in the presence of solvents with low dielectric constant, like toluene, chloroform and chlorobenzene where the dye exists as an ion pair, (Oliveira C. S. et al - unpublished data), e.g. the λ_{max} of CV^+ in chlorobenzene (dielectric constant = 5.69), shifts 10 nm to the red compared to water. Solvents with low dielectric constant have a poor solvation capacity, and therefore the dye and its counter ion exist as an ion-pair in such solvents. Most of the solvents in this study have high dielectric constants (18 to 78.5), and because of the high solvation capacity of these solvents the dye molecules do not exist as ion-pairs in these solvents.

The absorption spectra of diluted solutions of the symmetrical tri-para-amino-substituted dyes CV^+ and EV^+ display a characteristic shoulder on the short-wavelength side of the visible absorption band. The difference in frequency between the maximum

absorption and the shoulder's inflection point ($\Delta\nu$, values in wavenumber taken from the first derivative of the electronic spectrum) tended to increase upon increasing solvent dipolarity / polarizability (Π^* scale) and hydrogen-bond donor acidity (α scale), but with decreasing solvent hydrogen-bond acceptor basicity (β scale). Better linear relationships between $\Delta\nu$ and the Kamlet-Taft solvatochromic parameters Π^*, α and β (Kamlet M. J., 1983) were obtained when taking into consideration only solvents of the same family, e.g. the C_1 to C_4 alcohol series (Figure 4.2). Water typically gave anomalous results with regard to the dominant linear trends observed for $\Delta\nu$ as a function of the solvents' solvatochromic properties, while the non-hydroxylated solvents, acetone and acetonitrile, afforded a pronounced deviation when the dependence of $\Delta\nu$ on the hydrogen-bond donor acidity character (α scale) was taken into consideration. The behavior of acetone and acetonitrile is not surprising, since these two solvents cannot act as proton donors in solvent-to-solute hydrogen-bond interactions. The dominant trends observed for the solvent effect on the absorption spectra of $VPBBO^+$ and VBR^+ (Figure 4.3) exhibited opposite character as compared to those noticed in the cases of CV^+ and EV^+ (Figure 4.2). For the Victoria Blue dyes, the dominant trend was clearly characterized by a decrease in $\Delta\nu$ upon increasing Π^* and α and decreasing β (Figure 4.3).

All triarylmethanes considered in this investigation are known to form dye aggregates in aqueous media upon increasing dye concentration (Bartlett, J. A. and Indig, G. L., 1999). The formation of these aggregates is attested by the appearance of a hypsochromically shifted absorption band that overlaps with the spectral shoulder of the respective dye monomer observed in diluted solutions (Lueck H. B. et al, 1992). For

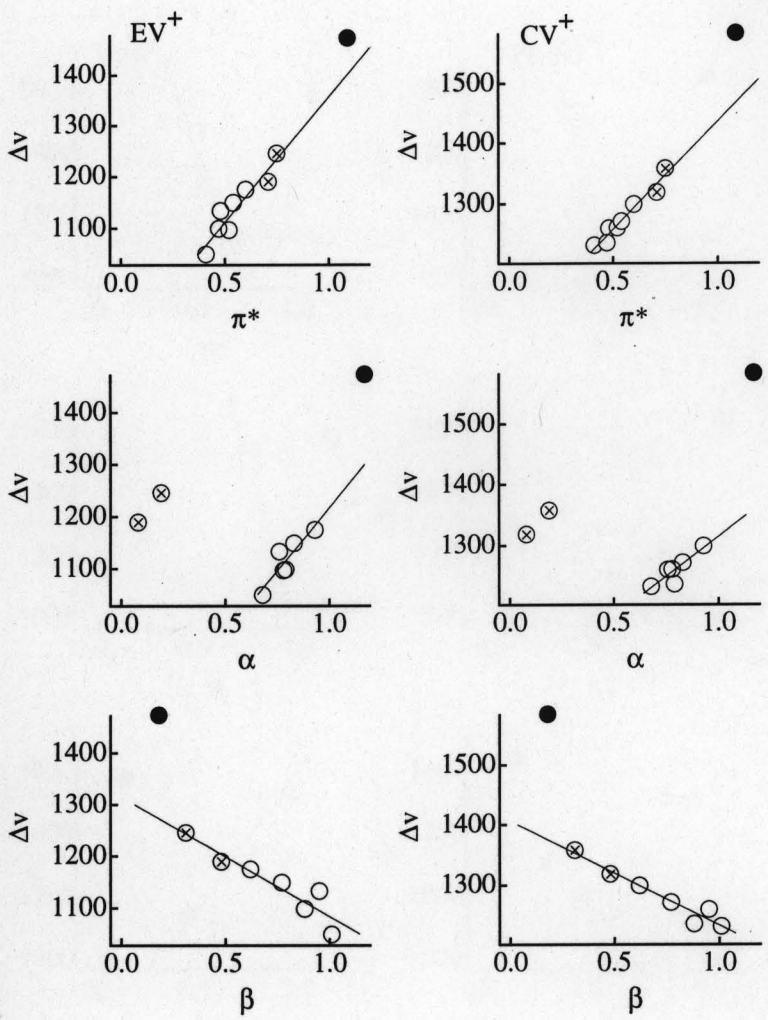

Figure 4.2. Solvatochromic effects on the magnitude of splitting ($\Delta\nu$) between the overlapping absorption bands of EV^+ (left column) and CV^+ (right column) in polar solvents. Empty circles, C_1 to C_4 alcohol series; full circle, water; crossed circle, acetone and acetonitrile.

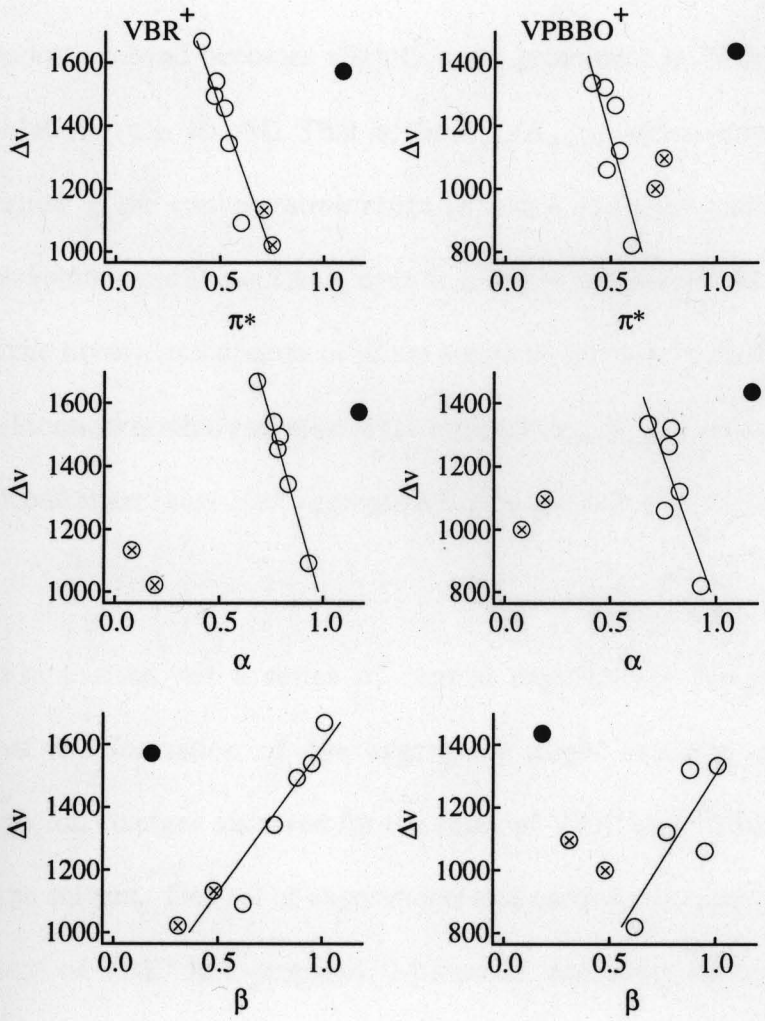

Figure 4.3. Solvatochromic effects on the magnitude of splitting ($\Delta\nu$) between the overlapping absorption bands of VBR^+ (left column) and $VPBBO^+$ (right column) in polar solvents. Empty circles, C_1 to C_4 alcohol series; full circle, water; crossed circle, acetone and acetonitrile. The poor resolution of the absorption spectra of $VPBBO^+$ in acetone and acetonitrile did not permit the accurate characterization of $\Delta\nu$ for this dye in these solvents.

example, the formation of EV^+ and $VPBBO^+$ aggregates in water can be easily characterized in 30 μM solutions, since the shoulder at the short-wavelength side of the maximum absorption band becomes slightly more prominent in 30 μM solutions than in more dilute solutions (e.g. 10 μM). That is, the $A_{max}/A_{shoulder}$ ratio decreases upon increasing dye concentration in the concentration range in which dye aggregation takes place. For dilute aqueous solutions of these TAM^+ dyes (*c.a.* 5 μM and lower) the $A_{max}/A_{shoulder}$ ratio is constant, and the normalized spectra of dilute solutions containing different concentrations are identical. Identical normalized spectra (or constant $A_{max}/A_{shoulder}$ ratio) indicate that below the 5 μM concentration range dye aggregation does not occur to any detectable extent in pure water.

We have carried out a series of control experiments designed to explore the possibility that the formation of dye aggregates might explain, at least in part, the pronounced spectral changes observed for the cases of VBR^+ and $VPBBO^+$ as a function of the nature of the solvent. One set of experiments was carried out using 10 μM, 1.0 μM, and 0.1 μM solutions of VBR^+ in 1-propanol, 2-propanol, and 1-butanol and of $VPBBO^+$ in 1-propanol and 1-butanol. The normalized spectra of the different VBR^+ and $VPBBO^+$ solutions in the individual solvents showed exactly the same spectral profile. Figure 4.4 shows the normalized spectra of VBR^+ and $VPBBO^+$ in 2-propanol and 1-propanol respectively. These results indicate that dye aggregation does not contribute to a measurable extent to the spectral changes observed in VBR^+ and $VPBBO^+$ solutions upon changing from aqueous to organic media. Additional evidence that supports the hypothesis that dye aggregation does not account for the solvent effects observed with VBR^+ and $VPBBO^+$ was

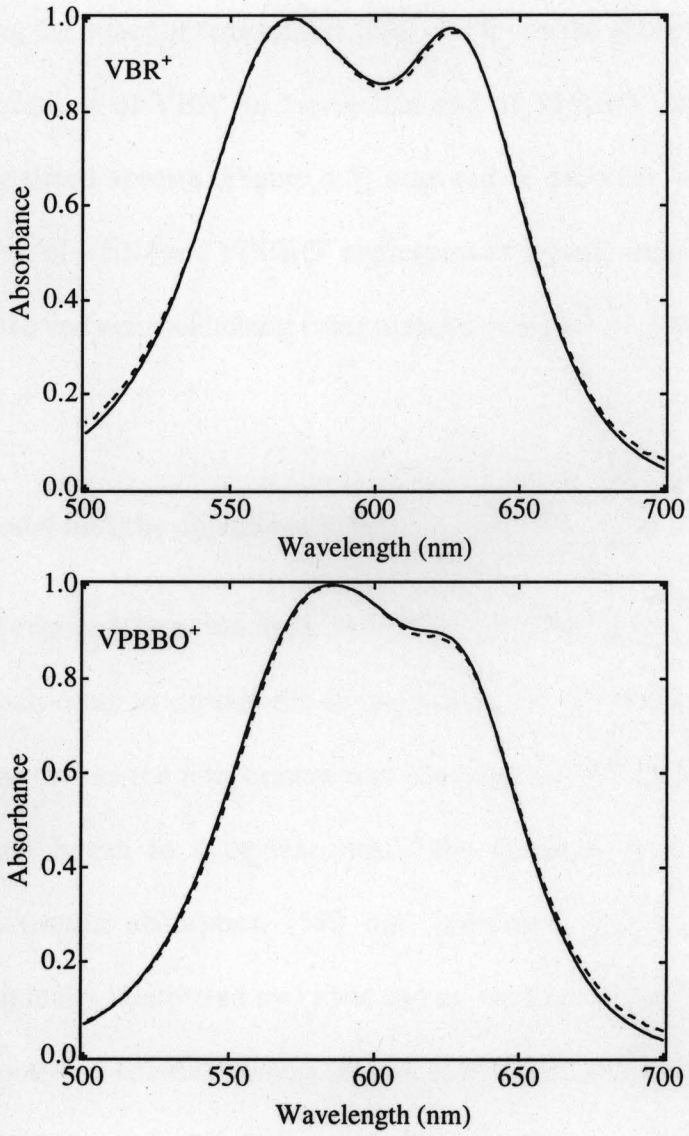

Figure 4.4 Normalized absorption spectra of VBR^+ and $VPBBO^+$ in 2-propanol and 1-propanol respectively. In both panels the dashed line represents a concentration of 0.1μM dye and the solid line represents a concentration of 10μM dye.

obtained by studying the effect of temperature (5°C - 50°C) on the absorption spectra of 10 μM and 1.0 μM solutions of VBR^+ in 2-propanol and of $VPBBO^+$ in 1-propanol and 1-butanol. The normalized spectra (Figure 4.5) acquired at different temperatures did not support the formation of VBR^+ and $VPBBO^+$ aggregates in organic media as the cause of the spectral changes observed upon switching from aqueous to organic media.

The Rotamer's Model and the objections to it:

Lewis et al proposed the existence of two CV^+ ground state rotational isomers in rapid equilibrium with each other to explain the absorption spectrum of this dye in ethanol. The key observation was that as the temperature was lowered, the 550 nm shoulder in the CV^+ absorption spectrum began to disappear, while the intensity of the transition at the wavelength of maximum absorption (589 nm) increased. The observed temperature dependence was originally interpreted by Lewis and co-workers as the result of a shift in the equilibrium between two rotational isomers present in solution, in favor of the lower-energy species as the temperature was lowered (Lewis G. N. et al, 1939; Lewis G. N. et al, 1942).

Due to steric restrictions, the aromatic rings of CV^+ and other cationic TAM^+ dyes are forced out of the molecular plane that contains the central carbon atom. The out-of-plane angle is modulated by both the repulsion between ortho-hydrogen atoms in adjacent aromatic rings and the restoration force that opposes rotation due to the double bond character of the twisted chemical bond. In the case of symmetrical molecules, such as the tri-para-amino-substituted CV^+, the repulsive and restorative forces acting on each distinct ring are expected

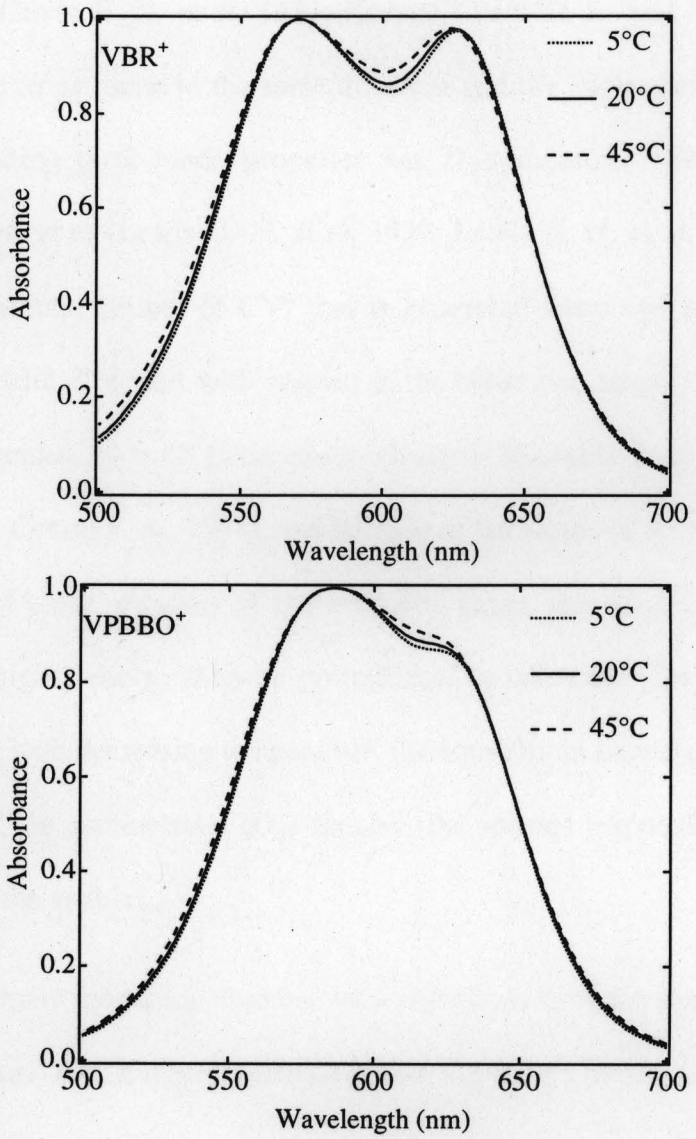

Figure 4.5 Normalized absorption spectra of VBR^+ and $VPBBO^+$ in 2-propanol and 1-propanol respectively, at different experimental temperatures. [Dye] = 10μM.

to be equivalent (Lewis G. N. et al, 1939; Korppi-Tommola J. and Yip R. W. 1981). When the aromatic rings rotate in the same direction and the angles between them are held constant, the resulting three-blade propeller has D_3 symmetry. The model originally developed by Lewis et al (Lewis G. N. et al, 1939; Lewis G. N. et al, 1942) proposes the existence of a rotational isomer of CV^+ that is generated when one of its aromatic rings rotates in the opposite direction with respect to the other two rings. This unsymmetrical propeller is represented by a C_2 point group (Korppi-Tommola J. and Yip R. W. 1981; Lueck, H. B. 1992; Cotton F. A., 1971), and because of the nature of the restorative force that opposes the out-of-plane rotation of the aromatic rings, the unsymmetrical rotamer is expected to have higher energy than its symmetrical counterpart. Therefore, the rotamers model predicts that with decreasing temperature, the equilibrium between the two rotamers is shifted in favor of the symmetrical (D_3) species (the species responsible for the stronger absorption band in the visible).

Lewis' rotamers model has faced several objections over the years. As observed by Korppi-Tommola and Yip (Korppi-Tommola J. and Yip R. W., 1981), no significant change in the absorption spectra of CV^+ in toluene takes place over the temperature range of + 46 °C to - 50°C, while in methanol the shoulder in the 550 nm region decreases with decreasing temperature, and practically disappears at -70°C. These authors suggest that their observations contradict the basis for the rotamers model, since there would be no reason why the equilibrium between the two rotamers would be significantly less temperature dependent in toluene than in methanol. They explain the effect observed in methanol in terms of changes in solvation of CV^+ with temperature. Therefore, the model of Korppi-Tommola

and Yip explains the spectroscopic behavior of CV^+ in solution in terms of solvation rather than the hypothetical existence of two rotational isomers in solution.

Lueck et al also presented results that do not support the rotamers model (Lueck H. B. et al, 1992). Based on semi-empirical molecular orbital calculations carried out using the intermediate neglect of differential overlap (INDO) method, these authors pointed out that the barrier separating the two rotamers is large compared to kT at room temperature. This suggests that it is unlikely that the shoulder observed in the absorption spectra of CV^+ in ethanol can be explained in terms of the presence of the unsymmetrical propeller in solution. Based on a combination of experimental measurements and theoretical calculations, the authors suggested that a solvent-induced symmetry-breaking process may be the cause of the appearance of the overlapped bands in the absorption spectra of CV^+. The proposed model explores the possibility that the loss in degeneracy of the symmetrical D_3 propeller can be produced by the electronic perturbation introduced by a solvent molecule located near one of the amino groups, or by the stabilization of the positive charge in one of the amino groups via a specific interaction with a solvent molecule. In this last case, in terms of resonance structures the amino group which accommodates the positive charge would be forced to assume a planar geometry while the other two amino groups would retain the tetrahedral configuration, and this solvent-induced difference in amino group configuration is a symmetry-breaking event.

The experimental results obtained in this laboratory add momentum to previous objections to the rotamers model, since they indicate that the magnitude of the splitting between the overlapped absorption bands of the highly symmetrical TAM^+ dyes CV^+ and

EV^+ is dependent upon solvent solvatochromic parameters. However, since multiple interacting solvent effects may be taking place simultaneously, only qualitative comments can be drawn based on the data shown in Figure 4.2. Accordingly, since the Π^* scale represents an index of the ability of the solvent to stabilize a dipole or charge due to its dielectric effect (Kamlet M. J., 1983), the observed increase in $\Delta\nu$ upon increasing Π^* is consistent with the hypothesis that an electronic rather than a mechanical perturbation is responsible for the loss in degeneracy of the symmetric D_3 propeller (Lueck H. B. et al, 1992). Besides, the results of semi-empirical molecular orbital calculations carried out by Lueck et al have indicated that the stronger the dipole located near one of the amino groups of the D_3 propeller the larger the expected splitting between its overlapping bands (Lueck H. B. et al, 1992). This theoretical prediction is in agreement with our experimental data. The linear relationships observed between $\Delta\nu$ and the solvatochromic parameters α and β further emphasizes the solvation dependence of the spectroscopic behavior of CV^+ and EV^+ in condensed phase. Although it is not clear why the data obtained in water typically display anomalous characteristics, the deviations observed in acetone and acetonitrile arise from the fact that these two solvents do not function as proton donors in solvent-solute interactions. More recently Ishikawa et al (Ishikawa M. et al, 1999) have reported a model to explain the absorption spectra of CV^+ in methanol and other alcohols in which they hypothesize the existence of two solvation isomers in fast equilibrium with one another. In this model the symmetric (D_3) propeller is thought to be in equilibrium with a pyramidal (C_3) isomer formed when the central carbon atom is strongly solvated with an alcohol molecule.

The spectroscopic behavior of VBR^+ and $VPBBO^+$ in solution

The lower energy levels of the TAM^+ dyes displaying lower molecular symmetry, VBR^+ and $VPBBO^+$, are not degenerate. Consequently, these dyes are expected to display relatively well resolved $S_0 \rightarrow S_1$ and $S_0 \rightarrow S_2$ absorption bands in solution. Indeed, the presence of two well defined absorption bands was readily noticed in the electronic spectra of VBR^+ and $VPBBO^+$ in the C_1 to C_4 alcohol series, although the resolution of these bands was diminished in the other solvents considered in this study (Figure 4.1). The experiments carried out to explore the effects of dye concentration and temperature on the electronic spectra of VBR^+ and $VPBBO^+$ performed in a variety of solvents have clearly indicated that, within the concentration range investigated, the spectroscopic doublet observed in the electronic spectra of the Victoria Blue dyes cannot be attributed to the formation of dye aggregates in solution. Since the occurrence of aggregation can be easily characterized in water but not in the alcohols investigated herein, the hydrophobic effect can be hypothesized to play an important role in the aggregation phenomena. However, we have also observed that the spectral profiles of VBR^+ and $VPBBO^+$ are concentration dependent in chloroform (1 μM to 10 μM range), which is evidence either for the formation of dye aggregates or ion pairs (Figure 4.6). As previously reported (Lueck H. B. et al 1992), while the aggregation of tri-para-amino substituted dyes is readily observed in aqueous media, the bi-para-amino substituted TAM^+ dye Malachite Green (*N,N,N',N'*-tetramethylpararosaniline) does not undergo aggregation to a significant extent in water. These observations suggest that the hydrophobic effect is not the only thermodynamic parameter controlling the aggregation

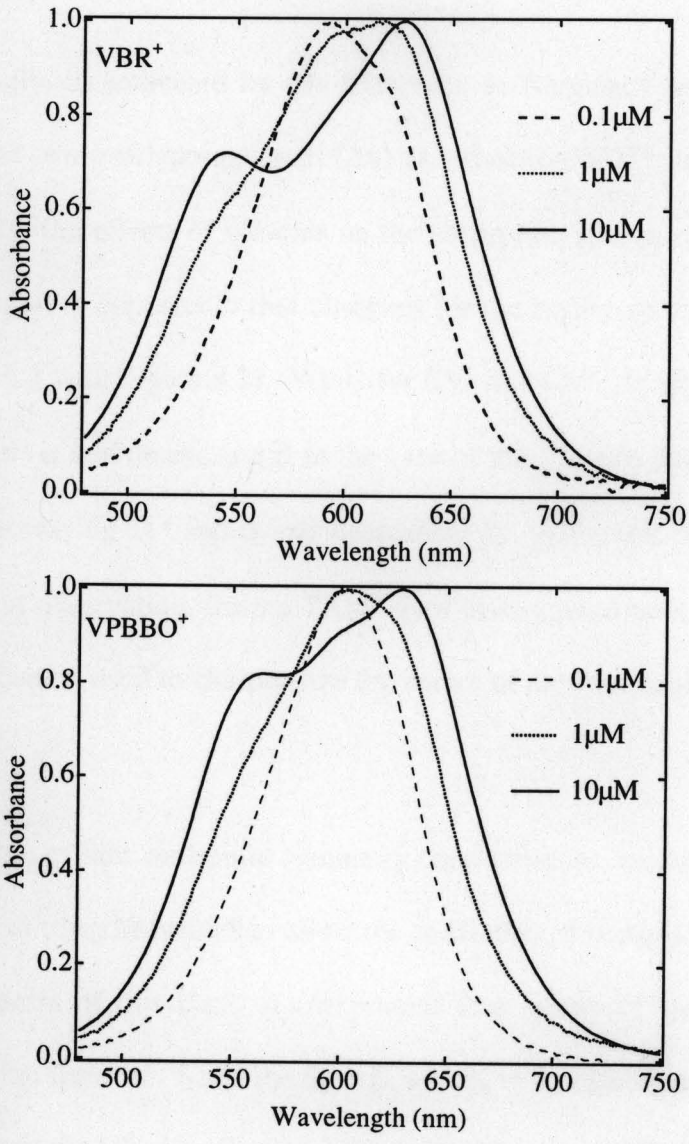

Figure 4.6 Normalized absorption spectra of VBR^+ and $VPBBO^+$ in chloroform. T = 25°C.

phenomena, and that the contribution of structure to TAM^+ aggregation is not completely understood (Bartlett J. A. and Indig G. L. 1999, Lueck H. B. et al 1992).

Interestingly, as indicated by the difference in frequency between the maximum absorption and the two overlapping bands ($\Delta\nu$) as a function of Π^*, α, and β, the dominant trends observed for the effects of solvents on the absorption spectra of $VPBBO^+$ and VBR^+ exhibit behavior that is opposite to that observed for the highly symmetrical CV^+ and EV^+ (compare Figure 4.3 with Figure 4.2). While for EV^+ and CV^+, $\Delta\nu$ typically increased with increasing Π^* and α and decreasing β in the case of the Victoria Blue dyes, $\Delta\nu$ tended to decrease upon increasing Π^* and α and decreasing β. Although this behavior may not represent a general observation, for the TAM^+ dyes investigated here, the effect of solvent properties on $\Delta\nu$ can be used to characterize the nature of the overlapping visible absorption bands.

The question of how molecular symmetry considerations can be combined with other structural aspects of triarylmethanes to allow the prediction of some of the characteristics of the electronic spectra of this class of compounds is a matter of substantial interest. A pertinent observation follows. While the $S_0 \rightarrow S_1$ and $S_0 \rightarrow S_2$ transitions in t-butanol are well separated in the case of Malachite Green (maxima at 622 nm and 429 nm, respectively), they appear as overlapping bands in VBR^+ and $VPBBO^+$. Apparently, for these three compounds the availability (or lack thereof) of the third amino group in the para position of the aromatic rings is an important factor with regard to the control of the energy gap between the first two excited singlet states in these dyes.

CONCLUSIONS:

The observed solvent-dependence on the magnitude of the splitting between the overlapping absorption bands indicates that the occurrence of specific interactions involving the TAM^+ dyes and the solvent molecules is the event that lowers the symmetry of the D_3 propeller, giving rise to two nondegenerate states or two solvation isomers. The observed solvent effects on the absorption spectra of the TAM^+ dyes displaying lower symmetry, VBR^+ and $VPBBO^+$, are distinct from those observed for CV^+ and EV^+, because the nature of the overlapped absorption bands is different in these two distinct sets of TAM^+ dyes. The difference in energy between the $S_0 \rightarrow S_1$ and $S_0 \rightarrow S_2$ electronic transitions in the nonsymmetrical TAM^+ molecules is apparently strongly dependent upon the number of amino groups in the para position of the aromatic rings, since the lack of one amino group in Malachite Green leads to a much large splitting between these transitions than those observed in the case of VBR^+ and $VPBBO^+$.

The solvents explored in this study cause a blue shift in the λ_{max} relative to water, even though the extinction coefficient of the dyes in these solvents is close to that in water. This indicates that if the dyes were experiencing an environment that is less polar than the bulk aqueous phase, the observed spectral signature would be a blue shift, with very little change in dye extinction coefficient. However, if the dye were to exist as an ion pair, the spectral signature would be a red shift in the λ_{max} as observed in the presence of solvents with low dielectric constant (Oliveria C. S. et al – unpublished data). In the binding experiments with different model biological hosts (Chapters 6, 7 and 8) blue shifts and hypochromic effects were observed at high dye to macromolecule concentration ratios, while at low dye to

macromolecule concentration ratios a red shift in λ_{max} was obtained. The blue shifts at high dye to macromolecule concentration ratios cannot be attributed to simple changes in polarity of the surrounding environment, because there is a concomitant decrease in the extinction coefficient. As will be demonstrated in the subsequent chapters under conditions of high biopolymer loading, the observed blue shift in the absorption spectra of TAM^+ dyes is more appropriately explained in terms of dye aggregation. The red shift in λ_{max} at low dye to bioploymer ratio probably indicates that the dye molecules exist as an ion pair at these concentration regimes, or in other words, that the binding of TAM^+ dyes to biopolymer polyelectrolytes results from a substantial contribution of electrostatic interactions between these dyes and negatively charged macromolecular residues. This red shift was also observed upon partitioning of TAM^+ dyes in micelles and LDL, suggesting that ion-pairing is an important factor for the solubilization of TAM^+ dyes in highly non-polar environments.

Chapter 5. Binding of Triarylmethane Dyes to Cyclodextrins and Detergents

RESULTS AND DISCUSSION:

To corroborate the binding data obtained with the various model biological hosts (HK, DNA and LDL), binding of TAM^+s to certain simple non-biological macromolecules and supramolecular structures was also undertaken. These non biological molecules included anionic (sodium dodecyl sulfate) and non-ionic (Triton X 100) detergents and the two cyclodextrins (β and γ cyclodextrins).

Titrations with anionic detergent, Sodium Dodecyl Sulfate (SDS):

Spectrophotometric titrations were carried out in which the concentration of dye was kept constant and the surfactant (SDS) concentration was increased in small increments. The surfactant concentration regimes explored included both pre-micellar and micellar concentrations. Figure 5.1 shows the effect of the surfactant on the uv-vis spectra of the four TAM^+s (CV^+, EV^+, VBR^+ and $VPBBO^+$). In the presence of SDS at concentrations below the CMC (CMC of SDS in water = 8mM) (Sarkar M. and Poddar S., 2000), a distinct change in spectroscopic signature was observed. With increasing detergent concentration (concentrations much lower than the aqueous CMC), there was a decrease in absorbance and a marked blue shift in the spectrum of each of the four TAM^+s (solid curves in Figure 5.1). According to the molecular exciton theory these pronounced blue shifts and hypochromic effects are attributed to the formation of H-type aggregates. With further increase in detergent concentration (concentrations still below the aqueous CMC), there is a region where the absorbance and the spectroscopic signature remain constant. Beyond this region,

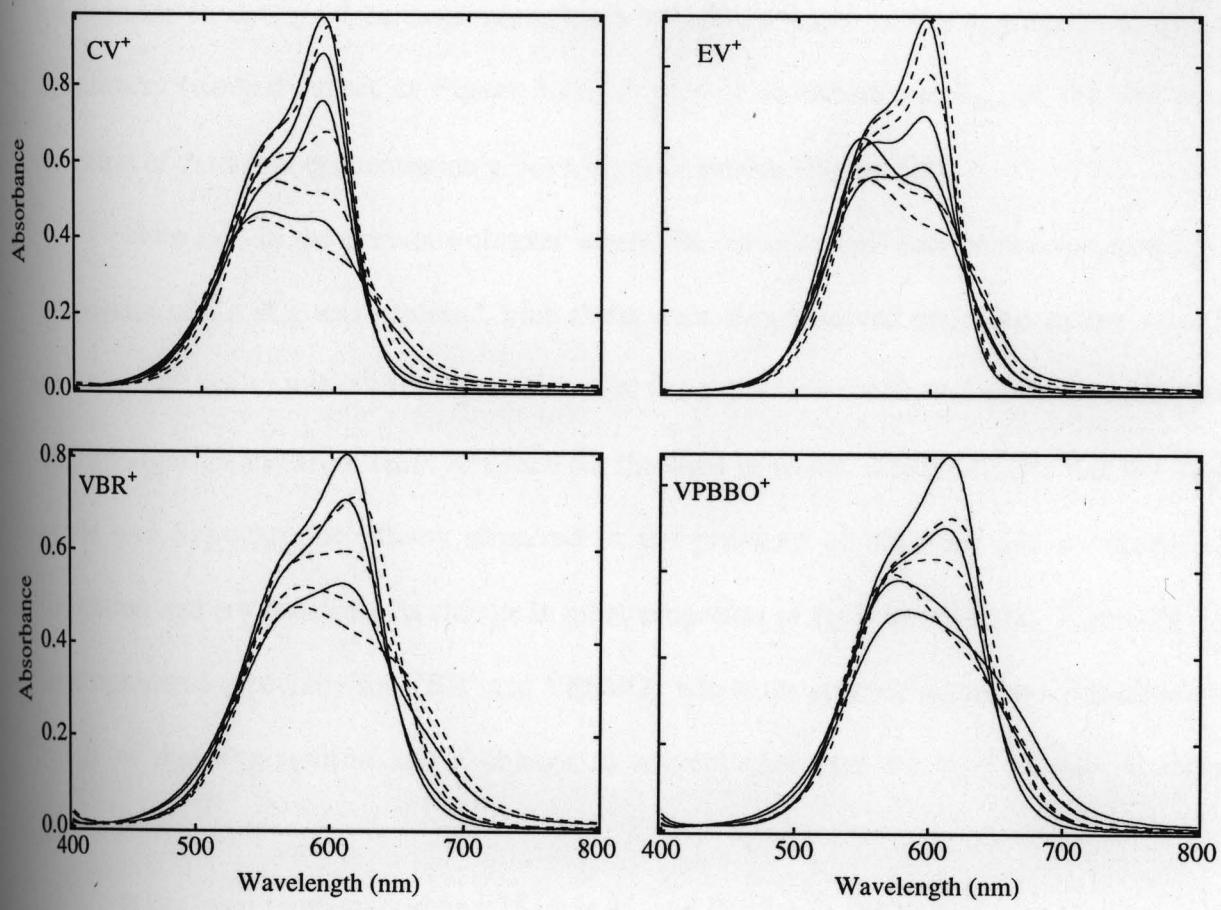

Figure 5.1 Effect of SDS on the absorption spectra of TAM^+ dyes. From the top, in order of decreasing absorption at λ_{max} (solid lines) the SDS concentrations were (μM): 0.0, 4.3, 57.7, 297 for CV^+; 0.0, 0.1, 1.7, 20 for EV^+; 0.0, 2.6, 7.6 for VBR^+; 0.0, 0.3, 1.0, 1.7 for $VPBBO^+$ From the bottom starting at the dashed lines, in order of increasing absorption at λ_{max}, the SDS concentrations were (mM): 0.9, 3.2, 4.7, 8.0 for CV^+; 0.9, 1.9, 4.7, 8.0 for EV^+; 1.1, 3.2, 4.7, 8.0 for VBR^+; 0.9, 4.7, 8.0 for $VPBBO^+$. T = 25°C; $[TAM^+]$ = 10 μM.

an increase in detergent concentration, leads to a dissociation of the aggregates to dye monomers (dashed curves in Figure 5.1). A plot of absorbance at λ_{max} of the dye as a function of detergent concentration gives a biphasic profile (Figure 5.2).

Note that in the previous chapter where the effect of solvents on the spectroscopic properties of TAM^+s was explored, blue shifts were also observed upon decreasing solvent polarity (π^* scale) relative to water. However the extinction coefficient of the dyes did not change significantly from those obtained for the dyes in water. This indicates that the blue shifts and hypochromic effects observed in the presence of SDS are due to aggregate formation and not because of a change in other properties of the bulk solution. This needs to be emphasized especially for VBR^+ and $VPBBO^+$, where the spectral signatures obtained as a result of dye aggregation and a change in solvent character are very similar in their appearance.

It has been previously shown (Sarkar M. and Poddar S., 2000) that in the presence of negatively charged surfactant molecules like sodium dodecyl sulfate (SDS), aggregation type spectroscopic signatures characteristic of the formation of H-type dye aggregates (blue shifts and hypochromism) were obtained below CMC for CV^+. Upon increasing SDS concentration beyond its CMC, the aggregates redistributed as monomers into the non-polar core of the micelle. Similar such results were observed in the titrations carried out in this laboratory with the other three TAM^+s. However the CMC in the presence of the dye was not similar to that observed in pure water. Hence the redistribution of TAM^+s as monomers occurs at detergent concentrations that are *circa* 4.7mM. Dye aggregation is a phenomenon that is usually observed under conditions of high dye concentration and high ionic strength (Lueck H. B., 1992; Bartlett J. A. and Indig G. L., unpublished data), but anionic detergents

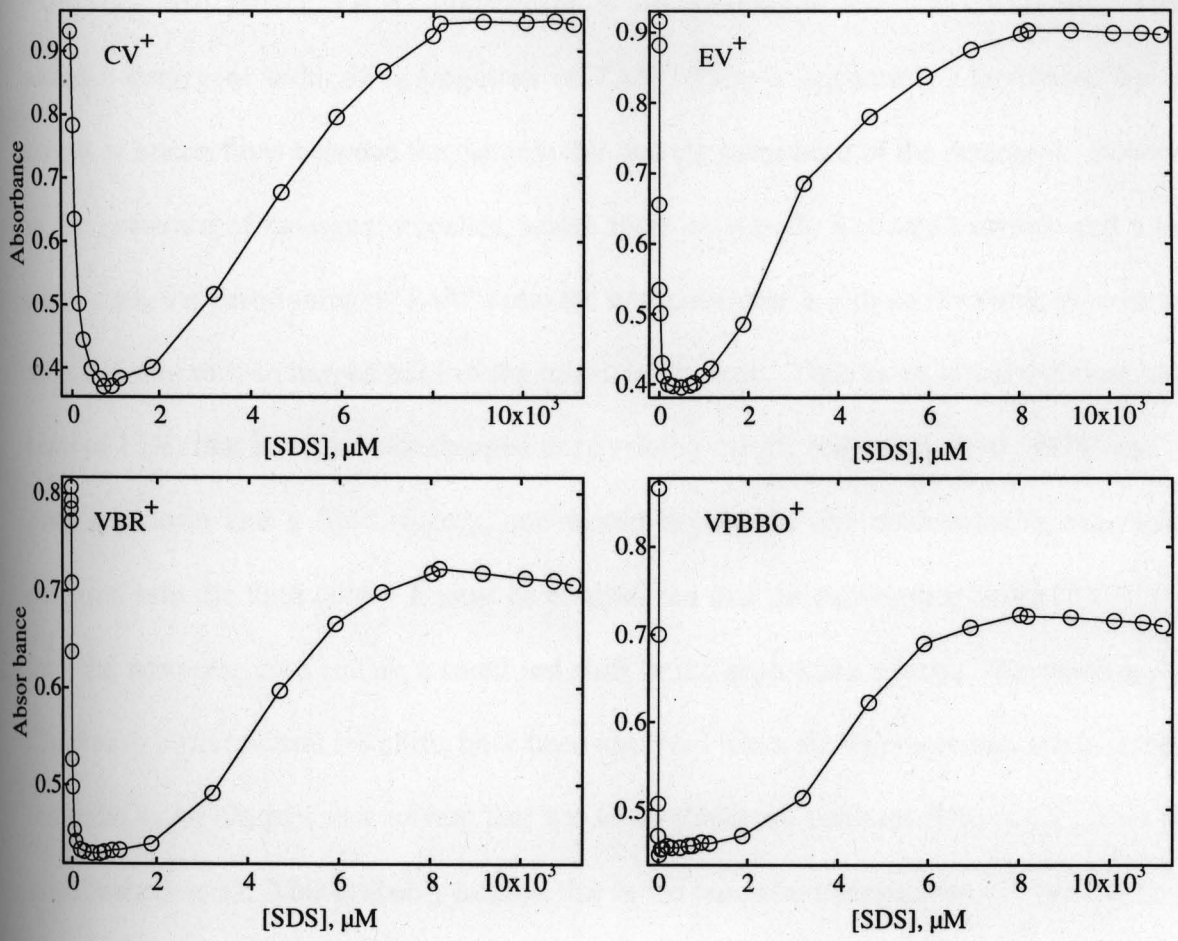

Figure 5.2 Plots of absorbance values at the λ_{max} of the dye, when free in solution as a function of SDS concentration. The detergent concentration regime includes both pre-micellar and micellar concentrations. T = 25°C; [TAM^+] = 10 μM.

like SDS also induce TAM^+ aggregation at submicromolar dye concentrations. The anionic detergent induced aggregation of TAM^+ dyes is apparently facilitated by non covalent interactions between the cationic dye and the polar head of the detergent. However, in the presence of detergent micelles, where there exist both, a charged surface and a non-polar core, the partitioning of TAM^+s into the non-polar core is a more favorable process than their binding to the charged head of the micellar structure. Thus as an initial estimate in the case of LDL that is negatively charged at physiological pH (Ghosh S. et al, 1974) and has both a protein and a lipid moiety, one would expect the dye molecules to extensively partition into the lipid core. It must be emphasized that the partitioning of the TAM^+ dyes into the nonpolar core causes a small red shift in the absorption spectra. As mentioned in Chapter 4, such spectral red shifts have been observed when the dye molecule and its counter ion exist as an ion pair in a solvent that has a low dielectric constant (Oliveira C. S. et al - unpublished data). This probably implies that in the nonpolar micelle core the dye molecules exist predominantly as ion pairs.

Titrations with non-ionic detergent Triton X 100 (TX 100):

Spectrophotometric titrations were also carried out with nonionic detergents and TAM^+s in a similar manner as in the case of SDS. The concentration of dye was kept constant and the surfactant (TX 100) concentration was increased in small increments. The surfactant concentration regimes explored included both pre-micellar and micellar concentrations. The inset of Figure 5.3 shows the effect of the surfactant on the uv-vis spectra of TAM^+s (EV^+ and CV^+). Since Triton X 100 is a nonionic surfactant, there should be no substantial aggregation of the dye molecules because of the absence of a ionic head,

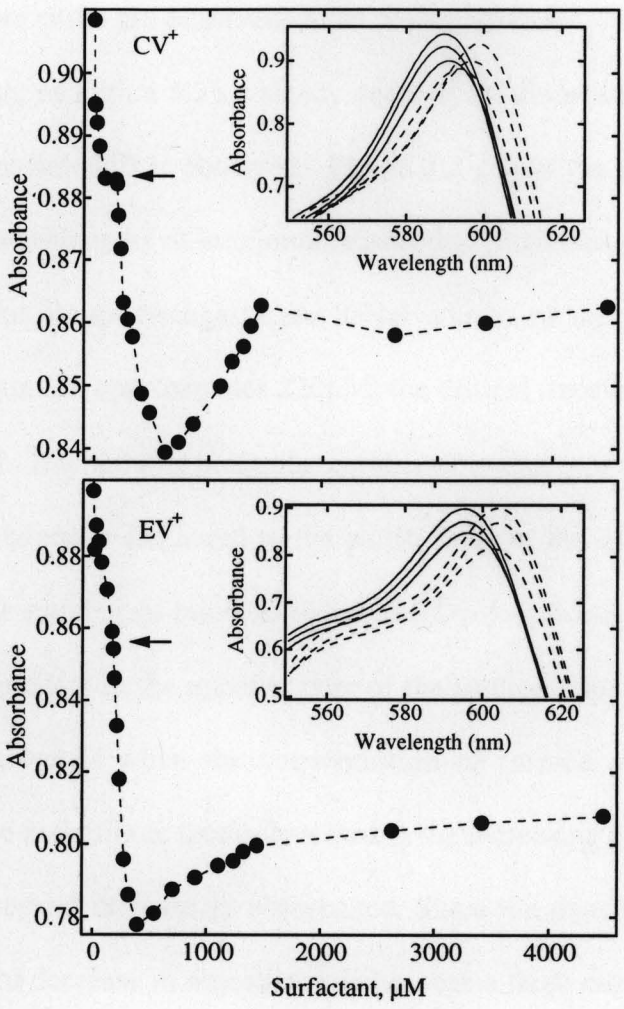

Figure 5.3 Plots of absorbance values of CV^+ and EV^+ at the λ_{max} of the dye, when free in solution as a function of Triton X 100 concentration. The insets show the effect of Triton X 100 on the absorption spectra of TAM^+ dyes. From the top, in order of decreasing absorption at λ_{max} (solid lines) the Triton X 100 concentrations were (mM): 0.0, 0.17, 0.32 for CV^+ and 0.0, 0.12, 0.20 for EV^+; and from the bottom starting at the dashed lines, in order of increasing absorption at λ_{max}, the Triton X 100 concentrations were (mM): 0.54, 1.23, 10 for CV^+ and 0.40, 3.42, 9.1 for EV^+. T = 25°C; $[TAM^+]$ = 10 μM. The arrow indicates CMC of Triton X 100 (220μM).

and indeed no blue shifts are observed in the uv-vis titrations. Instead as is more clearly evident in the inset of Figure 5.3 , a steady decrease in absorbance followed by an increase and a concomitant red shift is observed. Figure 5.3 shows the plots of absorbance of CV^+ and EV^+ at their wavelengths of maximum absorption plotted as a function of the surfactant concentration. An abrupt change in the initial portion of the plot is observed when the surfactant concentration approximates 220μM, the critical micelle concentration for TX 100 (Rharbi Y., 1999). Beyond this point, the number of micelles in the system increase and the decrease in absorbance is attributed to the partitioning of the dye inside the micellar core. Initially, when the number of micelles is lower ([Dye]>[Micelles]), a large number of dye molecules accommodate in the micellar core of the formed micelles, resulting in a decrease in absorbance, however when the concentration of formed micelles increases the dye molecules begin to redistribute themselves within the increasing number of micelles, and this results in the observed increase in absorbance. Since the dyes have substantial lipophilic character the initial decrease in absorbance is because a large number of dye molecules find themselves in the micelle core. This decreases the overall absorbance of the dye, since this large number of dye molecules within the nonpolar micelle core, now constitute a small volume of the system under spectroscopic investigation. This decrease is referred to as the sieve effect (Rabinowitch E. I., 1951, Gupta, B. D., 1986; McClendon J. H. et al, 1990), which occurs due to the localization of pigments which in turn lowers the net absorption, especially at the absorption peak, due to mutual shading of the pigment molecules.

It should be noted that the sharp decrease in absorbance takes place at lower TX 100 concentrations in the case of EV^+ compared to CV^+ (Figure 5.3) and this difference can be attributed to the different partition coefficients of these dyes. EV^+ (P = 237) is much more

lipophilic than CV^+ (P = 2.4) (Indig G. L. et al, 2000) and therefore tends to partition more efficiently into the micellar core, and this causes the observed steep decrease in absorbance and a more pronounced dip in the biphasic profile compared to CV^+. This red shift at high detergent concentrations (above CMC) has been observed in solvents with low dielectric constants like toluene where the dye exists as an ion pair (Oliveria C.S. et al -unpublished data) and is similar to that observed with SDS micelles, suggesting that the dye probably partitions into the nonpolar micellar core as an ion pair.

Fluorescence spectroscopy was also used to study dye detergent interactions, and as shown in Figure 5.4, the fluorescence of CV^+ and EV^+ remains practically constant up to a certain concentration regime and then shows an enhancement with increasing surfactant concentration. The abrupt increase in fluorescence occurs at the CMC, and at concentrations below the CMC; there is no significant change in the fluorescence of the dye. There is an approximate eighteen-fold increase in fluorescence upon partitioning of EV^+ into micelles, and an approximate eight-fold increase in fluorescence of CV^+ under similar conditions. In low viscosity media TAM^+ dyes have very short singlet life times typically in the 1-5 picosecond range, and, therefore, have poor fluorescence quantum yields (10^{-5} to 10^{-4}), due to the fast rotational relaxation processes that occur via rotation of their aromatic rings. However, in more viscous environments or in restricted reaction spaces, the TAM^+ dyes experience loss of rotational degrees of freedom and this results in an increase in fluorescence. The increase in fluorescence upon partitioning into the micelle core is probably because the micellar core offers steric hindrance to the free rotational relaxation processes of these dyes or because of an increase in the viscosity of the micelle core(micelle core has a viscosity of 25 cp, Henderson C. N. and Selinger B. K., 1981) as compared to water.

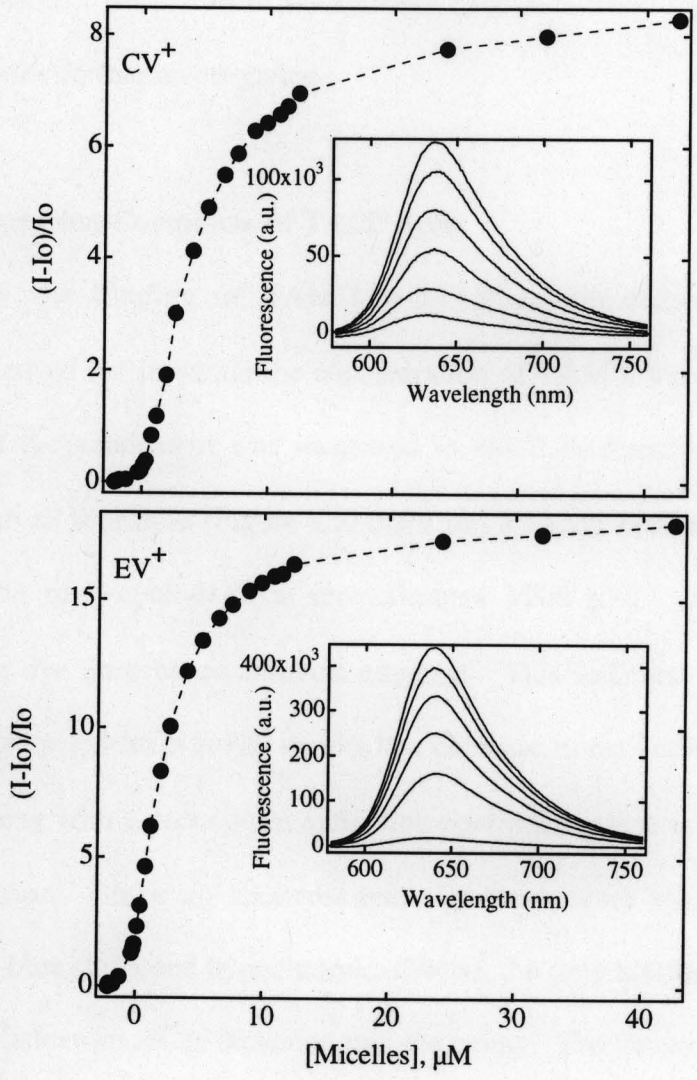

Figure 5.4 Plots of fluorescence of EV^+ and CV^+ as a function of Triton X 100 concentration. Io = Fluorescence intensity in the absence of detergent, I = Fluorescence intensity in the presence of detergent. The insets show the effect of Triton X 100 on the fluorescence spectra of TAM^+ dyes. From the bottom, in order of increasing fluorescence the Triton X 100 concentrations were (mM): 0.0, 0.33, 0.48, 0.73, 1.36 and 4.50. T = 25°C; $[TAM^+]$ = 10 μM.

Whether other intrinsic properties of the micellar core also affect fluorescence quantum yields would require further investigation.

Formation of Inclusion Complexes of TAM^+ dyes:

To study the binding of TAM^+s to β-cyclodextrin, similar spectrophotometric titrations were carried out in which the concentration of TAM^+s was kept constant and the concentration of β-cyclodextrin was increased in small increments. In the case of β-cyclodextrin, with all four dyes (Figure 5.5) there was a steady decrease in absorbance until the concentration of β-cyclodextrin approximates 1000 μM. Beyond 1000 μM β-cyclodextrin, the dye absorbance remains constant. This indicates that the inclusion of TAM^+s into the β-cyclodextrin cavity results in a decrease in extinction coefficient (Figures 5.5 and 5.6). Along with a decrease in extinction coefficient, there is also a red shift of the absorption spectrum. Since no spectroscopic signatures were obtained to suggest dye aggregation (e.g. blue shifts and hypochromic effects), the only binding event that occurs in the case of β-cyclodextrins, is an inclusion into the cavity. The cavity of the β-cyclodextrin is large enough to accommodate the aromatic rings of molecules like benzoic acid and certain halobenzenes (Fromming K. et al, 1994). The included molecule will be oriented in the host in such a position as to achieve maximum contact between the hydrophobic part of the guest and the apolar β-cyclodextrin cavity. One can therefore envision the TAM^+ molecule included into the β-cyclodextrin cavity such that the aromatic ring with alkyl substituted amino groups is inside the cavity, and the rest of the molecule with the positive charge placed outside the cavity. Unlike the scene encountered with the anionic detergents, there is no

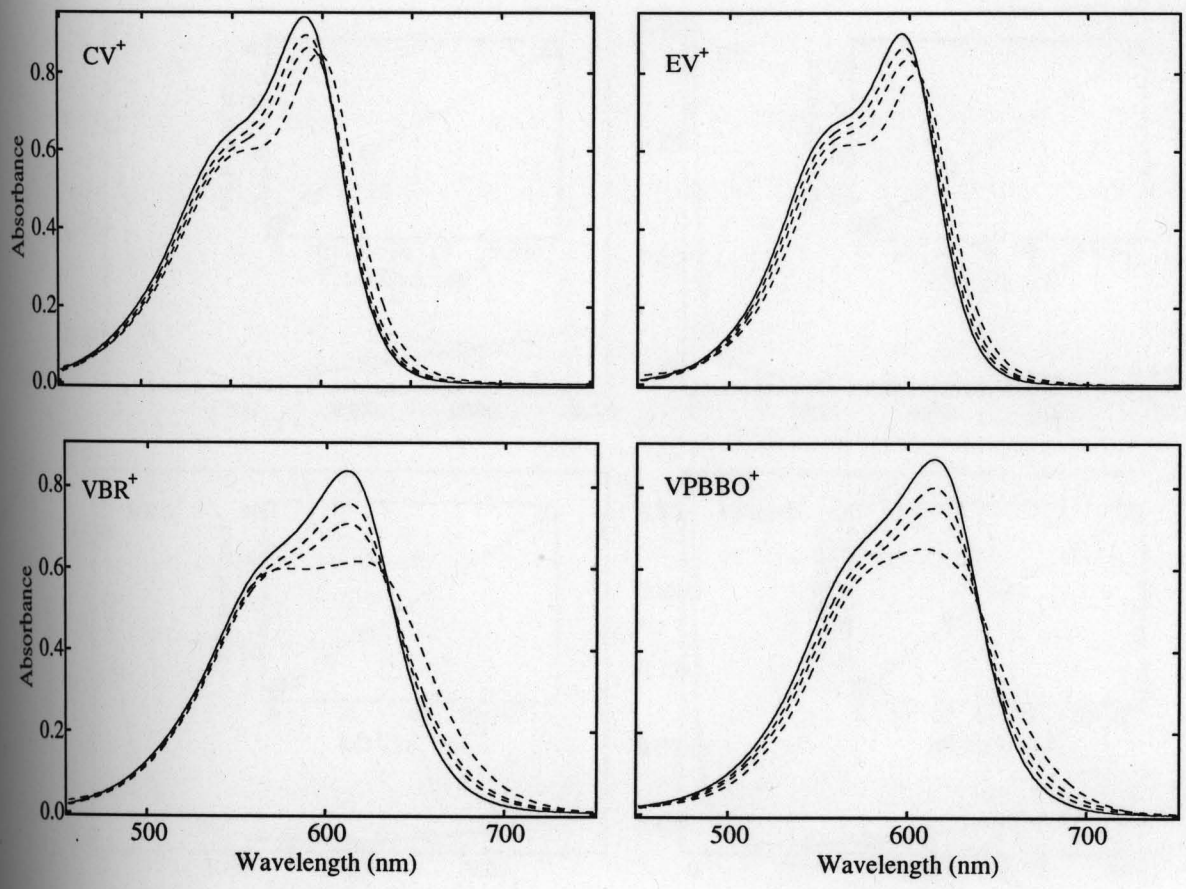

Figure 5.5 Effect of β-cyclodextrin on the absorption spectra of TAM^+ dyes. The solid line represents the spectrum of TAM^+ dye when free in solution, in each of the above four panels. From the top, in order of decreasing absorption at λ_{max} (dashed lines) the β-cyclodextrin concentrations were (mM): 0.04, 0.12, 8.70 for CV^+; 0.01, 0.24, 7.82 for VBR^+; 0.02, 0.04, 8.7 for EV^+ and $VPBBO^+$. T = 25°C; [TAM^+] = 10 μM.

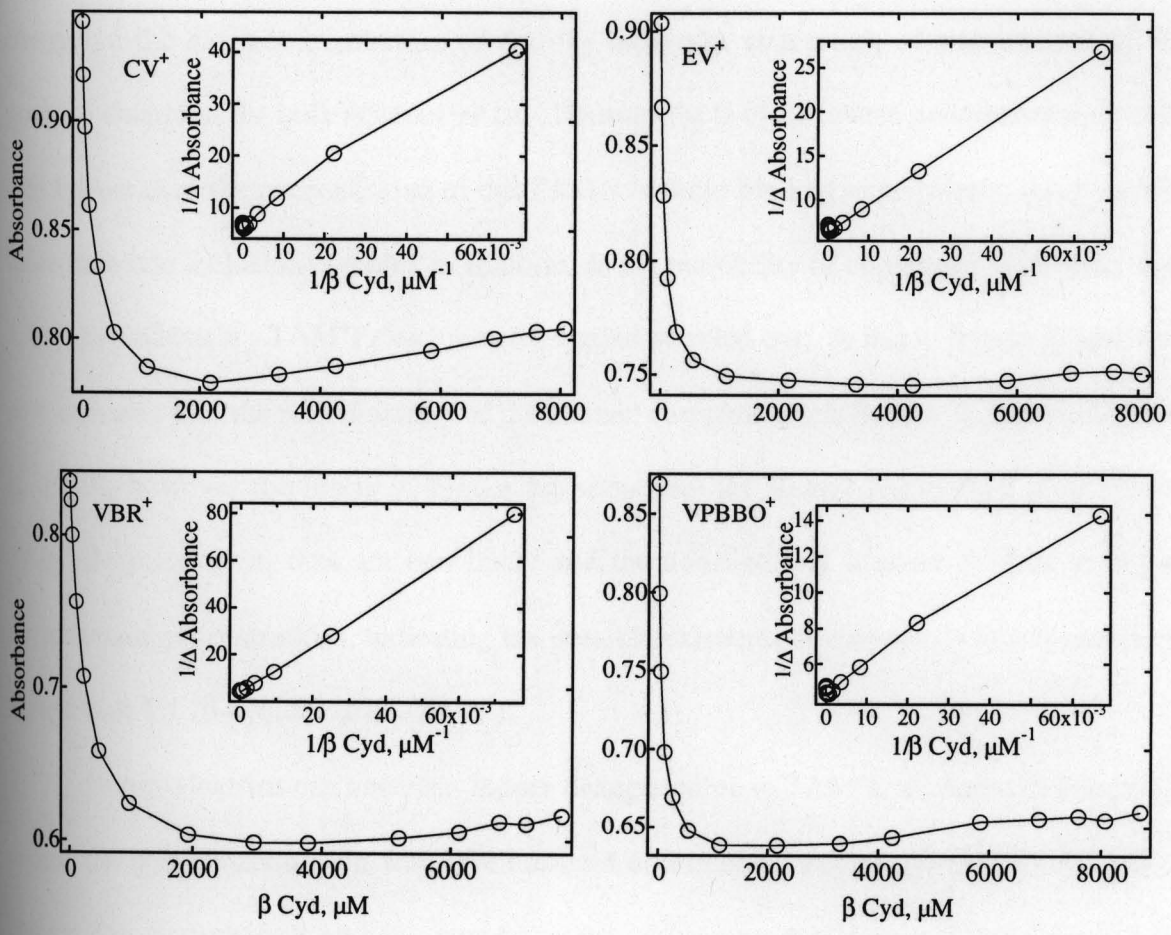

Figure 5.6 Plots of absorbance values at the λ_{max} of the dye, when free in solution as a function of β-cyclodextrin concentration. T = 25°C; [TAM^+] = 10 μM. The insets show the corresponding Benesi-Hildebrand plots. Δ Absorbance is the difference in dye absorbance in the presence and absence of β-cyclodextrin.

localization of the positive charge, and therefore aggregation is not induced in the presence of β-cyclodextrins. The red shift obtained upon inclusion could probably result from a change in the electronic structure of the dye molecule as a result of stabilization of the positive charge in the bulk aqueous phase. Because the β-cyclodextrin concentration is 1000 fold higher than the concentration of the TAM^+s in these binding experiments, there may be more than one inclusion complex in solution, so the possibility of complexes with other than 1:1 (β-cyclodextrin : TAM^+) stoichiometry cannot be ruled out. A linear Benesi-Hildebrand plot indicates that the stoichiometry of the formed complex is 1:1(Benesi H. and Hildebrand J., 1949), however the insets of Figure 5.6 show that the Benesi-Hildebrand plots for the TAM^+-β-cyclodextrin data are non linear and the non-linearity is more evident at higher cyclodextrin concentrations, indicating the possible existence of complexes of stoichiometry higher than 1:1 (β-cyclodextrin : TAM^+).

β-cyclodextrins can however induce deaggregation in TAM^+s, as shown in Figure 5.7 where the dye concentration was kept constant at a concentration regime high enough to induce dye aggregation and the concentration of β-cyclodextrin was increased in small increments. For dyes like EV^+ and $VPBBO^+$ that aggregate very efficiently, it is clear from Figure 5.7 that an increase in β-cyclodextrin concentration results in a decrease in the absorbance of the blue shifted peak that is attributed to the dimer and a concomitant increase in the absorbance of the peak attributed to the monomer. At high cyclodextrin concentrations (8000μM), the spectrum of the of the monomer is red shifted indicating that the dye molecules are included into the cavity at this concentration regime.

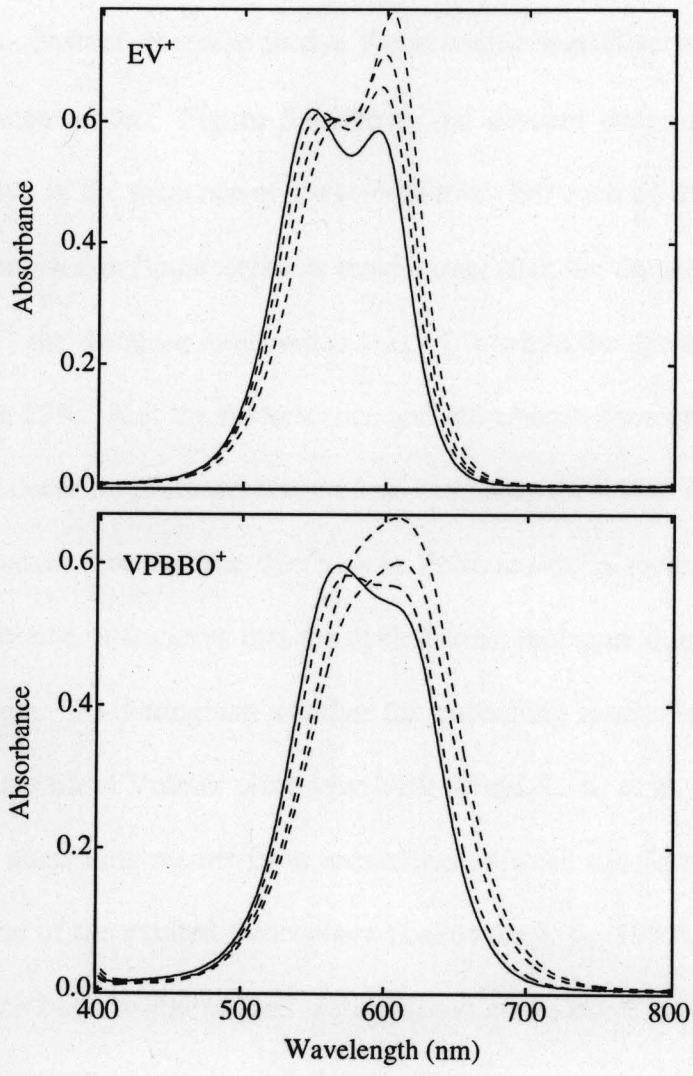

Figure 5.7 Effect of β-cyclodextrin on the absorption spectra of TAM^+ dyes, when present in a state of aggregation. The solid line represents the spectrum of TAM^+ dye in an aggregated state, in each of the above four panels. From the bottom, in order of increasing absorption at λ_{max} (dashed lines) the β-cyclodextrin concentrations were (mM): 0.04, 0.1, 1 for EV^+ and 0.05, 0.5, 5 for $VPBBO^+$. T = 25°C; [TAM^+] = 100 μM.

Fluorescence titrations were also carried out in a similar manner to the uv-vis titrations, and a constant decrease in dye fluorescence was observed with increasing β-cyclodextrin concentration. Figure 5.8 shows the percent decrease in absorbance and fluorescence of dye in the presence of β-cyclodextrin. For each of the dyes as observed in Figure 5.8, the decrease in fluorescence is much larger than the decrease in absorbance e.g., in the case of CV^+ the decrease in absorbance is 15 % while the decrease in fluorescence is slightly more than 25%. Had the fluorescence and absorbance decreased to the same extent, then the observed decrease in fluorescence could have been attributed to a simple decrease in absorbance. However, because the decrease in fluorescence is more pronounced than the decrease in absorbance, it suggests that the cyclodextrin molecule quenches the excited sate of the dye molecule. To distinguish whether the quenching results from static or dynamic quenching processes Stern Volmer plots were built (Fraiji, L. K. et al, 1992; Lakowicz J. R., 1999). Dynamic quenching results from encounters between the fluorophore and quencher during the life time of the excited fluorophore (Lakowicz J. R., 1999). Upon encounter the fluorophore returns back to the ground state without emission of a photon. Based on the distance between energy acceptor and donor encounters can be classified as collisional (Dexter mechanism, where two molecules are separated by a distance that equals the sum of their molecular radii) or long distance (Forster mechanism, where two molecules are separated by a distance greater than their collisional diameters (~50 to 100 A°). Static quenching is due to 'non fluorescent' ground state complex formation between donor and quencher.

Figure 5.9 shows the corresponding Stern-Volmer plots for the quenching data presented in the inset of Figure 5.8. In Stern Volmer plots, ($F/Fo = 1+ k_q[Q]$) F is the

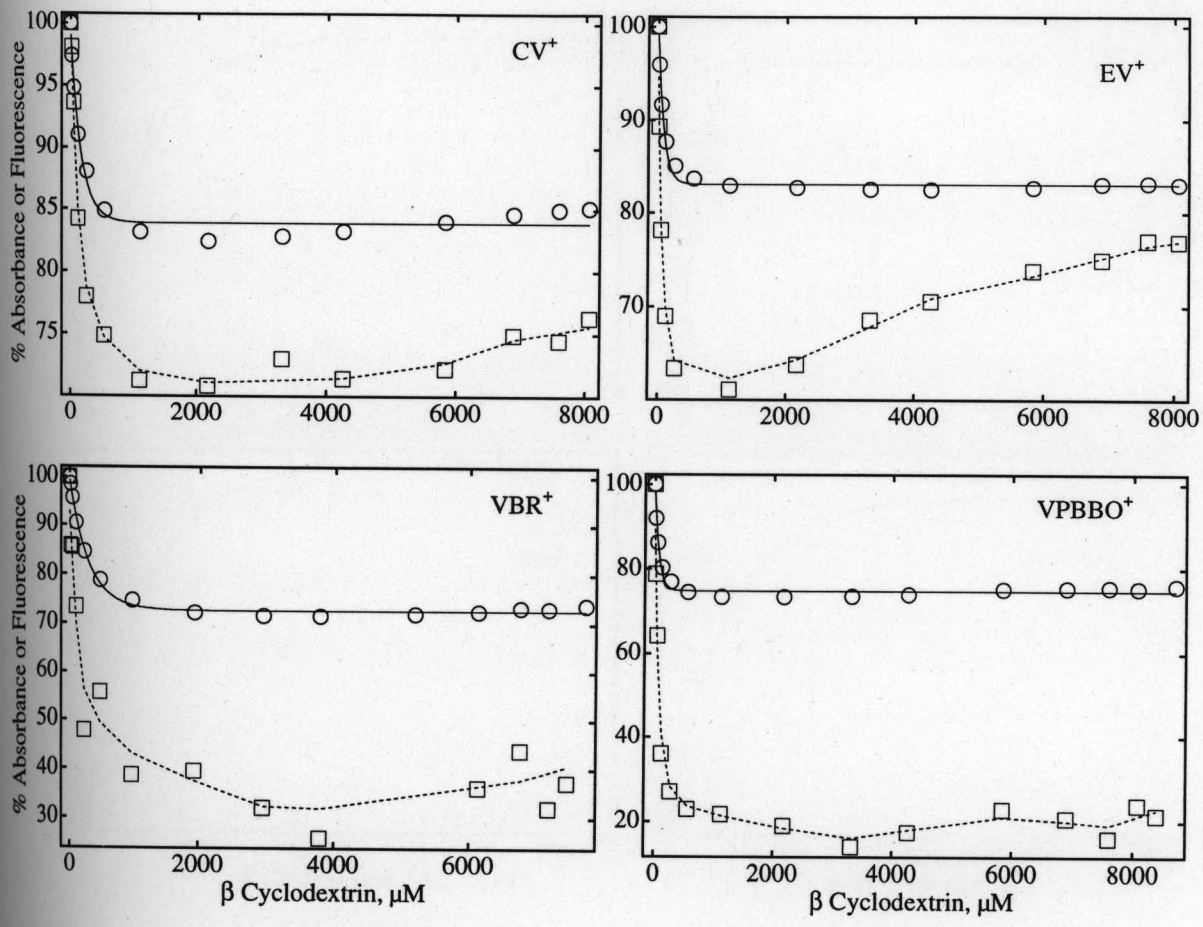

Figure 5.8 Effect of β-cyclodextrin on the percent fluorescence and absorbance of TAM^+ dyes. T = 25°C; $[TAM^+]$ = 10 μM. 100% fluorescence or absorbance represents the parameter measured in the absence of β-cyclodextrin. Squares represent fluorescence while circles represent absorbance.

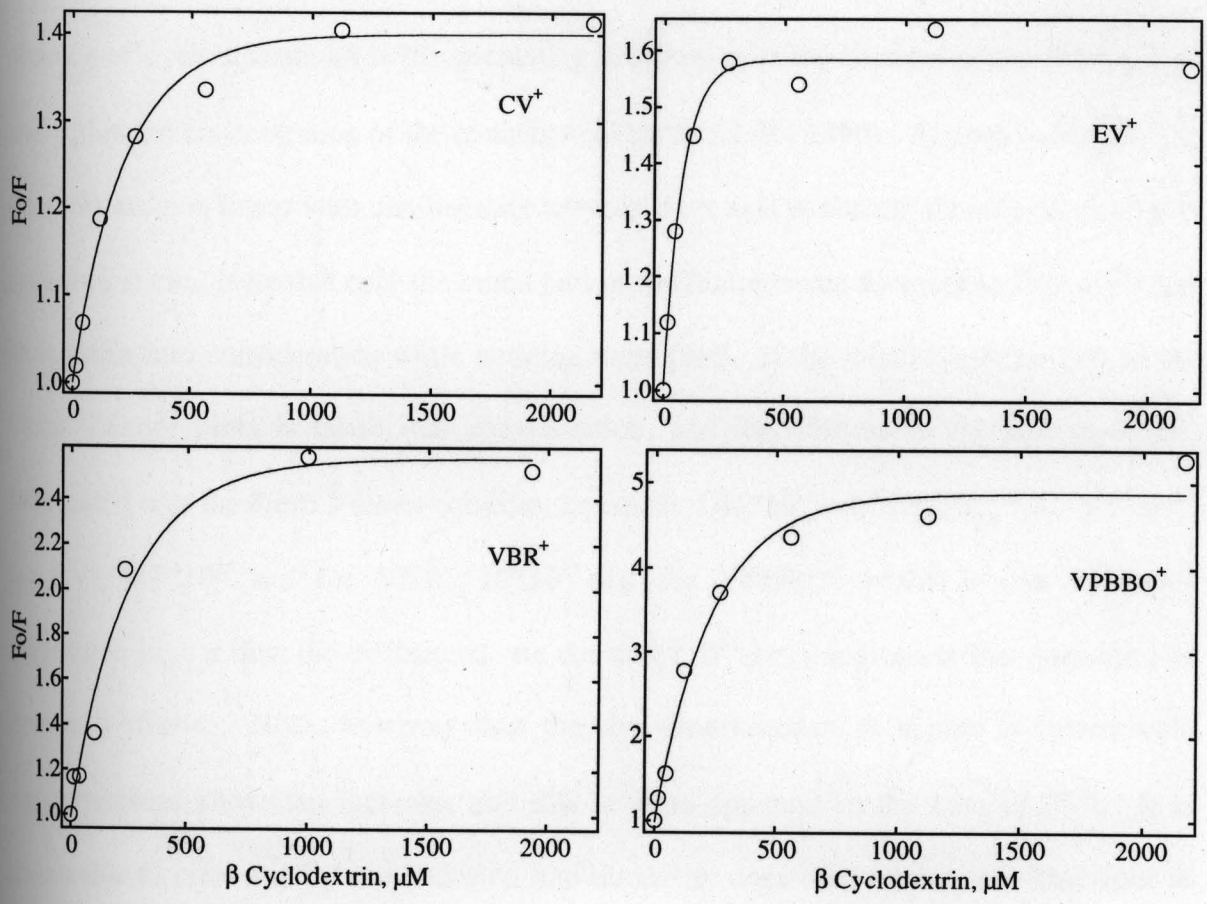

Figure 5.9 Stern Volmer plots built from data presented in Figure 5.8. Fo = fluorescence in the absence of β-cyclodextrin, F = Fluorescence in the presence of β-cyclodextrin.

fluorescence of dye in the presence of cyclodextrin, Fo is the fluorescence of dye in the absence of cyclodextrin, kq is the quenching constant, τ_o is the lifetime of the fluorophore and [Q] is the concentration of the quencher (Lakowicz J. R., 1999). As seen in Figure 5.9, the plots are non linear with non linearity towards the x axis indicating that the quenching is primarily static. Note that only the initial part of the fluorescence decrease in Figure 5.8 has been taken into consideration while building these plots. If the initial linear portion of the Stern Volmer plots is taken into consideration, and the lifetime of the dye (τ_o= 1ps) substituted into the Stern Volmer equation, kq equals $1.03*10^{15}$ sec^{-1} for CV^+, $3.67*10^{15}$ sec^{-1} for EV^+, $4.7*10^{15}$ sec^{-1} for VBR^+, $10*10^{15}$ sec^{-1} for $VPBBO^+$, which is five orders of magnitude higher than the diffusional rate constant (10^{10} sec^{-1}), indicating that quenching is primarily static. Note, however that the dye fluorescence at higher β-cyclodextrin concentrations shows an increase, and this is more apparent in the case of EV^+. It is reasonable to presume that the inclusion into the cavity does offer some steric hindrance to the free rotational relaxation processes of TAM^+s, and this process may in fact be competing with the quenching process. As indicated by the non linear Benesi-Hildebrand plots (insets of Figure 5.6), the existence of complexes of stoichiometry other than 1:1 (β-cyclodextrin : TAM^+) is possible at high β-cyclodextrin concentrations, and this might offer the necessary steric hindrance to the free rotational relaxation processes of TAM^+ dyes.

Titrations with γ-Cyclodextrin:

Previous experiments carried out by others (Bernad Bernad, M. J. et al, 1999; Hidefumi H. et al, 1985) with γ-cyclodextrin and CV^+ using uv-vis spectroscopy, induced

circular dichroism and the method of continuous variation have shown that complexes with 1:2 (Cyclodextrin:Dye) stoichiometry are formed. Spectroscopic evidence was obtained in the form of blue shifts and hypochromic effects, for the formation of CV^+ dimers in the presence of γ-cyclodextrin. Similar experiments carried out in our laboratory confirmed these findings with CV^+ (Figure 5.10), however with EV^+, no such dye aggregation signature was obtained. Instead a plot of absorbance versus γ-cyclodextrin concenteration gives a biphasic profile where there is an initial decrease in absorbance followed by an increase, probably indicating the formation of more than one type of inclusion complex, with the stoichiometries ranging from 1:1 to 2:1 or 3:1, (γ-cyclodextrin:EV^+). The inclusion complexes formed with cyclodextrins are usually governed by geometric rather than chemical factors (Fromming K., et al 1994). There is conflicting opinion in the literature about the formation of the 1:2 (γ-cyclodextrin : CV^+) complex. Bernad Bernad and co-workers assume that one guest molecule of CV^+ enters the cyclodextrin cavity by the narrow edge and the other one through its wide part, resulting in a dimer within the cavity (Bernad Bernad, M. J. et al, 1999). They base their assumption on data obtained using two dimensional NMR and molecular mechanics studies. However Hidefumi H. et al believe that the cavity of γ-cyclodextrin is large enough to accommodate the entire dimer (Hidefumi H. et al, 1985). They have used a molecular model that considers the fit of the guest molecule into the host cavity, based on molecular size.

The fluorescence titrations with CV^+ reveal a biphasic profile, where there is an initial decrease in fluorescence and this is followed by an increase with increase in γ-cyclodextrin concentration as shown in the inset of Figure 5.11. Figure 5.12 shows the percent absorbance

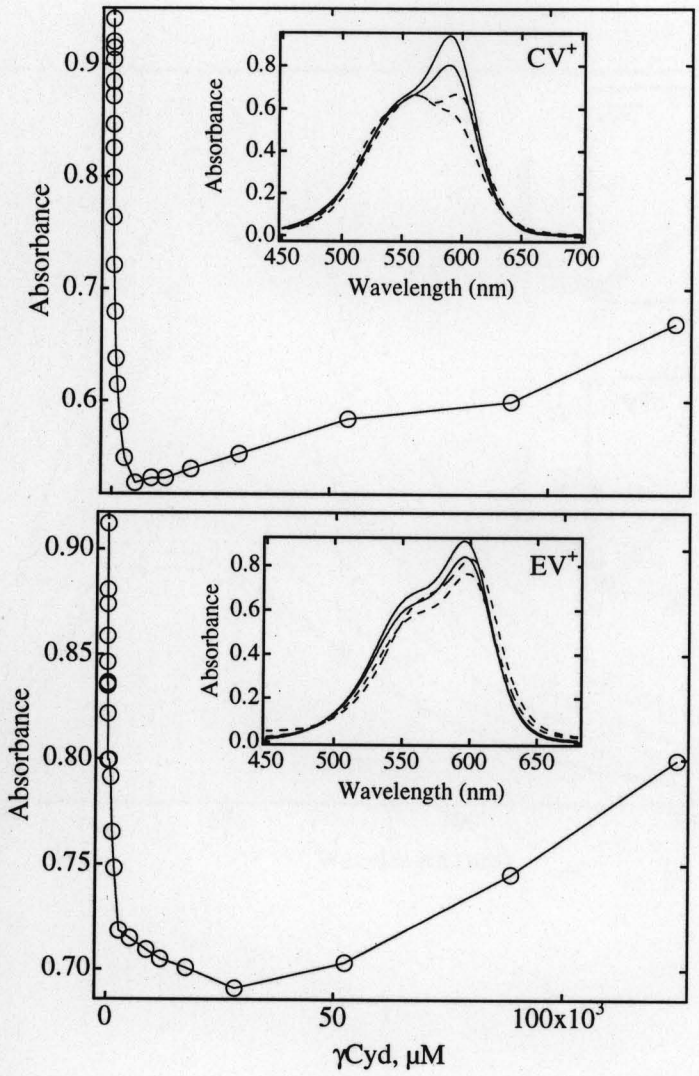

Figure 5.10 Plots of absorbance values at the λ_{max} of the dye, when free in solution as a function of γ-cyclodextrin concentration. The inset shows the effect of γ-cyclodextrin on the absorption spectra of TAM^+ dyes. From the top, in order of decreasing absorption at λ_{max} (solid lines) the γ-cyclodextrin concentrations were (mM): 0.0 and 0.12. From the bottom starting at the dashed lines, in order of increasing absorption at λ_{max}, the γ-cyclodextrin concentrations were (mM): 1.8 and 129. T = 25°C; $[TAM^+]$ = 10 μM.

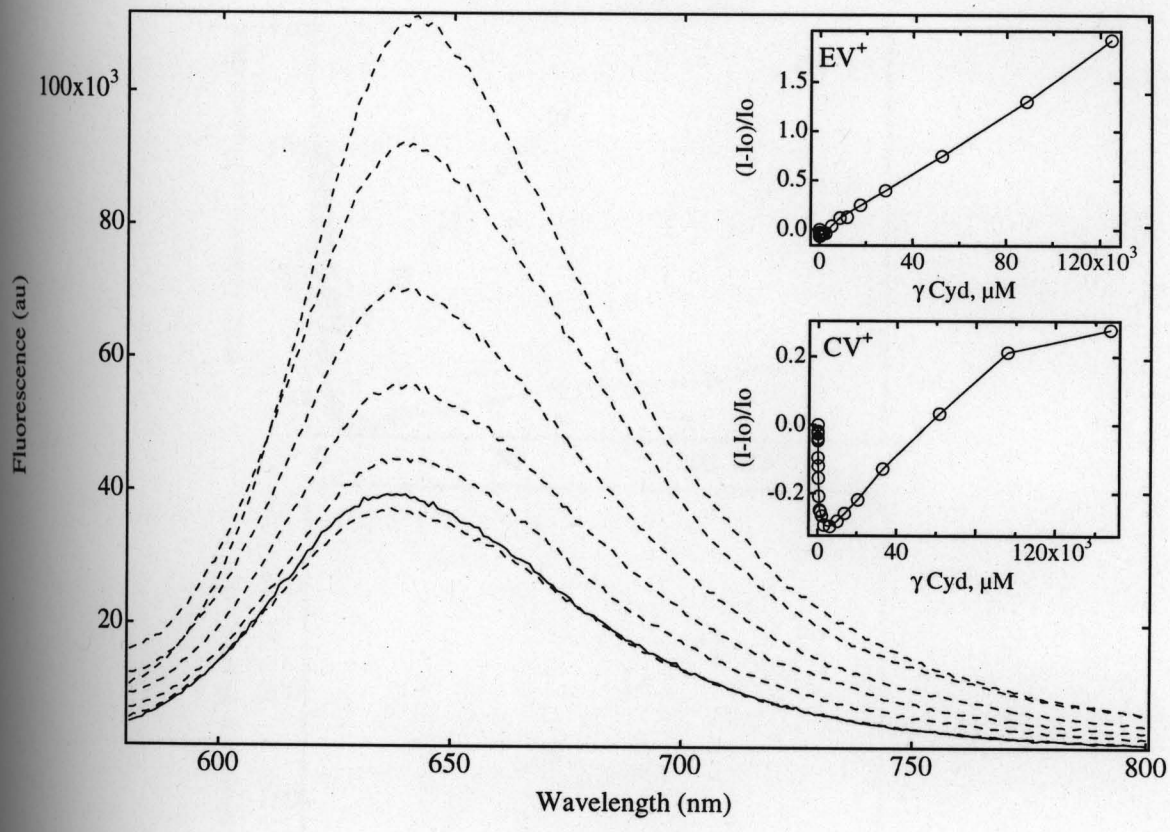

Figure 5.11 Effect of γ-cyclodextrin on the fluorescence spectra of EV^+. The inset shows the effect of γ-cyclodextrin on the flourescence of TAM^+ dyes. The solid line represents the spectrum of the dye in the absence of γ-cyclodextrin . From the bottom starting at the dashed lines, in order of increasing fluorescence, the γ-cyclodextrin concentrations were (mM): 0.28, 11.0, 28.0, 52.5, 88.6 and 124.8. T = 25°C; $[TAM^+]$ = 10 μM.

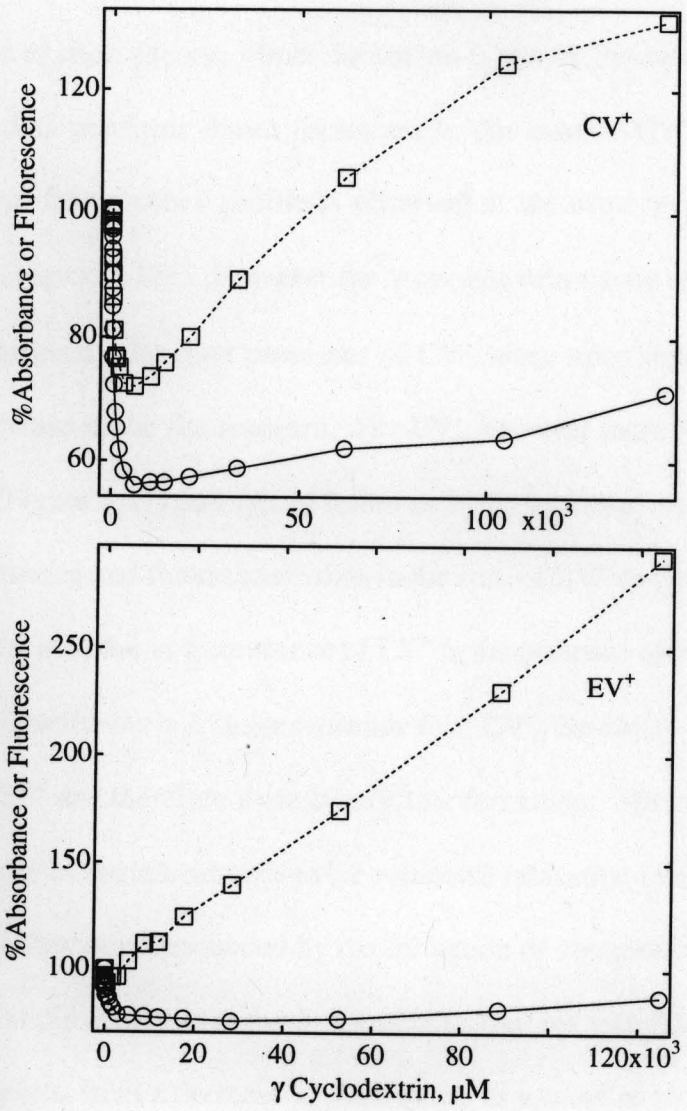

Figure 5.12 Effect of γ-cyclodextrin on the percent fluorescence and absorbance of TAM^+ dyes. T = 25°C; $[TAM^+]$ = 10 μM. 100% fluorescence or absorbance represents the parameter measured in the absence of γ-cyclodextrin. Squares represent fluorescence while circles represent absorbance.

and fluorescence plotted as a function of the γ-cyclodextrin concentration. According to the molecular exciton theory, dimer formation leads to fluorescence quenching and the fluorescence data confirms dimer formation in the case of CV^+, because the dip in the absorbance and fluorescence profile is observed at the same γ-cyclodextrin concentration (*circa* 6mM – Figure 5.12) . However the γ-cyclodextrin cavity also offers steric hindrance to the free rotational relaxation processes of CV^+, since upon redistribution of CV^+ dimers there is an increase in the fluorescence. For EV^+, however there is a small initial dip in the fluorescence (Figure 5.11) and this is followed by an increase. Also as observed in Figure 5.12, the absorbance and fluorescence data in the case of EV^+ do not overlap. Instead there is an almost 200% increase in fluorecence of EV^+ in the presence of γ-cyclodextrin. Since EV^+ with its ethyl substituents is a larger molecule than CV^+, the cavity cannot accommodate two molecules of EV^+ and therefore there is no dimer formation. The increase in fluorescence is probably because of steric hindrance to the rotational relaxation motions of its aromatic rings, which could be further compounded by the formation of complexes of higher stoichiometry. The small initial dip observed in the fluorescence titrations with EV^+ probably represents the decrease that results from a decrease in absorbance, as a result of inclusion.

CONCLUSIONS:

The data obtained with the anionic detergent SDS and its corresponding micelles indicates that below the CMC, dye aggregation occurs in the presence of this detergent, presumably assisted by the non covalent interaction of the cationic dyes with the negatively charged head of the detergent. Above the CMC there is a preferential partitioning of the TAM^+s into the nonpolar core, rather than an electrostatic interaction with the dye molecule

and the micelle head. The plot of absorbance vs. detergent concentration results in a biphasic profile with the descending arm of the biphasic profile representing the formation of TAM^+ aggregates and the ascending arm representing the redistribution of these aggregates as monomers in the micellar core. The region of the well represents a concentration regime at which the system is optimized to detect spectroscopic signatures of aggregates and is therefore a region that represents maximum concentration of aggregates. With the nonionic micelles, TAM^+s extensively partition into the nonpolar core of the nonionic micelles, and partitioning is the only binding event that also results in a biphasic profile when absorbance is plotted as a function of detergent concentration. The biphasic profile in this case however is obtained because of a non-homogenous distribution of the chromophore in the micelles (Rabinowitch E. I., 1951). The higher viscosity of the micellar environment (Henderson C. N. and Selinger B. K., 1981) provides resistance to the free rotational relaxation movements of the TAM^+s, resulting in an increase in their fluorescence quantum yields.

In the case of cyclodextrins, inclusion complexes were obtained with TAM^+s . The β cyclodextrin cavity was not large (~6.6 A°) (Connors K. A., 1997) enough to accommodate two molecules of the TAM^+ dye and therefore no dye aggregation was observed in the presence of β cyclodextrin. However deaggregation of the dye as monomers could be achieved in the presence of β cyclodextrin. The decrease in the fluorescence of TAM^+s in the presence of β cyclodextrin is because of static quenching. γ cyclodextrin that has a larger cavity dimension (~8.4 A°) (Connors K. A., 1997) than the β cyclodextrin cavity, was large enough to accommodate two dye molecules of the N-methyl substituted CV^+, but the same was not true for the N-ethyl substituted TAM^+, EV^+. Thus the inclusion of CV^+ into the γ

cyclodextrin cavity allows dimer formation, but in the case of EV^+ because of size constraints, dye dimers are not observed.

Thus as observed in the solvents listed in Table 4.1 in Chapter 4, blue spectral shifts were obtained relative to water with the extinction coefficient of the dye being similar or higher than that obtained in water. In the presence of SDS, blue shifts and hypochromic effects were observed below the CMC, indicating aggregate formation. Above the CMC, along with redistribution as a monomer, red shifts were obtained indicating dye partitioning into the nonpolar micellar core as an ion pair. In the case of nonionic detergents, no aggregation type spectroscopic signatures were obtained indicating that the dye does not undergo any significant aggregation in the presence of nonionic detergents. In the case of cyclodextrins, the inclusion of CV^+ into the γ cyclodextrin cavity allows dimer formation, but in the case of β cyclodextrin no aggregation was observed for all TAM^+ dyes considered in this study. Thus the data obtained with solvent effects in combination with the data on detergents and cyclodextrins provides important guidelines for the interpretation of the binding data of TAM^+ dyes to the model biological hosts discussed in the subsequent chapters of this thesis, namely HK, DNA and LDL.

Chapter 6. Binding of Triarylmethane dyes to HK and Photoreactivity of HK-TAM^+ Noncovalent Complexes.

RESULTS AND DISCUSSION:

Binding studies with HK:

Spectrophotometric titrations:

Electronic spectroscopy was used to characterize the binding of TAM^+s to HK. Titrations were carried out in which the dye concentration was kept constant at 10μM, and the concentration of HK (titrant) was increased in small increments. Figure 6.1 shows the effect of HK concentration on the absorption spectrum of TAM^+ dyes. Initially upon increasing HK concentration up to the 4.8μM range, a decrease in maximum dye absorption takes place with a concomitant increase in ratio between the absorption values observed at the wavelengths of shoulder and maximum of the respective TAM^+ spectra. Beyond 4.8μM HK an increase in enzyme concentration resulted in an increase in TAM^+ absorption, along with a red shift in the absorption spectrum.

The spectroscopic signature typical of the formation of H-type dimers of tri para substituted TAM^+ dyes in solution is the appearance of a hypsochromically shifted absorption band that overlaps with the spectral shoulder of the TAM^+ dye monomer. Because TAM^+ dimers absorb less light than their respective isolated monomers, hypochromic effects are also observed upon dye dimerization. Therefore both the decrease in A_{max} and the increase in $A_{shoulder}/A_{max}$ ratio observed in the absorption spectra of TAM^+ dye upon increasing HK

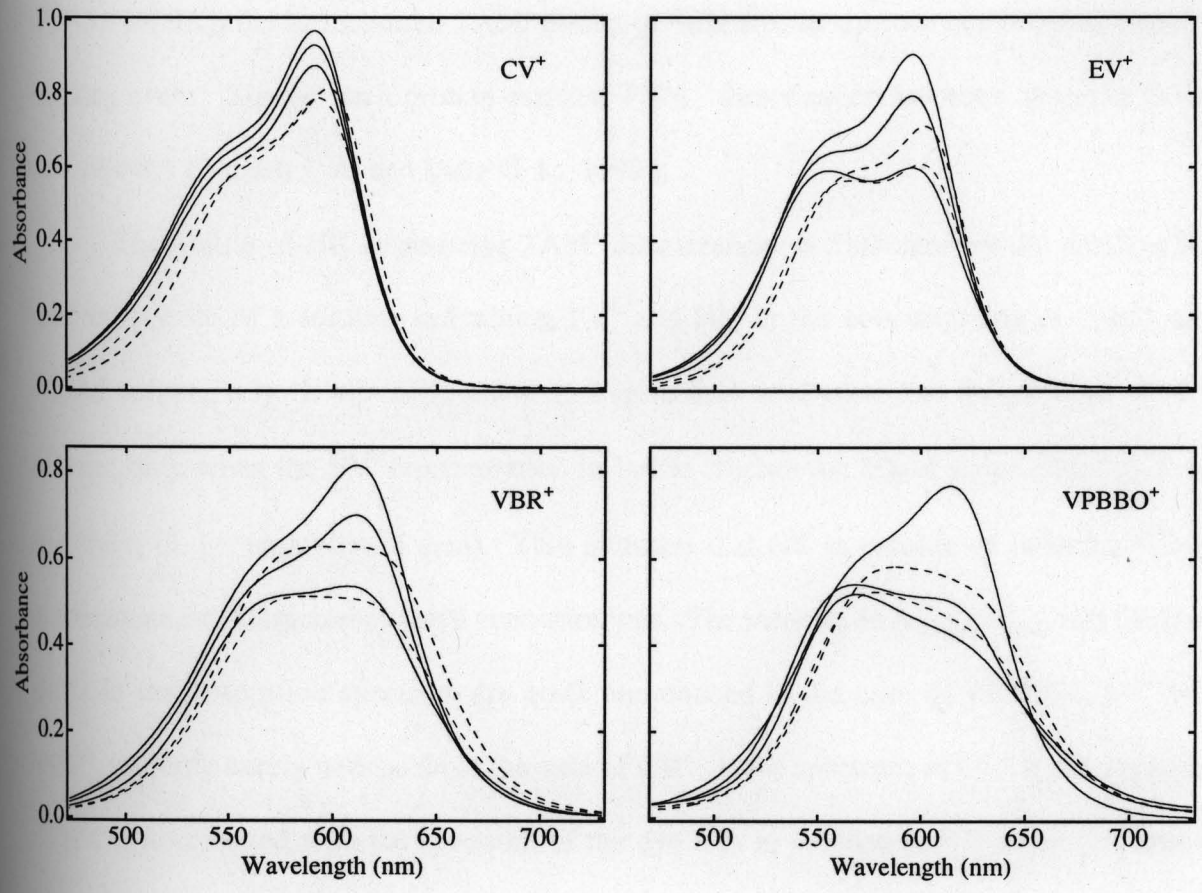

Figure 6.1 Effect of HK on the absorption spectra of TAM^+ dyes. From the top, in order of decreasing absorption at λ_{max} (solid lines) the HK concentrations were (μM): 0.0, 0.6, 4.8. From the bottom starting at the dashed lines, in order of increasing absorption at λ_{max}, the HK concentrations were (μM): 45, 148 (for EV^+, VBR^+, and $VPBBO^+$), or 45, 250 (for CV^+). Tris buffer 50 mM, pH 7.6; T = 25°C; $[TAM^+]$ = 10 μM.

concentration from 0 to 4.8μM indicates that under conditions of high protein loading ([TAM^+]>[HK]) the formation of TAM^+ dimers is facilitated in aqueous media by the protein binding event. Similar such protein-assisted TAM^+ dimerization has been observed in the case of BSA (Bartlett J. A. and Indig G. L., 1999).

The ability of HK in assisting TAM^+ dimerization is illustrated by the fact that the spectral profile of a solution containing EV^+ and HK in the concentration of 10μM and 4.8μM respectively (lower solid curve in Figure 6.1) is observed in the absence of this protein, only when the EV^+ concentration in buffer reaches the 80μM range (Bartlett J. A. and Indig G. L., unpublished data). This indicates that HK is capable of inducing TAM^+ dimerization at submicromolar dye concentrations. The increase in $A_{shoulder}/A_{max}$ and the blue shifts in the absorption spectrum are quite pronounced in the case of $VPBBO^+$, EV^+ and VBR^+, but only barely noticeable in the case of CV^+. If the spectrum of CV^+ in the presence of HK is normalized with the spectrum of the dye free in solution just a minor increase is observed in $A_{shoulder}/A_{max}$ ratio as indicated in Figure 6.2. This implies that CV^+ does not undergo significant dimerization upon HK binding. In the case of $VPBBO^+$, EV^+ and VBR^+, more pronounced effects are observed (Figure 6.2). Dye dimerization is related to the partition coefficient of the dye, therefore dyes with higher partition coefficients like EV^+ and $VPBBO^+$ (with P values of 237 and 180 respectively) show higher aggregation tendencies compared to dyes with lower partition coefficients like CV^+ (P = 2.4) and VBR^+ (P = 39) (Indig, G. L. et al, 2000).

Spectrophotometric titrations of dyes with HK were carried out in two different media viz. buffer containing 50mM Trizma HCl, pH = 7.6 and water adjusted to a pH of 7.6. In

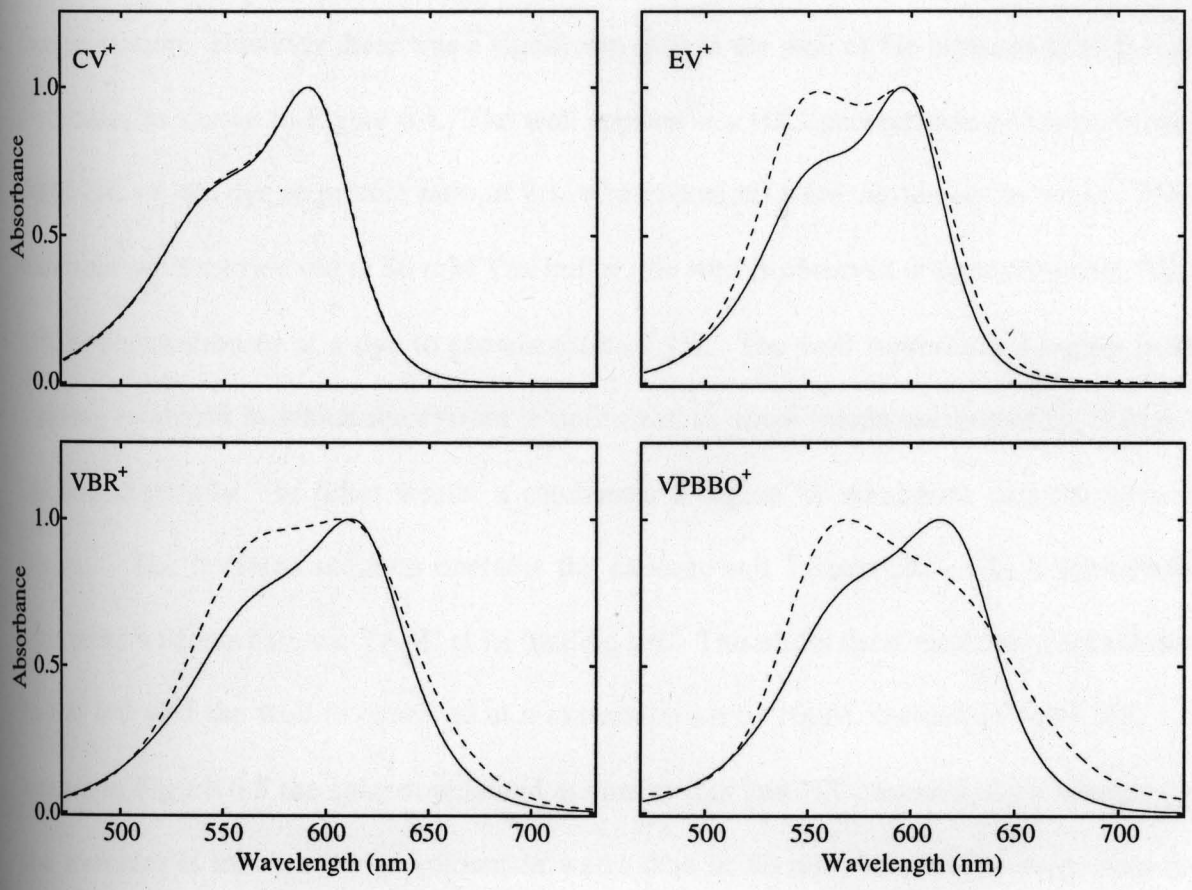

Figure 6.2 Normalized absorption spectra of TAM^+ dyes. The solid line represents the spectrum of the dye in the absence of HK. The dashed line represents the spectrum of the dye in the presence of 4.8 μM HK. Tris buffer 50 mM, pH 7.6; T = 25°C; [TAM^+] = 10 μM.

both these titrations (compare Figures 6.1 and 6.3) the spectral signatures were similar and biphasic profiles were obtained when the absorbance was plotted as a function of HK concentration. However there was a significant shift in the well of the biphasic profile in the two cases as shown in Figure 6.4. The well appears at a HK concentration of approximately 5μM HK or at a dye to protein ratio of 2:1, when titrations were carried out in water. When titrations were carried out in 50 mM Tris buffer, the well is observed at approximately 10μM HK concentration or at a dye to protein ratio of 1:1. The well represents a region in the binding isotherm in which the system is optimized to allow maximum detection of dimers spectroscopically. In other words it represents a region of maximum concentration of dimers. The buffered medium contains the cationic salt Trizma HCl, which presumably competes with the cationic TAM^+ at its binding site. This shifts the dimerization equilibrium to the left and the well is observed at a concentration of 10μM, instead of 5μM HK. As shown in Figure 6.5 the spectra obtained at similar dye and HK concentrations reveals that the shoulder is much more prominent in water than in 50 mM Tris buffer, indicating that dimerization is much more pronounced when the medium is water as opposed to 50 mM Tris buffer.

The binding data was also plotted using the mole ratio method (Chriswell, C. D. and Schilt, A. A., 1975). Figure 6.6 shows that the stoichiometry of the complex is close to 2:1, for EV^+, VBR^+ and $VPBBO^+$, indicating that there are approximately two dye molecules per enzyme molecule. Since the spectroscopic signature provides evidence for dimer formation at that concentration regime, it is reasonable to presume that the enzyme probably has only one binding site for the dye molecule. For CV^+, the ratio at the well is close to 0.5, indicating that the dye was not bound as a dimer, but largely as a monomer at that concentration regime.

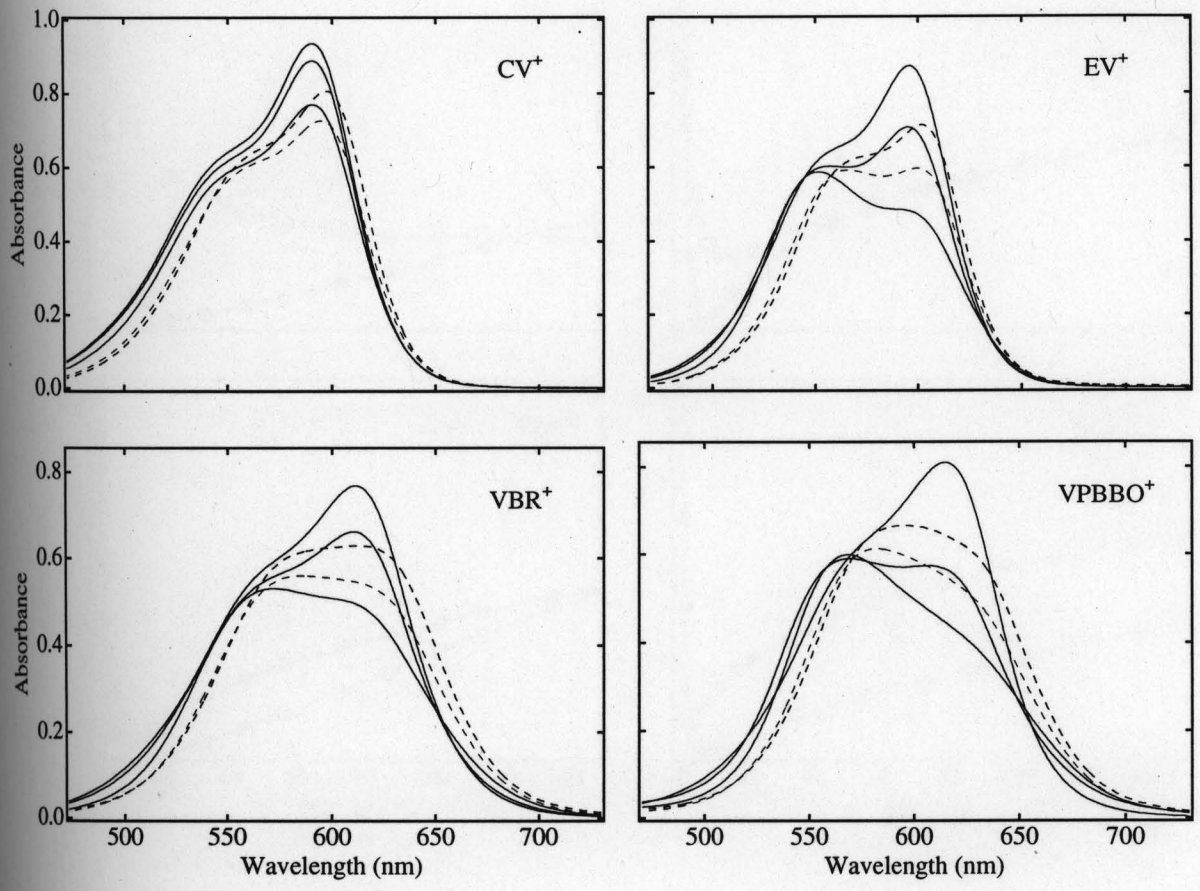

Figure 6.3 Effect of HK on the absorption spectra of TAM^+ dyes. From the top, in order of decreasing absorption at λ_{max} (solid lines) the HK concentrations were (μM): 0.0, 0.6, 4.8. From the bottom starting at the dashed lines, in order of increasing absorption at λ_{max}, the HK concentrations were (μM): 45, 148 (for EV^+, VBR^+, and $VPBBO^+$), or 45, 250 (for CV^+). Water, pH 7.6; T = 25°C; $[TAM^+]$ = 10 μM.

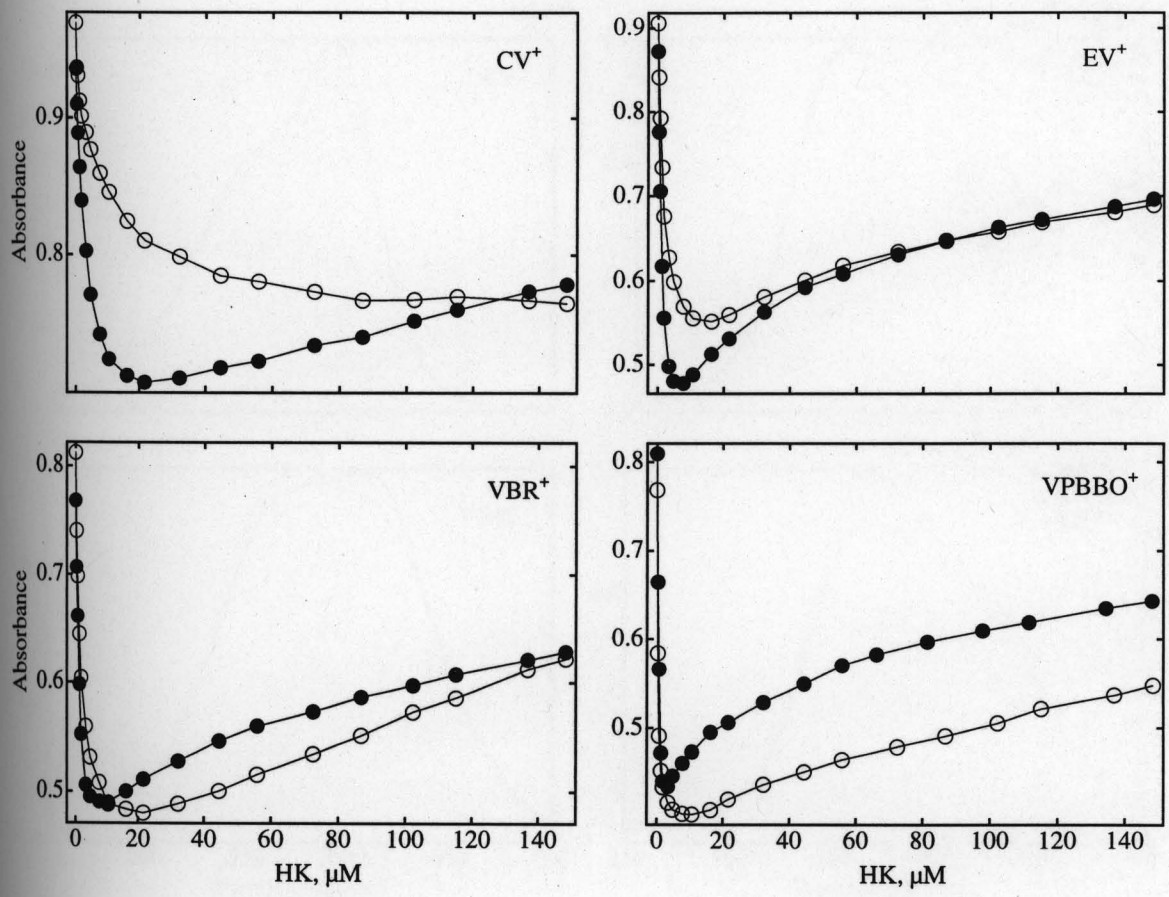

Figure 6.4 Plots of absorbance values at the λ_{max} of the dye as a function of HK concentration. The solid circles represent titration points obtained in medium containing water adjusted to pH 7.6, the open circles represent water 50mM Tris buffer. T = 25°C; $[TAM^+]$ = 10 μM.

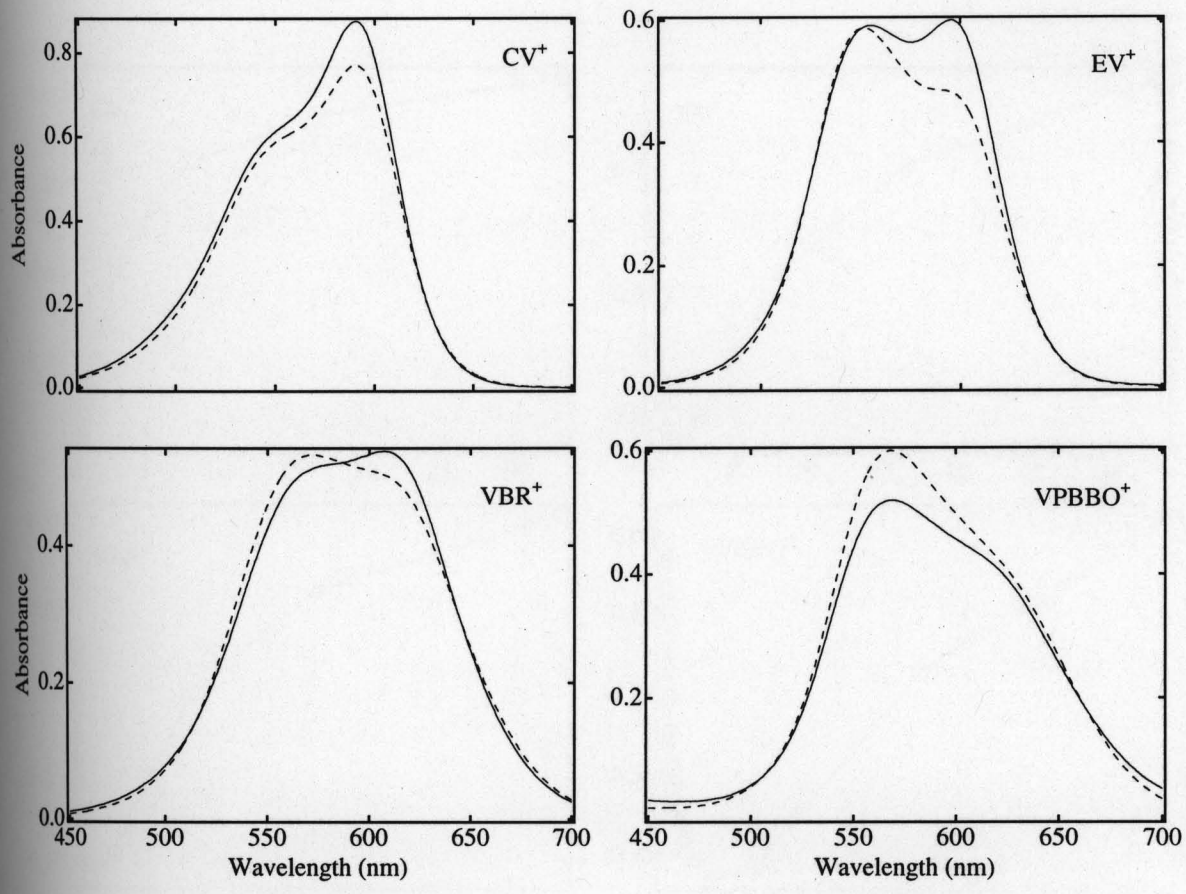

Figure 6.5 Absorption spectra of TAM dyes in the presence of 4.8μM HK in two different media viz. 50mM Tris buffer and water, adjusted to pH = 7.6. The dashed lines represent the TAM spectrum in the presence of water, the solid lines represent spectra in 50mM Tris buffer. T= 25°C; [TAM^+] = 10 μM.

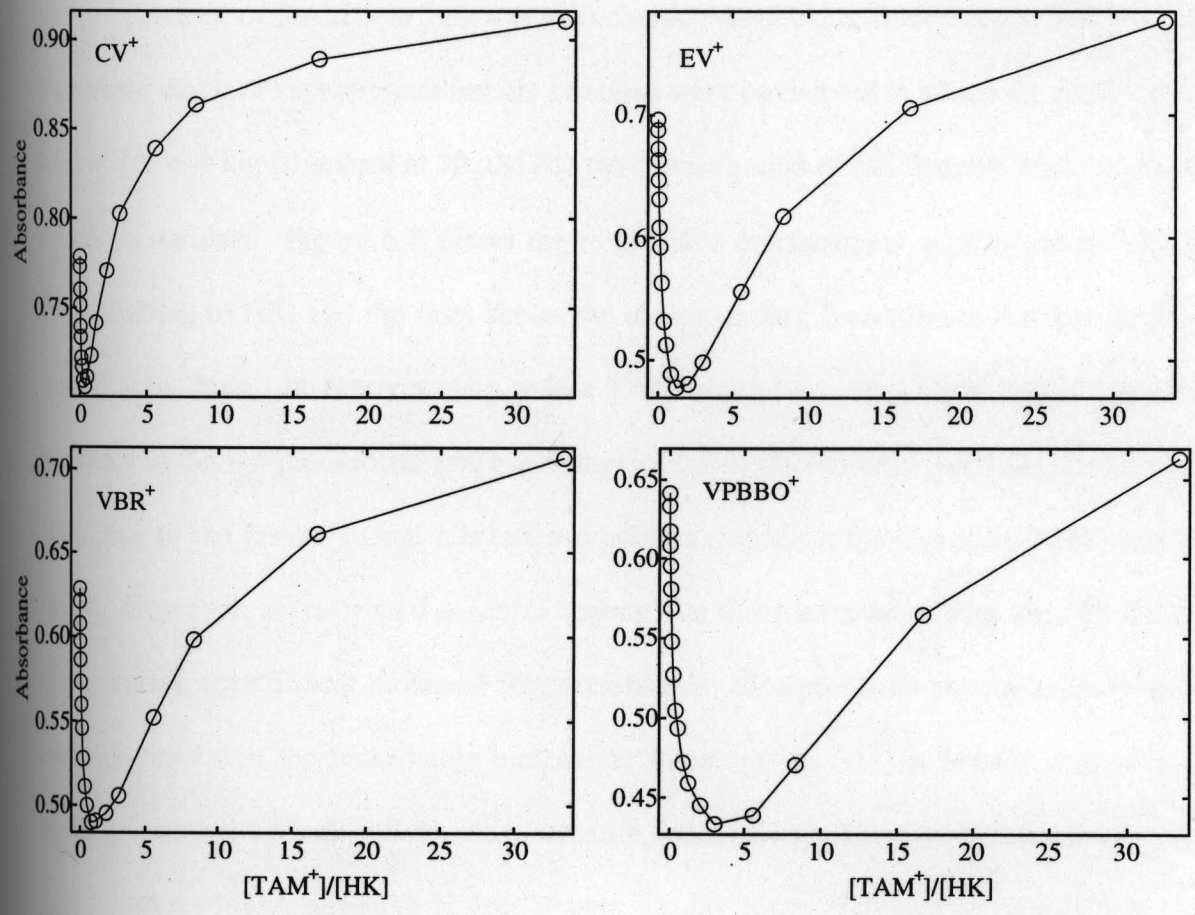

Figure 6.6 Plots of absorbance values at the λ_{max} of TAM^+ dyes as a function the dye to protein mole ratio. Water adjusted to pH 7.6, T = 25°C; $[TAM^+]$ = 10 μM.

Fluorescence Titrations:

Binding of TAM^+s to HK was also characterized using fluorescence spectroscopy. Titrations similar to spectrophotometric titrations were carried out in which the concentration of the dye was kept constant at 10 μM and the concentration of HK (titrant) was increased in small increments. Figure 6.7 shows the remarkable enhancement in fluorescence of EV^+ upon binding to HK, and the inset shows the corresponding fluorescence binding isotherms for all four dyes. In low viscosity media TAM^+ dyes have very short singlet life times typically in the 1-5 picosecond range and therefore poor fluorescence quantum yields (10^{-5} to 10^{-4}), due to the fast rotational relaxation processes that occur via rotation of their aromatic rings. However, in restricted reaction spaces like those encountered in the HK binding environment, the efficient modes of nonradiative relaxation processes are sterically hindered, and this results in the remarkable increase in fluorescence. At the plateau region of the binding isotherm basically all dye molecules are noncovalently bound to HK as a monomer.

Interestingly, although H type dimers display lower fluorescence yields than their respective dye monomers the increase in fluorescence quantum yield of TAM^+ monomers upon binding is larger than the decrease in fluorescence quantum yield of the TAM^+ dimers. As a result, the protein binding effect on the fluorescence of TAM^+ dyes in aqueous solutions is a net enhancement in intensity, even when considering the HK concentration regime in which dye aggregation takes place. For this reason the combined employment of electronic and fluorescence spectroscopy is a requirement for the detailed investigation of noncovalent

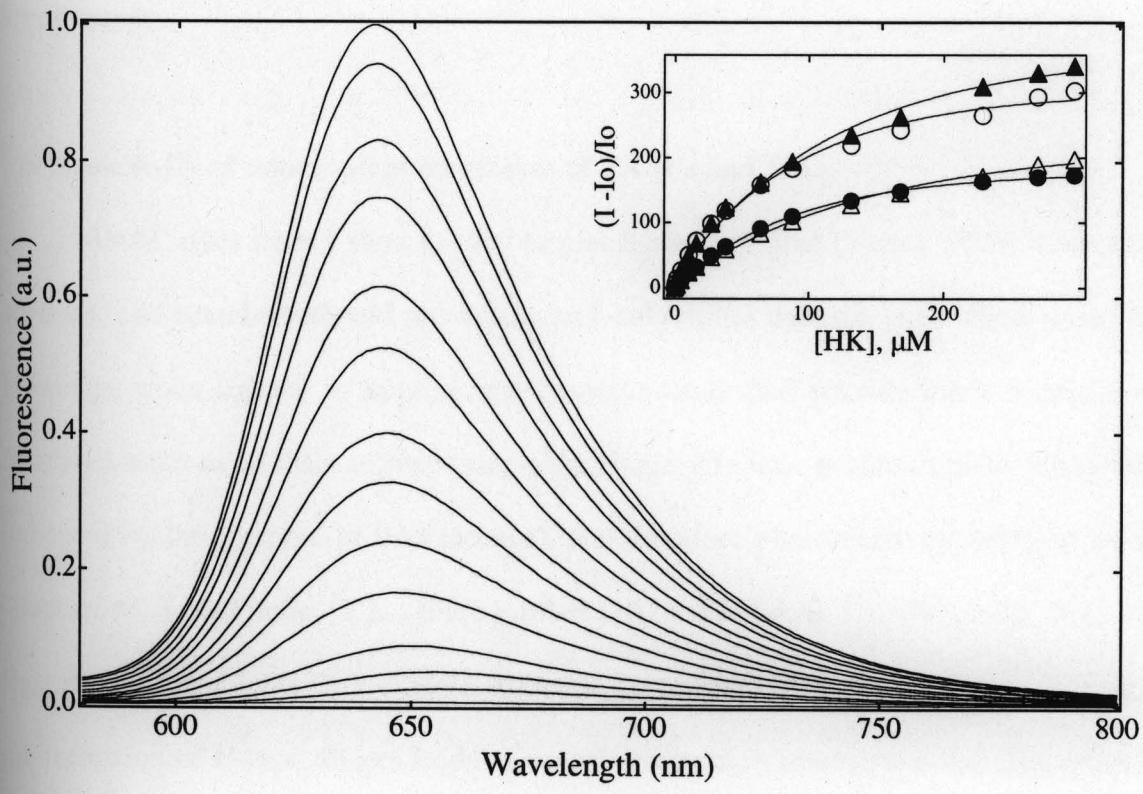

Figure 6.7 Effect of HK on the fluorescence spectrum of EV^+. From the bottom, in order of increasing fluorescence at the HK concentrations were (μM): 0.0, 4.65, 16.1, 27.2, 37.9, 87.8, 131.5, 168, 229 and 269. The inset shows the corresponding fluorescence binding isotherms for all four dyes. I = fluorescence intensity in the presence of HK, Io = fluorescence intensity in the absence of HK. Water, pH 7.6; T= 25°C; $[TAM^+]$ = 10 μM. CV^+ - solid circles; EV^+ - open circles, VBR^+ - open triangles, $VPBBO^+$ - solid triangles.

complexes of TAM^+ dyes with macromolecules. While fluorescence spectroscopy is appropriate to characterize the HK-dye monomer complexes, it is of limited use for the detection of HK-dye dimer complexes, which can be conveniently detected using electronic spectroscopy.

Photoreactivity of noncovalent complexes of TAM^+s and HK:

TAM^+ dyes have a short excited singlet lifetime (1-5ps) (Vogel, 1985) when free in solution, and therefore should not induce any substantial damage under these conditions. However, when located in binding microenvironments that provide steric restrictions to rotational motions of their aromatic rings, the singlet life time is substantially enhanced (as indicated by the increase in fluorescence), and therefore photoreactivity tends to increase (Baptista M. S. and Indig, G. L., 1998; Bartlett J. A. and Indig, G. L., 1999; Indig G. L. 1997; Baptista M. S. and Indig G. L., 1997). Besides, as predicted by the molecular exciton theory, the formation of H-type dimers leads to an enhancement in intersystem crossing efficiency and this typically should lead to enhanced photoreactivity (Kasha M. et al, 1965). Thus the photoreactivity of TAM^+ dyes when bound as monomers and aggregates to a biopolymer could be substantially different.

In order to explore how the formation of TAM^+ aggregates may affect the photoinduced inactivation of the enzymatic activity, samples representing a concentration regime of HK and dye that favors maximum formation of dimers on the enzyme template (lower solid curves in Figure 6.1) were subjected to photolysis. Photolysis was carried out at different time intervals and enzyme activity measured immediately after photolysis. There was no dark inhibition of the enzymatic activity for the time period of the experiment as

suggested by parallel controls in the dark with samples containing enzyme and dye in similar concentration regimes as in the photolysed samples.

Figure 6.8 shows some of the enzyme activity curves obtained with HK-TAM^+ complexes when photolysed and when kept in the dark. As mentioned in the experimental section the absorbance at 340 nm (formation of β–NADPH) plotted as a function of time can be used to measure enzyme activity. The slope of the initial linear portion of the curves gives an estimate of the rate constant. Rate constants for each such curve were thus estimated and used to obtain relative values of enzyme activity.

Under conditions of maximal TAM^+ aggregation, (Figure 6.1–bottom solid curves), the correlations observed between dye photobleaching and biopolymer damage suggest that the higher the degree of aggregation of a particular TAM^+ dye, the lower the photoinduced damage inflicted on the host enzyme (Figure 6.9). The binding experiments or spectrophotometric titrations suggested that among the four dyes the aggregation tendencies decreased in the following order $VPBBO^+ > EV^+ > VBR^+ > CV^+$. The ability to induce photoinhibition of enzymatic activity however followed the opposite trend $CV^+ > VBR^+ > EV^+ > VPBBO^+$. The dyes displaying the highest levels of aggregation upon binding to HK, namely $VPBBO^+$ and EV^+, were the ones associated with the lowest inhibitory effects (28% and 25% respectively) towards enzymatic activity of HK. While these photosensitizers were extensively bleached upon laser irradiation, little damage was inflicted by them on the enzyme. On the other hand CV^+, the TAM^+ dye that displays minor aggregation tendencies upon biopolymer binding was the one that most efficiently inactivated the enzyme upon photolysis (47% inhibition).

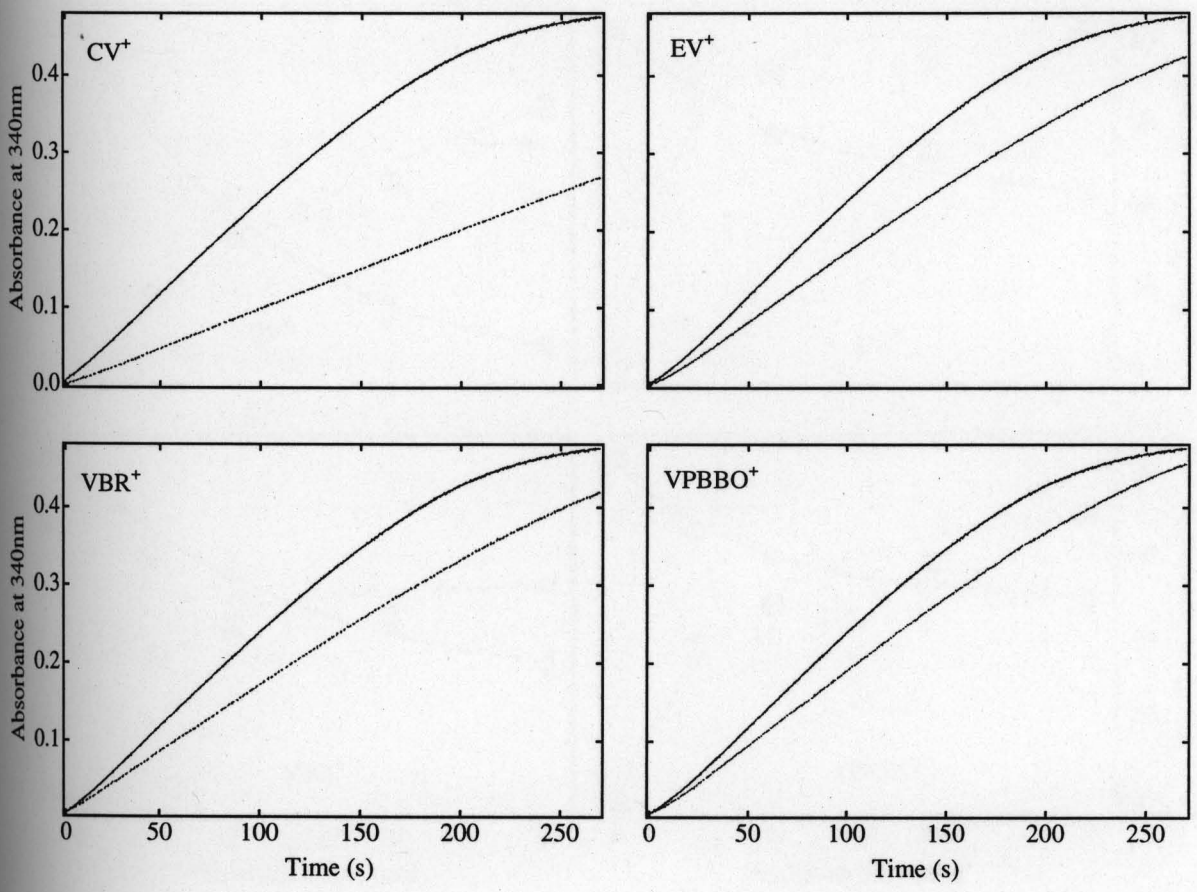

Figure 6.8 Enzyme activity assay monitoring the formation of β-NADPH at 340nm as a function of time. The solid lines represent controls, (HK + Dye in the dark and HK alone; superimposed lines). The dotted lines represent photolysed samples. [HK] = 4μM, [TAM^+] = 10μM, pH = 7.6, T = 30°C. Laser excitation at 532 nm, 10 Hz, 180 mJ/pulse.

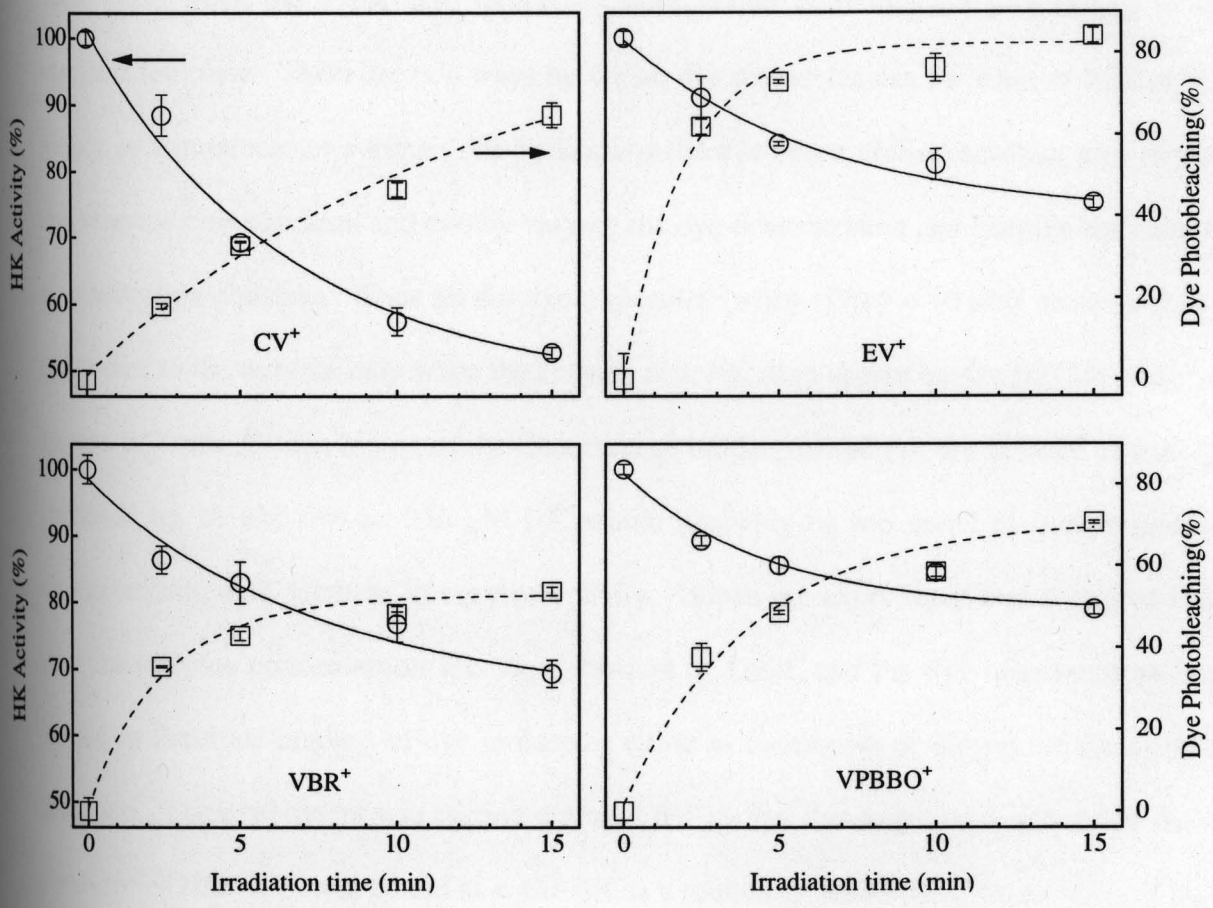

Figure 6.9 TAM^+ photobleaching (right axis; dashed lines) and decrease in HK enzymatic activity (left axis, solid lines) upon photolysis of HK-TAM^+ noncovalent complexes. Laser excitation at 532 nm, 10 Hz, 180 mJ/pulse. Tris buffer 50 mM, pH 7.6; T ≈ 22 ± 2 °C; [TAM^+] = 10 μM, [HK] = 4.0 μM.

To gain further evidence on whether dye aggregates decrease the efficiency of HK damage, a comparative evaluation of the extent of photoinhibition of HK activity was measured, when the TAM^+ dye molecules were bound as monomers and dimers to the enzyme template. There are two ways by which dye molecules can be made to bind to HK either as a monomer or a dimer, one by keeping the dye concentration constant and varying the enzyme concentration and two by varying the dye concentration and keeping the enzyme concentration constant. Since all the dye molecules (when [Dye] = 10 μM) are bound as a monomer to the enzyme only when the enzyme concentration approximates 250 μM (Inset of Figure 6.7 - the plateau region of the fluorescence binding isotherm), the amount of damage inflicted by 10 μM dye on 250 μM HK would probably be too small to permit precise characterization of decrease in enzyme activity. Hence the experiment was designed such that the enzyme concentration was kept constant at 4 μM, and the dye concentration was varied to facilitate binding of dye molecules either as monomers or dimers on the enzyme template. The experiment was carried out with EV^+, a dye that aggregates efficiently in the presence of HK. EV^+ was bound to 4 μM HK as a monomer, when the concentration of EV^+ was 2 μM and as a dimer when the concentration of EV^+ was 10 μM. The insets of Figure 6.10 show the spectral signatures of the dye in the presence of HK at the above-mentioned concentrations. The number of dye molecules required to bring about 13% inhibition was approximately $1.4*10^{16}$ when the dye was bound as a dimer, but as a monomer 14% inhibition of enzyme activity was achieved with the consumption of only $3.1*10^{15}$ dye molecules (Figure 6.10). Since the payload of dye molecules required to bring about an approximately similar extent of photoinhibition is substantially higher when the dye is bound as a dimer, it indicates that the dimer is inefficient compared to the monomer at

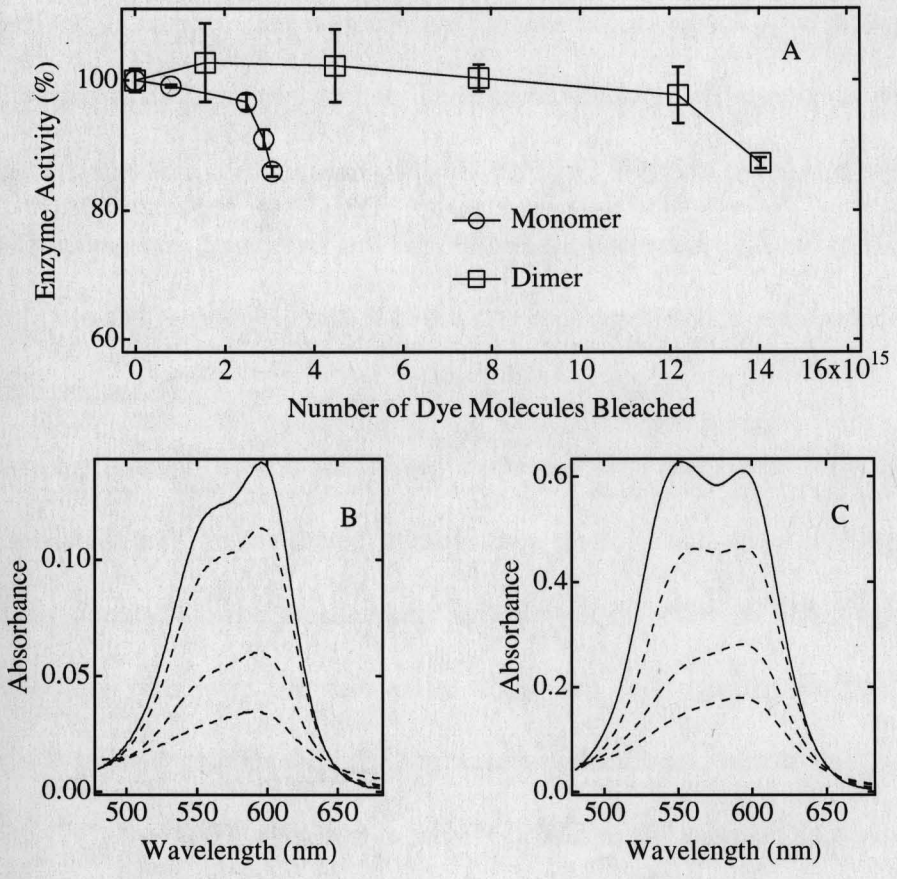

Figure 6.10 Decrease in HK enzymatic activity upon photolysis of HK-EV^+ noncovalent complexes (Panel A). Laser excitation at 532 nm, 10 Hz, 100 mJ/pulse. Tris buffer 50 mM, pH 7.6; T ≈ 22 ± 2 °C; [HK] = 4.0 μM. Panels B and C show the spectral changes upon photolysis of HK-EV^+ complexes when EV^+ is bound to HK as a monomer (Panel B; [EV^+] = 2μM) and dimer (Panel A; [EV^+] = 10μM) respectively.

inducing HK damage. Also as shown in Panel C of Figure 6.10, the spectra obtained upon photobleaching indicate that with decrease in dye concentration upon photolysis the dye begins to bind primarily as a monomer to the enzyme template. The point at which damage to HK begins (in the case of the dimer) closely parallels with the point at which substantial dye molecules have been consumed and mostly dye monomers are bound to HK. This adds further impetus to the hypothesis that it is the dye monomer that is responsible for most of the observed damage.

Thus as predicted by the molecular exciton theory dyes that form aggregates or dimers are indeed more photoreactive, because they photobleach more efficiently, but such photobleaching occurs through mechanisms that are not effective in inducing HK damage. The dye molecules that form the composite dimer are destroyed in the process, leaving behind little dye to react directly with the host macromolecule and induce damage. However, in the case of CV^+, the TAM^+ dye that is largely bound to the enzyme as a monomer at the concentration regime under consideration, because of its close proximity to the enzyme, it can involve itself in photoinduced electron transfer events with the host macromolecule that ultimately bring about inhibition of enzymatic activity.

Previous experiments conducted in this lab with BSA-TAM^+ complexes have shown that TAM^+s are capable of photoprotease activity (Baptista M. S. and Indig G. L., 1998). Upon 532 nm photolysis of BSA-TAM^+ complexes two protein fragments were formed, each weighing 8.5kDa and 58kDa respectively. To explore whether an analogous photofragmentation process would explain the inhibitory effects observed towards HK, the photolysed HK-TAM^+ complexes were subjected to SDS polyacrylamide gel electrophoresis. However the HK migration pattern in SDS-PAGE was exactly the same for the photolysed

([HK] = 4μM, [TAM^+] = 10μM) and control (neither dye nor light) HK samples (Figure 6.11). Though a slight fading of bands was observed in the photolysed samples, especially for CV^+, no new band was detected. These results suggest that the decrease in enzyme activity cannot be attributed to any photoprotease activity, with this activity understood as cleavage of the macromolecule in large (detectable) fragments.

While the gel electrophoresis experiments did not bring about any information on the nature of photoinduced damage of HK mediated by TAM^+ dyes, evidence on structural changes that are likely to be associated with the observed inhibitory effects were obtained using fluorescence spectroscopy. Using CV^+ as a representative TAM^+ dye, it was observed that the 532 nm photolysis of HK-TAM^+ complexes leads to a decrease in the fluorescence band attributed to the tryptophan and tyrosine residues present in the protein (excitation at 280 nm, emission maximum at 334nm). This decrease in fluorescence intensity (Figure 6.12 – Panel A) occurs in parallel with a small shift of the emission band to the red region of the spectrum. For the HK-CV^+ complex, after 15 minutes of irradiation, a 7 nm bathochromic shift was observed, along with a 25% decrease in the intensity of this band. This behavior is typically associated with conformational changes in polypeptides where one or more tryptophan residues originally buried in hydrophobic macromolecular environments are exposed to the bulk aqueous media (Lakowicz J. R., 1999, Kim J. S. and Kim H., 1996).

Fluorescence spectroscopy also provided a second line of evidence on the structural damage of HK mediated by TAM^+ dyes. The intensity of the fluorescence band observed at 450 nm when HK is excited at 360 nm was found to increase fivefold upon 532 nm photolysis in the presence of CV^+ (Figure 6.12 – Panel B). This increase in fluorescence

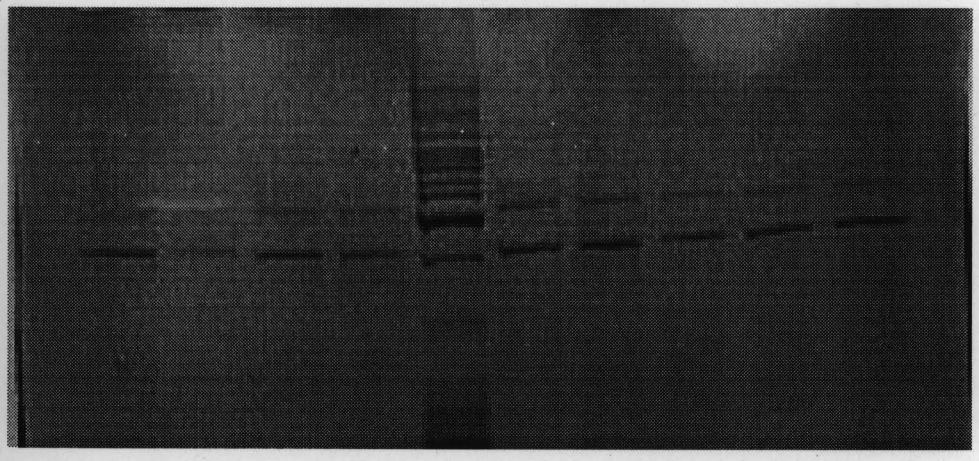

Figure 6.11 Picture of SDS polyacrylamide gel that was run to detect protein fragmentation. From the extreme left samples are represented as follows: Lane 1- CV^+ + HK ; Lane 2 - CV^+ + HK + light; Lane 3 - EV^+ + HK ; Lane 4 - EV^+ + HK + light; Lane 5 – Molecular weight marker ; Lane 6 - HK; Lane 7 – VBR^+ + HK; Lane 8 - VBR^+ + HK + light ; Lane 9 – $VPBBO^+$ + HK; Lane 10 - $VPBBO^+$ + HK + light.

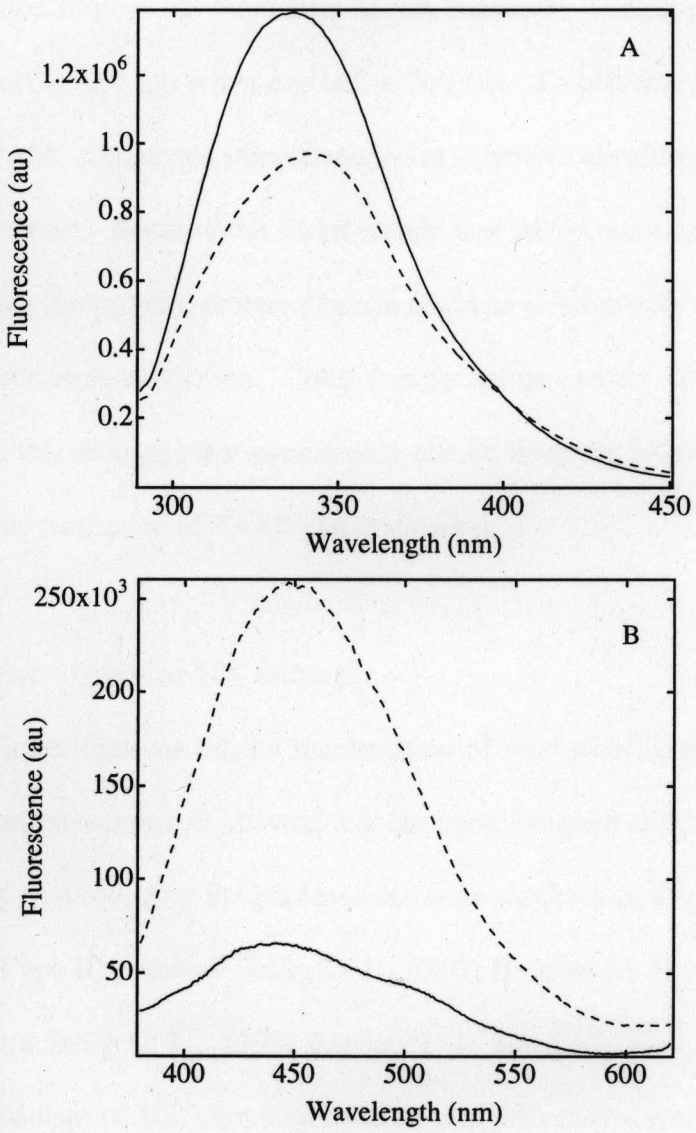

Figure 6.12 Evidence for photodamage in HK using fluorescence spectroscopy. Samples were excited at 280 nm to detect changes in Tryptophan fluorescence (Panel A) and at 360nm to detect increase in fluorescence at 450 nm (Panel B). The solid line represents control (HK + dye in the dark), the dashed line represents photolysed sample. Samples were photolysed using the 532 nm line of a Nd:YAG laser operating at 10 Hz, (180 mJ/pulse). Tris buffer 50 mM, pH 7.6; T = 22 ± 2 °C; [TAM^+] = 10 μM, [HK] = 4.0 μM, Photolysis time = 15 minutes.

cannot be attributed to possible formation of low molecular weight photoproducts that coincidentally emit at 450 nm when excited at 360 nm. To test this possibility, photolysed samples of HK-TAM^+ complexes were subjected to extensive ultrafiltration using fresh buffer as replacement solvent. Because the fluorescence was still present in the final resuspended fractions containing the protein, protein damage could be satisfactorily identified as the actual cause of the fluorescence at 450 nm. Control experiments carried out in the absence of dye also indicate that this damage, that presumably results from the oxidation of an amino acid residue requires the mediation of TAM^+ dye to develop.

Effect of molecular oxygen on HK damage:

Previous investigations on the mechanisms of photosensitization of TAM^+ dyes in complex biological environments showed that the photodynamic effects observed with these dyes are primarily controlled by the photosensitization mechanism Type I, rather than by the singlet oxygen, (Type II) pathway (Indig G. L., 1997; Baptista M. S. and Indig G. L., 1997; Baptista M. S. and Indig G. L., 1998; Bartlett J. A. and Indig G. L., 1999). To explore whether the mechanism of HK photoinactivation was primarily controlled by a free radical process, a comparative evaluation of the degree of macromolecular damage mediated by CV^+ in two different media, viz. buffered D_2O and aqueous buffer was carried out. In addition the degree of HK damage was also compared in air equilibrated and nitrogen purged samples. Because the lifetime of singlet oxygen is approximately seven fold longer in D_2O than in water (Rodgers M. A., 1982), the role of singlet oxygen in processes that take place in aqueous solution is typically amplified when water is replaced by D_2O as the reaction medium. The replacement of water by D_2O, lead to a decrease in the efficiency with which

CV^+ mediates the inactivation of HK. Under the experimental conditions described in the legend of Figure 6.13, after 15 minutes of photolysis of the HK-CV^+ complex, the inactivation was twofold higher in water than in D_2O (Figure 6.13). Because the absorption spectra of HK-CV^+ complexes were identical both in water and in D_2O, the differences observed in HK damage cannot be attributed to differences in the efficiency with which CV^+ binds to HK in these two different solvents. Along the same lines, the levels of dye photobleaching in water was equivalent to that observed in the case of D_2O, and therefore the observed results cannot be attributed to differences in bleaching efficiencies of CV^+ in the two different media. Interestingly, the twofold increase in inhibition of HK activity in water as compared to D_2O suggests that the mechanism of HK damage may be controlled by a proton coupled electron transfer event (Shafirovich V. et al, 1999; Shafirovich V. et al, 1995; O'Connor D. et al, 1994).

CONCLUSIONS:

Studies on the binding of TAM^+s to HK using spectrophotometric titrations revealed that under conditions of high biopolymer loading ([Dye] > [HK]), the formation of dye aggregates is assisted by the enzyme even when the dye concentration in solution is at the micromolar range. HK-assisted dimer formation is particularly efficient with the ethyl substituted TAM^+s, namely EV^+ and $VPBBO^+$. The tendency to aggregate decreases in the following order $VPBBO^+ \geq EV^+ > VBR^+ > CV^+$. The remarkable increase in fluorescence upon binding of TAM^+s to HK indicates that the dye finds itself in a binding environment in which the fast rotational relaxation processes are sterically hindered. This implies that there

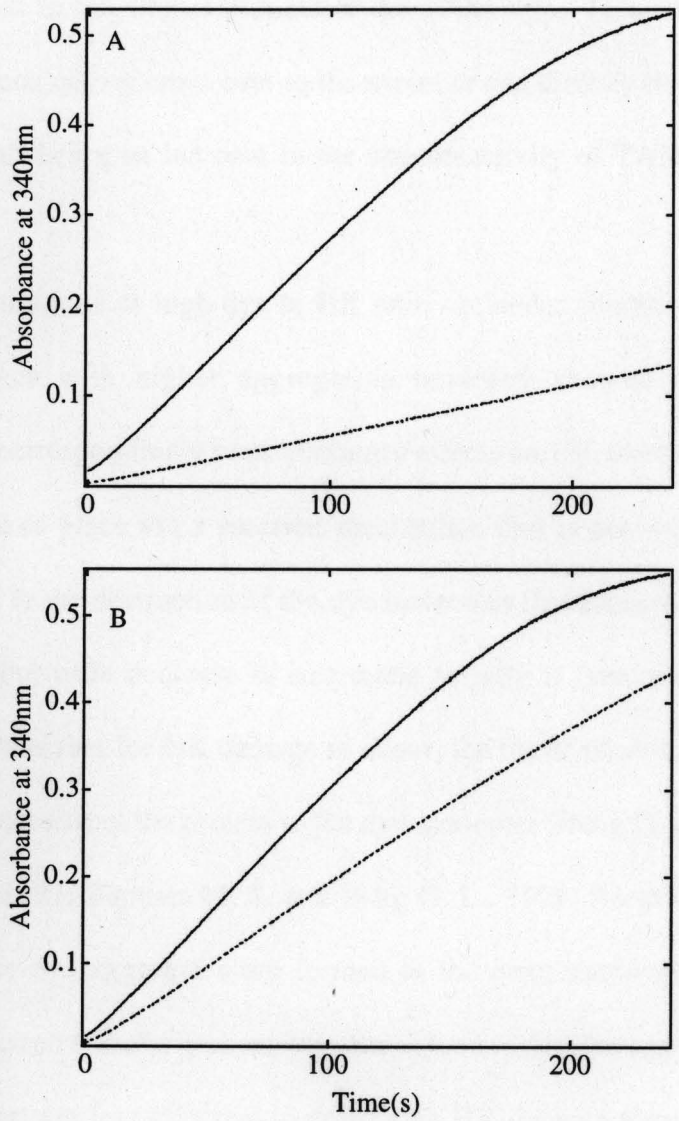

Figure 6.13 Decrease in HK enzymatic activity upon photolysis of HK-CV^+ noncovalent complexes in buffered water (Panel A) and D_2O (Panel B). The solid line represents control (HK + dye in the dark), the dotted line represents photolysed sample. Laser excitation at 532 nm, 10 Hz, 100 mJ/pulse. Tris buffer 50 mM, pH 7.6; T ≈ 22 ± 2 °C; [HK] = 4.0 μM; [CV^+] = 10μM, Photolysis time = 15 minutes.

is an enhancement in the singlet lifetime of the TAM^+ dye. This long-lived singlet can therefore either intersystem cross over to the triplet or can directly interact with the substrate, with the net result being an increase in the photoreactivity of TAM^+s when noncovalently bound to HK.

Under conditions of high dye to HK ratio i.e. under conditions of maximum TAM^+ dimerization, dyes with higher aggregation tendency showed higher photobleaching efficiencies, but correspondingly poor inhibitory effects on HK activity. The photobleaching of dye dimers takes place via a reaction mechanism that is not effective in inducing HK damage. It leads to the destruction of the dye molecules that form the composite dimer with high efficiency, but little decrease in enzymatic activity is concomitantly observed. This observation suggests that for HK damage to occur, the initial photoinduced electron transfer event must take place from the protein to the dye monomer (Indig G. L., 1997; Baptista M. S. and Indig G. L., 1997; Baptista M. S. and Indig G. L., 1998; Bartlett J. A. and Indig G. L., 1999). When the dye aggregates are formed in the macromolecular template, the initial photoinduced electron transfer presumably takes place within the aggregate to produce a pair of dye radicals that are less effective in promoting HK damage than the hole created in the host macromolecule by abstraction of one electron by the excited monomer. The ability to induce photoinhibition of enzymatic activity therefore followed the trend $CV^+ > VBR^+ > EV^+ \geq VPBBO^+$, which is opposite to the trend observed for dye aggregation ($CV^+ < VBR^+ < EV^+ \leq VPBBO^+$).

Although there was no apparent evidence for protein fragmentation, evidence for structural damage in protein was obtained in protein using fluorescence spectroscopy. Photoinduced inactivation of HK mediated by CV^+ can take place via oxygen independent

pathways. Evidence for this was obtained in comparative experiments involving air-equilibrated and nitrogen purged samples and in experiments in which the aqueous medium was replaced with D_2O.

Chapter 7. Binding of Triarylmethane Dyes to DNA and Photoreactivity of DNA-TAM^+ Noncovalent Complexes.

RESULTS AND DISCUSSION:

Binding Studies:

Spectrophotometric Titrations:

As in the case of HK in the preceding chapter, both electronic and fluorescence spectroscopy was used to characterize the binding of TAM^+s to DNA. Titrations were carried out in a similar manner in which the concentration of dye was kept constant at 10μM and the concentration of DNA (titrant) was increased in small increments. Figure 7.1 shows the effect of DNA concentration on the absorption spectrum of the TAM^+s. Initial increases in DNA concentration up to the 20μg/ml range resulted in a decrease in maximum dye absorption along with a simultaneous pronounced blue shift in the absorption spectrum. Further increments in DNA concentration (beyond 20μg/ml) resulted in an increase in absorption at the original wavelength of maximum absorption of the dye free in solution (dashed curves in Figure 7.1). A plot of absorbance values at the λ_{max} of the dye when free in solution as a function of DNA concentration resulted in a biphasic profile (Figure 7.2). Though the effect of DNA on the absorption spectra of TAM^+ dye is analogous to that of HK, substantially larger spectroscopic shifts were observed in the case of EV^+ and $VPBBO^+$ in the presence of DNA than in the case of HK (compare Figures 6.1 and 7.1).

As predicted by the molecular exciton theory the formation of trimers and other H type TAM^+ aggregates, should lead to larger hypsochromic shifts in the absorption spectra of

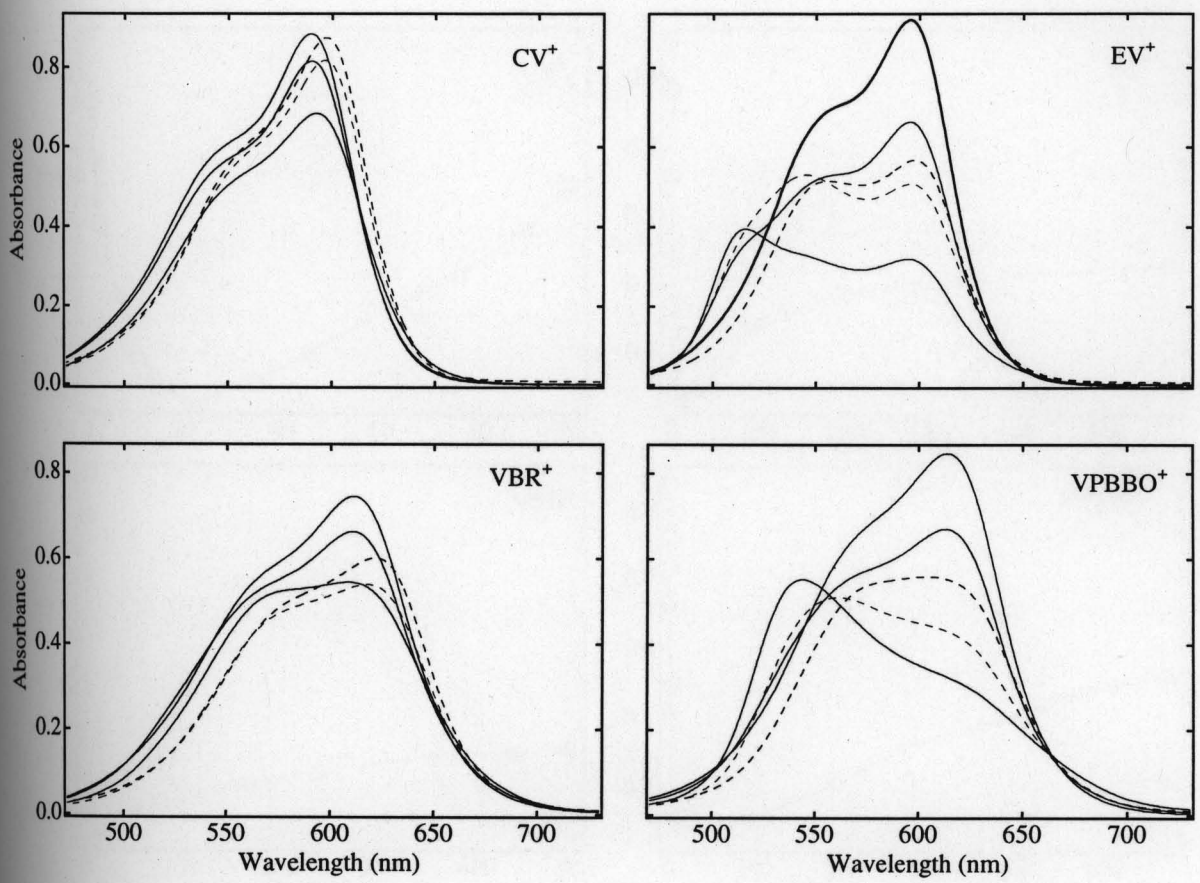

Figure 7.1 Effect of DNA on the absorption spectra of TAM^+ dyes. From the top, in order of decreasing absorption at λ_{max} (solid lines) the DNA concentrations were (μg/ml): 0.0, 0.6, 20. From the bottom starting at the dashed lines, in order of increasing absorption at λ_{max}, the DNA concentrations were (μg/ml): 100, 400. Phosphate buffer 10 mM, pH 7.3; T = 25°C; $[TAM^+]$ = 10 μM.

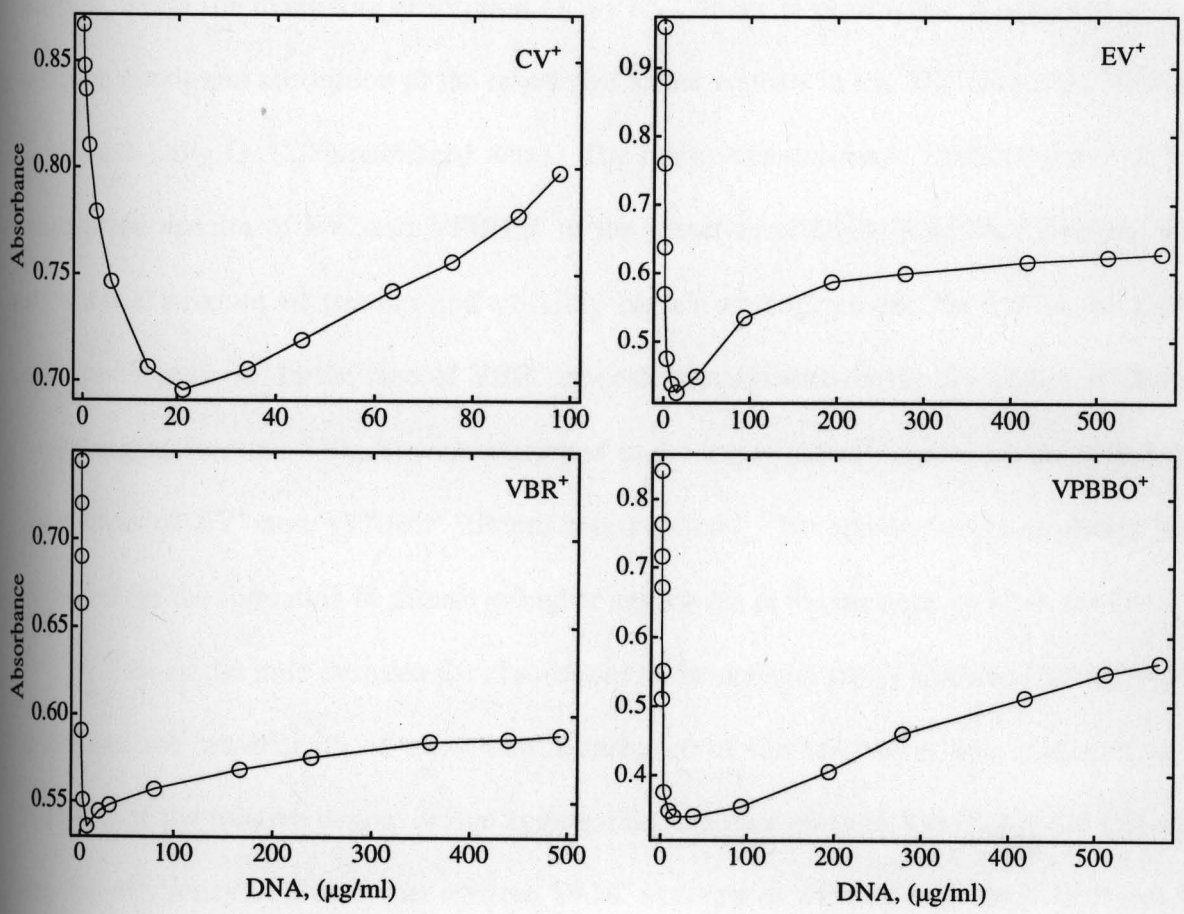

Figure 7.2 Plots of absorbance values at the λ_{max} of the dye, as a function of DNA concentration. Data obtained from titrations carried out in Figure 7.1.

these dyes, as compared to the shifts observed upon dimerization (Kasha M. et al, 1965). Indeed, while the maximum absorption of the EV^+ dimer in pure water is observed at 538 nm, the maximum absorption of the respective trimer appears in the 520 nm region (Bartlett J. A. and Indig G. L., unpublished data). The larger hypsochromic shifts observed in the absorption spectra of EV^+ and $VPBBO^+$ in the presence of DNA indicates therefore, that substantial amount of trimers and possibly higher aggregates are formed in the DNA microenvironment. In the case of VBR^+ modest enhancements in the absorption at shorter wavelengths (around 520nm) were observed under experimental conditions in which the formation of EV^+ and $VPBBO^+$ trimers was maximal. No spectroscopic evidence was obtained for the formation of trimers or higher aggregates in the presence of DNA for CV^+.

Taking the ratio between the absorbance at the wavelength of the blue shifted TAM^+ band and the wavelength of maximum absorbance of the respective dye monomer as a measure of the relative degree of dye aggregation, the data presented in Figure 7.3 indicate that the efficiency of biopolymer assisted TAM^+ aggregation mediated by DNA decreases in the following order: $VPBBO^+ > EV^+ > VBR^+ > CV^+$. This order is analogous to the trend observed for the relative efficiencies with which these dyes aggregate upon increasing their concentration in pure water (Bartlett J. A. and Indig G. L., unpublished data). Those showing higher lipophilic character like the ethyl substituted EV^+ and $VPBBO^+$ show higher aggregation tendencies than those showing lower lipophilic character, the methyl substituted CV^+ and VBR^+. The binding data obtained with spectrophotometric titrations was also plotted using the mole ratio method (Figure 7.4).

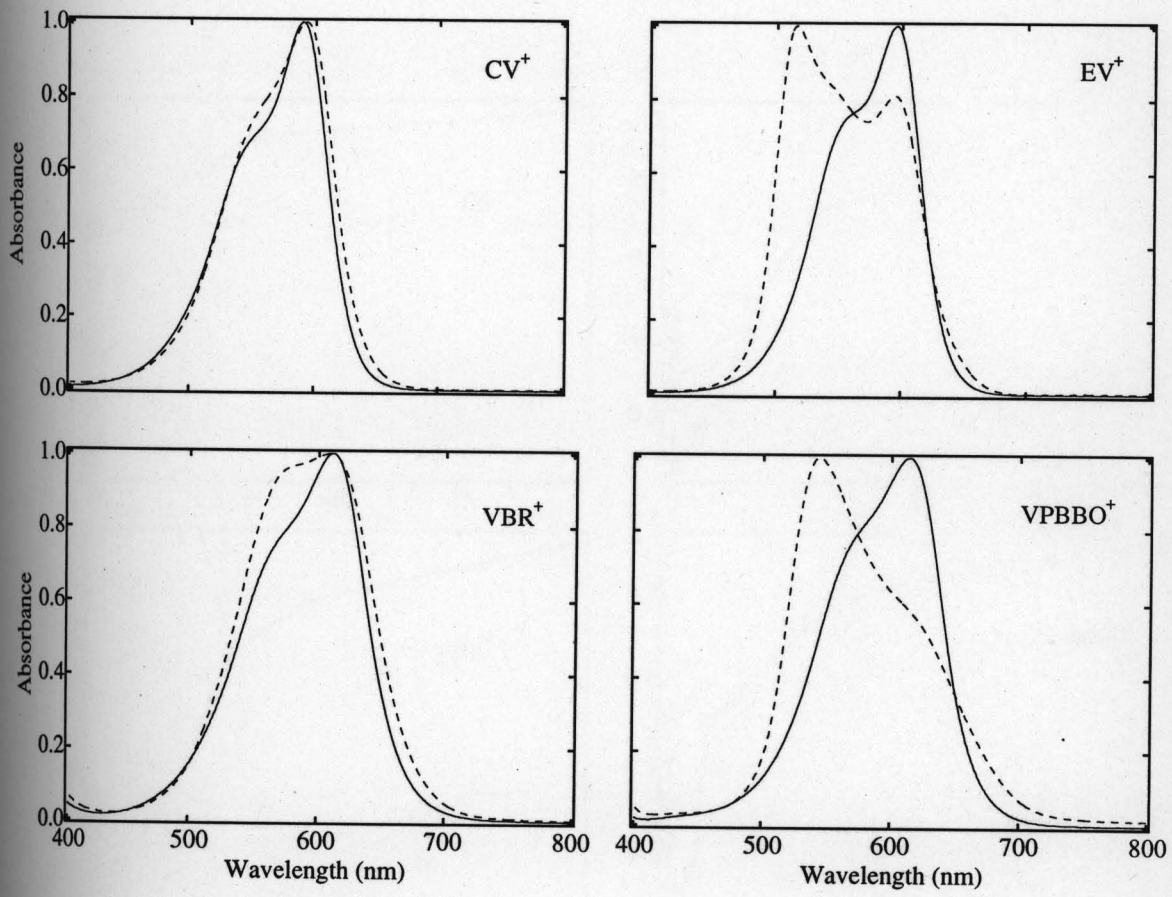

Figure 7.3 Normalized absorption spectra of TAM^+ dyes, in the absence (solid lines) and in the presence of 20μg/ml (dashed lines). The solid line represents the spectrum of the dye in the absence of DNA. The dashed line represents the spectrum of the dye in the presence of 20μg/ml DNA. Phosphate buffer, 10 mM, pH 7.6; T = 25°C; $[TAM^+]$ = 10 μM.

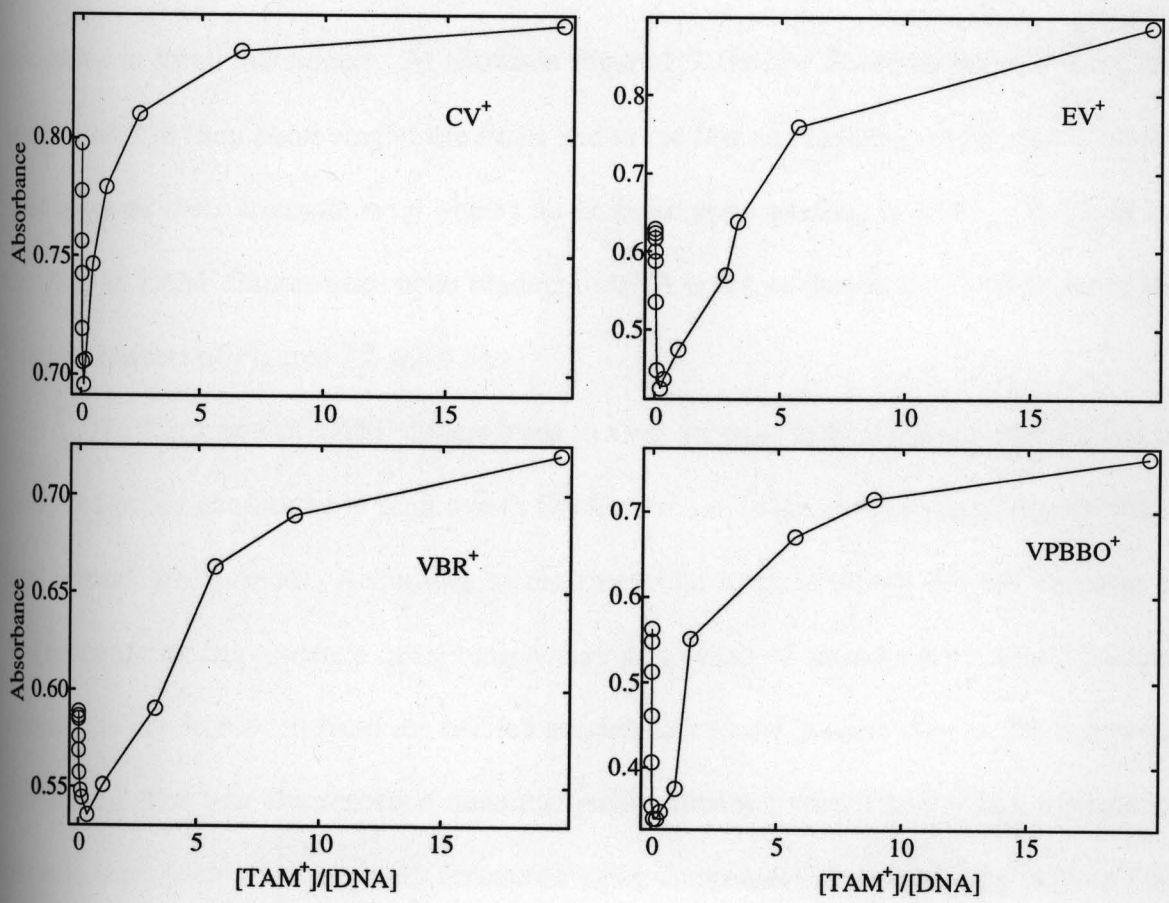

Figure 7.4 Plots of absorbance values at the λ_{max} of the TAM^+ dye, as a function of mole ratio of the concentration dye to DNA. Phosphate buffer 10 mM, pH 7.3; T = 25°C; $[TAM^+]$ = 10 μM. To calculate the molar concentration of DNA an extinction coefficient of 6600 M^{-1} cm^{-1} per nucleotide at 260 nm was used (Minchin R. F., 1987).

Fluorescence Titrations:

Fluorescence spectroscopy was used to characterize the binding of TAM^+s to DNA. The concentration of TAM^+ was kept constant at 10μM and the concentration of DNA was increased in small increments. As shown in Figure 7.5, the low fluorescence of TAM^+s, that is attributed to their short singlet life times and to the fast non radiative rotational relaxation processes of their aromatic rings shows an increase upon binding to DNA. However the increase in TAM^+ fluorescence upon binding to DNA is not as enhanced as in the case of HK (compare insets of Figures 7.5 and 6.7).

The formation of TAM^+ dimers leads to a net decrease in fluorescence and this can be observed under conditions of high dye to DNA ratio, i.e. in the concentration regime where dye dimers are formed. According to the molecular exciton theory the net decrease in fluorescence or fluorescence quenching occurs as a result of formation of dimers because transitions are forbidden from the excited singlet state to the ground state in the composite molecule. The low fluorescence quantum yields obtained with TAM^+-DNA complexes permits the observation of dimer formation using fluorescence spectroscopy (Figure 7.6). This was however, not the case with HK-TAM^+ complexes because the fluorescence quantum yield was much enhanced, upon binding of a dye monomer to HK. Hence the small decreases in fluorescence due to dimer formation are hidden or buried under the large increases in fluorescence quantum yield.

In the case of CV^+-DNA complex, there is only a small imperceptible change in slope as seen in Figure 7.6, since CV^+ a dye that displays a minor aggregation tendency is bound to DNA largely as a monomer. For the other TAM^+ dyes, the fluorescence curves show a small initial dip and the fluorescence then increases steadily with increase in DNA concentration

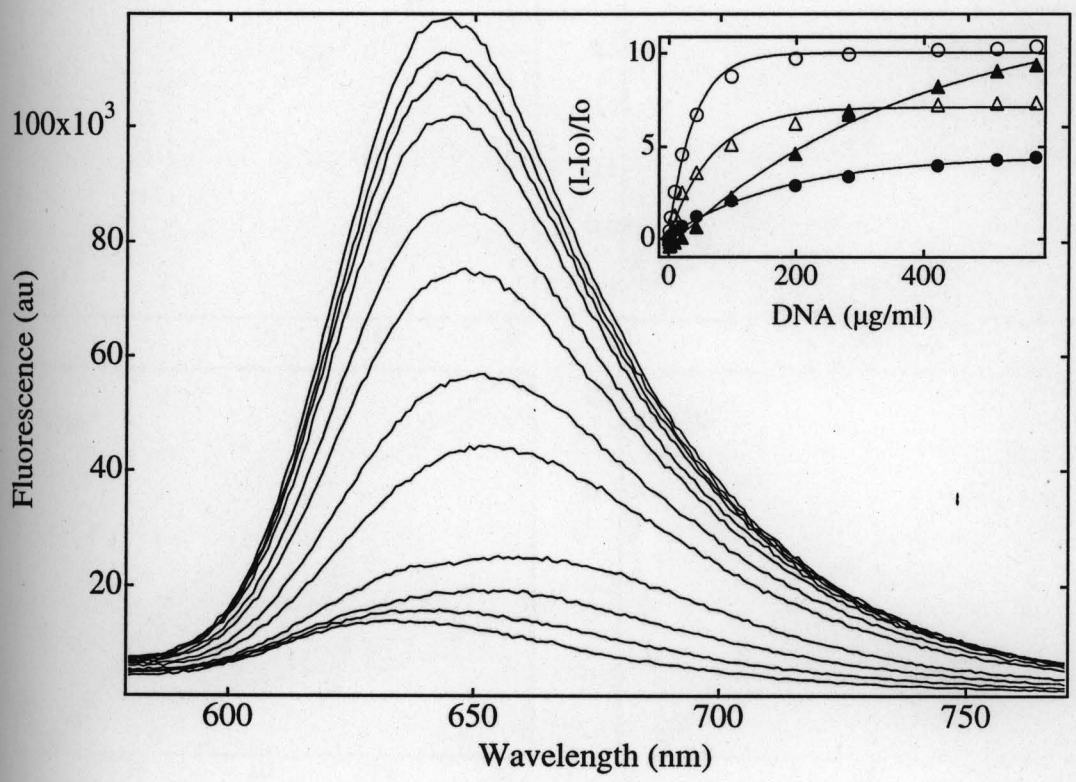

Figure 7.5 Effect of DNA on the fluorescence spectrum of CV^+. From the bottom in order of increasing fluorescence, the DNA concentrations (μg/ml) were: 0.0, 1.16, 2.81, 6.05, 13.9, 21.1, 34.2, 45.2, 63.5, 75.6, 83.8 and 97.86. The inset shows the corresponding fluorescence binding isotherms for all four dyes. I = fluorescence intensity in the presence of DNA, Io = fluorescence intensity in the absence of DNA. Phosphate buffer 10 mM, pH 7.3; T = 25°C; $[TAM^+]$ = 10 μM. CV^+ - closed circles; EV^+ - open circles, VBR^+ - open triangles, $VPBBO^+$ - closed triangles.

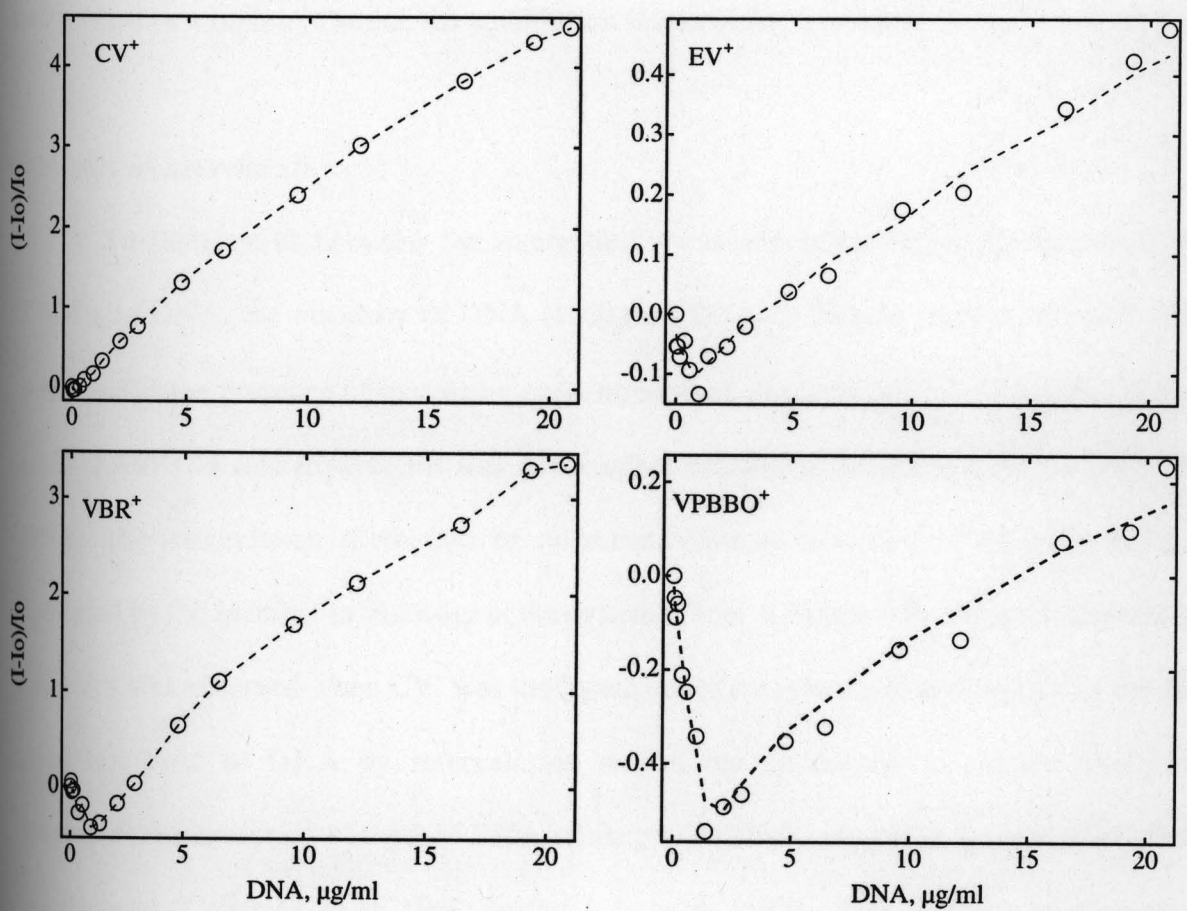

Figure 7.6 Effect of DNA on the fluorescence of TAM^+ dyes at high dye to DNA concentration ratios. I = fluorescence intensity in the presence of DNA, Io = fluorescence intensity in the absence of DNA. Phosphate buffer 10 mM, pH 7.3; T = 25°C; $[TAM^+]$ = 10 µM.

(Figure 7.6). The small initial dip represents the concentration regime in which dimers are formed or a region in which the equilibrium favors dimer formation.

Viscosity measurements:

To distinguish between the intercalative and non intercalative binding mode of TAM^+s to DNA, the viscosity of DNA (100μg/ml DNA or 303μM nucleotide bases) was measured in the presence of increasing concentration of ethidium bromide and CV^+. Use of other TAM^+s in this experiment was not feasible because of co-precipitation of dye and DNA. The intercalation of ethidium bromide resulted in an elongation of the DNA helix as indicated by the increase in viscosity of the system (Panel A-Figure 7.7). No such increase in viscosity was observed when CV^+ was the ligand under consideration, indicating that the dye does not bind to DNA by intercalation within the concentration regime explored. Intercalation increases the length of DNA, while groove binding typically has a smaller effect on viscosity (Cohen G. et al, 1969; Seifert J. L. et al, 1999). The helix lengthening ratio $L/Lo = (\eta/\eta o)^{1/3}$, was calculated from the viscometric data and plotted as a function of ligand to DNA ratio (Panel B – Figure 7.7), where L = helix length in the presence of ligand, Lo = Helix length in the absence of ligand, η = viscosity of DNA in the presence of ligand, ηo = viscosity of DNA in the absence of ligand. Previous reports on the binding of CV^+ to DNA have also concluded that crystal violet is a non-intercalating dye (Norden B. et al, 1977; Muller W. et al, 1975).

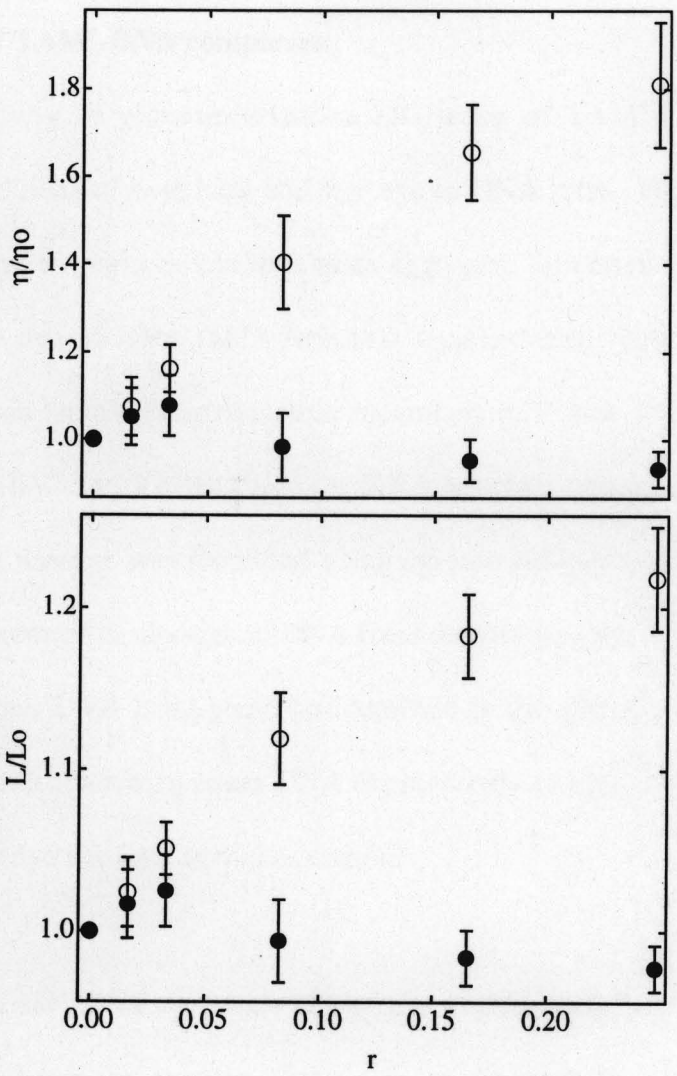

Figure 7.7 Viscometric analysis of DNA binding mode. Samples contained 100 μg/ml DNA in 10 mM phosphate buffer, pH = 7.6, T = 25°C. Aliquots of CV^+ and ethidium bromide were added to DNA in small increments. The ratio of dye to DNA is represented by r, and each data point is an average of five readings. L = helix length in the absence of ligand, Lo = helix length in the presence of ligand, η = viscosity of DNA in the presence of ligand, ηo = viscosity of DNA in the absence of ligand.

Photoreactivity of TAM^+-DNA complexes:

Photoreactivity or photosensitization efficiency of TAM^+-DNA complexes was studied under conditions of both high and low dye to DNA ratio. High dye to DNA ratios represent concentration regimes that maximize aggregate formation (lower solid curves in Figure 7.1). Low dye to DNA ratios represent concentration regimes in which the dye molecules have been largely redistributed as monomers (CV^+ and VBR^+) or monomers and lower aggregates (EV^+ and $VPBBO^+$) on the DNA template (upper most dashed curves in Figure 7.1). DNA damage was identified using agarose gel electrophoresis and quantified through the measurement of changes in DNA band density as a function of irradiation time. No new well-defined DNA band could be identified in the gel after photolysis. In these experiments solutions containing either DNA exposed only to light, only to dye (and kept in the dark) or neither dye nor light served as controls.

Photoreactivity of TAM^+-DNA complexes at high dye to DNA ratios:

Figure 7.8 shows the pictures of the gels for the four dyes, when their respective complexes with DNA were photolysed under conditions that facilitate TAM^+ aggregation. The dyes displaying the highest levels of aggregation upon macromolecular binding, namely $VPBBO^+$ and EV^+, were the ones associated with the lowest photonuclease activity towards DNA. This can be inferred from the right hand panels of Figure 7.8, since all lanes in the case of these two dyes show the presence of visible DNA. On the other hand in the case of CV^+, a continuous fluorescent streak appears in Lane 9, the lane representing a sample of CV^+-DNA subjected to five minutes of photolysis. From Lane 5 onwards the fluorescent streak fades and is difficult to capture photographically. This indicates that DNA has

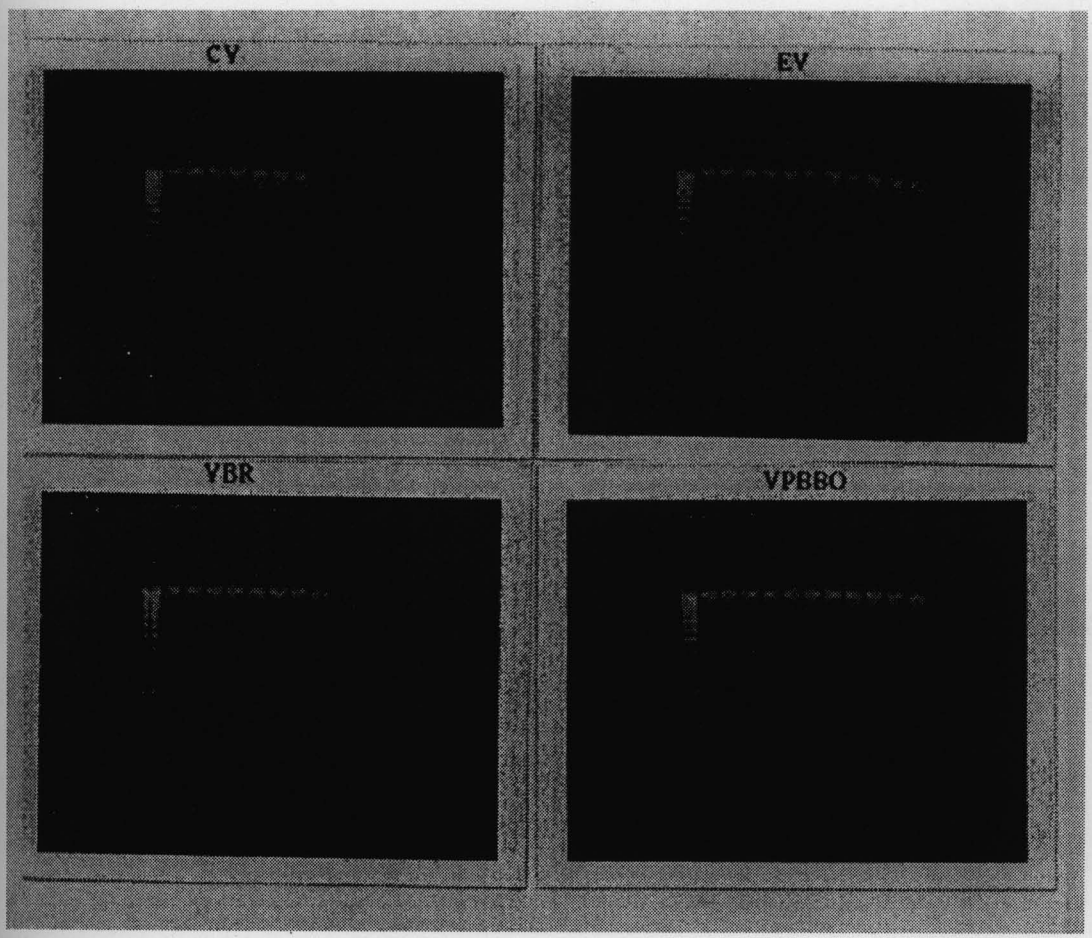

Figure 7.8 Pictures of agarose gels that were run to detect DNA damage. For each of the panels, lanes are represented as follows from the extreme left of each gel: Lane 1- DNA marker; Lane 2 - DNA; Lane 3 - TAM^+ + DNA; Lane 4 - DNA + light; Lanes 5 to 12 - TAM^+ + DNA + light. The photolysis time points (in minutes) represented by each lane are as follows: Lane 5 – 0.5; Lane 6 - 1; Lane 7 – 1.5; Lane 8 – 2.0; Lane 9 –5; Lane 10 –10.0; Lane 11 –15.0 and Lane 12 - 30.

undergone extensive double strand cleavage. The same fluorescent streak appears in Lane 11 for VBR^+, a lane that represents a sample of VBR^+-DNA subjected to fifteen minutes of photolysis.

The correlation observed between dye photobleaching and DNA damage suggest that higher the degree of aggregation of a particular TAM^+ dye, the lower the photoinduced damage inflicted by this dye on the host macromolecule (Figure 7.9). While EV^+ and $VPBBO^+$, dyes that form trimers and higher aggregates were extensively destroyed upon laser irradiation, little damage was inflicted by them on DNA, in a manner analogous to that observed in the case of HK. Once again, CV^+, the dye displaying minor aggregation tendencies upon biopolymer binding was the one that most efficiently inflicted DNA damage.

Photoreactivity of TAM^+-DNA complexes at low dye to DNA ratios:

Photoreactvity of TAM^+-DNA complexes was also evaluated in the concentration range where dye molecules are redistributed as monomers (CV^+ and VBR^+) and as monomers or dimers plus lower aggregates (EV^+ and $VPBBO^+$) on the DNA template (10μM dye and 400μg/ml DNA) and the spectra obtained under these conditions are the topmost dashed curves in Figure 7.1. DNA damage was assessed in a similar manner as described previously.

Table 7.1 tabulates the comparative evaluation of the four dyes with respect to their photobleaching efficiency and photonuclease activity, when bound as monomers and aggregates. When EV^+ is bound as an aggregate to the DNA template, a 77.3% dye bleaching leads to 4.9 μg/ml DNA damage, but when bound as a monomer or a lower

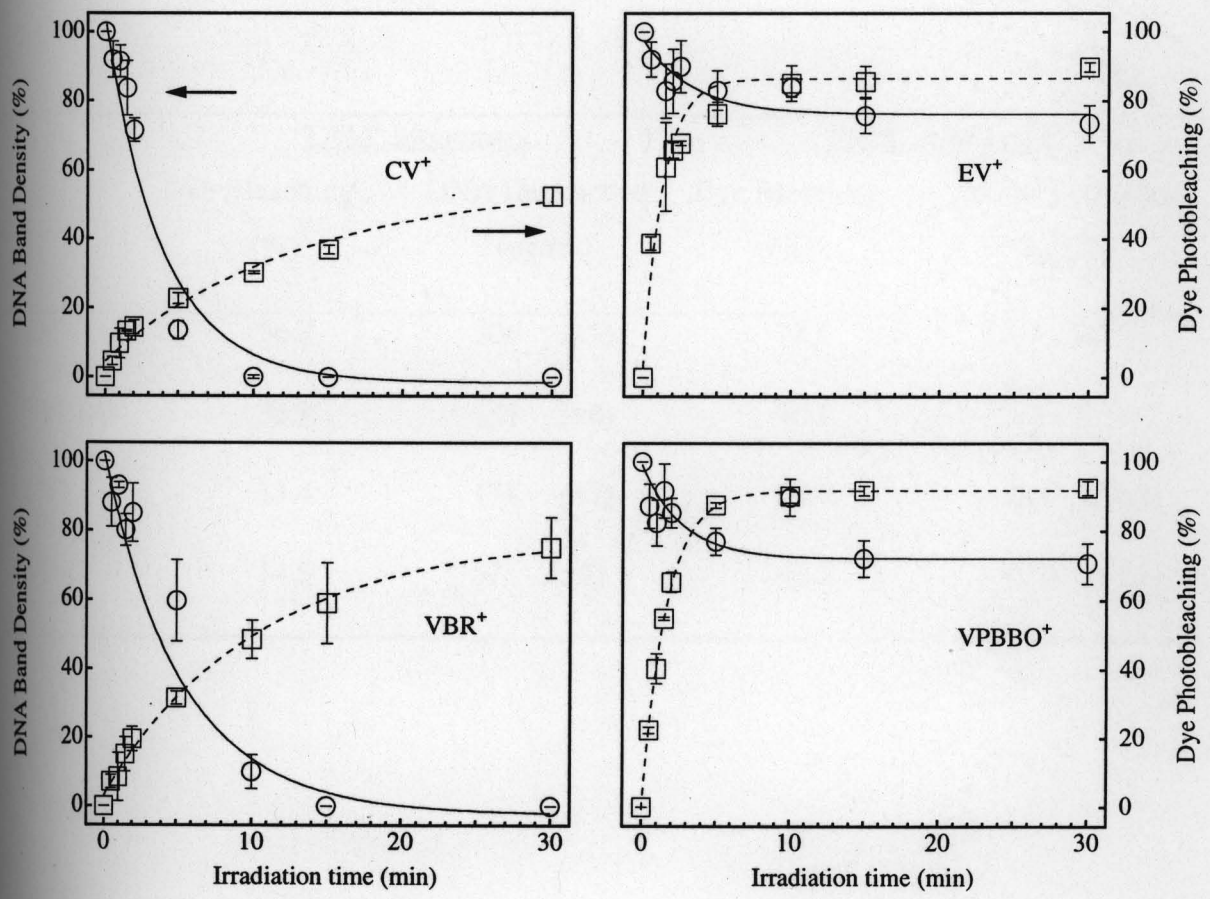

Figure 7.9 TAM^+ photobleaching (right axis; dashed lines) and decrease in DNA band density (agarose gel electrophoresis; left axis, solid lines) upon photolysis of DNA-TAM^+ noncovalent complexes. Laser excitation at 532 nm, 10 Hz, 180 mJ/pulse. Phosphate buffer 10 mM, pH 7.3; T = 22 ± 2 °C; [TAM^+] = 10 μM, [DNA] = 20 μg/ml.

	[a]TAM^+ Monomers		[b]TAM^+ Aggregates	
	Dye Bleaching (%)	DNA Destruction (μg/ml)	Dye Bleaching (%)	DNA Destruction (μg/ml)
EV^+	36.7	106 (±5)	77.3	4.9 (±0.3)
$VPBBO^+$	33.9	141 (±6)	85.1	2.2 (±0.1)
CV^+	13.4	174 (±7)	23.9	18.8 (±0.3)
VBR^+	14.5	57 (±2)	40.4	10.9 (±0.1)

Table 7.1 Comparative evaluation between TAM monomer and aggregates. Samples photolysed at 150 mJ/pulse for 10 minutes, Phosphate buffer 10 mM, pH = 7.6, T = 22 ± 2°C. [a]DNA-TAM^+ with dye bound as a monomer, [DNA] = 400 μg/ml, [TAM^+] = 10μM. [b]DNA-TAM^+ with dye bound as a monomer, [DNA] = 20 μg/ml, [TAM^+] = 10 μM.

aggregate to the DNA template, a 36.7% bleaching leads to 106 μg/ml DNA damage. In the case of $VPBBO^+$, a 85.1% bleaching leads to 2.2 μg/ml DNA damage when bound as a higher aggregate, but when bound as a dimer or a lower aggregate, a 33.9% bleaching leads to 141 μg/ml DNA damage. Thus the dyes when bound as monomers or lower aggregates are much more photoreactive than when bound as higher aggregates and the same trend is conserved with CV^+ and VBR^+. The table also indicates that under both these conditions CV^+ is the dye that exhibits maximum photonuclease activity.

To further confirm whether dye aggregation decreases the efficiency of DNA damage, additional experiments were carried out with EV^+ a dye that aggregates efficiently. The experimental strategy involved keeping the DNA concentration constant and varying the dye concentration. The various panels of Figure 7.10 show the spectral signatures of EV^+ obtained at different dye concentrations in the presence of 20 μg/ml DNA. With 10μM EV^+ the spectral signature is that of a higher aggregate, with 6μM EV^+ the signature is that of a mixture of trimers and dimers, with 3μM EV^+ the dye molecules are largely bound as monomers. The number of dye molecules bleached during the photolysis of these different complexes and the corresponding damage done to DNA is shown in Figure 7.10. To destroy approximately 40% of the initial DNA, the EV^+ trimer (and possibly higher aggregates) need $9.7*10^{15}$ dye molecules, while upon decreasing aggregation number the same degree of damage is observed after consumption of $1.6*10^{15}$ dye molecules (when the dye molecules are bound mostly as dimers), and $5.3*10^{14}$ dye molecules (when the dye is bound largely as monomers). It is once again very apparent that upon reducing the degree of dye aggregation, the number of dye molecules required to inflict photoinduced DNA damage decreases.

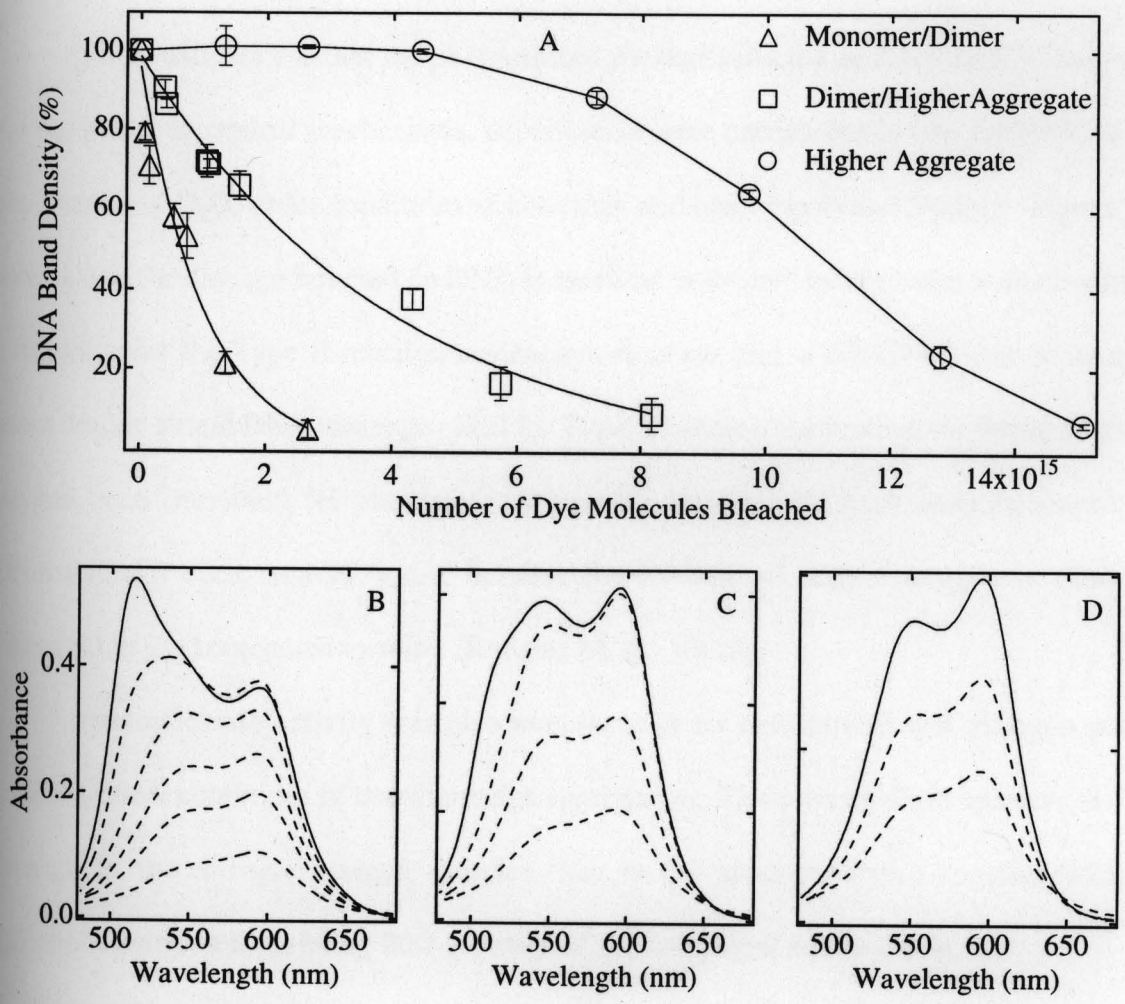

Figure 7.10 Decrease in DNA band density upon photolysis of DNA-EV^+ noncovalent complexes (Panel A). Laser excitation at 532 nm, 10 Hz, 100 mJ/pulse. Phosphate buffer 10 mM, pH 7.3; T = 22 ± 2 °C; [DNA] = 20 μg/ml. In panels B, C and D the solid lines represent the spectral signature of EV^+ under different aggregation regimes. Panel B - [EV^+] = 10 μM (presence of trimers and possibly higher TAM^+ aggregates); Panel C - [EV^+] = 6 μM (enrichment of dimers); Panel D - [EV^+] = 3 μM (high monomer content). The dashed lines represent absorption spectra obtained as a result of dye photobleaching during photolysis.

Effect of Oxygen on DNA Damage:

To investigate whether the photoinduced damage inflicted on DNA by CV^+ can occur via oxygen independent mechanisms, experiments were carried out in two different media, viz. water and D_2O, under conditions of both high and low biopolymer loading. Figure 7.11 reveals that the damage inflicted on DNA is identical in the two media under both conditions, indicating that the Type II reaction mechanism does not play a significant role in bringing about double strand DNA cleavage. Had the Type II reaction mechanism involving singlet oxygen been important for photonuclease activity, there would have been an increase in DNA damage compared to water, because the lifetime of singlet oxygen is enhanced sevenfold in D_2O compared to water (Rodgers M. A., 1982).

Photonuclease activity was also monitored in air equilibrated and nitrogen purged samples, under conditions of maximum dye aggregation. There was a slight increase in DNA damage in the nitrogen purged samples than in the air-equilibrated samples with the difference between them being 20% (average of 6 independent measurements).

CONCLUSIONS:

Spectrophotometric titrations revealed that binding of TAM^+s to DNA at high dye to DNA concentration ratios leads to the formation of dye trimers and higher aggregates on the DNA template at submicromolar dye concentration for EV^+ and $VPBBO^+$, while for VBR^+ only the formation of dye dimers was observed. CV^+ however, was largely bound as a

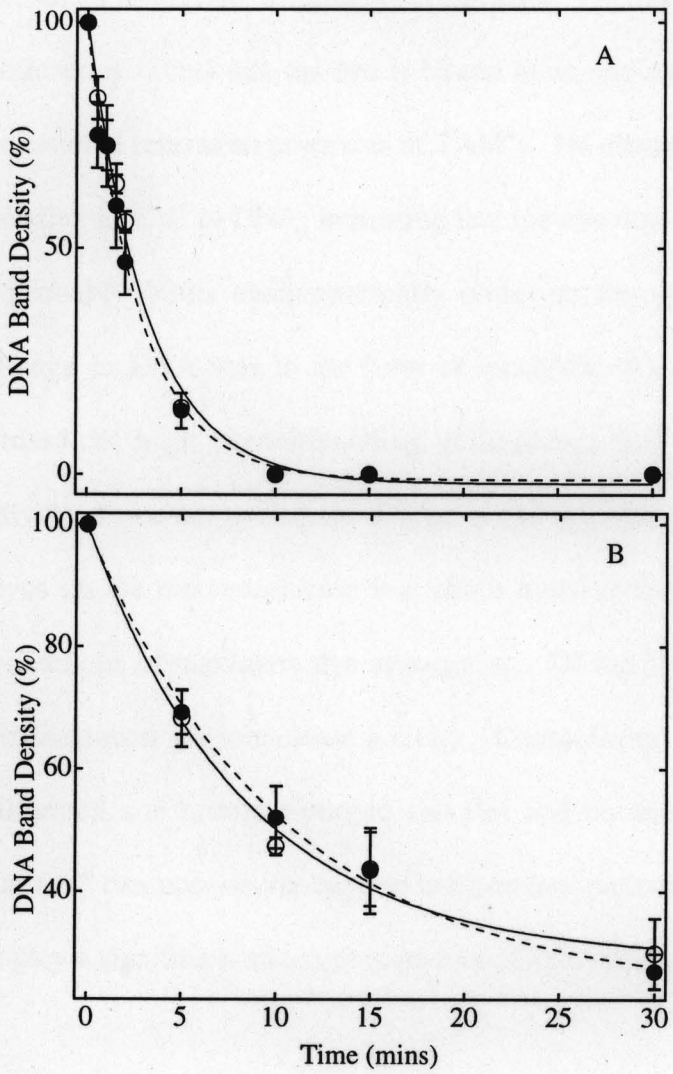

Figure 7.11 Decrease in DNA band density upon photolysis of DNA-CV^+ noncovalent complexes in buffered water and D_2O. The solid line and solid circles represent photolysis in water, the dashed line and open circles represent D_2O. Laser excitation at 532 nm, 10 Hz, 100 mJ/pulse. Phosphate buffer 10 mM, pH 7.6; T ≈ 22 ± 2 °C, [CV^+] = 10μM. Panel A represents high DNA loading (DNA 20μg/ml), Panel B represents low DNA loading (DNA = 400μg/ml).

monomer to the DNA template at this concentration regime. Titrations using fluorescence spectroscopy reveal that the dye is bound in an environment, that offers steric hindrance to the rotational relaxation processes of TAM^+s. No change in DNA viscosity was observed, upon binding of CV^+ to DNA, indicating that the dye does not intercalate between base pairs, but probably binds electrostatically either to the minor or major groove. Photoinduced damage in DNA was in the form of extensive double strand breaks. Dye aggregation resulted in high photobleaching efficiencies but correspondingly poor photonuclease activity. Upon decreasing the degree of dye aggregation, the damage inflicted by each of the dyes on the macromolecule was much more pronounced than the damage observed under conditions of maximum dye aggregation. Of the four TAM^+s, CV^+ was the dye that exhibited maximum photonuclease activity. Comparative experiments carried out between air-equilibrated and nitrogen-purged samples and between samples in D_2O and water indicate that CV^+ can operate via oxygen independent pathways and that the Type II pathway does not play a significant role in photoinduced DNA damage.

Chapter 8. Binding of Triarylmethane Dyes to LDL and Photoreactivity of LDL-TAM^+ Noncovalent Complexes.

RESULTS AND DISCUSSION:

Binding Studies:

Spectrophotometric Titrations:

UV-VIS spectrophotometric titrations were carried out in a similar manner as in the case of HK and DNA, in which the concentration of dye was kept constant and the concentration of LDL was increased in small increments. Figure 8.1 shows the spectroscopic signature of TAM^+s in the presence of increasing concentration of LDL. As shown in Figure 8.1 the absorbance of TAM^+s showed a steady decrease till a certain LDL concentration was reached (solid curves) and beyond this point further increase in LDL concentration lead to an increase in absorbance (dashed curves). Thus a biphasic profile was obtained when the absorbance at the wavelength of maximum absorption of dye free in solution was plotted as a function of the LDL concentration (Figure 8.2). At high LDL concentrations, a red shift in the absorption spectrum was obtained. As discussed previously in Chapters 4 and 5, a red spectral shift is observed when the dye molecule is present as an ion pair in solvents with low dielectric constant like toluene, chloroform and chlorobenzene (Oliveria C. S.- unpublished data), or when the dye partitions into the non-polar micelle core as an ion pair. This red shift therefore indicates that the dye is partitioning into the lipid phase (that constitutes 80% of the LDL mass) as an ion pair. However, no blue shift was observed as in the case of HK and

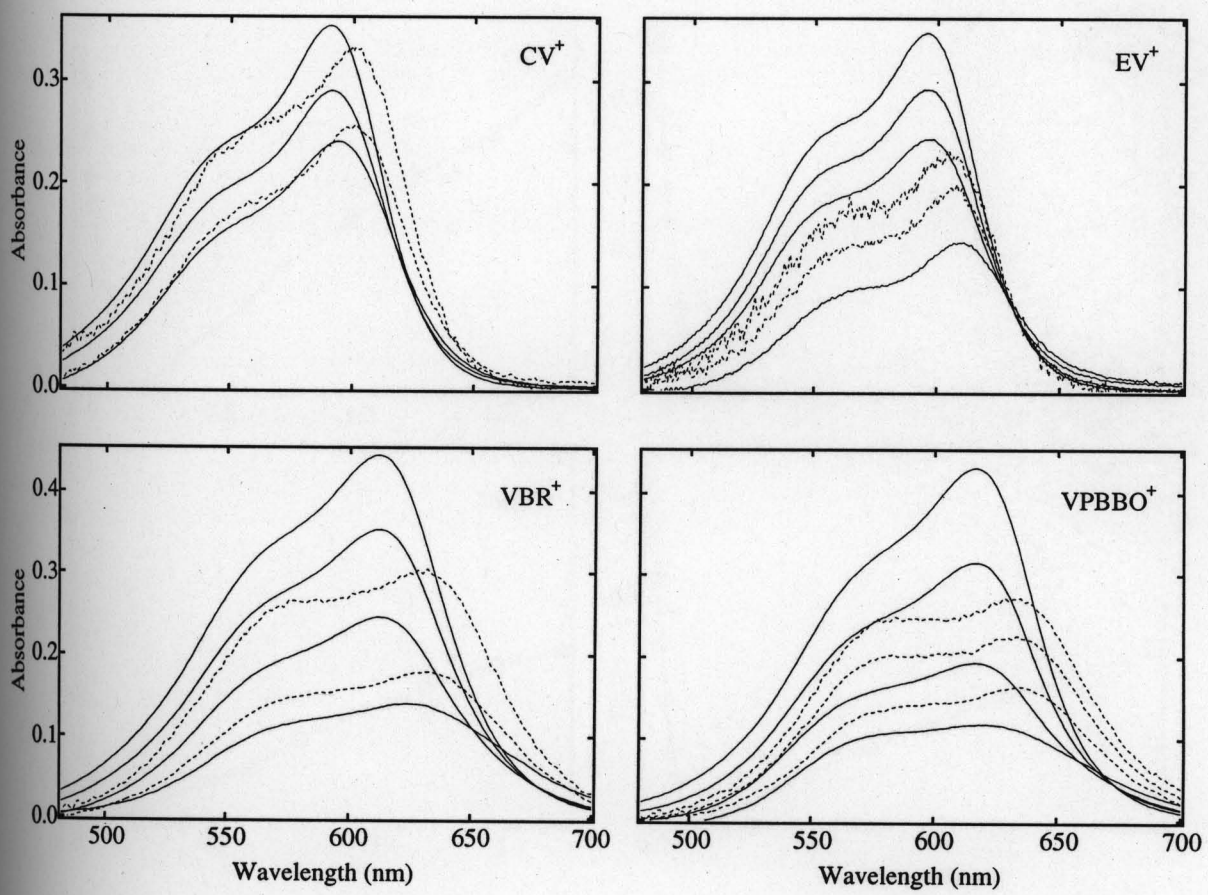

Figure 8.1 Effect of LDL on the absorption spectra of TAM^+ dyes. From the top, in order of decreasing absorption at λ_{max} (solid lines) the LDL concentrations were (μM): 0.0, 0.02, 0.1 for CV^+; 0.0, 0.02, 0.03, 0.44 for EV^+; 0.0, 0.02, 0.03, 0.14 for VBR^+; 0.0, 0.01, 0.03, 0.07, for $VPBBO^+$;. From the bottom starting at the dashed lines, in order of increasing absorption at λ_{max}, the LDL concentrations were (μM): 0.6, 1.5 for CV^+; 1.4, 2.26 for EV^+; 0.44, 1.2 for VBR^+; 0.63, 1.2, 1.7 for $VPBBO^+$; Phosphate buffer, pH 7.6; T = 25°C; $[TAM^+]$ = 5μM.

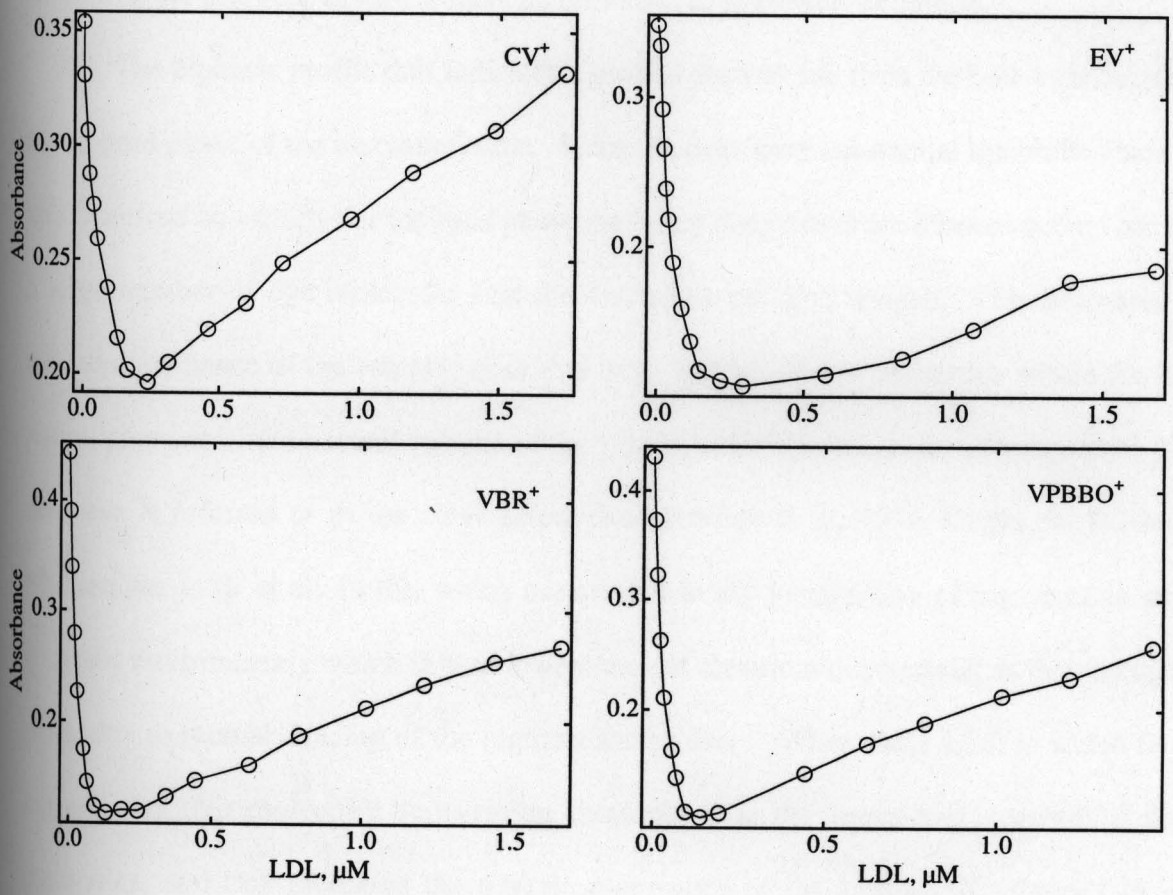

Figure 8.2 Plots of absorbance values at the λ_{max} of the dye, as a function of LDL concentration. Phosphate buffer, pH 7.6; T = 25°C; [TAM^+] = 5μM.

DNA, at high dye to LDL ratio, indicating that the change in spectroscopic signature of TAM^+s in the presence of LDL cannot be attributed to aggregate formation.

The biphasic profile thus indicates a gradual partitioning from the bulk aqueous phase to the lipid phase of the macromolecule. Since the dyes have substantial lipophilic character and therefore an affinity for the lipid phase the initial decrease in absorbance occurs because a large number of dye molecules find themselves in the lipid droplet. This decreases the overall absorbance of the sample, since this large number of dye molecules within the lipid phase, now constitute a small volume of the system under spectroscopic investigation. This decrease is referred to as the sieve effect (Rabinowitch E. I., 1951, Gupta, B. D., 1986; McClendon J. H. et al, 1990), which occurs due to the localization of pigments in small confined environments which in turn lowers the net absorption, especially at the absorption peak, due to mutual shading of the pigment molecules. When more LDL is added to the system, the dye molecules redistribute themselves in the increasing number of LDL molecules, and this increases the overall absorbance of the sample, represented by the ascending portion of the biphasic profile. This behavior is analogous to that observed in the case of nonionic detergent micelles (Triton X 100). Moreover, normalization of the TAM^+ spectrum obtained at 0.1μM LDL (or at the LDL concentration regime near the well) with the spectrum of TAM^+ free in solution (Figure 8.3) does not show pronounced increases in the shoulder with respect to the peak as observed in the case of HK and DNA (Figures 6.2 and 7.3 respectively), but a red shift in the λ_{max} of each TAM^+, which is further evidence pointing to a lack of dye aggregation in the LDL binding environment.

The absorbance data was also plotted according to the mole ratio method (Figure 8.4). For CV^+ and EV^+, the well appears at a ratio of 15 and 16 (Dye : LDL) respectively, while

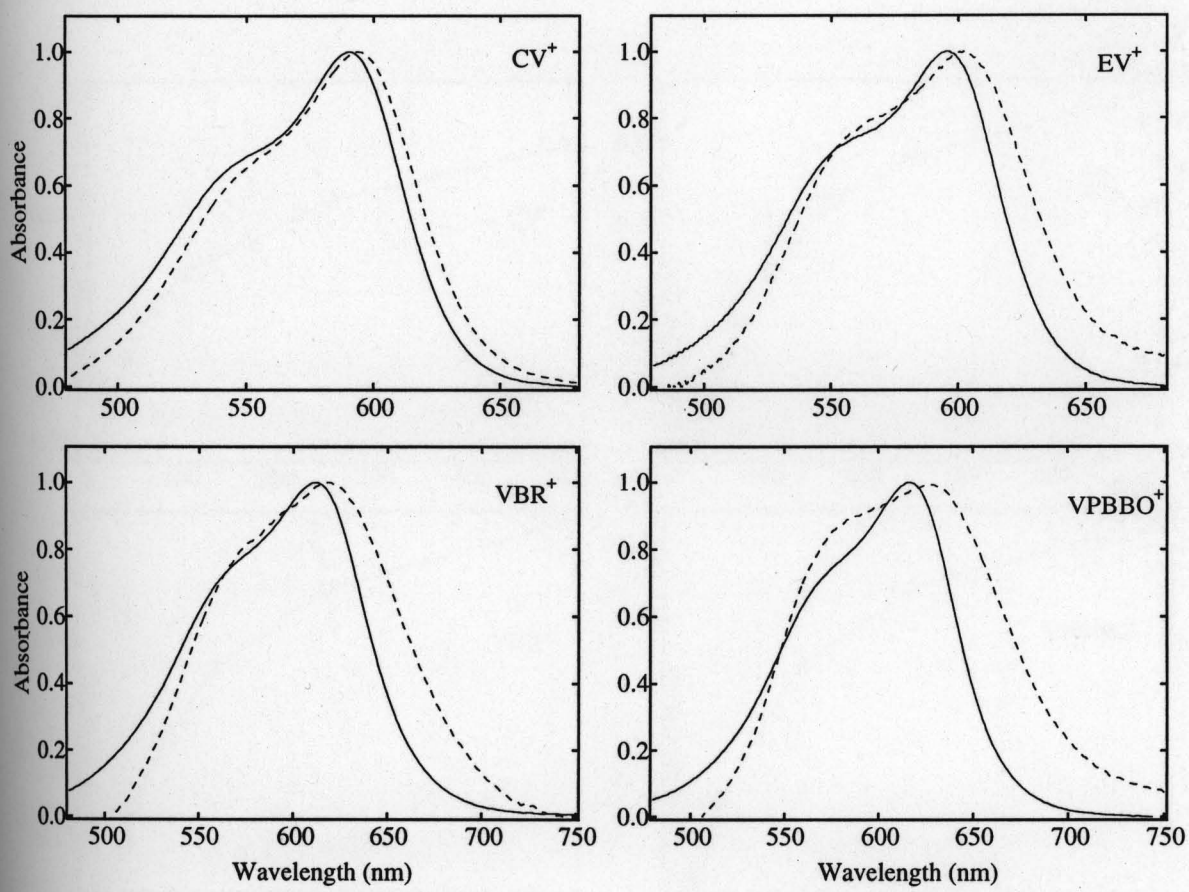

Figure 8.3 Normalized absorption spectra of TAM^+ dyes. The solid line represents the spectrum of the dye in the absence of LDL. The dashed line represents the spectrum of the dye in the presence of 0.1μM LDL. Phosphate buffer, pH 7.6; T = 25°C; $[TAM^+]$ = 5μM.

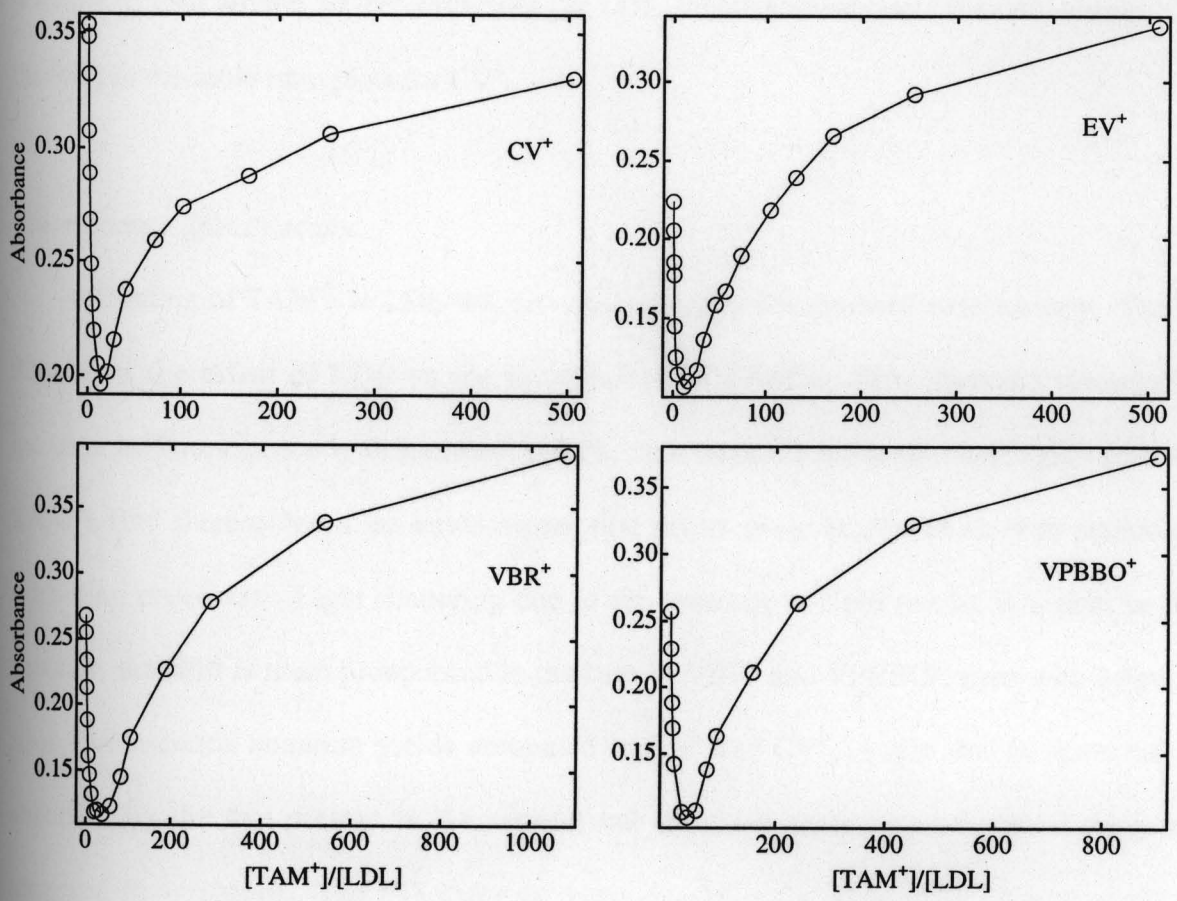

Figure 8.4 Plots of absorbance values at the λ_{max} of the dye, when free in solution as a function of mole ratio of the concentration dye to LDL. Phosphate buffer, pH 7.6; T = 25°C; $[TAM^+]$ = 5μM.

for VBR^+ and $VPBBO^+$ the well appears when the ratio equals 35 (Dye : LDL). Ultrafiltration experiments with CV^+ and LDL have shown that with 0.1μM LDL it is possible to load around 20 dye molecules per LDL, which approximates the ratio obtained at the well in the mole ratio plots for CV^+.

Fluorescence Spectroscopy:

Binding of TAM^+s to LDL was also studied using fluorescence spectroscopy. Figure 8.5 shows the effect of LDL on the fluorescence of TAM^+s. This observed remarkable increase in fluorescence with increase in LDL concentration indicates once again that the TAM^+s find themselves in an environment that offers steric hindrance to their rotational relaxation processes. Light scattering due to the presence of lipid results in a shift in the baseline, the shift is more pronounced in the case of VBR^+ and $VPBBO^+$, dyes with inherent poor fluorescence quantum yields compared to EV^+ and CV^+. Light that is scattered is absorbed by the dye present in the sample and therefore cannot be subtracted from the observed fluorescence. The PTI software however allows the integration of peak areas of each individual signal, by drawing a straight line between the two wavelengths under consideration and integrating the area within this defined region. The increase in fluorescence of EV^+ in the presence of LDL is 120 fold, while the enhancement in fluorescence is only eighteen fold in the case of the EV^+-micellar systems. This difference might arise either from the higher viscosity of the LDL lipid core or from a combination of this contribution with the contribution associated with the formation of dye-apoB complexes, since in the presence of a protein like HK, the enhancement in fluorescence of EV^+ is 140 fold, which is close to LDL (120 fold).

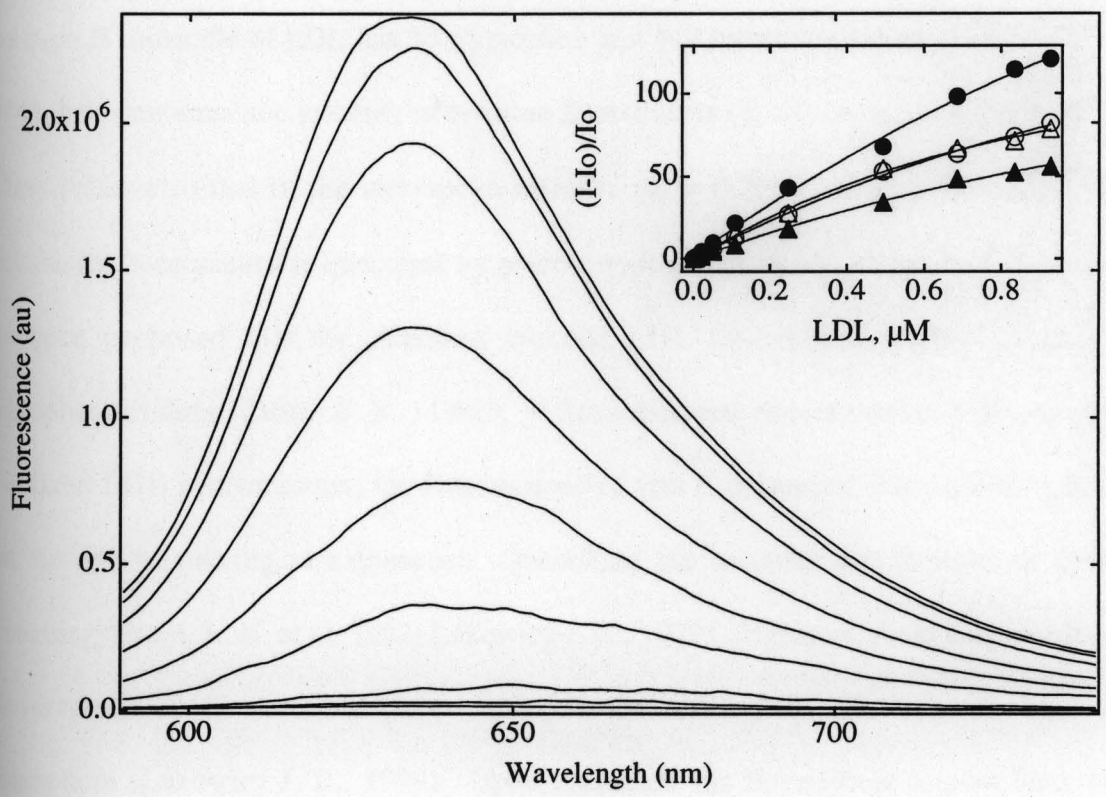

Figure 8.5 Effect of LDL on the fluorescence spectrum of EV^+. From the bottom, in order of increasing fluorescence the LDL concentrations were (μM): 0.0, 0.01, 0.02, 0.05, 0.11, 0.25, 0.5, 0.7, 0.84, 0.93. The inset shows the corresponding fluorescence binding isotherms for all four dyes. I = fluorescence intensity in the presence of LDL, Io = fluorescence intensity in the absence of LDL. Phosphate buffer, pH 7.6; T = 25°C; $[TAM^+]$ = 5μM. CV^+ - solid circles; EV^+ - open circles, VBR^+ - open triangles, $VPBBO^+$ - solid triangles.

Tryptophan/Tyrosine Quenching:

Binding was also studied by monitoring the quenching of intrinsic LDL fluorescence. The Apo B molecule of LDL has 37 tryptophan and 148 tyrosine residues (Shen S. H. et al, 1986), however since the intensity of tyrosine fluorescence ($\phi_f = 0.14$, $\varepsilon_{max} = 1.4*10^3\ M^{-1}cm^{-1}$) is less relative to that of the tryptophan residues ($\phi_f = 0.20$, $\varepsilon_{max} = 5.6*10^3\ M^{-1}cm^{-1}$) and because its fluorescence is quenched by nearby tryptophans due to energy tranfer events, it has been proposed that the observed intrinsic LDL fluorescence is due primarily to tryptophan residues (Cantor C. R. , 1980). When increasing concentration of dye was added to a fixed LDL concentration, the fluorescence of apo B decreased (Figure 8.6) indicating that the dye was acting as a quencher. Quenching can be either due to static or dynamic quenching (Fraiji, L. K. et al, 1992; Lakowicz J. R., 1999). Dynamic quenching results from encounters between the fluorophore and quencher during the life time of the excited fluorophore (Lakowicz J. R., 1999). Upon encounter the fluorophore returns back to the ground state without emission of a photon. Based on the distance between energy acceptor and donor encounters can be classified as collisional (Dexter mechanism, where two molecules are separated by a distance that equals the sum of their molecular radii) or long distance (Forster mechanism, where two molecules are separated by a distance greater than their collisional diameters (~50 to 100A°). Static quenching is due to 'non fluorescent' ground state complex formation between donor and quencher.

Stern Volmer plots, $F/Fo = 1+ kq\tau_o[Q]$, (Lakowicz J. R., 1999) were built to distinguish between dynamic and static quenching, where F is the fluorescence of apo B in the presence of dye, Fo is the fluorescence of apo B in the absence of dye, kq is the quenching constant, τ_o is the lifetime of the fluorophore and [Q] is the concentration of the

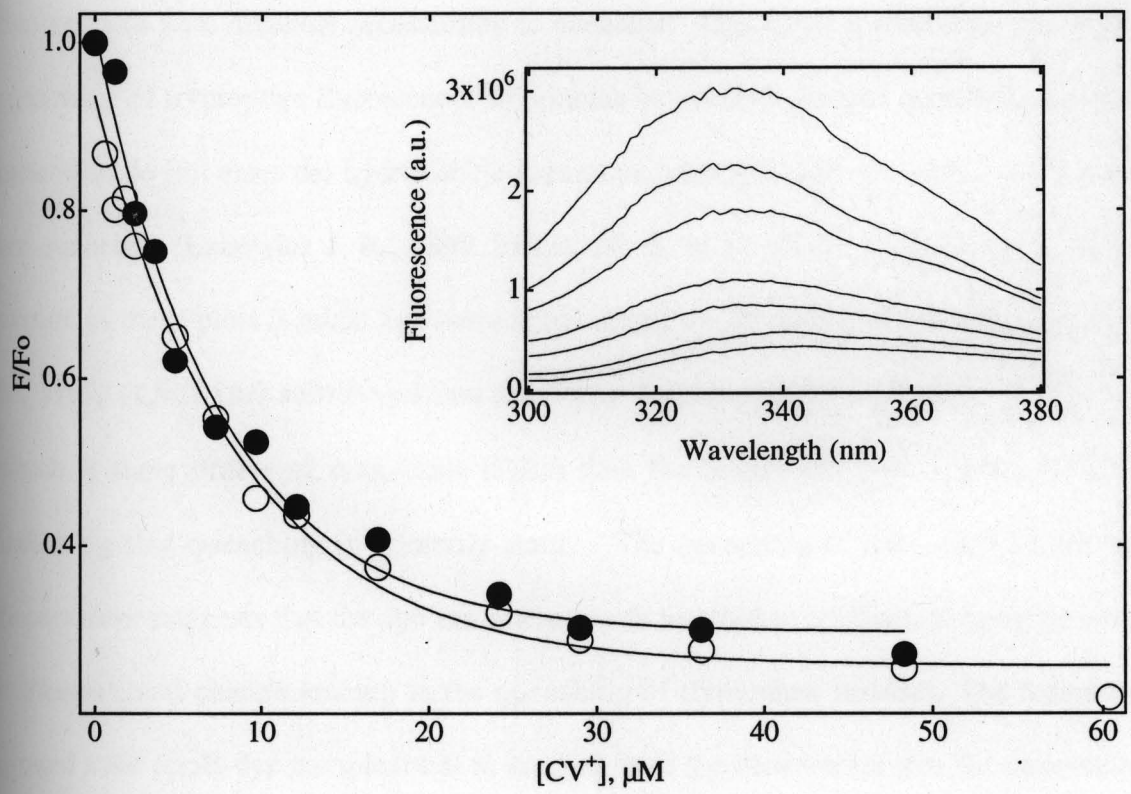

Figure 8.6 Effect of CV^+ on the intrinsic fluorescence of LDL at two different concentrations viz. 0.1 μM and 0.15 μM. Solid circles represent 0.1μM LDL and open circles represent 0.15μM LDL. Fo = fluorescence in the absence of dye, F = Fluorescence in the presence of dye. Each point represents an average of two samples. Inset shows the changes in the fluorescence spectrum of apoB. From top in order of decreasing fluorescence the concentration of CV^+ (μM) is: 0.0, 0.6, 4.8, 9.7, 17, 36, 60. Phosphate buffer 10mM, pH = 7.3, T = 25°C.

quencher. As observed in Panel A of Figure 8.7, Stern Volmer plots were nonlinear with non-linearity towards the x-axis, suggesting that there exist different populations of fluorophores with different accessibility to quencher. This result is frequently found for the quenching of tryptophan fluorescence in proteins by polar or charged quenchers, since these molecules do not enter the hydrophobic core of proteins and therefore only surface residues are quenched (Lakowicz J. R., 1999, Eflkin, M. R. et al 1976). Also if the initial linear portion of these plots is taken into consideration, and the lifetime of tryptophan (Lakowicz J. R., 1999) (τ_o= 3.1ns) substituted into the Stern Volmer equation, kq equals $3.4*10^{13}$ sec^{-1}, which is three orders of magnitude higher than the diffusional rate constant (10^{10} sec^{-1}), indicating that quenching is primarily static. The quenching of the intrinsic LDL apo B fluorescence suggests that the dye can interact with tryptophan residues of ApoB or induce a conformational change leading to the quenching of tryptophan residues. The formation of ground state apoB-dye complexes is in keeping with the observation that the enhancements in TAM^+ fluorescence yields is substantially higher in the presence of LDL as compared to micelles.

Modified Stern Volmer plots were also built to estimate about the proportion of fluorophore not accessible to quencher. $F/\Delta F = 1/f_a k_q[Q] + 1/f_a$ represents the modified form of the Stern Volmer equation (Lakowicz J. R., 1999), where F = Fluorescence in the presence of quencher, Fo = Fluorescence in the absence of quencher, k_q is the Stern-Volmer quenching constant, [Q] is the concentration of the quencher and f_a is the fraction accessible to quencher. The y-intercept of the modified Stern Volmer plot gives f_a. The Panel B in Figure 8.7 shows that f_a approximates 0.8 implying that about 80% of the population of fluorophores is accessible to quencher. Victorov A. V. and coworkers have reported that

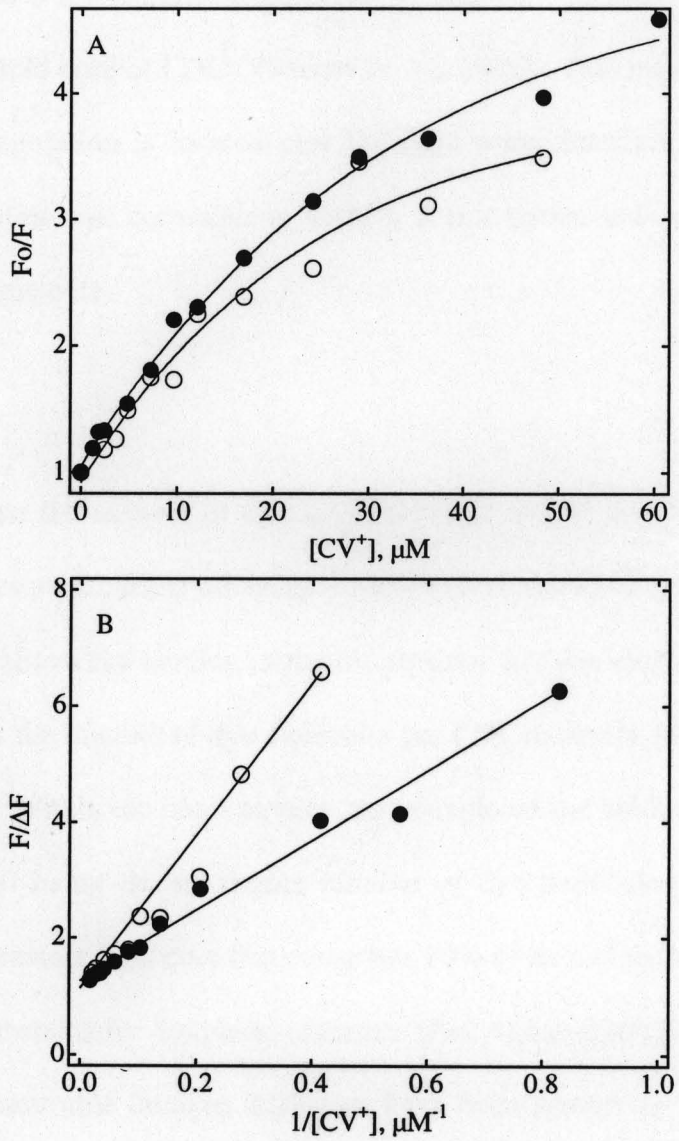

Figure 8.7 Stern Volmer (Panel A) and Modified Stern Volmer plots (Panel B) built from data presented in Figure 8.6. Open circles represent 0.1μM LDL and solid circles represent 0.15μM LDL. Fo = fluorescence in the absence of dye, F = Fluorescence in the presence of dye. Each point represents an average of two samples.

only 50% of the apo B fluorescence is quenched by an ionic quencher like iodide, which cannot access the lipid core of LDL (Victorov A. V., 1989). This implies that only 50% of the fluorophore population is located near the lipid water interface. Since 80% of the fluorophore population was accessible to TAM^+s, it is a further indication that TAM^+s can partition into the lipid core.

Ultrafiltration:

To determine the number of dye molecules that can be loaded per LDL molecule ultrafiltration studies were carried out using a molecular cut-off filter of 30,000 Daltons. The inset of Figure 8.8 shows the binding isotherms obtained in these experiments, while Figure 8.8 itself represents the number of dye molecules per LDL molecule plotted as a function of dye concentration. Within the concentration range explored the binding appears to be non-saturable, with 400 being the maximum number of dye molecules per LDL molecule. Because LDL possesses a lipid core that comprises 80% of its molecular composition, a dye like CV^+ with a substantially lipophilic character (P=2.4) can partition into the lipid core. Similar such non-saturable binding isotherms have been previously obtained in binding studies with LDL and various insecticides using equilibrium dialysis (Maliwal, B. P. and Guthrie, F. 1980), which suggested that the interaction was a partitioning rather than a stoichiometric binding process. Using rough estimates for molecular volume (Girolami G. S., 1994) it was inferred that 400 dye molecules could only occupy 5% of the total LDL volume suggesting that very little perturbation should be expected in the supramolecular structure of LDL upon dye binding.

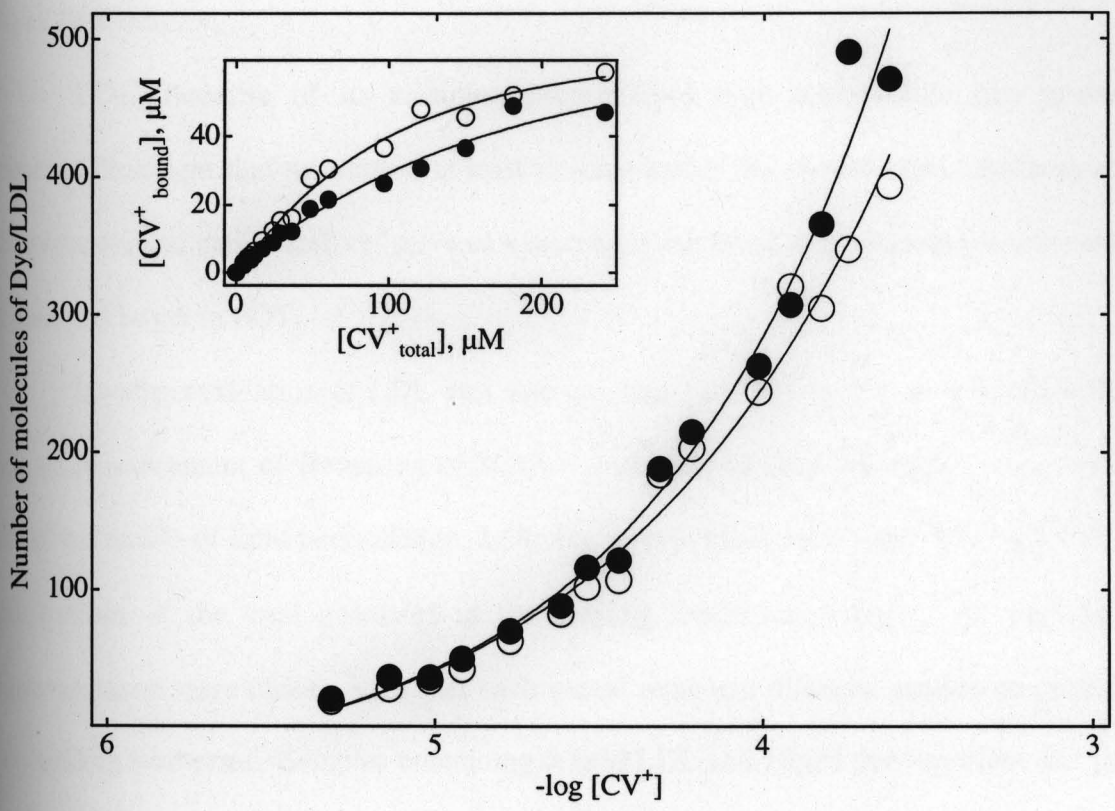

Figure 8.8 Plot of number of dye molecules bound per LDL as a function of dye concentration. Data was obtained using ultrafiltration with a molecular cut off filter of 30,000 Daltons. Open circles represent 0.1μM LDL and solid circles represent 0.15μM LDL. The inset shows the corresponding binding isotherms. Phosphate buffer 10mM, pH = 7.3.

Photoreactivity of TAM^+-LDL complexes

Lipid Peroxidation:

LDL, because of its complex protein-lipid type architecture can provide a microenvironment that resembles, at least to some extent the protein-lipid interfaces of cell membranes, and can, therefore, serve as a biological model of a cell membrane that could be a potential target in PDT.

Lipid peroxidation of LDL was assayed using the Thiobarbituric acid method that, allows measurement of formation of MDA – a product of lipid peroxidation. In order to study the extent of lipid peroxidation, LDL was kept constant at 0.1μM (the region close to the bottom of the well observed in the binding isotherms, Figure 8.2), and the dye concentrations were chosen such that each would represent different aspects or portions of the binding isotherms. Samples containing 0.1μM LDL and 10μM dye represent that part of the descending arm of the biphasic profile that is close to the region of the well. When the dye concentration was lowered to 1μM, cuvettes with a 10 cm pathlength were used to increase the limit of detection of MDA formation.

The results of lipid peroxidation are presented in Table 8.1. The percent yield of MDA increased with increase in dye concentration, indicating that greater damage occurred when a larger number of dye molecules are present in the lipid core. Note that this was not the case with HK and DNA, where an increase in dye concentration lead to a decrease in macromolecular damage (Figures 6.10 and 7.10 respectively). This is probably because the mode of binding of TAM^+s to LDL is different from that observed in the case of HK and DNA. Higher dye concentrations in the case of HK and DNA lead to the formation of dye aggregates, which are extensively bleached through a reaction mechanism that is not

	High $[TAM^+]/[LDL]$	Low $[TAM^+]/[LDL]$
TAM^+	[MDA], μM	[MDA], μM
CV^+	0.231(± 0.011)	0.082 (± 0.005)
EV^+	0.153 (± 0.007)	0.086 (± 0.000)
VBR^+	0.305 (± 0.010)	0.079 (± 0.010)
$VPBBO^+$	0.223 (± 0.002)	0.072 (± 0.020)

Table 8.1 Effect of photosensitizer on lipid peroxidation of LDL. The LDL concentration was 0.1 μM for each of the samples. At high $[TAM^+]$ to LDL ratios, the $[TAM^+]$ concentration was 10μM, at low $[TAM^+]$ to LDL ratios, the $[TAM^+]$ concentration was 1μM. Samples were photolysed to complete dye bleaching and absorbance of MDA was measured at 532 nm. Laser excitation at 532 nm, 10 Hz, 180 mJ/pulse. T = 22 ± 2 °C.

efficient in causing damage to the host macromolecule. In the case of LDL, since partitioning into the lipid core is a dominant part of the binding phenomenon, and because no evidence for dye aggregation upon LDL binding has been found, lipid peroxidation proceeds in a concentration dependent manner. VBR^+ seems to be the most effective of the four dyes in inducing lipid peroxidation.

To investigate whether TAM^+s bring about changes in apoB (the protein associated with LDL), photolysed samples and appropriate controls were excited at 280 nm to monitor changes in tryptophan fluorescence. Figure 8.9 shows that with increasing photolysis times, there is a steady decrease in tryptophan fluorescence and a shift to the red in the emission spectrum of the tryptophan residues. Thus similar to the HK case, there was a decrease in the tryptophan fluorescence and a red shift in the emission spectrum. As in the case of HK, however the detection of fluorescence at 450 nm, when excited at 360 nm was not feasible. This is because LDL has an inherent fluorescence at 450 nm, which is quenched in the presence of the dye, probably as a result of dye binding to LDL. As the dye concentration decreases during photolysis, the LDL fluorescence at 450 nm increases even if no damage to the protein takes place, making the detection of oxidative damage difficult.

CONCLUSIONS:

Spectrophotometric and fluorescence titrations (tryptophan quenching) show that TAM^+s bind to both, the protein and the lipid portion of LDL, with partitioning into the lipid core representing the dominant part of the binding phenomenon. The spectroscopic behavior of TAM^+ dyes in the presence of LDL indicates that no detectable amount of dye aggregates are formed upon binding to the lipoprotein. Fluorometric titrations also reveal that binding to

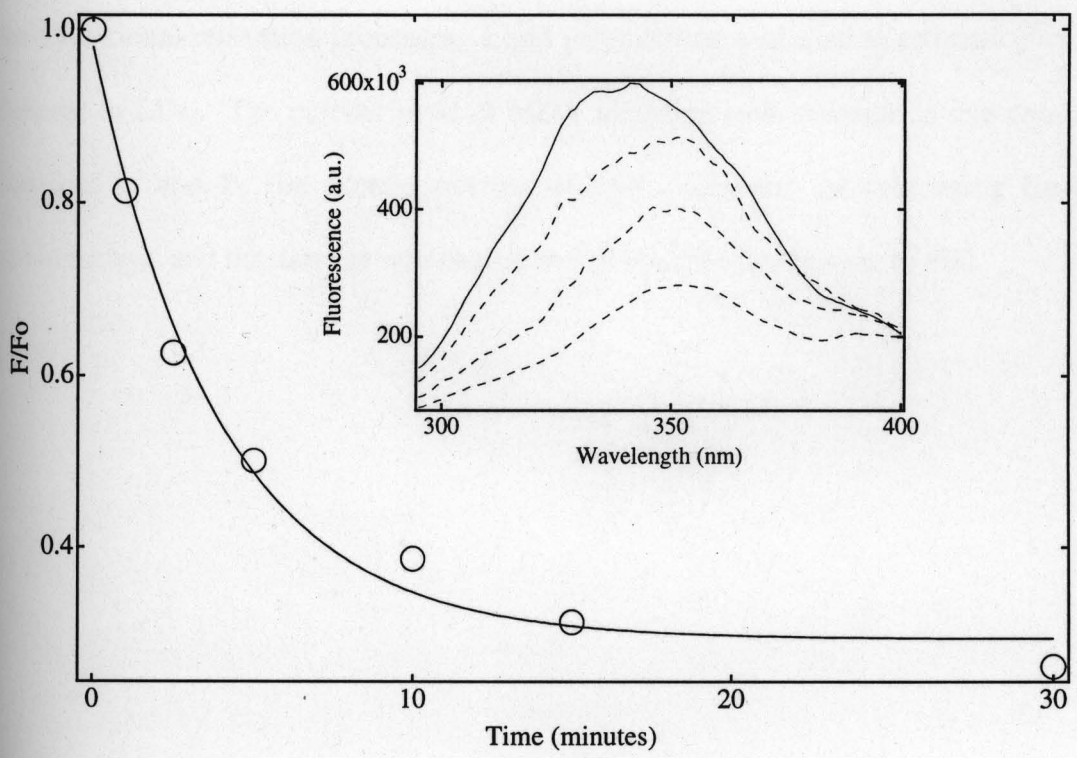

Figure 8.9 Effect of photolysis on the intrinsic LDL fluorescence. Inset shows the decrease in apo B fluorescence. From top in order of decreasing fluorescence intensity the photolysis time periods were as follows: 0, 1, 3 and 6 minutes. Fo = fluorescence in the absence of dye, F = Fluorescence in the presence of dye. [LDL] = 0.1μM, [TAM^+] = 10μM, Phosphate buffer 10mM, pH = 7.3. Laser excitation at 532 nm, 10 Hz, 180 mJ/pulse. T = 22 ± 2 °C.

LDL leads to an increase in the fluorescence quantum yields of the dyes, as would be expected when these dyes find themselves in an environment that offers steric hindrance to their rotational relaxation processes. Lipid peroxidation was used to estimate photoinduced damage in LDL. The percent yield of MDA increased with increase in dye concentration. Damage to apo B, the protein portion of LDL, was also evident using fluorescence spectroscopy, and the damage was similar to that observed in the case of HK.

Chapter 9. Mathematical Models

In this chapter we have explored some of the limitations of the Scatchard analysis with regard to the interpretation of experimental data on the binding of small molecules to macromolecules. We have also explored how changes in both the magnitude of binding constants and in the experimental parameter under analysis (here the molar extinction coefficient of the ligand) affect the profile of the binding isotherms associated with three distinct types of complexes. The library of binding isotherms generated in this exercise can assist in the preliminary assessment of the nature of noncovalent complexes generated upon binding of a small chromophore to a macromolecule. The models considered in this chapter are the following:

A. Macromolecules with one ligand binding site with dye molecules binding as a monomer at that site

B. Macromolecules with two ligand binding sites with dye molecules binding as a monomer at each site

C. Macromolecules with one binding site where the dye molecules can bind to that site either as a monomer or a dimer.

In all these models it was assumed that the dye does not aggregate to any significant extent when free in solution. Another assumption was that the macromolecule does not contribute to sample absorbance in the spectroscopic region where the dye (monomers and

aggregates) absorbs light. In the case of models A, B and C, synthetic data were generated and corresponding Scatchard plots were built.

RESULTS AND DISCUSSION :

A. Macromolecules with one ligand binding site with dye molecules binding as a monomer at that site

Consider a dye molecule D binding to protein P with one binding site to form a complex PD with a binding constant k. The absorbance of this system is thus a sum of the contributions of two species viz. the free dye D and the complex PD.

Symbols :

Pt = Total Protein

Dt = Total Dye

P = Free Protein

D = Free Dye

PD = Complex of protein and dye with 1:1 stoichiometry

ε_D = Extinction coefficient of dye free in solution

ε_{PD} = Extinction coefficient of dye bound as monomer to the protein

k = Binding constant

Abs = Absorbance

Equations:

$$P + D \overset{k}{\leftrightarrow} PD$$

$$k = \frac{[PD]}{[P][D]} \qquad (1)$$

$$[Pt] = [P] + [PD] \qquad (2)$$

$$[Dt] = [D] + [PD] \qquad (3)$$

Rearranging Equations (2) and (3)

$$[P] = [Pt] - [PD] \qquad (4)$$

$$[D] = [Dt] - [PD] \qquad (5)$$

Substituting Eqautions (4) and (5) in (1) gives equation (6)

$$k = \frac{[PD]}{([Pt] - [PD])([Dt] - [PD])} \qquad (6)$$

Solving for [PD]

$$[PD] = \frac{k[Pt] + k[Dt] + 1 \pm \sqrt{(-k[Pt] - k[Dt] - 1)^2 - 4k^2[Dt][Pt]}}{2k} \qquad (7)$$

The absorbance of the system is given by Equation (8)

$$Abs = \varepsilon_D [D] + \varepsilon_{PD}[PD] \qquad (8)$$

From (5)

$$Abs = \varepsilon_D([Dt] - [PD]) + \varepsilon_{PD}[PD] \qquad (9)$$

For each pair of [Pt] and [Dt] values, the respective concentration of [PD] complex in solution can be solved using equation (7), and [D] can be solved using equations (5) and (7).

The absorbance obtained from equation (9) can then be plotted against [Pt]. The unknown variables in this model are k and ε_{PD}. Reasonable guess values were used as estimates for these variables and the equations were solved accordingly to obtain the concentrations of both, bound and free ligand and corresponding Scatchard plots were built. The Scatchard equation for a macromolecule with one binding site is represented by equation (10).

$$\frac{\nu}{[D]} = nk - \nu k \qquad (10)$$

where ν = number of moles of dye bound per mole of macromolecule, [D] is the free dye concentration, n = number of binding sites and k is the binding constant. Panels A an B of Figure 9.1 show the plots of absorbance plotted as a function of macromolecule concentration. In Panel A, the binding event increases the extinction coefficient, while in Panel B, the assumption is made that the binding event decreases the extinction coefficient of the dye molecule. Panel C shows the corresponding linear Scatchard plot which is in accordance with what should be obtained for a macromolecule with one binding site.

Figure 9.2 shows a family of curves that were obtained by varying the extinction coefficient of the dye when bound to the macromolecule. As observed in Panel A of Figure 9.2, with increasing extinction coefficient (ε_{PD}) the absorbance of the system increases and with decreasing extinction coefficient, there is a net decrease (Panel B, Figure 9.2). When the extinction coefficient of the bound dye was equal to that of the dye free in soultion ($\varepsilon_{PD} = \varepsilon_D$), there was no change in the absorbance of the system. Figure 9.3 shows changes in the absorbance plots when the binding constant is varied. A higher binding constant leads to an increase in the net absorbance, when $\varepsilon_{PD} > \varepsilon_D$ (Panel A), and a decrease in the absorbance when $\varepsilon_{PD} < \varepsilon_D$ (Panel B). This indicates that the absorbance profiles in the case of a macromolecule with one binding site will either increase or decrease monotonically depending on the values that the variables (k and ε_{PD}) assume.

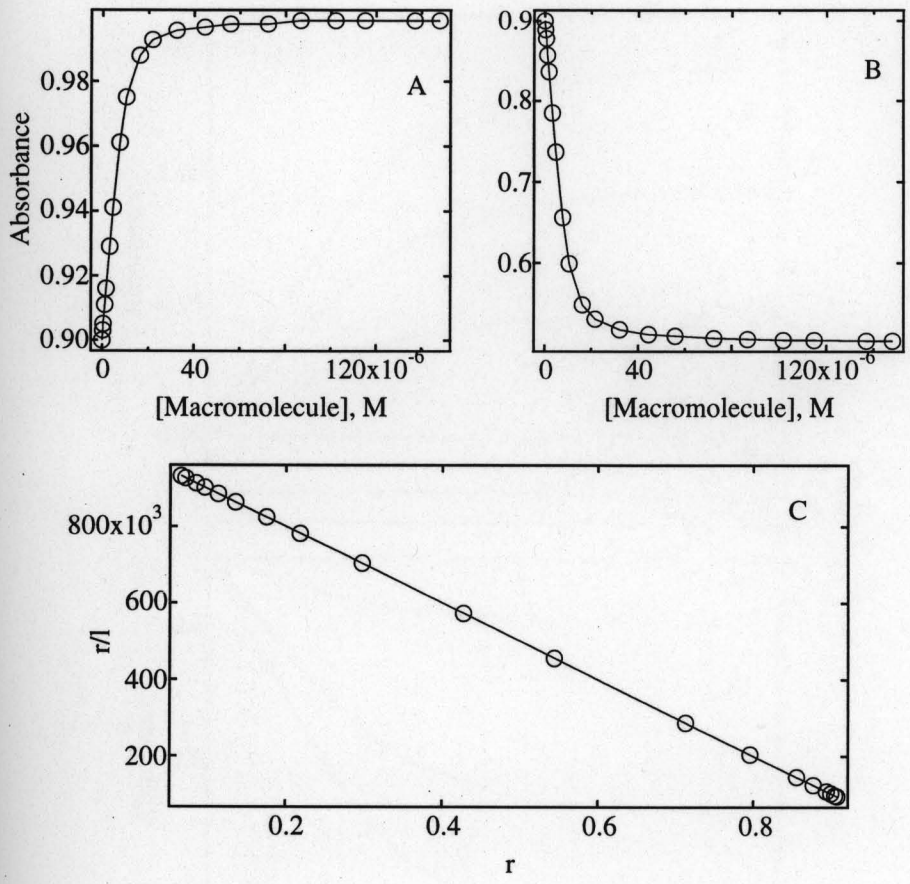

Figure 9.1 Plots obtained using Model A. ε_D was fixed at $9*10^4 M^{-1}cm^{-1}$, [Dt] was fixed at $10*10^{-6}$M, [Pt] was varied from 0 to $1.5*10^{-4}$ M and the variables were k and ε_{PD}. In Panel A, $\varepsilon_{PD} = 10*10^4 M^{-1}cm^{-1}$, $k = 1*10^6 M^{-1}$; in Panel B $\varepsilon_{PD} = 5*10^4 M^{-1}cm^{-1}$, $k = 1*10^6$. Panel C shows the corresponding Scatchard plot, r = [Bound Dye]/[Protein], l = [Free Dye]

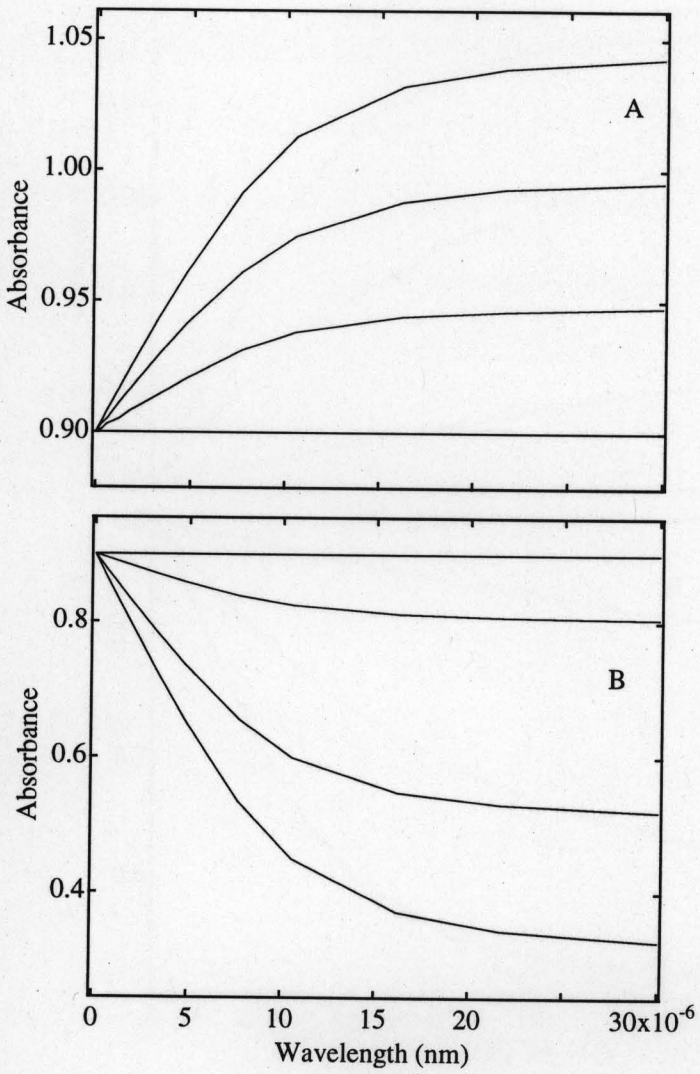

Figure 9.2 Plots obtained (using Model A) by varying ε_{PD}. ε_D was fixed at $9*10^4 M^{-1}cm^{-1}$, [Dt] was fixed at $10*10^{-6}$M, [Pt] was varied from 0 to $3*10^{-5}$ M, k was fixed at $1*10^6 M^{-1}$. In Panel A, from the bottom in order of increasing absorbance, the values of ε_{PD} ($M^{-1}cm^{-1}$) were $9*10^4$, $9.5*10^4$, $10*10^4$, $10.5*10^4$; in Panel B from the top in order of decreasing absorbance the values of ε_{PD} ($M^{-1}cm^{-1}$) were $9*10^4$, $8*10^4$, $5*10^4$, $3*10^4$.

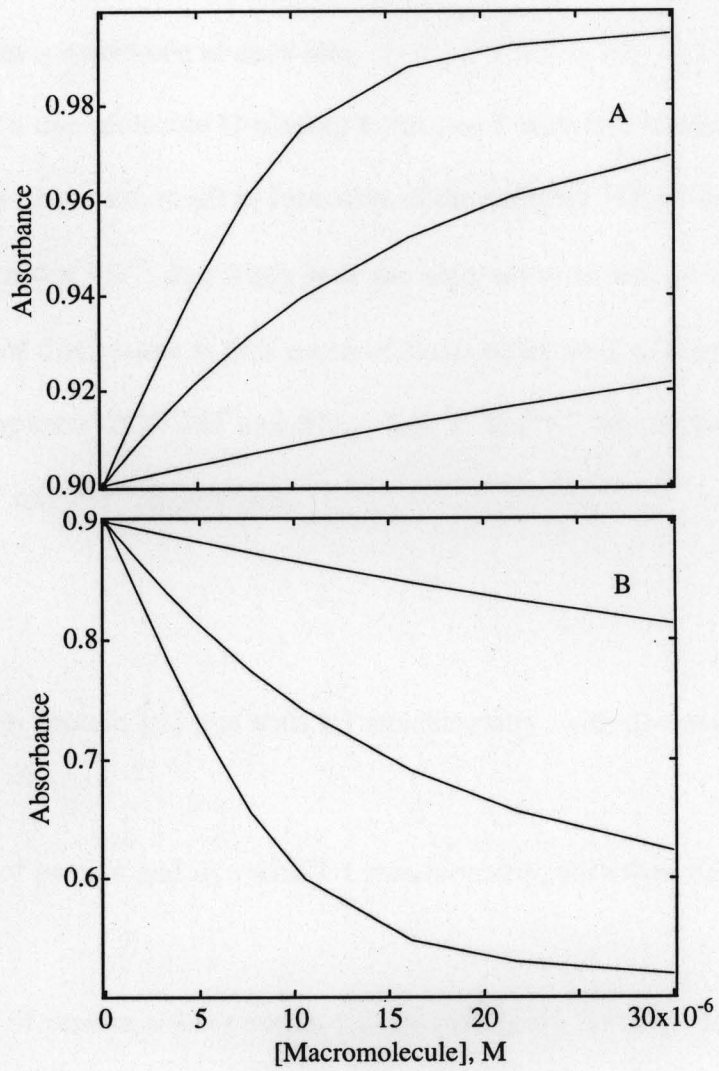

Figure 9.3 Plots obtained (using Model A) by varying k. ε_D was fixed at $9*10^4 M^{-1}cm^{-1}$, [Dt] was fixed at $10*10^{-6}$M, [Pt] was varied from 0 to $3*10^{-5}$ M. In Panel A ε_{PD} was fixed at $10*10^4 M^{-1}cm^{-1}$ and from the bottom in order of increasing absorbance, the values of k (M^{-1}) were $1*10^6$, $1*10^5$, $1*10^4$; in Panel B ε_{PD} was fixed at $5*10^4 M^{-1}cm^{-1}$ and from the top in order of decreasing absorbance the values of k (M^{-1}) were $1*10^6$, $1*10^5$, $1*10^4$.

B. Macromolecules with two independent binding sites with dye molecules binding as a monomer at each site

Consider a dye molecule D binding to protein P with two binding sites. Let binding of dye molecules to one site result in formation of the complex PD′ while binding to the other site result in complex PD″; and when both the sites are occupied let the complex be PD_2. The absorbance of this system is thus a sum of the contributions of four species viz. the free dye D, the complexes PD′, PD″and PD_2. Let k′ and k″ be the binding constants for formation of PD′ and PD″ respectively.

Symbols:

PD′ = Complex of protein and dye with 1:1 stoichiometry, with dye molecule binding at the first site

PD″= Complex of protein and dye with 1:1 stoichiometry, with dye molecule binding at the second site

PD_2 = Complex of protein and dye with 1:2 stoichiometry, with dye molecules occupying both sites

k′= Binding constant for first site

k″= Binding constant for second site

ε_D= Extinction coefficient of dye free in solution

$\varepsilon_{PD'}$= Extinction coefficient of dye bound at the first binding site

$\varepsilon_{PD''}$= Extinction coefficient of dye bound at the second binding site

Abs = Absorbance

Equations:

$$P + D \overset{k'}{\leftrightarrow} PD' \quad \text{..... (Binding to first site)}$$

$$P + D \overset{k''}{\leftrightarrow} PD'' \quad \text{..... (Binding to second site)}$$

$$PD' + D \overset{k''}{\leftrightarrow} PD_2 \quad \text{..... (Binding to second site)}$$

$$PD'' + D \overset{k'}{\leftrightarrow} PD_2 \quad \text{..... (Binding to first site)}$$

$$k' = \frac{[PD']}{[P][D]} \quad (1) \qquad k' = \frac{[PD_2]}{[PD''][D]} \quad (2)$$

$$k'' = \frac{[PD'']}{[P][D]} \quad (3) \qquad k'' = \frac{[PD_2]}{[PD'][D]} \quad (4)$$

From Equations (1), (2), (3) and (4), $[PD_2]$ can be expressed in terms of free protein and free dye concentrations.

$$[PD_2] = k'[PD''][D] = k'k''[P][D]^2 \quad (5)$$

OR

$$[PD_2] = k''[PD'][D] = k'k''[P][D]^2 \quad (5)$$

Total dye and total protein concentrations can be expressed by equations (6) and (7) respectively

$$[Dt] = [D] + [PD'] + [PD''] + 2[PD_2] \quad (6)$$

$$[Pt] = [P] + [PD'] + [PD''] + [PD_2] \quad (7)$$

Substituting for [PD′], [PD″] and $[PD_2]$ from equations (1), (3) and (5) respectively in equations (6) and (7) gives equations (8) and (9).

$$[Dt] = [D] + k'[P][D] + k''[P][D] + 2k''k'[P][D]^2 \quad (8)$$

$$[Pt] = [P] + k'[P][D] + k''[P][D] + k''k'[P][D]^2 \quad (9)$$

From (9), [P] can be expressed as:

$$[P] = \frac{[Pt]}{1 + k'[D] + k''[D] + k'k''[D]^2} \quad (10)$$

Equation (8) can also be written as:

$$[Dt] = [D] + [P](k'[D] + k''[D] + 2k'k''[D]^2) \quad (11)$$

Substituting for [P] in (11) from (10)

$$[Dt] = [D] + [Pt]\frac{(k'[D] + k''[D] + 2k'k''[D]^2)}{1 + k'[D] + k''[D] + k'k''[D]^2} \qquad (12)$$

Solving for [D] gives a cubic equation in [D]

$$a[D]^3 + b[D]^2 + c[D] + d = 0 \qquad (13)$$

where,

$$a = k'k''$$

$$b = k' + k'' + 2k'k''[Pt] - k'k''[Dt]$$

$$c = 1 + (k' + k'')([Pt] - [Dt])$$

$$d = -[Dt]$$

The absorbance of this system is given by equation (14)

$$Abs = \varepsilon_D[D] + \varepsilon_{PD'}[PD'] + \varepsilon_{PD''}[PD''] + (\varepsilon_{PD'} + \varepsilon_{PD''})[PD_2] \qquad (14)$$

From equations (1) and (10) one can obtain [PD'],

$$[PD'] = \frac{k'[Pt][D]}{1 + k'[D] + k''[D] + k'k''[D]^2} \qquad (15)$$

From equations (3) and (10) one can obtain [PD″],

$$[PD''] = \frac{k''[Pt][D]}{1 + k'[D] + k''[D] + k'k''[D]^2} \qquad (16)$$

From equations (5) and (10) one can obtain [PD_2],

$$[PD_2] = \frac{k''k'[Pt][D]}{1 + k'[D] + k''[D] + k'k''[D]^2} \qquad (17)$$

Substituting equations (15), (16) and (17) in (14) gives the absorbance values that can then be plotted against [Pt]. [PD′], [PD″] and [PD_2] were solved using equations (15), (16) and (17). The values of these complexes were then substituted in equation (14) and solved for absorbance, which was then plotted against [Pt]. The same equations can be obtained if the Scatchard equation (equation 19) for a protein with two types of binding sites is used as the initial starting point.

$$\nu = \frac{n_1 k_1[D]}{1 + k_1[D]} + \frac{n_2 k_2[D]}{1 + k_2[D]} \qquad (19)$$

where ν is the number of moles of dye bound per mole of macromolecule, [D] is the free dye concentration, n_1 and n_2 are the number of binding sites in the first and second type of independent sites respectively, and k_1 and k_2 are the binding constants for the first and second type of independent sites respectively (Scatchard G., 1949).

The unknown variables in this model are k′, k″, $\varepsilon_{PD''}$, $\varepsilon_{PD'}$. Reasonable guess values were used as estimates for these variables and the equations were solved accordingly to obtain the concentrations of both, bound and free ligand and corresponding Scatchard plots were built. Panel A of Figure 9.4 shows the plots of absorbance as a function of macromolecule concentration and Panel B shows the corresponding non-linear Scatchard plot which is in accordance with what should be obtained for a macromolecule with two independent classes of binding sites.

Figure 9.5 shows the family of curves obtained by varying k′, when the other variables are fixed. Panel A shows that with increasing k′ ($k' > 1*10^6\ M^{-1}$) the absorbance increases. The well appears at approximately the same region (*circa* $5*10^{-6}$M) in Panel A though a slight shift to the left is observed with increasing changes in k′. Panel B shows that with decreasing k′ ($k' < 1*10^6 M^{-1}$) the absorbance decreases. The well also disappears with decreasing k′, and the biphasic nature of the profile is lost within the macromolecular concentration regime considered here.

Figure 9.6 shows the family of curves obtained by varying k″, when the other variables are fixed. Panel A shows that with decreasing k″ ($k'' < 1*10^5\ M^{-1}$) the absorbance increases. The well shifts to the left with decreasing k″, and eventually disappears as k″assumes much lower values. On the other hand in Panel B with increasing k″ ($k'' > 1*10^5 M^{-1}$) the absorbance decreases. The well becomes broader and eventually disappears with increasing k″, and the biphasic nature of the profile is lost within the considered macromolecular concentration regime.

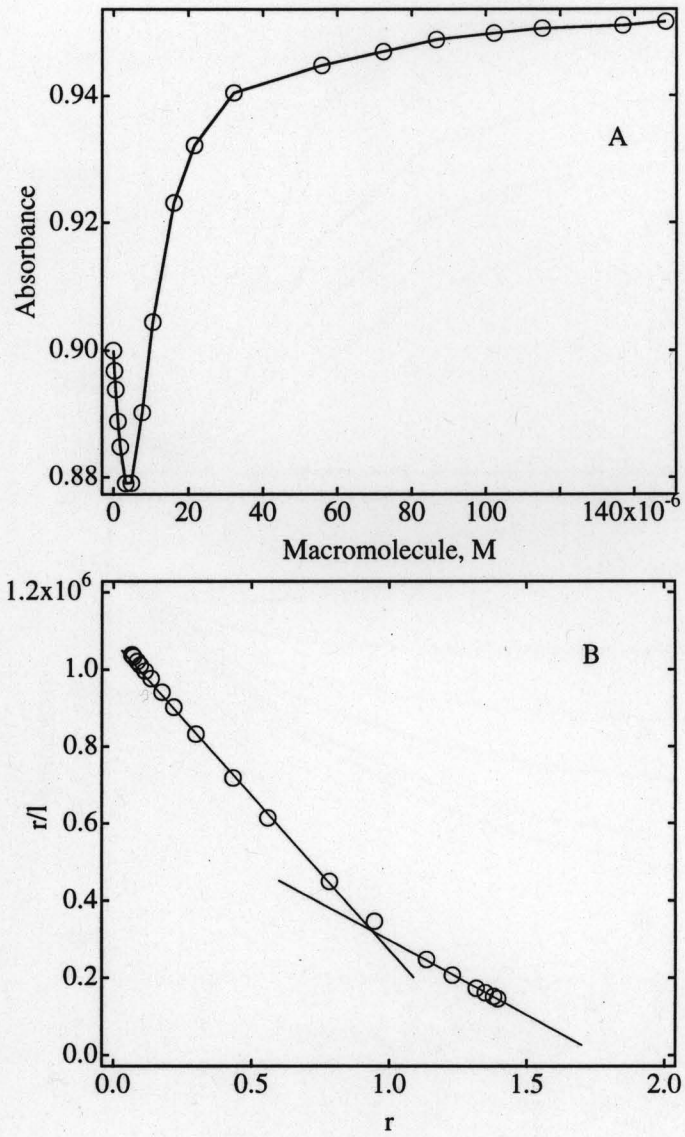

Figure 9.4 Plot obtained using Model B (Panel A). $\varepsilon_D = 9*10^4 M^{-1}cm^{-1}$, [Dt] $=10*10^{-6}$ M, [Pt] was varied from 0 to $3*10^{-5}$ M, $\varepsilon_{PD'} = 10*10^4 M^{-1}cm^{-1}$, $\varepsilon_{PD''} = 5*10^4 M^{-1}cm^{-1}$, $k' = 1*10^6 M^{-1}$, $k'' = 1*10^5 M^{-1}$.

Panel B shows the corresponding Scatchard plot, r = [BoundDye]/[Protein], l = [Free Dye].

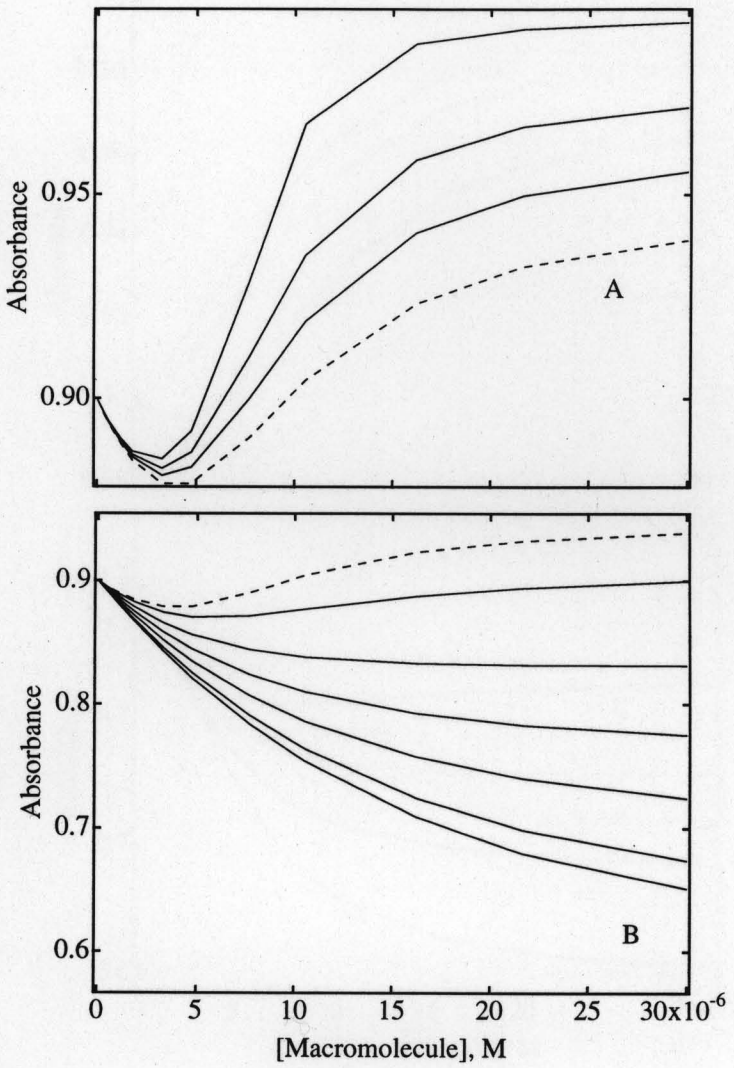

Figure 9.5 Plots obtained (using Model B) by varying k′. The fixed variables were : ε_D = $9*10^4M^{-1}cm^{-1}$, [Dt] =$10*10^{-6}$ M, $\varepsilon_{PD'} = 10*10^4M^{-1}cm^{-1}$, $\varepsilon_{PD'} = 10*10^4M^{-1}cm^{-1}$, $\varepsilon_{PD''} = 5*10^4M^{-1}cm^{-1}$, $k'' = 1*10^5M^{-1}$. [Pt] was varied from 0 to $3*10^{-5}$ M. In Panel A, in order of increasing absorbance from the dashed line $k'(M^{-1}) = 1*10^6$, $1.5*10^6$, $2.5*10^6$, $1*10^7$; In Panel B, in order of decreasing absorbance from the dashed line $k'(M^{-1}) = 1*10^6$, $0.5*10^6$, $0.2*10^6$, $0.5*10^5$, $0.2*10^5$, $0.1*10^5$.

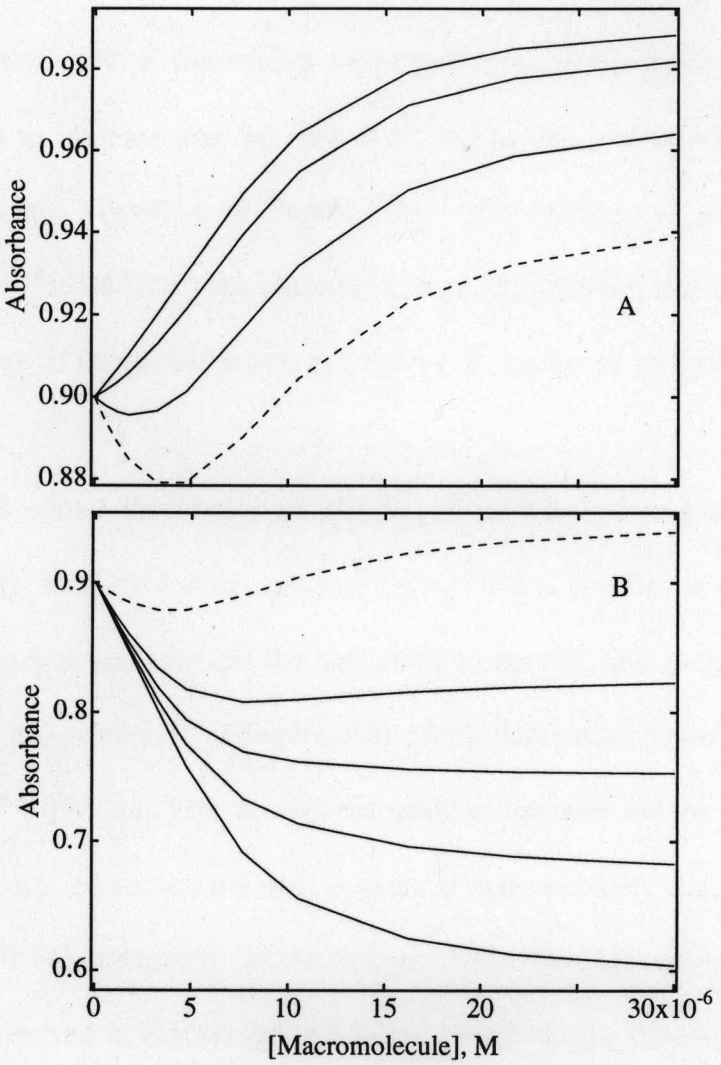

Figure 9.6 Plots obtained (using Model B) by varying k″. The fixed variables were : ε_D = $9*10^4M^{-1}cm^{-1}$, [Dt] =$10*10^{-6}$ M, $\varepsilon_{PD'} = 10*10^4M^{-1}cm^{-1}$, $\varepsilon_{PD'} = 10*10^4M^{-1}cm^{-1}$, $\varepsilon_{PD''} = 5*10^4M^{-1}cm^{-1}$, k′= $1*10^6M^{-1}$. [Pt] was varied from 0 to $3*10^{-5}$ M. In Panel A, in order of increasing absorbance from the dashed line k″ (M^{-1}) = $1*10^5$, $0.5*10^5$, $0.2*10^5$, $0.1*10^5$. In Panel B, in order of decreasing absorbance from the dashed line k′(M^{-1}) = $1*10^5$, $5*10^5$, $1*10^6$, $2*10^6$, $5*10^6$.

Figure 9.7 shows the family of curves obtained by varying $\varepsilon_{PD'}$, when the other variables are fixed. With increasing extinction coefficient ($\varepsilon_{PD'}>10*10^4M^{-1}cm^{-1}$) the absorbance tends to increase and the well shifts to the left, and eventually disappears at higher values of $\varepsilon_{PD'}$ (Panel A of Figure 9.7). With decreasing values of extinction coefficient ($\varepsilon_{PD'}<10*10^4M^{-1}cm^{-1}$) the absorbance tends to decrease and the well disappears. The biphasic nature of the profile is lost and the curves appear to plateau (Panel B of Figure 9.7).

Figure 9.8 shows the family of curves obtained by varying $\varepsilon_{PD''}$ when the other variables are fixed. With increasing values of the extinction coefficient ($\varepsilon_{PD''}>5*10^4M^{-1}cm^{-1}$) the absorbance tends to increase and the well shifts to the left, and eventually disappears at higher values of $\varepsilon_{PD''}$ (Panel A of Figure 9.8). With decreasing values of the extinction coefficient ($\varepsilon_{PD''}<5*10^4M^{-1}cm^{-1}$) the absorbance tends to decrease and the well becomes more and more prominent. Moreover the well appears at approximately the same concentration regime (*circa* $5*10^{-6}M$), irrespective of the changes in $\varepsilon_{PD''}$ (Panel B – Figure 9.8).

Thus as observed in Figures 9.5 to 9.8, the profile shape, the appearance of the well and the shifts are very much influenced by changes in the parameter values.

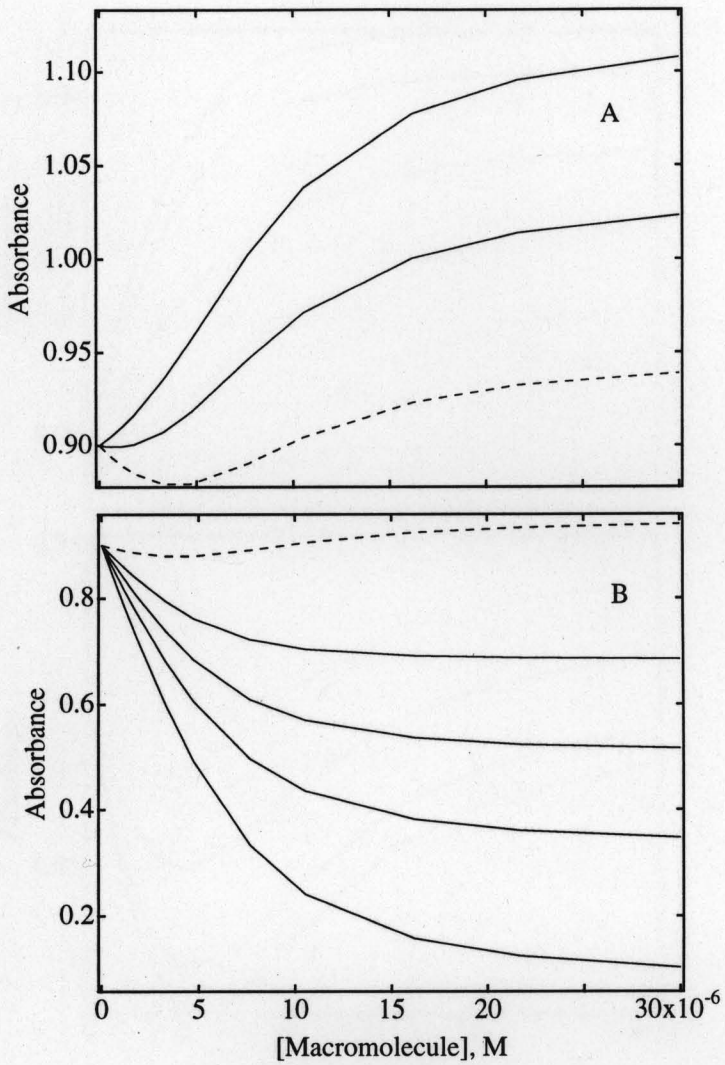

Figure 9.7 Plots obtained (using Model B) by varying $\varepsilon_{PD'}$. The fixed variables were : $\varepsilon_D = 9*10^4 M^{-1}cm^{-1}$, [Dt] $=10*10^{-6}$ M, $\varepsilon_{PD''} = 5*10^4 M^{-1}cm^{-1}$, $k' = 1*10^6 M^{-1}$, $k'' = 1*10^5 M^{-1}$. [Pt] was varied from 0 to $3*10^{-5}$ M. In Panel A, in order of increasing absorbance from the dashed line $\varepsilon_{PD'}$ ($M^{-1}cm^{-1}$) = $10*10^4$, $11*10^4$, $12*10^4$. In Panel B, in order of decreasing absorbance from the dashed line $\varepsilon_{PD'}$ ($M^{-1}cm^{-1}$) = $10*10^4$, $7*10^4$, $5*10^4$, $3*10^4$, $0.1*10^4$.

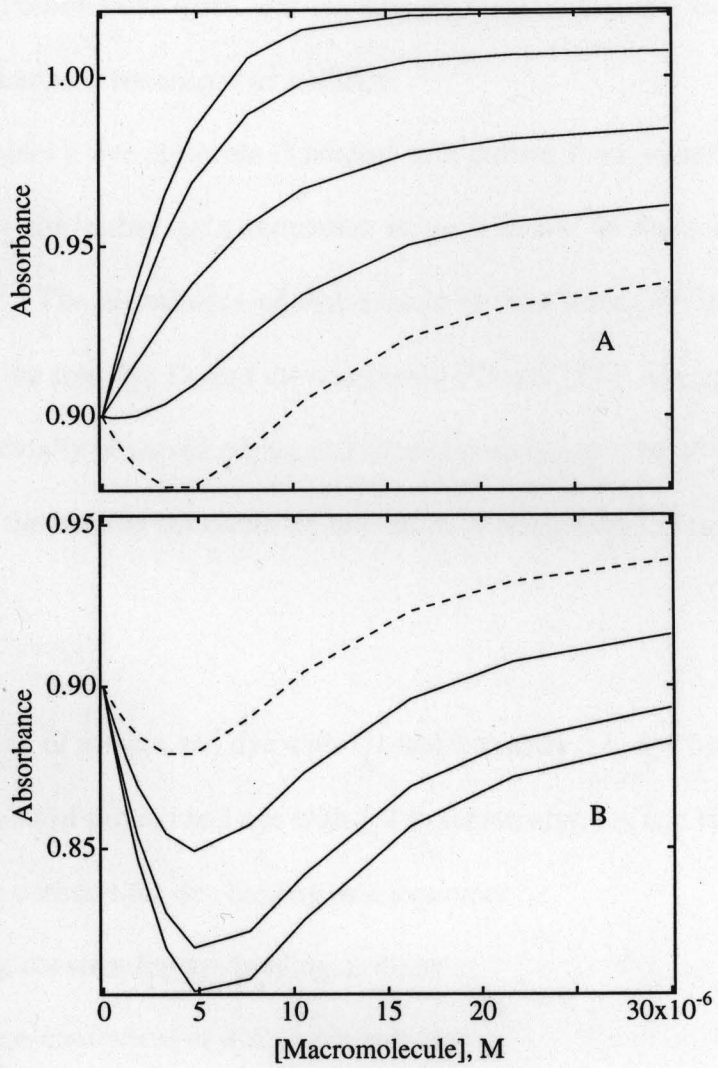

Figure 9.8 Plots obtained (using Model B) by varying $\varepsilon_{PD''}$. The fixed variables were : $\varepsilon_D = 9*10^4 M^{-1}cm^{-1}$, [Dt] $=10*10^{-6}$ M, $\varepsilon_{PD'} = 10*10^4 M^{-1}cm^{-1}$, $\varepsilon_{PD'} = 10*10^4 M^{-1}cm^{-1}$, $k' = 1*10^6 M^{-1}$, $k'' = 1*10^5 M^{-1}$. [Pt] was varied from 0 to $3*10^{-5}$ M. In Panel A, in order of increasing absorbance from the dashed line $\varepsilon_{PD''}$ ($M^{-1}cm^{-1}$) = $5*10^4$, $7*10^4$, $9*10^4$, $11*10^4$, $12*10^4$. In Panel B, in order of decreasing absorbance from the dashed line $\varepsilon_{PD''}$ ($M^{-1}cm^{-1}$) = $5*10^4$, $1*10^4$, $3*10^4$, $0.1*10^4$.

C. Macromolecules with one binding site where the dye molecules can bind to that site either as a monomer or a dimer.

Consider a dye molecule D binding to a protein P with one binding site. Let the dye bind to this site either as a monomer or as a dimer to form complexes PD and PD_2 respectively. The absorbance of this system is thus a sum of the contributions of three species viz. the free dye D, and the complexes PD and PD_2. The protein does not absorb in the experimentally observed region and therefore does not contribute to the absorbance. Let k_1 and k_2 be the binding constants for formation of complexes PD and PD_2 respectively.

Symbols:

PD = Complex of protein and dye with 1:1 stoichiometry, i.e. dye binding as a monomer

PD_2 = Complex of protein and dye with 1:2 stoichiometry, i.e. dye binding as a dimer

k_1 = Binding constant for dye binding as a monomer

k_2 = Binding constant for dye binding as dimer

ε_D = Extinction coefficient of dye free in solution

ε_{PD} = Extinction coefficient of dye bound as monomer

ε_{PD2} = Extinction coefficient of dye bound as dimer

Abs = Absorbance

Equations

$$P + D \overset{k_1}{\leftrightarrow} PD \qquad \text{(Dye binding as a monomer)}$$

$$PD + D \overset{k_2}{\leftrightarrow} PD_2 \qquad \text{(Dye binding as a dimer)}$$

$$k_1 = \frac{[PD]}{[P][D]} \qquad (1)$$

$$k_2 = \frac{[PD_2]}{[PD][D]} \qquad (2)$$

The total dye and protein concentrations are defined by equations (3) and (4) respectively

$$[Pt] = [P] + [PD] + [PD_2] \qquad (3)$$

$$[Dt] = [D] + [PD] + 2[PD_2] \qquad (4)$$

Equation (5) can be obtained by substituting equations (1) and (2) in equation (3).

$$[Pt] = [P] + k_1[P][D] + k_1k_2[P][D]^2 \qquad (5)$$

Equation (6) can be obtained by substituting equations (1) and (2) in equation (4).

$$[Dt] = [D] + k_1[P][D] + 2k_1k_2[P][D]^2 \qquad (6)$$

Equation (5) can be rearranged to give equation (7)

$$[Pt] = [P](1 + k_1[D] + k_1k_2[D]^2) \qquad (7)$$

The free protein concentration [P], can be expressed in the form of equation (8), by rearranging equation (7)

$$[P] = \frac{[Pt]}{1 + k_1[D] + k_1k_2[D]^2} \qquad (8)$$

Substituting for [P] in equation (6)

$$[Dt] = [D] + [Pt]\frac{k_1[D] + 2k_1k_2[D]^2}{1 + k_1[D] + k_1k_2[D]^2} \qquad (9)$$

Equation (9) when simplified gives a cubic equation in [D].

$$a[D]^3 + b[D]^2 + c[D] + d = 0 \qquad (10)$$

where,

$a = k_1k_2$

$b = -(k_1k_2[Dt] - k_1 - 2k_1k_2[Pt])$

$c = 1 + k_1[Pt] - k_1[Dt]$

$d = -[Dt]$

The absorbance of this system is given by equation (11)

$$Abs = \varepsilon_D[D] + \varepsilon_{PD}[PD] + \varepsilon_{PD_2}[PD_2] \qquad (11)$$

[PD] and [PD_2] can be obtained from equations (12) and (13) respectively

From equations (1) and (8), [PD] can be expressed as:

$$[PD] = \frac{k_1[Pt][D]}{1 + k_1[D] + k_1k_2[D]^2} \qquad (12)$$

From equations (2) and (12), [PD_2] can be expressed as:

$$[PD_2] = \frac{k_1k_2[Pt][D]^2}{1 + k_1[D] + k_1k_2[D]^2} \qquad (13)$$

Substituting for [PD] and [PD_2] in equation (11) from equations (12) and (13) gives absorbance values which can then be plotted against [Pt]. [PD] and [PD_2] were solved using equations (12) and (13). The values of these complexes were then substituted in equation (11) and solved for absorbance which was then plotted against [Pt], and the plots are biphasic as shown in Panel A of Figure 9.9. The unknown variables in this model are k_1, k_2, ε_D, ε_{PD} , ε_{PD2}. Realistic values were used as estimates for these variables and the equations

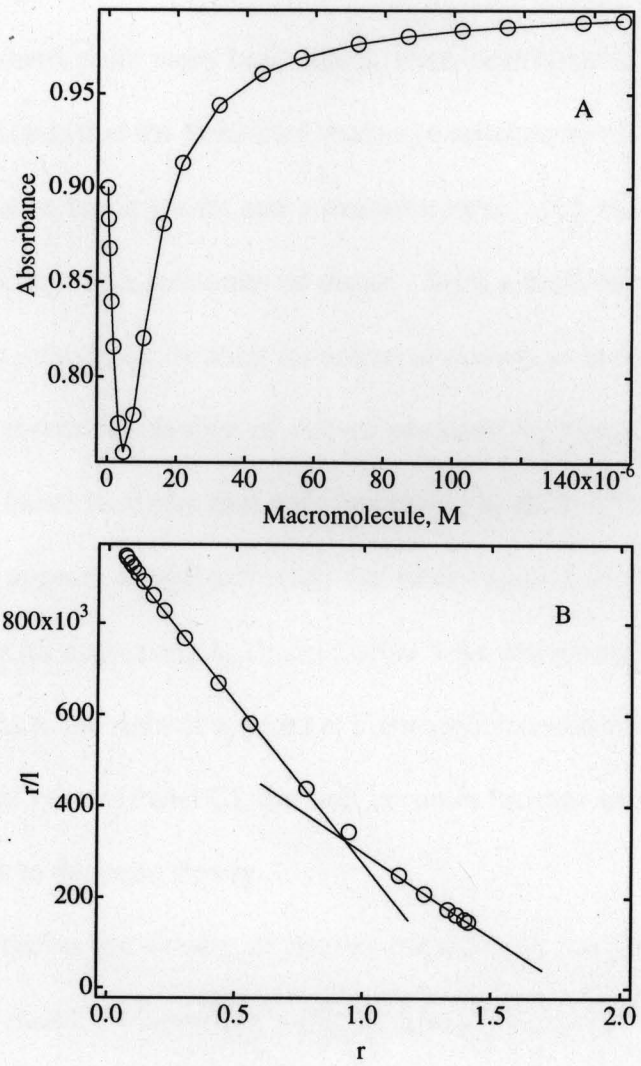

Figure 9.9 Plot obtained using Model C (Panel A). $\varepsilon_D = 9*10^4 M^{-1}cm^{-1}$, [Dt] $=10*10^{-6}$ M, [Pt] was varied from 0 to $1.5*10^{-4}$ M, $\varepsilon_{PD1} = 10*10^4 M^{-1}cm^{-1}$, $\varepsilon_{PD2} = 5*10^4 M^{-1}cm^{-1}$, $k_1 = 1*10^6 M^{-1}$, $k_2 = 1*10^5 M^{-1}$.

Panel B shows the corresponding Scatchard plot, r = [BoundDye]/[Protein], l = [Free Dye].

were solved accordingly to obtain the concentrations of both, bound and free ligand and corresponding Scatchard plots were built which were non-linear as shown in Panel B of Figure 9.9. This indicates that the Scatchard analysis cannot permit the distinction between a macromolecule with two binding sites and a macromolecule with one binding site, to which the ligand can bind either as a monomer or dimer. Such a distinction can only be made if there is spectroscopic evidence indicating formation of dimers, as in the case of TAM^{+}s.

Figure 9.10 shows the family of curves obtained by varying k_1, when the other variables are fixed. Panel A shows that with increasing k_1 ($k_1 > 1*10^6\ M^{-1}$) the absorbance increases. The well appears at approximately the same region (*circa* $5*10^{-6}$M) in Panel A. Panel B shows that with decreasing k_1 ($k_1 < 1*10^6 M^{-1}$) the absorbance decreases at a slower rate and the well shifts to the right or appears at higher macromolecule concentrations. When k_1 assumes even lower values (Panel C), the well becomes broader with decreasing k_1 and the absorbance also tends to decrease slowly.

Figure 9.11 shows the family of curves obtained by varying k_2, when the other variables are fixed. Panel A shows that with decreasing k_2 ($k_2 < 1*10^5\ M^{-1}$) the absorbance increases. The well shifts to the left with decreasing k_2 and eventually disappears as k_2 assumes much lower values. On the other hand in Panel B with increasing k_2 ($k_2 > 1*10^5 M^{-1}$) the absorbance decreases and the well becomes broader as the absorbance remains constant over a larger macromolecule concentration range.

Figure 9.12 shows the family of curves obtained by varying ε_{PD2} when the other variables are fixed. With increasing extinction coefficient ($\varepsilon_{PD2} > 5*10^4 M^{-1}cm^{-1}$) the absorbance tends to increase though the well appears at the same macromolecule concentration (*circa* $5*10^{-6}$ M) (Panel A of Figure 9.8). However, as observed in Panel B of

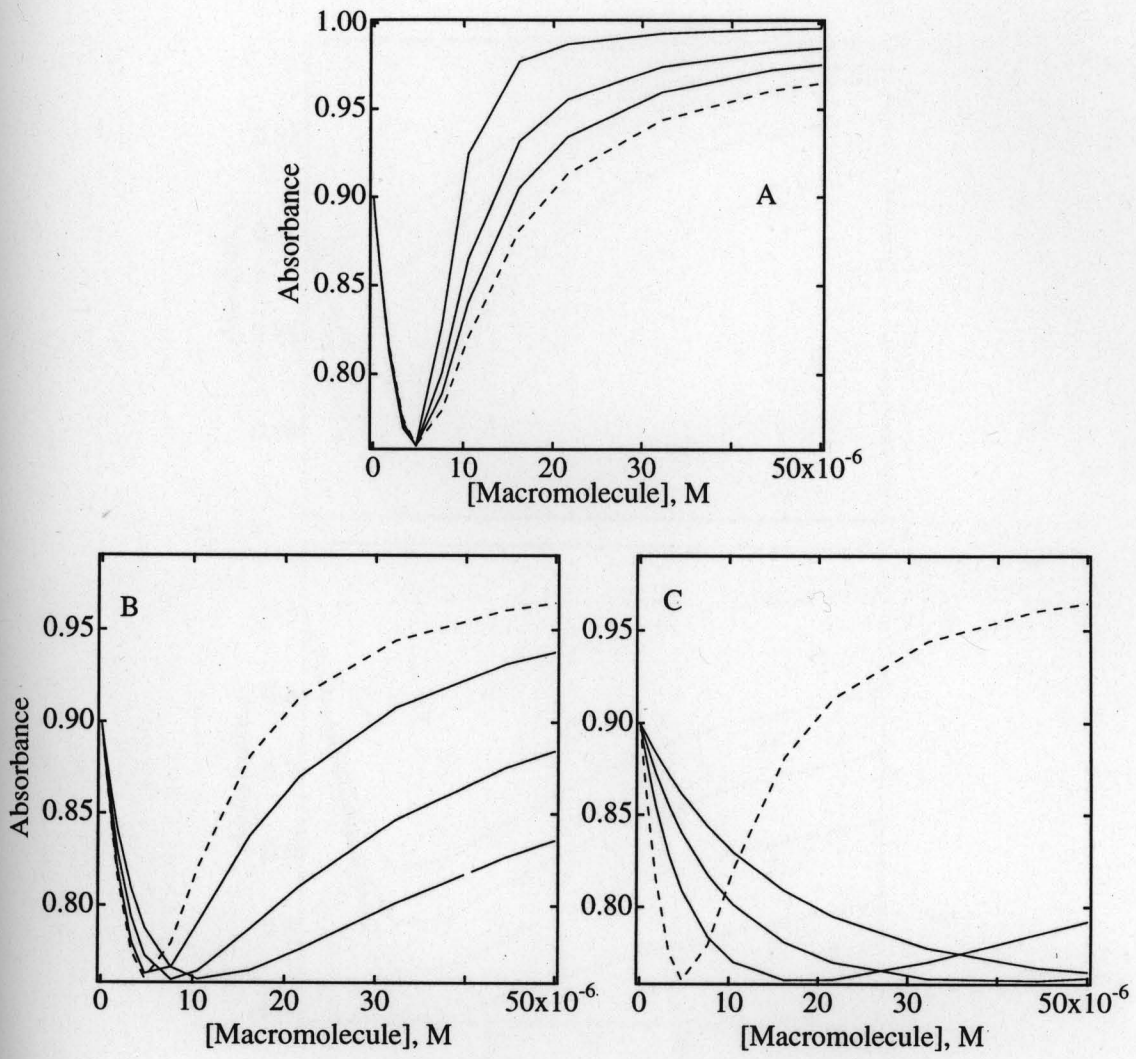

Figure 9.10 Plots obtained (using Model C) by varying k_1. The fixed variables were : $\varepsilon_D = 9*10^4 M^{-1}cm^{-1}$, [Dt] $=10*10^{-6}$ M, $\varepsilon_{PD1} = 10*10^4 M^{-1}cm^{-1}$, $\varepsilon_{PD2} = 5*10^4 M^{-1}cm^{-1}$, $k_2 = 1*10^5 M^{-1}$. [Pt] was varied from 0 to $3*10^{-5}$ M. In Panel A in order of increasing absorbance from the dashed line k_1 (M^{-1}) = $1*10^6$, $1.5*10^6$, $2.5*10^6$, $1*10^7$; in Panel B in order of decreasing absorbance from the dashed line k_1 (M^{-1}) = $1*10^6$, $0.5*10^6$, $0.2*10^6$; in Panel C in order of decreasing absorbance from the dashed line k_1 (M^{-1}) = $1*10^6$, $0.5*10^5$, $0.2*10^5$, $0.1*10^5$.

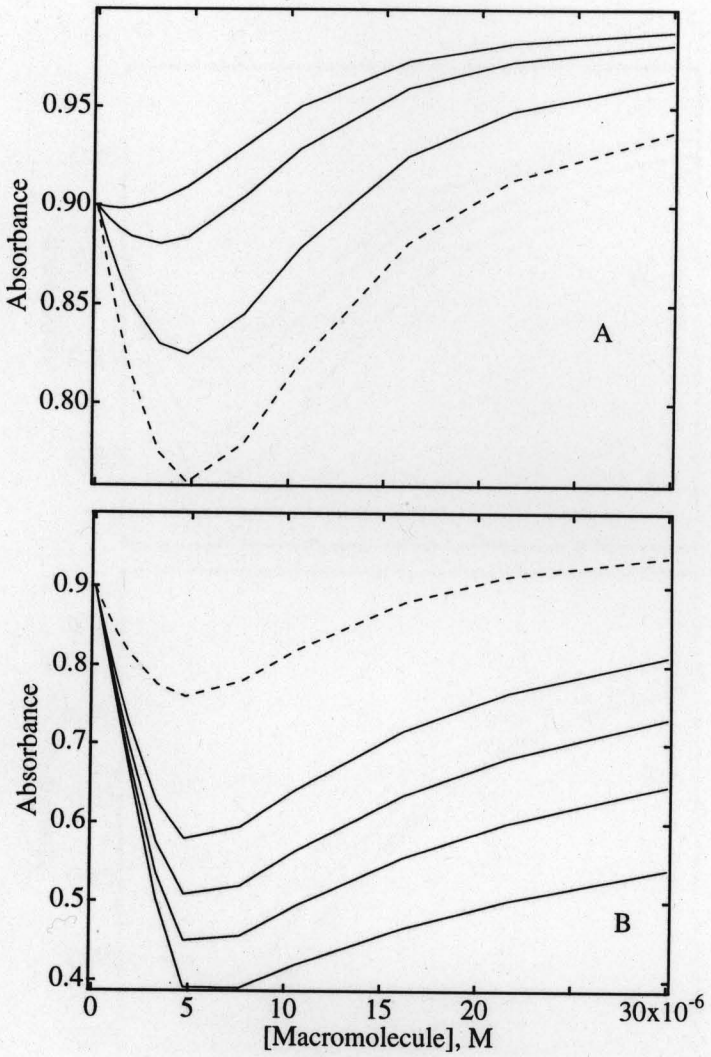

Figure 9.11 Plots obtained (using Model C) by varying k_2. The fixed variables were : $\varepsilon_D = 9*10^4 M^{-1}cm^{-1}$, [Dt] $=10*10^{-6}$ M, $\varepsilon_{PD1} = 10*10^4 M^{-1}cm^{-1}$, $\varepsilon_{PD2} = 5*10^4 M^{-1}cm^{-1}$, $k_1 = 1*10^6 M^{-1}$. [Pt] was varied from 0 to $3*10^{-5}$ M. In Panel A, in order of increasing absorbance from the dashed line k_2 (M^{-1}) = $1*10^5$, $0.5*10^5$, $0.2*10^5$, $0.1*10^5$. In Panel B, in order of decreasing absorbance from the dashed line k_2 (M^{-1}) = $1*10^5$, $5*10^5$, $1*10^6$, $2*10^6$, $5*10^6$.

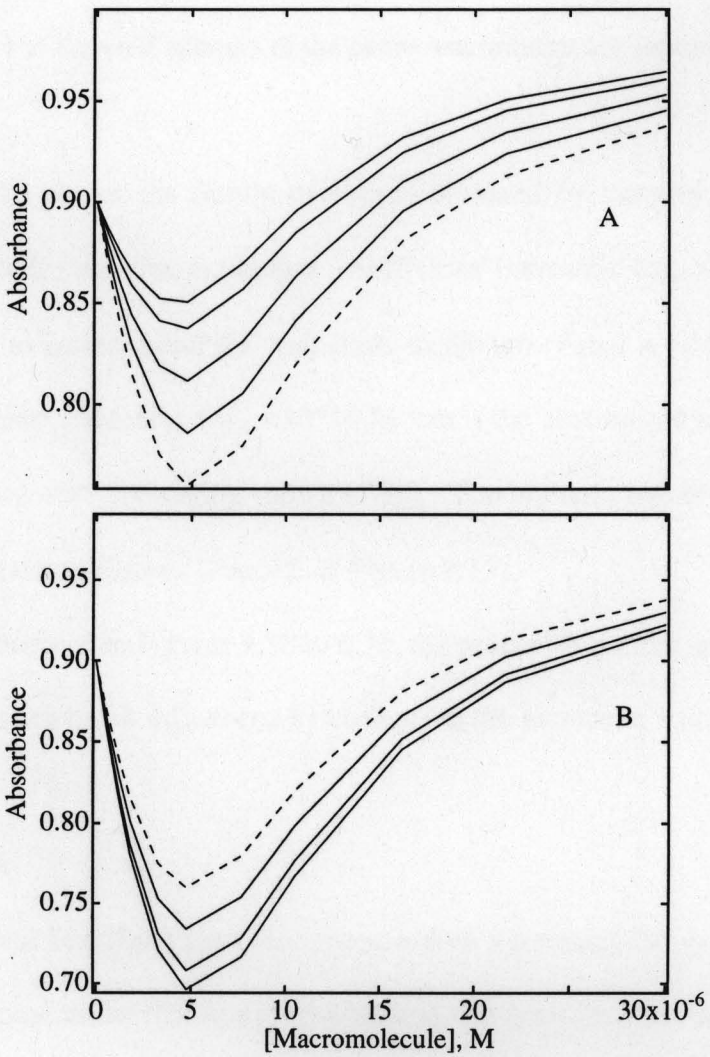

Figure 9.12 Plots obtained (using Model C) by varying ε_{PD2}. The fixed variables were : $\varepsilon_D = 9*10^4 M^{-1}cm^{-1}$, [Dt] $=10*10^{-6}$ M, $\varepsilon_{PD1} = 10*10^4 M^{-1}cm^{-1}$, $k_1 = 1*10^6 M^{-1}$, $k_2 = 1*10^5 M^{-1}$. [Pt] was varied from 0 to $3*10^{-5}$ M. In Panel A, in order of increasing absorbance from the dashed line ε_{PD2} ($M^{-1}cm^{-1}$) = $5*10^4$, $7*10^4$, $9*10^4$, $11*10^4$, $12*10^4$. In Panel B, in order of decreasing absorbance from the dashed line ε_{PD2} ($M^{-1}cm^{-1}$) = $5*10^4$, $1*10^4$, $3*10^4$, $0.1*10^4$.

Figure 9.12, with decreasing extinction coefficient ($\varepsilon_{PD2}<5*10^4M^{-1}cm^{-1}$) the absorbance tends to decrease but the well appears at the same macromolecule concentration (*circa* $5*10^{-6}$ M).

Figure 9.13 shows the family of curves obtained by varying ε_{PD1} when the other variables are fixed. As the extinction coefficient increases ($\varepsilon_{PD1}>10*10^4M^{-1}cm^{-1}$), the absorbance tends to increase and the well shifts to the left (Panel A of Figure 9.13). As the extinction coefficient decreases ($\varepsilon_{PD1}<10*10^4M^{-1}cm^{-1}$) the absorbance tends to decrease and the well disappears with decreasing values of ε_{PD1}. The biphasic nature of the profile is lost and the curves appear to plateau (Panel B of Figure 9.13).

Thus as observed in Figures 9.10 to 9.13, the profile shape, the appearance of the well and the shifts are very much influenced by changes in the parameter values.

CONCLUSIONS:

The classical Scatchard analysis approach does not permit the distinction between the aggregation of ligand molecules in a single binding site from the existence of different types of binding sites for that ligand. This limitation of the Scatchard analysis precludes its use in the analysis of binding data that involves distinct noncovalent interactions, like self-association and macromolecular binding that occur simultaneously in the case of TAM^+s. The visual inspection of the biphasic profiles obtained using Models B and C show that the well of the biphasic profile mostly appears at approximately $5*10^{-6}M$ ([Dt] = $10*10^{-6}M$), indicating that there are two dye molecules per macromolecule. While the ratio of dye to macromolecule at the well may be true for both cases, each case is distinctly different, because the macromolecule in Model C, has only one ligand binding site, while in Model B,

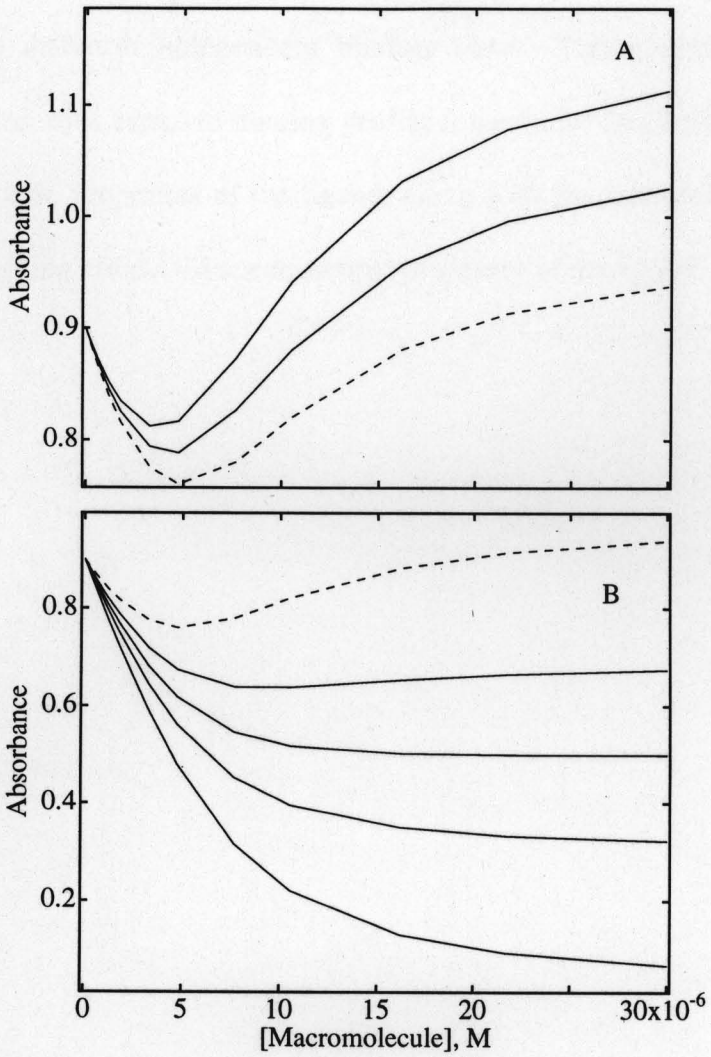

Figure 9.13 Plots obtained (using Model C) by varying ε_{PD1}. The fixed variables were : $\varepsilon_D = 9*10^4 M^{-1}cm^{-1}$, [Dt] $=10*10^{-6}$ M, $\varepsilon_{PD2} = 5*10^4 M^{-1}cm^{-1}$, $k_1 = 1*10^6 M^{-1}$, $k_2 = 1*10^5 M^{-1}$. [Pt] was varied from 0 to $3*10^{-5}$ M. In Panel A, in order of increasing absorbance from the dashed line ε_{PD1} ($M^{-1}cm^{-1}$) = $10*10^4$, $11*10^4$, $12*10^4$. In Panel B, in order of decreasing absorbance from the dashed line ε_{PD1} ($M^{-1}cm^{-1}$) = $10*10^4$, $7*10^4$, $5*10^4$, $3*10^4$, $0.1*10^4$.

it has two different independent binding sites. This indicates that the rigorous interpretation of a biphasic binding profile requires the availability of information on the solvatochromic properties of the ligand, along with the knowledge of the extent to which exciton coupling affects the spectroscopic properties of the ligand.

Chapter 10. Conclusions and Suggestions for Future Work

CONCLUSIONS:

1. The study on the effects of solvents on the spectroscopic properties of TAM^+s, supports previous objections to the rotamers model, since they indicate that the magnitude of the splitting between the overlapped absorption bands of the highly symmetrical TAM^+ dyes, CV^+ and EV^+ is dependent upon solvent solvatochromic parameters.

2. The spectral signatures of TAM^+s (blue shifts and hypochromic effects) obtained in the presence of HK and DNA suggest that dye aggregation, a phenomenon that is usually observed at high dye concentrations and high ionic strength, occurs in the presence of these biopolymers at submicromolar dye concentration. The observation of dye aggregate formation in the presence of SDS at concentrations below the CMC indicates that the interaction of TAM^+ dyes with the negative head of the detergent facilitates aggregation, suggesting that similar interactions take place in the presence of HK and DNA. The tendency to aggregate decreases in the following order $VPBBO^+ \geq EV^+ > VBR^+ > CV^+$.

3. The observed remarkable increase in fluorescence upon binding of TAM^+s to a macromolecule indicates that the dye finds itself in a binding environment in which the fast nonradiative rotational relaxation processes are sterically hindered. This not only increases the fluorescence quantum yields, but also leads to an enhancement in the singlet lifetime of the TAM^+. This long-lived singlet can either intersystem cross to the triplet or can directly

interact with the substrate, resulting in an increase in the photoreactivity of TAM^+s when noncovalently bound to a biopolymer.

4. The ability to cause photoinhibition of enzymatic activity and photoinduced DNA damage followed the trend $CV^+ > VBR^+ > EV^+ > VPBBO^+$, which is the opposite of the trend observed for dye aggregation ($CV^+ < VBR^+ < EV^+ < VPBBO^+$). Thus the magnitude of photoinduced macromolecular damage in the case of HK and DNA decreases with the increasing degree of aggregation. Comparative evaluation between monomers and aggregates of the same dye also revealed that the monomers are capable of inducing damage to DNA and HK much more efficiently than aggregates.

5. Among the TAM^+ dyes investigated here, CV^+ is the one showing better clinical potential. CV^+ is the dye that brings about maximum damage to HK and DNA, and it has been previously demonstrated that it is the only dye exhibiting selective destruction of leukemia cells (Indig et al, 2000).

6. TAM^+s interact with both the protein and the lipid portion of LDL, but partitioning into the lipid core represents the major binding event. No experimental evidence has been found for the formation of TAM^+ aggregates upon binding to LDL. TAM^+s can induce lipid peroxidation upon photolysis of the TAM^+–LDL complexes, and the degree of lipid peroxidation increases with increasing dye concentration.

7. The Scatchard analysis cannot permit the distinction between the aggregation of ligand molecules in a single binding site from the existence of different types of binding sites for that ligand. This distinction requires the analysis of binding data based on the molecular exciton theory and the knowledge of solvatochromic effects on the electronic spectra of TAM^+ dyes.

SUGGESTIONS FOR FUTURE WORK:

Dye aggregation can reduce tumor cell selectivity in PDT (Figure 10.1). Because the tumor cells have an elevated mitochondrial membrane potential compared to normal cells, it is conceivable that upon increasing dye concentration the formation of dye aggregates will develop earlier in tumor cells than in the normal cells. Accordingly, under high dye concentration regimes, any excess dye in targeted cells above the level of dye aggregation would decrease the efficiency with which these photosensitizers inactivate mitochondrial biopolymers like DNA and HK, while a lower dye concentration in the surrounding normal tissue (below the dye aggregation range) would be associated with higher photosensitization efficiency. Therefore it is reasonable to infer that maximum selectivity towards tumor cells is achieved when the final dye concentration in these cells falls below the aggregation range, and is kept at a minimum in the surrounding normal tissues. If this hypothesis based on *in vitro* data is true, then mitochondrial targeting with cationic photosensitizers would represent a case in PDT in which the use of lower rather than higher doses might be associated with better therapeutic effects. Moreover the use of lower dye doses may also help in reducing undesirable side effects like systemic toxicity. A systematic study could be carried out to

At Low Photosensitizer Dose :

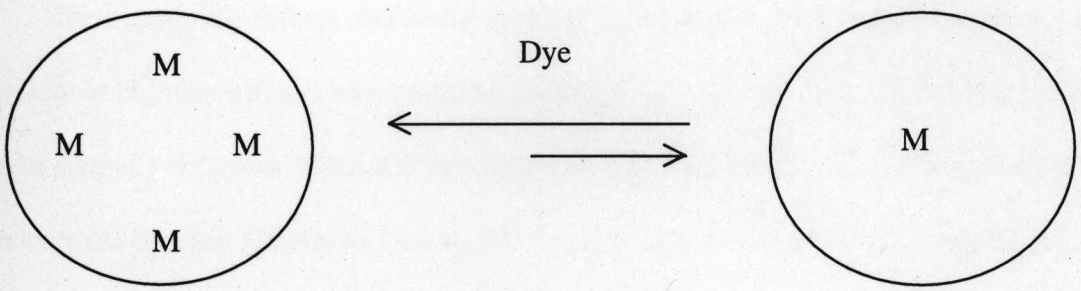

At High Photosensitizer Dose :

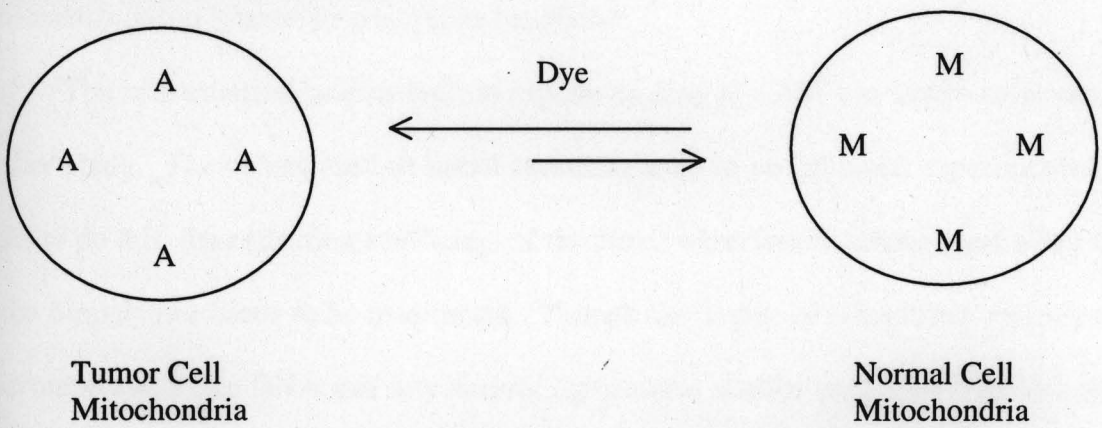

Figure 10.1 Dye aggregation can affect the selectivity in PDT. Cells on the left represent tumor cell mitochondria and cells on the right hand represent normal cell mitochondria. M – Monomer, A – Aggregates. Low photosensitizer dose leads to the binding of dye molecules as monomers in the tumor cell mitochondria, leading to beneficial therapeutic effects. High photosensitizer dose (above the level of dye aggregation) leads to binding of dye aggregates in the tumor cell mitochondria and dye monomers in the normal cell mitochondria, reducing selectivity.

prove this hypothesis initially at the cellular level under conditions of high and low dye concentrations.

The synergistic effects that could possibly be obtained using a combination of anionic and cationic photosensitizers also could be explored. It is possible that the reaction pathways may be entirely different when the two types of photosensitizers are used in combination. Moreover the binding affinity to various PDT targets may be different or compromised when both types of photosensitizers are present in the neoplastic tissue. If they are injected together *in vivo* and fail to bring about the desired therapeutic effects, then using them in conjunction but in separation may prove beneficial

The mathematical models built to explain binding of TAM^{+}s to macromolecules need further study. The values used as initial estimates need to be validated experimentally. In order to do this, the extinction coefficient of the dimer when free in solution and when bound to the biopolymer needs to be determined. Though the degree of complexity increases with macromolecules like DNA and low density lipoprotein, similar such mathematical models can be built and evaluated.

Appendix I (Model A)

Since Igor Pro does not allow the use of certain characters like primes, subscripts, superscripts etc., within a macro, some of the symbols were replaced as shown below.

For a protein with one ligand binding site, with ligand binding as a monomer :

Pt = Total Protein

Dt = Total Dye

P = Free Protein

D = Free Dye

K = Binding constant

EpsD = ε_D = Extinction coefficient of dye

EpsPD = ε_{PD} = Extinction coefficient of dye bound as monomer to the protein

Absor = Absorbance

Macro :

```
Function/D Compute_PD(k, Pt, Dt)
        Variable/D k, Pt, Dt
        Variable/D PD
PD = ((k*Pt + k*Dt +1)/(2*k) ) - ((((-k*Pt - k*Dt -1)^2 - (4*k^2*Dt*Pt))^0.5)/(2*K))
        printf "Pt - %e, Dt- %e, PD- %e\r", Pt, Dt, PD
        return PD
End
Function/D Compute_Absor(EpsPD, EpsD, Dt, PD)
```

```
	Variable/D  EpsPD, EpsD, Dt, PD
	Variable/D Absor
	Absor = EpsD*Dt - EpsD*PD + EpsPD*PD
	printf  "Absor- %e\r", Absor
	return Absor
End
```

Appendix II (Model B)

For protein with two ligand binding sites, with ligand binding as a monomer at each site:

Pt = Total Protein

Dt = Total Dye

P = Free Protein

D = Free Dye

k1= k′= Binding constant for first binding site

k2= k″= Binding constant for second binding site

EpsD = ε_D = Extinction coefficient of dye

EpsPD1 = $\varepsilon_{PD'}$ = Extinction coefficient of dye bound at the low affinity site

EpsPD2 = $\varepsilon_{PD''}$ = Extinction coefficient of dye bound at the high affinity site

Macro:

```
Function/D SolveForD(k1, k2, Pt, Dt, D_guess)
        Variable/D k1, k2, Pt, Dt, D_guess;
        Variable/D a, b, c;
        Variable/D D, f_guess, f_d_guess, D_new, epsilon;

        a = 2*Pt-Dt + (k1+k2)/(k1*k2);
        b = (1 + (Pt-Dt)*(k1+k2))/(k1*k2);
        c =-Dt/(k1*k2);
        epsilon = 1e-14;
```

```
|       printf "Pt - %e, Dt- %e, a - %e, b - %e, c - %e\r", Pt, Dt, a, b, c;

        D_new = D_guess;
        do
                D = D_new;
                f_guess = D^3 + a*D^2 + b*D + c; || f(D)
                if (f_guess == 0)
                        break;
                endif
                f_d_guess = 3*D^2 + 2*a*D + b;  || f'(D)
                D_new = D - (f_guess/f_d_guess);
|               printf "f_guess - %e, F_d_guess - %e, D_new - %e\r", f_guess,
f_d_guess,D_new;
        while (abs(D - D_new) > epsilon)

        printf "Soln -%e\r", D;
        return D;
End

Function/D Computed_Absorbance(EpsD, EpsPD1, EpsPD2, k1, k2, Pt, D)
        Variable/D EpsD, EpsPD1, EpsPD2,k1, k2, Pt, D
        Variable/D Absorbance, denom
```

```
        denom = (1+k1*D) * (1+k2*D);
        Absorbance =EpsD*D + (EpsPD1 * k1 + EpsPD2 * k2) * D * Pt / denom  + (EpsPD1
        + EpsPD2)*((k1*k2*Pt*D^2)/denom);
        printf  "Absorbance- %e\r", Absorbance
        return Absorbance
End

Macro twosite (Pt_data_name, EpsD, EpsPD2, EpsPD1, k1,k2)
    String    Pt_data_name;
    variable k1, k2, EpsD, EpsPD2, EpsPD1
       prompt Pt_data_name,  "Pt data :", popup,WaveList("*",";","")
       prompt k1,      "Input  k1: "
       prompt k2,      "Input  k2: "
       prompt EpsD,   "Input  EpsD: "
       prompt EpsPD1, "Input  EpsPD1: "
       prompt EpsPD2, "Input  EpsPD2: "

       Make /O/D/N=(numpnts($Pt_data_name)) Pt_Values=$Pt_data_name
       Make /O/D/N=(numpnts($Pt_data_name)) D_Values
       Make /O/D/N=(numpnts($Pt_data_name)) Abs_Wave

       Display Abs_Wave vs Pt_Values
```

```
Edit Abs_Wave

Edit D_Values


D_Values = SolveForD(k1, k2, Pt_Values, 10e-6, 1e-5);

Abs_Wave = Computed_Absorbance(EpsD, EpsPD1, EpsPD2, k1, k2, Pt_Values,
D_Values)

EndMacro
```

Note that to solve the cubic equation in D, the Newton-Raphson method was used. For finding the roots of the function 'f(x)' it works by starting with an initial guess 'x_guess' and progressively refining the estimate. Briefly, it computes the series x_0, x_1, x_2, ..., x_n, x_n+1, ...

The series is computed as:

$x_0 = x\_guess$

$x_{n+1} = x_n - f(x_n)/f'(x_n)$

Given this series, the root is x_n such that ($|x_{n+1} - x_n| < epsilon$) for a constant value of 'epsilon' (the acceptable error in the estimate of the root).

Appendix III (Model C)

For protein with one binding site that is capable of binding both, ligand monomers and ligand dimers.

Pt = Total Protein

Dt = Total Dye

P = Free Protein

D = Free Dye

k1 = k_1 = Binding constant for dye binding as a monomer

k2 = k_2 = Binding constant for dye binding as dimer

EpsD = ε_D = Extinction coefficient of dye

EpsPD1= ε_{PD} = Extinction coefficient of dye bound as monomer

EpsPD2 = ε_{PD2} = Extinction coefficient of dye bound as dimer

Abs = Absorbance

Macro:

```
Function/D SolveForD(k1, k2, Pt, Dt, D_guess)
        Variable/D k1, k2, Pt, Dt, D_guess;
        Variable/D a, b, c, D_new, D, f_guess, f_d_guess, epsilon;

        a = -Dt +2*Pt + 1/k2;
        b = (1 + k1*(Pt - Dt))/(k1 * k2);
        c =-Dt/(k1 * k2);
        epsilon = 1e-20;
```

```
|       printf "Pt - %e, Dt- %e, a - %e, b - %e, c - %e\r", Pt, Dt, a, b, c;

        D_new = D_guess;
        do
                D = D_new;
                f_guess = D^3 + a*D^2 + b*D + c; || f(D)
                if (f_guess == 0)
                        break;
                endif
                f_d_guess = 3*D^2 + 2*a*D + b;  || f'(D)
                D_new = D - (f_guess/f_d_guess);
|               printf "f_guess - %e, F_d_guess - %e, D_new - %e\r", f_guess,
f_d_guess,D_new;
        while (abs(D - D_new) > epsilon)

        printf "Soln -%e\r", D;
        return D;

End

Function/D Comput_Absorbance(EpsD, EpsPD1, EpsPD2, k1, k2, Pt, D)
        Variable/D EpsD, EpsPD1, EpsPD2,k1, k2, Pt, D
```

```
        Variable/D Absorbance

        Absorbance =EpsD* D + EpsPD1 *(( k1 * D * Pt) / (1 + k1*D + k1*k2*D^2)) +
EpsPD2*((k1*k2*Pt*D^2)/(1+k1*D+k2*k1*D^2))
        printf  "Absorbance- %e\r", Absorbance
        return Absorbance
End

Macro monodimers (Pt_data_name, EpsD, EpsPD2, EpsPD1, k1,k2)
    String   Pt_data_name;
    Variable k1, k2, EpsD, EpsPD2, EpsPD1
        prompt Pt_data_name,  "Pt data :", popup,WaveList("*",";","")
        prompt k1,      "Input  k1: "
        prompt k2,      "Input  k2: "
        prompt EpsD,   "Input  EpsD: "
        prompt EpsPD1, "Input  EpsPD1: "
        prompt EpsPD2, "Input  EpsPD2: "

        Make /O/D/N=(numpnts($Pt_data_name)) Pt_Values=$Pt_data_name
        Make /O/D/N=(numpnts($Pt_data_name)) D_Values
        Make /O/D/N=(numpnts($Pt_data_name)) Abs_Wave

        Display Abs_Wave vs Pt_Values
```

```
Edit Abs_Wave

Edit D_Values

D_Values = SolveForD(k1, k2, Pt_Values, 10e-6, 1e-5);

Abs_Wave = Compute_Absorbance(EpsD, EpsPD1, EpsPD2, k1, k2, Pt_Values,
D_Values)

EndMacro
```

Note that to solve the cubic equation in D, the Newton The Newton-Raphson method was used. For finding the roots of the function 'f(x)' it works by starting with an initial guess 'x_guess' and progressively refining the estimate. Briefly, it computes the series x_0, x_1, x_2, ..., x_n, x_n+1, ...

The series is computed as:

$x_0 = x\_guess$

$x_{n+1} = x_n - f(x_n)/f'(x_n)$

Given this series, the root is x_n such that ($|x_{n+1} - x_n| < epsilon$) for a constant value of 'epsilon' (the acceptable error in the estimate of the root).

REFERENCES:

Allison B. A.; Pritchard P. H.; Levy J. G., Evidence for low density lipoprotein receptor mediated uptake of benzoporphyrin derivative, B. J. Cancer, 69, 833-839, 1994.

Arora K. K.; Pederson P. L., "Functional significance of mitochondrial bound hexokinase in tumor cell metabolism," J. Biol. Chem., 263: 17422-17428, 1988

Baptista M. S.; Indig G. L., "Effect of BSA binding on the photophysical and photochemical properties of triarylmethane dyes", J. Phys. Chem. B, 102:4678-4688, 1998.

Baptista M. S.; Indig G. L., "Mechanism of photobleaching of EV non-covalently bound to BSA", Chem. Comm., 1791-1792, 1997.

Bartlett J. A.; Indig, G. L., "Spectroscopic and photochemical properties of Malachite Green noncovalently bound to bovine serum albumin", Dyes and Pigments, 43: 219-226, 1999.

Bartlett J. A., Indig G. L., "Effect of self-association and protein binding on the photochemical reactivity of triarylmethanes. Implications of noncovalent interactions on the competition between photosensitization mechanisms Type I and Type II", Photochem and Photobiol. 70: 490-498, 1999.

Bartlett J. A.; Indig, G. L. unpublished data

Benesi H; Hildebrand J. "A spectrophotometric investigation of the interaction of iodine with aromatic hydrocarbons", J. Am. Chem. Soc. 71: 2703-2707, 1949.

Bernal S. D.; Lampidis, T. J.; Melsaac, R. M.; Chen, L. B., "Anticarcinoma activity of Rhodamine 123, a mitochondria specific dye", Science, 222: 169-172, 1983.

Barrett J. T.; Schoenlein, P. V.; Lipschultz, C., "Mitochondrial-DNA damage and cell survival following photodynamic therapy and ionizing radiation", Int. J. Radiat. Oncol., 27: 308-308 Suppl. 1, 1993.

Bernad Brenad, M. J.; Gracia-Mora, J.; Diaz, D.; Mendoza Diaz, G., "Molecular interactions and thermodynamic aspects of the complexation reaction between gentian violet and several cyclodextrins", J. Incl. Pheno. Macro., 34: 1-18, 1999.

Bonnett R. "Chemical Aspects of Photodynamic Therapy" Gordon and Breach Science Publishers: London, 2000.

Cantor C. R. and Schimmel P. R., Biophysical Chemistry, Part II. "Techniques for the study of biological structure and function," W,. N. Freeman and Co., San Francisco, 1980.

Chance B., "Fluorescent probe environment and the structural charge changes in energy coupling of mitochondrial membranes", Proc. Natl. Acad. Sci. USA, 67: 560-564, 1970.

Chen L. B., "Mitochondrial membrane potential in living cells", Ann. Rev. Cell. Biol., 4: 155-181, 1988

Chris de Schmidt P.; Verluis A. J.; Van Berkel T. J., "Properties of incorporation, redistribution and integrity of porphyrin-LDL complexes", Biochemistry, 32 : 2916-2922, 1993.

Chriswell, C. D.; Schilt, A. A., "New and improved techniques for applying the mole ratio method to the identification of weak complexes in solution", anal. Chem. 47: 1623-1629, 1975.

Cohen G.; Eisenberg, H. K., "Viscosity and sedimentation study of sonicated DNA-proflavine complexes", Biopolymers, 8: 45-55, 1969.

Connors K. A., "The stability of cyclodextrin complexes in solution", Chem. Rev., 97:1325-1357, 1997

Cotton F. A., "Chemical applications of Group Theory", Secon Ed, Wiley-Interscience , New York, 1971

Crane R. K.; Sols A., "The association of hexokinase with particulate fractions of brain and other tissue homogenates", J. Biol. Chem., 210: 597-606, 1954.

Davis, C. "Amino-fluorene-compounds and process for the preparation thereof" United States Patent Office, US 3,344,189, 1967.

Davis S.; Weiss, M. J.; Wong, J. R.; Lampidis, T. J.; Chen, L. B., "Mitochondrial and plasma membrane potentials cause unusual accumulation and retention of Rhodamine 123 by human breast adenocarcinoma derived MCF-7 cells", J. Biol. Chem, 260: 13844-13850, 1985

Docampo R.; Silva, N. J. M.;Cruz, F.S.; "Enhancement of the cytotoxicity of crystal violet against Trypanosoma Cruzi in the blood by ascorbate," Molec. and Biochem. Parasitol., 27:241-248, 1988.

Dougherty T. J., Photosensitizers:Therapy and detection of malignant tumors. Photochem. Photobiol. 45 : 879-889, 1987

Dougherty T. J., "Photochemistry in the treatment of cancer", Adv. Photochem., 17: 275-311, 1992.

Dougherty T. J.; Gomer, C. J.; Henderson, B. W.; Jori, G.; Kessel , D.; Korbelik, M.; Moan, J.; Peng, Q, "Photodynamic Therapy", Journal of the National Cancer Institute, 90: 889-905, 1998

Duxbury D. F., "The photochemistry and photophysics of triarylmethane dyes in solid and liquid media", Chem Rev., 93: 381-433, 1993.

Easterby, J.S. and O' Brien, M.J., "Purification and properties of pig-heart hexokinase", European Journal of Biochemistry, 38: 201-211, 1973.

Eflkin, M. R.; Ghiron, C. A., "Exposure of tryptophanyl residues in proteins. Quantitative determination by fluorescence quenching studies", Biochemistry, 15: 672-80, 1976.

Fanciulli M.; Paggi, M. G.; Bruno, T.; Delcarlo, C.; Bonetto, F.; Gentile, F. P.; Floridi, A., "Glycolysis in normal and in hexokinase-transfected NIH/3T3 cells", Oncol. Res. 6:405-409, 1994.

Fiedorowicz M.; Galindo J. R.; Julliard M.; Mamoni P.; Chanon M., Efficient Photodynamic action of Victoria Pure Blue BO, Photochem. Photobiol., 58 (3), 356-361, 1993. 20. Viola A., 1996

Fisher, A. M. R; Murphree, A. L.; Gomer, C. J. "Clinical and preclinical photodynamic therapy" Lasers Surg. Med. 17: 2-31, 1995

Fliss, M. S., Usadel, H.; Caballero, O. L.; Wu, L.; Buta, M. R.; Eleff, S. M.; Jen, J., Sidransky, D., "Facile detection of mitochondrial DNA mutations in tumors and bodily fluids", Science, 287: 2017-2019, 2000.

Foote C. S., "Mechanism of photosensitized oxidation", Science, 162:963-970, 1968

Foster T. H.; Murant R. S. ; Bryant R. G. ; Knox R. S. ; Gibson S. L. ; Hilf R., "Oxygen consumption and diffusion effects in photodynamic therapy", Radiat. Res., 126: 296-303, 1991.

Fraiji, L. K.; Hayes, D. M.; Werner, T. C., "Static and Dynamic fluorescence quenching, experiments for the Physical chemistry laboratory", J. Chem. Edu. 69: 424-428, 1992.

Fromming K.; Szejtli, J.; "Cyclodextrins in Pharmacy", in "Topics in Inclusion Science", Davies, J. E. D. Eds., Kluwer Academic Publishers, Dordrecht, The Netherlands, 1994

Gal D.; Mcdonald P. C. ; Porter J. C.; Simpson E. R., "Cholesterol metabolism in cancer cells in monolayer culture, III, Low-density lipoprotein metabolism", Int J. Cancer 28:315-319, 1981.

Gennaro A. R.; Chase, G. D.; Marderosian, A. D.; Harvey, S. C.; Hussar, D. A.; Medwick, T.; Rippie, E. G.; Schwartz, J. B.; Swinyard, E. A.; Gilbert, Z.L.; Remmington's Pharmaceutical Sciences, 18E, Mack Publishing Company, Eston PN, 1990.

Ghosh S., Basu, M. K.; Schweppe, J. S., "Interaction of 1-ANS with human low density lipoprotein", Biochim. Biophys. Acta, 337: 395-403, 1974.

Girolami G. S., "A simple 'Back of the envelope' method for estimating the densities and molecular volumes of liquids and solids", J. Chem. Edu., 71: 962-964, 1994

Glasoe P. K.; Long, F. A., "Use of glass electrodes to measure acidities in deuterium oxide", J. Phys. Chem, 64: 188-190, 1960.

Gots R. E.; Gorin, F. A.; Bessman, S.P., "Kinetic enhancement of bound hexokinase activity by mitochondrial respiration", Biochem. Biophys. Res. Commun., 49: 1249-1255, 1972.

Gotts R.E.; Bessman, S. P., "The functional compartmentation of mitochondrial hexokinase", Arch. Biochem. Biophys., 163: 7-14, 1974.

Gupta, B. D.; Borys, T.J.; Abrahamson, E. W., " Absorption spectrum of rhodopsin in rod outer segment suspension: role of sieve effect", Photochem. and Photopysics, 12: 253-258, 1986.

Havel R. J., "The formation of LDL : Mechanisms and Regulation", J. Lipid Res., 25: 1570-76, 1984.

Hidefumi H.; Toshima, N.; Uenoyama, S., "Inclusion formation of γ-Cyclodextrin. One host-two guest complexation with water-soluble dyes in the ground state", Bull. Chem. Soc. Jpn., 58: 1156-1164, 1985. et al, 1985

Henderson B. W.; Waldow, S. M.: Mang, T.S.; Potter, W. R.; Malone, P. B.; Dougherty , T. J., "Tumor destruction and kinetics of tumor cell death in two experimental mouse tumors following photodynamic therapy", Cancer Research, 45: 572-576, 1985.

Henderson C. N. and Selinger B. K., "Solvent effects on intramolecular excimer formation of dipyrenylalkanes", Journal of Photochemistry, 16:215-222, 1981.

Hochhauser D., "Relevance of Mitochondrial DNA in cancer", The Lancet, 356:181-182, 2000.

Hunter F. E.; Gebicky J. M.; Hoffesten P. E.; Weinstein J.; Scott A., "Swelling and lysis of rat liver mitochondria induced by ferrous ions", J. Biol Chem., 238: 828-835, 1963.

Indig G. L., Photochemistry of Triarylmethane dyes bound to proteins, Optical Methods for tumor treatment and detection : Mechanisms and Techniques in Photodynamic therapy V, SPIE. 2675, 228-237, 1996.Indig G. L., "Mechanism of dye bleaching upon laser excitation of CV bound to BSA", Chemistry Letters, 3, 243-244, 1997.

Indig, G. L.; Anderson, G. S.; Nichols, M. G.; Bartlett, J. A.; Mellon, W. S.; Sieber, F., "Effect of Molecular Structure on the performance of triarylmethane dyes as therapeutic agents for photochemical purging of autologous bone marrow grafts from residual tumor cells," J. Pharm. Sci., 89:88-99, 2000.

Ishikawa M.; Ye, J. Y.; Maruyama Y.; Nakatsuka H.; "Triphenylmethane dyes revealing heterogeneity of their nanoenvironment: Femtosecond, picosecond, and single-molecule studies", J. Phys. Chem. A 103:4319-4331, 1999.

Jones II, G.; Oh, C., Goswami, K., "the photochemistry of triarylmethane dyes bound to polyelectrolytes : photoinduced electron transfer involving bound dye monomers and dimers", J. Photochem. Photobiol. A: Chem, 57: 65-80, 1991.

Jones II G.; Oh C.; Indig G. L.,Organic dyes bound to polyelectrolytes : Photophysical probes of binding domains and biopolymer conformation, In Aquatic and Surface Photochemistry, (Helz G. R., Zepp R. G., and Crosby D. G., Eds.); Lewis Publishers, Boca Raton, 129-136, 1994.

Jori G.; Beltramini M.; Reddi E. ; Salvato B. ; Pagnan A. ; Ziron L. ; Tomio L. ; Tsanov T., "Evidence for a major role of plasma lipoproteins as hematoporphyrin carriers *in vivo*", Cancer Lett., 24:291-297, 1984.

Jori G.; Reddi E., The role of lipoproteins in the delivery of tumor-targeting photosensitizers, Int J. Biochem, 25 :1369-1375, 1993.

Jori G., "Factors controlling the selectivity and efficiency of tumor damage in photodynamic therapy", Lasers Med. Sci., 5, 115-120, 1990.

Kamlet, M. J.; Abboud J . L. M. ; Abraham M. H.; Taft, R. W., "Linear Solvation energy relationships. 23. A comprehensive collection of the solvatochromic parameters, π^*, α and β and more methods for simplifying the generalized solvatochromic equation," J. Org. Chem., 48: 2877-2887, 1983.

Kasha M.; Rawls H. R.; El-Bayoumi M. A., "The exciton model in molecular spectroscopy", Pure Appl. Chem., 11: 371-392, 1965.

Kim J. S. and Kim H., "Stability and folding of a mutant ribose-binding protein of Escherichia Coli", J. Protein Chem., 15: 731-736, 1996.

Korppi-Tommola J.; Yip R. W., "Solvent effects on the visible absorption spectrum of crystal violet", Can. J. Chem., 59: 191-194, 1981.

Kottke M.; Adams, V.; Riesinger, I.; Bremm, G.; Bosch, W.; Brdiczka, D.; Sandrti, G.; Panfili, E., "Mitochondrial boundary membrane contact sites in brain: Points of hexokinae and creatine kinase location, and control of Ca2+ transport," Biochim. Biophys. Acta 935: 87-102, 1988

Kowaltowski A. J.; Verseci, A. E., "Mitochondrial damage induced by oxidative stress", Free. Rad. Biol. Med., 26: 463-471, 1999.

Lakowicz J. R., "Protein Fluorescence" In "Principles of FluorescenceSpectroscopy", Second Ed. Kluwer Academic Publishers, New York, N.Y., 446-485, 1999.

Leuck H. B.; McHale J. L.; Edwards, W. D., "Symmetry-breaking solvent effects on the electronic structure and spectra of a series of triarylmethane dyes", J. Am. Chem. Soc., 114:2342-2348, 1992.

Leuck, H. B.; Rice, B. L.; McHale J. L., "Aggregation of triphenylmethane dyes in aqueous solution : dimerization and trimerization of crystal violet and ethyl violet," Spectrochim. Acta, 48:819-828, 1992.

Lewis G. N.; Calvin M., "The color of organic substances", Chem Rev, 25:273-328, 1939.

Lewis G. N.; Magel, T. T.; Lipkin, D., "Isomers of crystal violet. Their absorption and re-emission of light", J. Am. Chem. Soc., 64: 1774, 1782, 1942.

Lewis L. M.; Indig, G. L. "Solvent effects on the spectroscopic properties of triarylmethane dyes" Dyes Pigm. 46: 145-154, 2000.

Lewis L. M.; Indig, G. L., "Photonuclease activity of mitochondrial triarylmethane photosensitizers." Pharmac. Pharmacol. Letters, accepted, 2001.

Maliwal, B. P.; Guthrie, F. "Interaction of insecticides with human plasma lipoproteins", Chem. Biol. Interactions, 35: 177-188, 1981.

Mathews, J. M. "Numerical Methods for Mathematics, Science and Engineering", Prentice Hall, Eds, New Jersey, Second Edition, 1992.

Maziere′, J. C., "New Trends in Photobiology (Invited Review). The role of the low density lipoprotein receptor pathway in the delivery of lipophilic photosensitizers in PDT of tumors", Photochem. Photobiol. B. Biol., 8: 351-360, 1991.

McClendon J. H.; "On the interpretation of absorption spectra of leaves – I. introduction and the correction of leaf spectra for surface reflection", Photochem and Photobiol., 51: 203-210, 1990.

Miccoli L.; Beuderly-Thomas, A.; DePineux, G.; Sureau, F.; Oudard, S.; Dutrillaux, B.; Poupon, M. F.; " Light –Induced photoactivation of hypericin affects the energy metabolism of human glioma cells by inhibiting hexokinase bound to mitochondria", Cancer Research, 58:5777-5786, 1998.

Minchin, R. F., "Evidence for the reversible binding of Paraquat to deoxyribonucleic acid," Chem-Biol Interactions, 61: 139-149, 1987.

Moras-Souza H.; Bordin, J. O., "Strategies for prevention of transfusion associated Chaga's disease," Transfusion Medicine Reviews, 10: 161-170, 1996

Morgan J.; Potter, W. R.; Oseroff, A. R., "Comparison of Photodynamic targets in a carcinoma cell line and its mitochondrial DNA deficient derivative", Photochem. and Photobiol., 71: 747-757, 2000

Muller W. and Gautier, F., "Interactions of heteroaromatic compounds with nucleic acids. A - T-specific non-intercalating DNA ligands", European Journal of Biochemistry. 54 : 385-94, 1975.

Nicholls, D. G.; Ferguson, S.J., Bioenergetics 2. Academic Press, London, 1982.

Norden B.; Tjerneld, F., "Binding of methyl green to deoxyribonucleic acid by linear dichroism", Chem. Phys. Letters, 50: 508-512, 1977.

O'Connor D.; Shafirovich V.; Geacintov, N. E., "Influence of adduct stereochemistry and hydrogen-bonding solvents on photoinduced charge transfer in a covalent benzo[a]pyrene diol epoxide –nucleoside adduct on picosecond time scales", J. Phys. Chem. 98: 9831-9839, 1994.

Oliveira C. S.; Pozzi, K.; Baptista, M.S.; Indig, G. L., Triarylmethanes : A comprehensive spectrochemical study" - unpublished data

Paardekooper M.; Vanagompel, A. E.; Vansteveninck, J.; Vandenbroek, P. J. A.; "The effect of Photodynamic treatment of yeast with the sensitizer Chloroaluminium Phthalocyanine on various celluolar parameters", Photochem. Photobiol., 62: 561-567, 1995.

Pal M. K., Gosh, J. K., "Circular Dichroic and Spectrophotometric probes of the competitive binding of crystal violet between DNA and anionic polymers", Spectrochim Acta, 50: 119-126, 1994.

Pedersen P. L. , "Tumor Mitochondria and the bioenergetics of cancer cells", in Homburger, F. Eds, "Progress in experimental tumor research", Krager, Basel, 22: 190-274, 1978.

Pedersen P. L., "Bioenergetics of cancer cells - A brief orientation to this mini review series" J. Bioenerg. Biomembrane, 29:301-302, 1997.

Penso J.; Beitner R., "Clotrimazole and bifenazole detach hexokinase from mitochondria of melanoma cells", European Journal of Pharmacology, 342:113-117, 1998.

Ramirez L. E.; Lages-Silva, E.; Pianetti, G. M.; Rabelo, R. M. C.; Bordin, J. O.; Moras-Souza H., " Prevention of transfusion associated Chaga's disease by sterilization of Trypanosoma Cruzi, infected blood with gentian violet, ascorbic acid and light," Transfusion, 35:226-230, 1995.

Rabinowitch E. I., "Photosynthesis and related processes", Vol II(1) pg 672, Wiley Interscience, New York, N.Y.1951.

Rharbi Y.; Kitaev, V.; Winnik, M. A.; Haahn, K. A., "Characterizing aqueous micellar Triton X 100 solutions of a fluorescent model triglyceride", 15: 2259-2266, 1999.

Registry of Toxic Effects of Chemical Substances (RTECS). US Department of Health and Human Service, Centers for Disease Control and Prevention, 1997.

Rempel A., Mathupala, S. P.; Griffin, S.A.; Hawkins, A. L.; Perderson, P. L., "Glucose catabolism in cancer cells: Amplification of the gene encoding type II hexokinase", Cancer Research, 56:2468-2471, et al, 1996.

Reyftmann J. P.; Morliere P.; Goldstein S.; Santus R.; Duebertret L.; Lagrange D., "Interaction of human serum LDLs with porphyrins : a spectroscopic and photochemical study", Photochem. Photobiol. 40:721-729, 1984.

Rodgers M. A. J.; Snowden P. T., "Lifetimes of singlet oxygen in liquid water as determined by time-resolved infrared luminescence measurements", J. Am. Chem. Soc. 104, 5541-5543, 1982.

Rosenberger V.; Margalit R., "Thermodynamics of the binding of hematoporphyrin ester, a hematoporphyrin derivative-like photosensitizer and its components to human

serum albumin, human high density lipoprotein and human low density lipoprotein", Photochem. Photobiol., 58:627-630, 1993.

Rotenberg M.; Margalit R., "Deuteroporhyrin-albumin binding equilibrium. The effects of porphyrin self-aggregation studied for human and bovine proteins", Biochem J., 229:197-203, 1985.

Rouhi M., "Let there be light and let it heal", Chemical and Engineering News, 22-27, 1998.

Sarkar M. and Poddar S., "Studies on the interaction of surfactants with cationic dye by absorption spectroscopy", 221: 181-185, 2000.

Scatchard G., "The attraction of proteins for small molecules and ions", Ann. N. Y. Acad. Sci., 51: 660-672, 1949.

Schiller, R. L.; Coates, J. H.; Lincoln, S. F., "Kinetic and equilibrium studies of crystal violet-cyclodextrin inclusion complexes", J. Chem. Soc. Faraday Trans. 1, 80: 1257-1266, 1984Schatz G., "Mitochondria-beyond oxidative phosphorylation", Biochim. Biophys. Acta, 1271:123-126, 1995.

Schmidt-Erfurth V.; Baumann W.; Gragoudas E.; Flotte T. J.; Michaud N. A.,; Birngruber R.; Hasan T.; "Photodynamic therapy of Experimental Choroidal Melanoma using lipoprotein- delivered benzoporphyrin", Ophthalmology, 101: 89-99, 1994.

Sambrook, J.; Fritsch E. F.; Maniatis T., "Molecular cloning. A laboratory manual," 2nd Edition. Cold Spring Harbor laboratory, Cold Spring Harbor, New York, 1989.

Schumaker V. N.; Phillips M. L.; Chatterton J. E., "Apolipoprotein B and LDL structure : implications for biosynthesis of triglyceride rich lipoprotein", Adv. in Protein Chemistry, 45: 205-248, 1994.

Seifert J. L.; Connor, R. E.; Kushon, S. A.; Wang, M.; Armitage, B. A., "Spontaneous assembly of helical cyanine dye aggregates on DNA nanotemplates", J. Am. Chem. Soc. 121: 2987-2995, 1999.

Shen, S. H.; Yong, C. Y.; Chen, P. F.; Setzer, D.; Tanimura M.; Li, W. H.; Gotto, A. M.; and Chan, L., "The complete cDNA and amino acid sequence of human apolipoprotein B-100", J. Biol. Chem., 261:12918-12921, 1986.

Shafirovich V.; Courtney, S. H.; Naiqi, Y.; Geacintov, N. E., "Proton-coupled electron transfer, deuterium isotope effects, and fluorescence quenching in noncovalent benzo[a]pyrenetetraol-nucleoside complexes in aqueous solutions", J. Am. Chem. Soc., 117: 4920-4929, 1995.

Shafirovich V.; Dourandin, A.; Luneva, N. P.; Geacintov, N. E., "The kinetic deuterium isotope effect asa probe of a proton coupled electron transfer mechanism in the oxidation of guanine by 2-aminopurine radicals", 104: 137-139, 2000.

Singh K. K.; Russell, J.; Sigala, B.; Zhang, Y.; Williams, J.; Keshav, K. F., "Mitochondrial DNA determines the cellular response to cancer therapeutic agents", Oncogene, 18: 6641-6646, 1999.

Smith T. A., "Mammalian hexokinases and their abnormal expression in cancer", British Journal of Biomedical Science. 57:170-178, 2000.

Spady, D. K., "Lipoproteins in biological fluids and compartments : Synthesis, Interconversion and Catabolism". In "Lipoproteins as carriers of Pharmacological agents", Michael J. Shaw Eds, Marcel Decker Inc., N. Y.,1-44, 1991.

Steitz, T. A.; Anderson, W. A.; Fletterick, I.J.; Anderson, C.M.; "High resolution crystal structures of yeast hexokinase complexes with substrates, activators and inhibitors: evidence for an allosteric control site", J. Biol. Chem. 252:4494-4500, 1977.

Stewart F.; Bass, P.; Star, W., "What does photodynamic therapy have to offer radiation oncologists (or their patients)?", Radiotherapy and Oncology, 48: 233-248, 1998.

Stork W. H.; Lippitis, G. J. M. ; Mandel, M; "Association of crystal violet in aqueous solutions", J. Phys. Chem., 76: 1772-1775, 1972

Tall A. R.; Small D. M., "High Density Lipoproteins", New Engl. J. Med., 299:1232-1236, 1978.

Victorov A. V.; Medvedeva, N. V.; Gladkaya, E. M.; Morozkin, A. D.; Podrez, E. A.; Koshyk, V. A.; Yurkiv, V. A., "Composition and structure of lipopolysaccharide-human plasma low density lipoprotein complex. Analytical ultracentrifugation, P-NMR, ESR and fluorescence spectroscopy studies", Biochimic et Biophysica Acta, 984: 119-127, 1989.

Viitanen P. V.; Geiger, P.J.; Erickson- Viitanen S.; Bessman, S. P., "Evidence for hexokinase compartmentation in rat skeletal muscle mitochondria," J. Biol. Chem., 259: 9679-9686, 1984.

Vogel, M.; Rettig, W. "Efficient Intramolecular fluorescence quenching in triphenylmethane-dyes involving excited states with charge separation and twisted conformations", *Ber. Bursenges Phys. Chem.* 89: 962-968, 1985.

Wilbur K. M.; Bernheium F.; Shapiro O. W., "The thiobarbituric acid reagent as a test for the oxidation of unsaturated fatty acids by various agents", Arch. Biochem., 24: 305-313, 1949.

Wilson J. E., "Hexokinases", In "Reviews of Physiology, Biochemistry and Pharmacology,"126: 66-198, Springer-Verlag, NY, 1995

Wilson J. E.;Chung V., "Rat brain hexokinase : Further studies on the specificity of the hexose and hexose 6-phosphate binding sites", Arch. Biochem. Biophys. 269: 517-525, 1989.

Wong J. R.; Chen, L.B.;, "Recent Advances in the study of mitochondria in living cells", Adv. Cell Biol., 2:263-290, 1988.

Wong J. R., Ho, C; Mauch, P; Coleman, N.; Berman, S.; Chen, L. B., " Removal of carcinoma cells from contaminated bone marrow using lipophilic cation Rhodamine 123", Clinical Cancer Research, 1: 621-630, 1995.

Zhou C.; Milanesi C.; Jori G., "An ultrastructural comparative evaluation of tumors photosensitized by porphyrins administered in aqueous solution, bound to liposomes or in lipoproteins", Photochem. Photobiol., 48: 487-492, 1988.